Hydrogen bonding induced order in supramolecular polymers

Hydrogen bonding induced order in supramolecular polymers

PROEFSCHRIFT

ter verkrijging van de graad van doctor aan de
Technische Universiteit Eindhoven, op gezag van de
rector magnificus, prof.dr.ir. C.J. van Duijn, voor een
commissie aangewezen door het College voor
Promoties in het openbaar te verdedigen
op donderdag 24 november 2011 om 14.00 uur

door

Tristan Mes

geboren te Breda

Dit proefschrift is goedgekeurd door de promotor:

prof.dr. E.W. Meijer

Copromotor:
dr.ir. A.R.A. Palmans

Voor mijn ouders

Table of contents

1

Introduction of order and function via hydrogen bonding

Abstract. This introductory chapter gives an overview of supramolecular polymers that self-assemble into ordered functional objects via the formation of non-covalent bonds, with hydrogen bonding as the most important one. While the design principles of synthetic supramolecular polymers are often derived from natural polymers, the study of synthetic supramolecular polymers yields valuable information about complex phenomena in natural systems. The interplay between natural and synthetic supramolecular polymers serves to formulate the research aim and outline of this thesis.

1.1 Introduction

The pioneering work of Hermann Staudinger revealed that polymeric properties in solution and in the solid state result from the macromolecular nature of molecules.[1] Small repeating units connected by covalent bonds form long interacting chains that generate many of the material properties typical for polymers. Macroscopic properties of polymers are directly derived from the molecular structure of the repeating units. By using the present knowledge of polymer chemistry in combination with the virtually endless number of available monomeric building blocks, many polymers comprising tunable properties have become accessible. In contrast to synthetic polymers, natural polymers or biomacromolecules are made of a limited number of different monomeric building blocks but they possess a much higher degree of complexity and functionality. In organisms, thousands of different biomacromolecules are responsible for metabolism, growth, response to stimuli, reproduction and adaptation to external factors. Biomacromolecules possess the property to adopt different conformations to fulfill their specific function.[2] The functionality of biomacromolecules is embedded into their three dimensional structure. Intra- and intermolecular non-covalent interactions play a crucial role in the conformational changes and folding of biomacromolecules. These interactions play also a key role in supramolecular chemistry. Supramolecular chemistry refers to the area of chemistry where non-covalent interactions substitute the "traditional" covalent bond formation (Figure 1.1). A special case consists of supramolecular polymeric materials that have the potential of possessing the valuable properties of traditional polymers. This, in combination with the major advantage of their reversible binding character, can give rise to new, unique material properties.[3-6]

Macromolecule
covalent bonds

Supramolecular polymer
non-covalent interactions
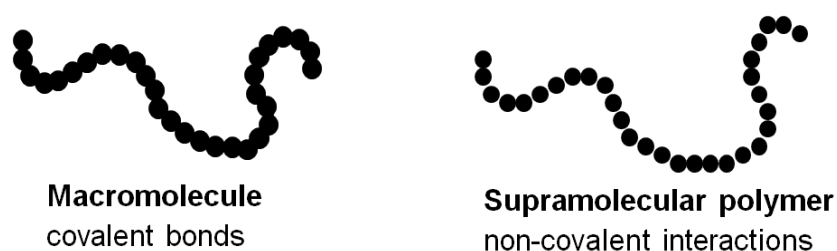
Figure 1.1 Schematic representation of a macromolecule consisting of covalent bonds and a supramolecular polymer formed by non-covalent interactions.

1.2 Supramolecular polymer chemistry

Supramolecular chemistry has been described as "chemistry beyond the molecule" in which well-defined non-covalent interactions determine assembly, disassembly, conformation and the function of the system.[7, 8] Supramolecular chemistry initially focused on the development of well-defined aggregates or supramolecular assemblies in solution by Cram,[9, 10] Lehn[7, 11, 12] and Pedersen[13-15] 40 years ago. Today, supramolecular chemistry has

grown into a broader field with many different applications, some of them are focused on the development of supramolecular polymers.[16-25] Supramolecular polymers consist of small monomeric building blocks, which have the ability to self-assemble into larger objects and exhibit true polymeric properties.

While the design principles of synthetic supramolecular polymers are often derived from natural (bio)polymers, the study of synthetic supramolecular polymers yields valuable information about complex phenomena in natural systems.[26-30] Due to reversible association, biological systems can also respond to external stimuli. By creating supramolecular systems with a similar design, smart materials can be developed. Nature uses supramolecular chemistry also for construction purposes to generate strength in polymeric materials. Examples are the proteins titin and silk fibroin. Titin is the largest single polypeptide that functions as a molecular spring and is responsible for the passive elasticity of muscles.[31, 32] Variations in the polypeptide sequence, and as a result in the supramolecular structure, are correlated with differences in mechanical properties of muscle tissue. Silk fibroin consists of small phase segregated crystalline domains embedded in a soft flexible matrix.[2] The crystalline domains act as physical cross-links and generate high strength and elasticity in the material. This principle is also applied in the synthetic polymer Spandex, in which hydrogen bonds are used to induce phase segregation, generating elastic material properties (Figure 1.2).[33, 34] Spandex is widely used in the textile industry for sports clothing under the commercial names Lycra® and Elastine®.
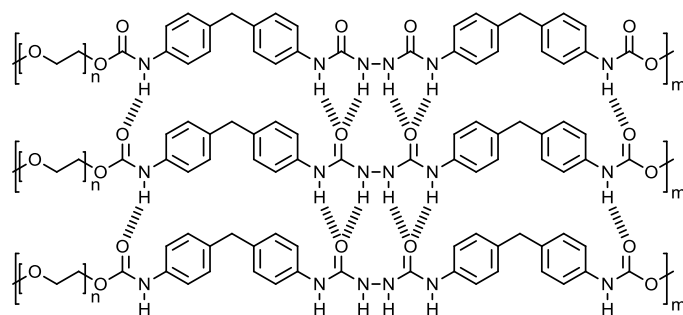
Figure 1.2 A (supra)molecular structure of spandex.[34]

The development of multiple hydrogen bonded supramolecular polymers, exhibiting true polymer material properties comparable with those of traditional covalent polymers in solution and in the solid state, gave a significant boost to the area of supramolecular polymers. Functionalization of low molecular weight polymers with supramolecular binding motifs allowed to combine the attractive features of traditional polymers with the reversibility and dynamic behavior of the supramolecular motif.[35-46] The strength and dynamic parameters of the supramolecular motif determine the resulting polymer properties. This concept is now widely applied and has evolved into a unique class of

materials that is able to respond to external stimuli and, when appropriately designed, can be applied in biomedical and electronic applications.

1.3 Supramolecular polymerization mechanisms

Complementary motifs, A-B, or self complementary motifs, A-A, are able to form polymeric structures such as linear polymers, copolymers and even supramolecular cross-linked networks under appropriate conditions. The degree of polymerization (DP) depends on the association constant, the concentration, the temperature and the polymerization mechanism. The polymerization mechanisms can be divided into two main classes: a) the isodesmic or multistage open association (MSOA) mechanism or b) the nucleation-elongation or cooperative mechanism (Figure 1.3).[47]

The isodesmic or MSOA polymerization is similar to the conventional step polymerization and is characterized by a polydispersity of 2 and a DP that strongly depends on the association constant of the linking supramolecular units. The chain length does not affect the association constant and the chain length increases with increasing concentration or decreasing temperature (Figure 1.3).[48]
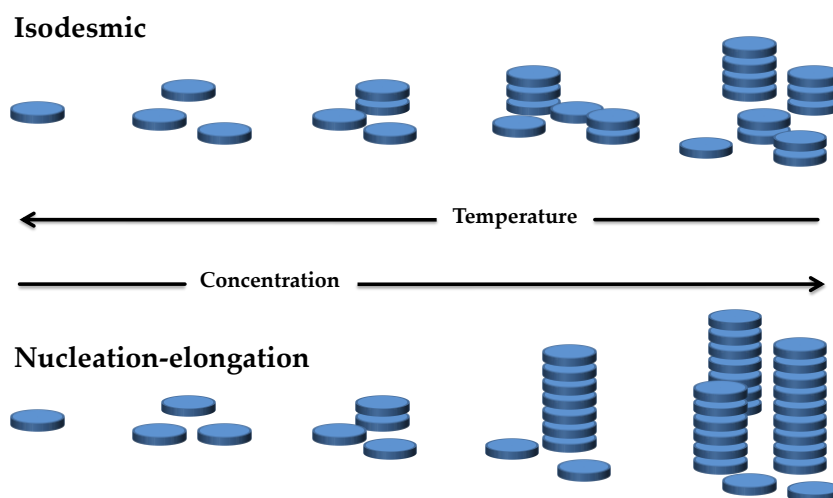
Figure 1.3 Schematic representations of the main supramolecular polymerization mechanisms.

In the nucleation-elongation or cooperative growth mechanism two steps can be distinguished.[49-53] The first step is less favorable and characterized by a low association constant and proceeds until a stable nucleus is formed. Due to a cooperative effect the addition of an additional monomer then occurs with an association constant that is higher. The supramolecular polymerization proceeds but now with a higher association constant. Long elongated polymer chains are only formed above a critical concentration or below a critical temperature. The formation of polymeric species is characterized by a sharp transition from a state dominated by free monomers to a state in which monomers are polymerized (Figure 1.3).

1.4 Hydrogen bonding

1.4.1 Hydrogen bonding strength

A number of non-covalent interactions can be applied in the formation of supramolecular polymers such as electrostatic interactions, hydrogen bonding, coordinative bonding, π-π interactions, van der Waals forces and solvophobic effects. A covalent bond has a typical bond strength of 350 kJ/mol while non-covalent bonds are much weaker. Van der Waals forces have a typical bond strength of 2 kJ/mol, hydrogen bonds of 20 kJ/mol and ion-ion interactions of 250 kJ/mol. Although hydrogen bonding is not the strongest interaction, it is widely used due to its directionality and versatility.[54, 55] A hydrogen bond is an interaction between a positive dipole or charge on hydrogen and an electronegative atom. The strength of a single hydrogen bond depends on the strength of the hydrogen bond donor (acidity) and acceptor (basicity) and ranges from weak C-H – π interactions to the very strong F-H – F-interaction (163 kJ/mol).[56] Supramolecular chemistry is often based on medium strength hydrogen bonds between N-H and O-H (donor groups, D) and C=N- and C=O (acceptor groups, A). Also the environment of the hydrogen bonding system (*e.g.* solvent) determines the strength of the interaction.[57]

A general approach to enhance binding strength in hydrogen bonding systems is the use of multiple hydrogen bonds in an array.[58, 59] Gong *et al*. reported a highly stable dimeric complex that is based on six hydrogen bonds with a dimerization constant of 1.3×10^9 M^{-1}.[60] However, increasing the number of hydrogen bonds in an array does not a priori result in a higher association constant.[61] This phenomenon was demonstrated by Jorgensen *et al*.[62, 63] and later extended by the group of Zimmerman[64] with threefold hydrogen bonding motifs as an example. Complexes between ADA – DAD exhibit an association constant of 10^2 M^{-1} in chloroform. DAA – ADD complexes exhibit association constants of 10^4 M^{-1} and the association constant of the AAA – DDD complex exceeds 10^5 M^{-1} in chloroform. The difference was attributed to attractive and repulsive secondary cross-interactions of donor and acceptor units in their counterpart (Figure 1.4). The additional repulsive or attractive interactions have a significant influence on the association constant. An association constant that is three orders of magnitude larger was obtained in the most ideal array. Schneider *et al*. calculated that the free association energy increases with 2.9 kJ/mol by every additional attractive interaction, introduced into the complex.[65]
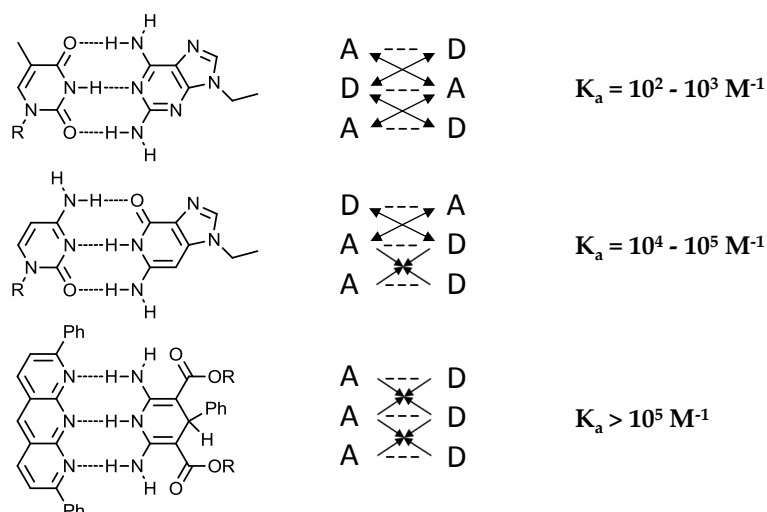
Figure 1.4 Stability of complexes of threefold hydrogen bonding motifs in chloroform.

The use of multiple hydrogen bonds in one complex has led to a rapid expansion of the development of strong hydrogen bonding motifs.[59, 66] Especially interesting are self-complementary binding motifs, since they do not suffer from stoichiometric issues in the formation of linear polymers. In our group, Beijer *et al*. developed various quadruple hydrogen bonding motifs showing a DADA array based on diaminotriazines.[67] Acetylated diaminotriazines exhibit a low binding constant of 170 M^{-1} (diacetyl) and 530 M^{-1} (monoacetyl) in chloroform. Interestingly, monoureido derivatized diaminotriazines exhibit a dimerization constant of 2 x 10^5 M^{-1}. Based on Schneider's calculations,[65] a large deviation in the expected and measured dimerization constant was observed. The difference was attributed to an intramolecular hydrogen bond between the ureido N-H and nitrogen in the triazine ring. This leads to a *cis* conformation of the ureido part and forces the carbonyl to be in a planar arrangement with respect to the ring, resulting in a preorganized ADAD array. Preorganization via intramolecular hydrogen bonding was also successfully applied in quadruple hydrogen bonding motifs with the more favorable AADD array. Sijbesma and Beijer introduced the 2-ureido-4[1*H*]-pyrimidinone (UPy), which is a preorganized quadruple hydrogen bonding motif.[48, 68, 69] The UPy possesses a tautomeric equilibrium between a keto-tautomer and an enol-tautomer. The UPy tautomers can dimerize via an ADAD or AADD array and exhibit dimerization constants of 9 x 10^5 M^{-1} and 6 x 10^7 M^{-1}, respectively.[70] Which of the possible tautomeric forms dominate, depends on the solvent and on the substituent on the isocytosine part. Corbin and Zimmerman developed a heterocyclic quadruple hydrogen bonding motif that does not suffer from weakening effects due to tautomerism (Figure 1.5).[71] Upon tautomerization, the relative spatial arrangement of the donor/acceptor substituents does not change, leading to mainly AADD hydrogen bonding arrays with corresponding association constants of 10^8 M^{-1} in toluene and 3 x 10^7 M^{-1} in chloroform.

Ratio in toluene (chloroform)	2% (6%)	39% (11%)	46% (43%)	13% (40%)
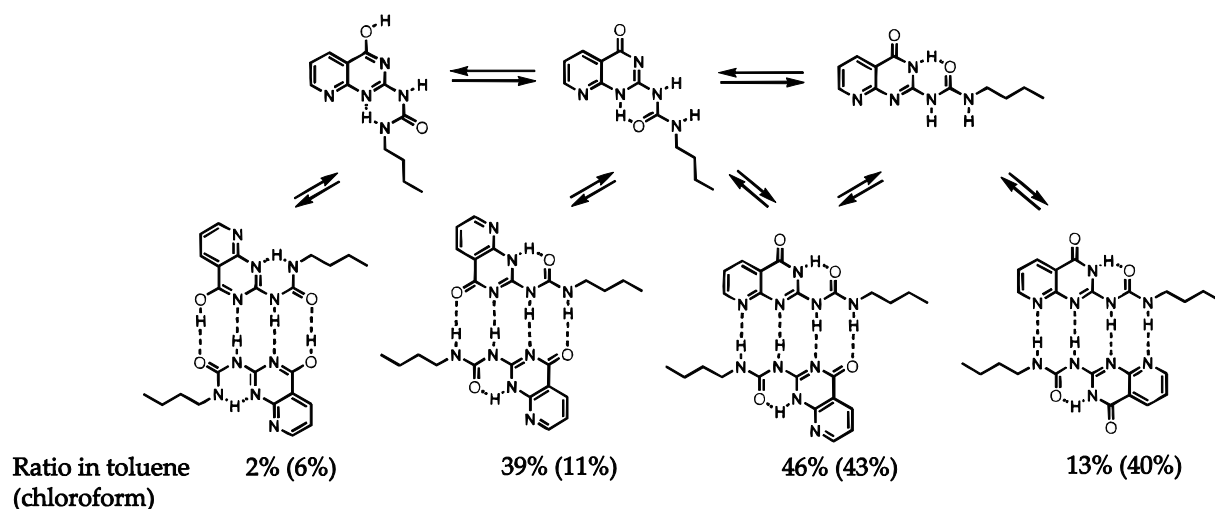
Figure 1.5 Ratio of tautomeric forms of the quadruple hydrogen bonding motif developed by Zimmerman *et al*. in toluene and chloroform.

1.4.2 Increasing binding strength

In general, an increase in the association constant of the supramolecular motif results in an increase in length of the supramolecular polymer and thus in an enhancement of their macroscopic properties. A different approach to increase macromolecular properties is to include additional interactions apart from hydrogen bonding. Phase segregation, hydrophobic interactions or others, may enhance the binding strength as well. For example, liquid crystalline behavior in main- or side-chain and columnar supramolecular polymers was observed in the initial reports on hydrogen bonded supramolecular polymers.[72-80] Liquid-crystalline behavior was the result of an increase in anisotropy due to the formation of ordered flexible and rigid domains in the supramolecular polymer. The induction of anisotropy by hydrogen bonding is a cooperative process because anisotropy favors alignment of the hydrogen bonding motifs resulting in a higher association. Lehn *et al*. observed this phenomenon in supramolecular chains, arranged in a helical fashion, that were formed by threefold hydrogen bonding between bifunctional uracil and bifunctional diaminopyridine motifs (Figure 1.6).[72] Both motifs separately did not show liquid crystalline behavior but only a mixture of both motifs, in a 1:1 ratio, showed the presence of a mesophase in a broad temperature range.
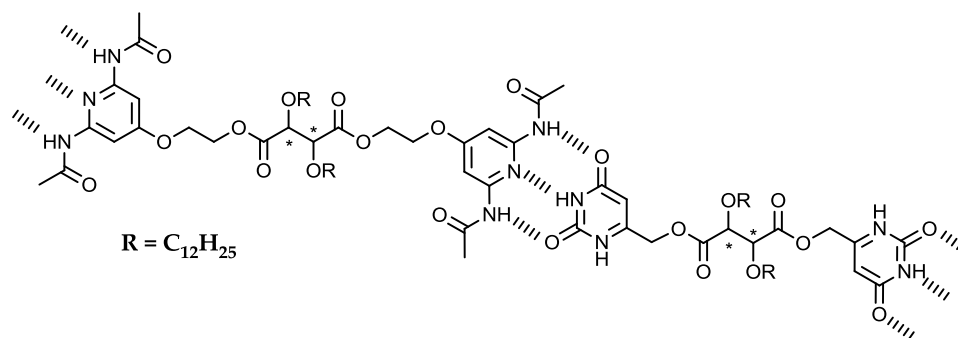
Figure 1.6 Formation of a supramolecular chain by threefold hydrogen bonding between bifunctional diuracil and bifunctional diaminopyridine motifs.

Liquid crystalline behavior in general originates from an intrinsic difference within one molecule, such as differences in flexibility or polarity. In the liquid crystalline phase these different parts are phase segregated resulting in ordered microdomains. In fact, phase segregation in general is a method to increase binding strength and to generate new material properties in supramolecular polymers.[36, 81-87] Phase segregation in traditional block copolymers originates from the immiscibility of both blocks. Depending on the composition of the blocks, small functional domains can be formed that give rise to new material properties. In supramolecular polymers, the formation of domains of hydrogen bonding motifs is a frequently used method to extend polymer chains in a supramolecular fashion. When domain formation takes place, the local concentration of the supramolecular motif increases and this results in a virtual increase of the association constant.[88] This principle was initially investigated by Stadler *et al*. who developed polybutadienes side-functionalized with phenylurazole motifs.[89-91] Hydrogen bonded phenylurazoles formed small, crystalline domains that behaved like conventional cross-links in a polymer matrix. The end-capping of telechelic poly(tetrahydrofuran) (pTHF) with the weak hydrogen bonding benzoic acid led to a significant increase of the material properties.[81] Rowan and coworkers found that even thermoplastic elastomeric properties were obtained after end-capping of pTHF with moderate hydrogen bonding motifs based on nucleobases.[83] Both telechelic polymers showed additional melting points that were attributed to the melting of the crystalline domains.

Since the intrinsic strength of a hydrogen bond highly depends on the solvent in which the supramolecular motif is employed, shielding of hydrogen bonds from the solvent can be a powerful tool to increase the association constant of a supramolecular motif.[92-94] This is because a polar environment is more capable to interact with hydrogen bonding motifs than an apolar environment and thus leads to a decrease of hydrogen bonding strength. The hydrophobic effect (or solvophobic effect) is a frequently applied methodology to shield hydrogen bonds from the environment.[95, 96] Moreover, hydrophobic compartmentalization is one of the main concepts in nature to create and stabilize supramolecular systems in water

environments.[2] Polarity differences within a biomacromolecule results in a specific arrangement of the polymer backbone creating polar and apolar domains. The apolar domains form a suitable environment for stable hydrogen bonds. Due to compartmentalization, the local concentration of hydrogen bonding motifs increases resulting in a higher association constant. The principles and consequences of the hydrophobic effect are similar to those of phase segregation.

1.5 Supramolecular networks

Supramolecular polymers utilizing multiple hydrogen bonding arrays in combination with the use of additional interactions to reinforce the supramolecular structure (*vide supra*), led to the development of supramolecular materials showing unique material properties and with applications envisioned in biomaterials,[16, 97, 98] self-healing materials,[18, 19, 99, 100] and hydrogels.[21, 22, 101, 102] Under suitable conditions, these supramolecular polymers display macroscopic material properties comparable to high molecular weight macromolecules. In general, the following design principles suffice to introduce excellent material properties in supramolecular polymers. First, the supramolecular polymer should consist of low molecular weight polymers (supramolecular monomer) bearing (self)-complementary supramolecular motifs in the main chain. Second, physical cross-linking occurs when oligotopic monomers (functionality >2) or ditopic monomers, with the tendency to phase segregate, are used. Oligotopic monomers can contain supramolecular motifs end-functionalized to,[43, 103-106] copolymerized with,[107, 108] or side-functionalized[109-117] to a polymeric backbone. Also, ditopic discotic molecules can form networks due to entanglement of long linear supramolecular polymers.[118, 119]

Chain extension and physical cross-linking by domain formation, as a result of phase segregation, proved to be an excellent method to obtain thermoplastic elastomeric material properties from low molecular weight polymers bearing relatively weak hydrogen bonding motifs. A systematic study on thermoplastic elastomeric behavior in supramolecular polymers was performed on bis-urea functionalized polymers. Bis-urea motifs end-capped to,[87] copolymerized with,[107, 108, 120] or side-functionalized[121] to amorphous polymers form strong intermolecular bifurcated hydrogen bonds. Hydrogen bonded bis-ureas motifs phase segregate into nanofibers and act as strong physical cross-links. Another example of an end-functionalized low molecular weight polymer with self-complementary binding motifs that shows promising material properties came from our group. Folmer *et al.* showed that telechelic poly(ethylene-*co*-butylene) (pEB) functionalized with UPy groups shows significantly better material properties than that of unfunctionalized pEB.[36] When UPys were introduced via a urethane or urea bond, a further increase of the material properties was obtained. The additional lateral interactions between urethanes or ureas resulted in the formation of phase segregated nanometer-sized fibers. The fibers act as strong multiple

cross-linking points in the polymer matrix (Figure 1.7).[84] Dankers *et al*. expanded this concept to bioactive materials by mixing in mono UPy functionalized peptides into biodegradable UPy functionalized polycaprolactone.[16]
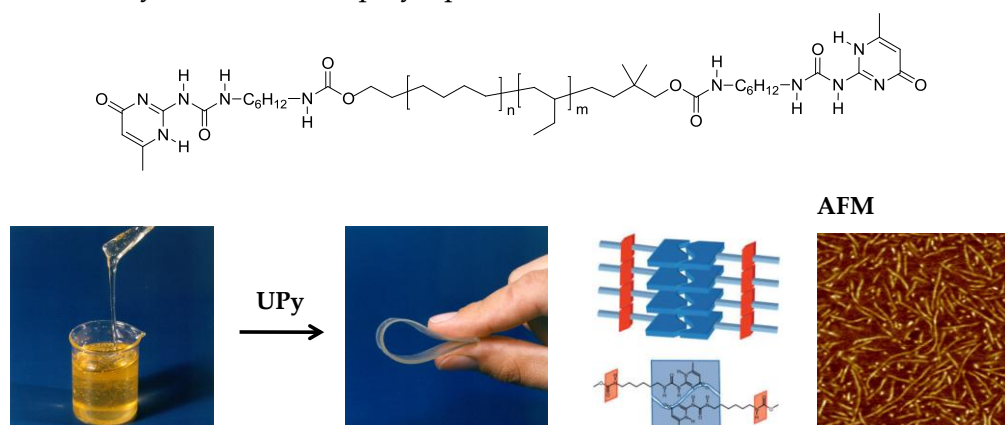
Figure 1.7 A thermoplastic elastomeric polymer was obtained after functionalization of telechelic pEB with UPy motifs via a urethane bond.

Side-functionalized polymers bearing supramolecular motifs, based on multiple hydrogen bonding arrays, were initially developed by the group of Rotello, inspired by the seminal work of ten Brinke and Ikkala using phenol-pyridine interactions.[122] A significant part of the work of Rotello is based on non-covalent functionalization of polymers with small molecules via hydrogen bonding. The modular approach of hydrogen bonding functionalization was denoted as "plug and play". In this approach non-covalent synthesis was used to create functional composite materials from organic polymers and a variety of small molecules that can influence the bulk material properties. One of the first examples was the functionalization of polystyrene bearing diaminotriazine-groups with flavin via threefold hydrogen bonding. Upon addition of flavin, the polymer morphology changed from a folded state, due to dimerization of diaminotriazine, to an unfolded state (Figure 1.8). With this strategy, recognition of guests in various polymeric host systems was demonstrated.[123-125]
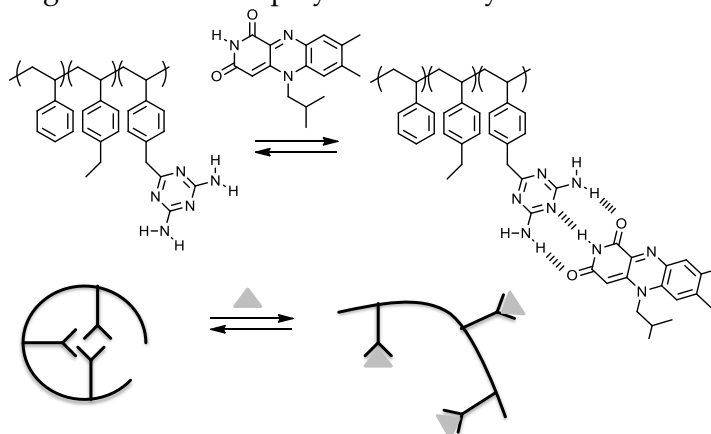
Figure 1.8 Hydrogen bonding attachment of flavin to diaminotriazine-functional polystyrene leads to unfolding of the polymer backbone.[125]

The group of Weck elaborated the concept of side-functionalized supramolecular polymers by the introduction of multiple non-covalent orthogonal binding sides in the side-chain.[126] They initially focused on the use of multiple hydrogen bonding motifs with competitive binding properties. Self-sorting or step-wise functionalization strategies were successfully used to obtain heterofunctional supramolecular copolymers.[127] A polynorbornene backbone side-functionalized with cyanuric acid and thymine motifs were functionalized with the Hamilton wedge and diaminopyridine, respectively, in a step-wise and one-pot approach (Figure 1.9). Subsequently, they expanded their tool box by using metal coordination and hydrogen bonding in an orthogonal fashion.[128, 129] The development of these polymers is aimed to increase the level of functionality in supramolecular polymers.
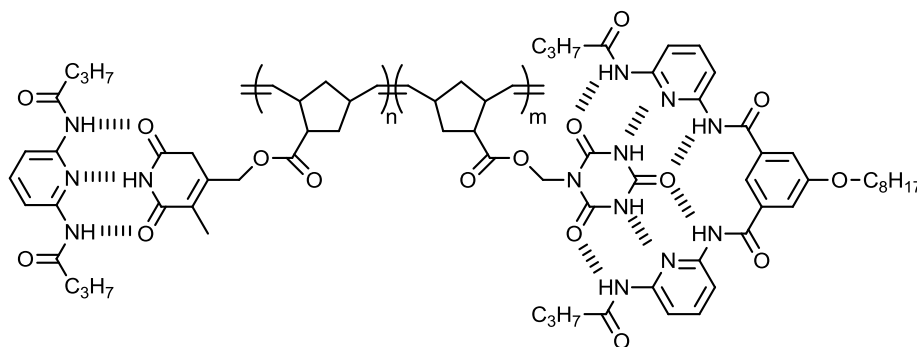
Figure 1.9 Heterofunctional supramolecular copolymer obtained by a step-wise and one-pot approach using orthogonal binding sites.

1.6 *C₃*-symmetrical compounds in supramolecular polymerizations.

Ditopic disc-shaped molecules with the ability to form linear, rodlike supramolecular polymers are a particularly interesting class of molecules.[25, 130-133] Disc-shaped molecules, which consist of a rigid planar aromatic core equipped with flexible side-chains often show thermotropic liquid crystalline behavior.[134] The non-covalent interactions between cores of consecutive discs are mainly based on π-π interactions and hydrogen bonding. The interdisc interactions are also significantly stabilized by solvophobic effects. The interdisc interactions are much stronger than intercolumnar interactions, promoting the formation of long polymers. At higher concentration, the long columnar structures interact and this can lead to the formation of gels. Many discotic compounds self-assemble in columnar aggregates, but we focus here on those in which the intermolecular non-covalent interactions are dominated by hydrogen bonding.

The group of Hanabusa investigated the self-assembly of a ditopic compound based on a *cis* cyclohexane-1,3,5-trisamide.[118, 135, 136] This compound consists of a cyclohexane core equipped with three alkyl side chains connected via amide bonds. Due to the *cis* arrangement of the cyclohexane core, all three amide bonds participate in uni-directional hydrogen bonding in apolar solvents, as evidenced by the single crystal X-ray structure produced by

the group of Hamilton (Figure 1.10A).[137] Due to the formation of long supramolecular polymers, transparent viscous solutions or gels were obtained depending on the solvent.

The group of van Esch developed a series of water soluble cyclohexane-1,3,5-trisamide derivatives that were successfully applied as low molecular weight hydrogelators (LMWGs) with thermo- and pH-responsive properties (Figure 1.10B).[94, 138, 139] Hydrogen bonding was stabilized by additional hydrophobic interactions from a hydrophobic shell around the core. The supramolecular structure and corresponding gelating properties were investigated in great detail. Van Bommel *et al.* demonstrated the potential of these LMWGs to be used as drug delivery systems.[140] One of the three side chains was functionalized with an *L*-phenylalanyl-amidoquinoline group (Figure 1.10C). The amidoquinoline group represents a model drug and could be released by enzymatic cleavage. They showed that enzymatic cleavage occurred significantly faster in the solution state than in the gel state. Controlled release was obtained by alteration of the sol-gel equilibrium with temperature.
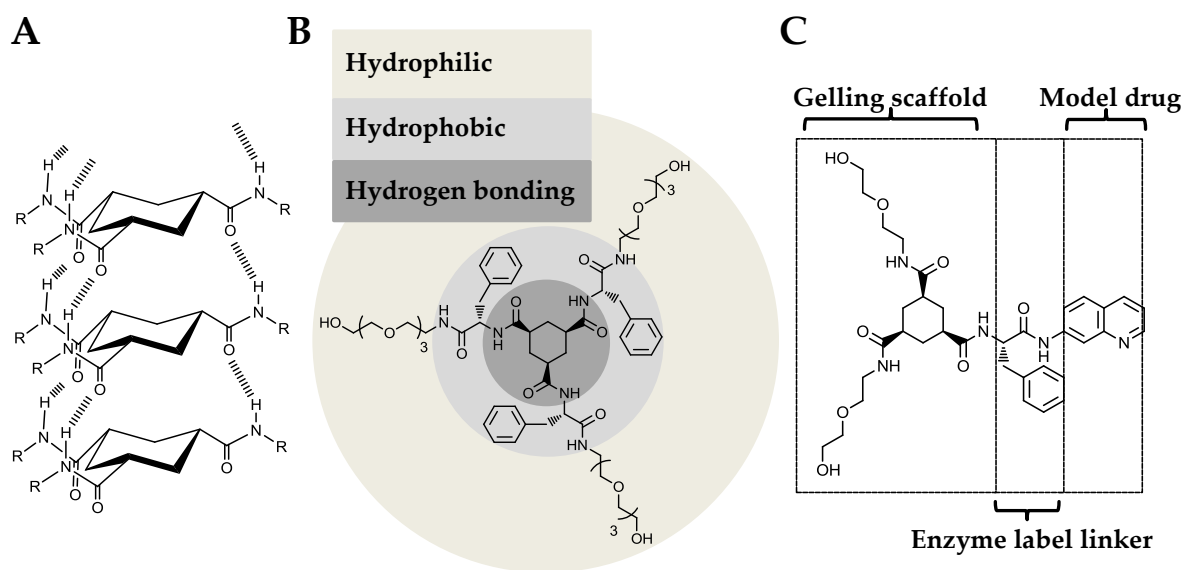
Figure 1.10 A) Single crystal X-ray structure of cyclohexane-1,3,5-trisamide. B) Molecular structure of a LWMG based on a cyclohexane-1,3,5-trisamides. C) Molecular structure of cyclohexane-1,3,5-trisamides, which are used to make bio-active hydrogels.

The benzene-1,3,5-tricarboxamide (BTA) motif consists of a benzene core and three side chains connected via three amide bonds. This motif forms a one dimensional polymer in solution and in the solid state, as a result of the threefold α-helix type arrangement of the intermolecular hydrogen bonds.[141-144] Lightfoot *et al*. produced a single crystal X-ray structure of tris(2-methoxyethyl)benzene-1,3,5-tricarboxamide (Figure 1.11, left).[145] The structure shows that all carbonyls in the amide are tilted. Usually, aromatic amides prefer a coplanar arrangement of the carbonyl with the aryl group. In this case a conflict originates

between the demands of conjugation and those of hydrogen bonding. This leads to the formation of helical supramolecular polymers (Figure 1.11 right). At higher concentration, long polymers gelate organic solvents due to intercolumnar interactions.[146, 147] BTAs also exhibit thermotropic liquid crystalline behavior in the solid state.[148]
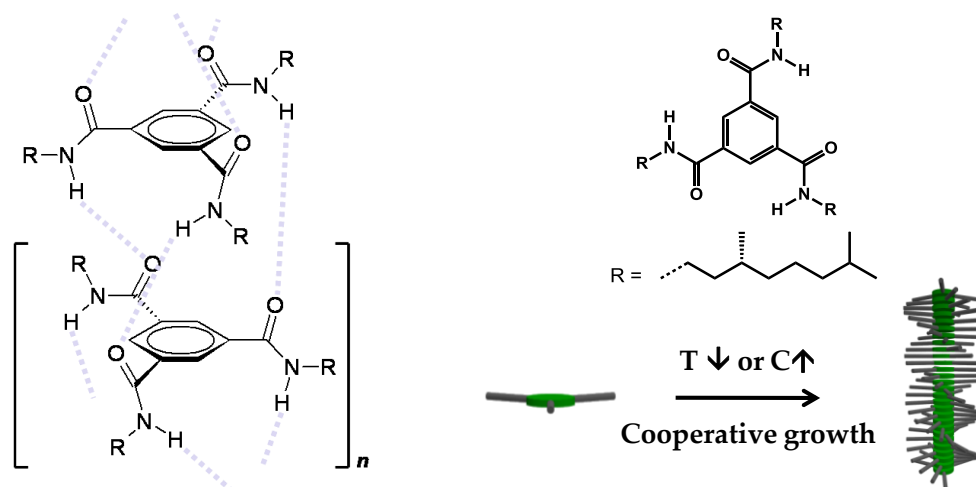
Figure 1.11 Single crystal X-ray structure of a benzene-1,3,5-tricarboxamide (left). Schematic representation of a helical supramolecular polymer of BTAs (right).

BTAs equipped with achiral side chains form an equimolar mixture of left- and right-handed columns. The introduction of one stereogenic centre into the alkyl side chain biases the formation of only one helicity due to an energy difference between both diastereomeric helicities. In this sense, the configuration of the stereocentre is transferred to the conformation of the supramolecular polymer. The addition of a small amount of chiral BTAs in a solution of achiral BTAs instantly directs the helicity to one handedness (Sergeants and Soldiers effect). These results are similar to those obtained in chiral polymers with covalent bonds and are explained by a cooperative effect due to the directionality of hydrogen bonds. Self-assembly of BTAs can be followed with circular dichroism (CD) and ultraviolet (UV) spectroscopy. CD measurements showed that the temperature-dependent aggregation can be described by a nucleation-elongation mechanism.[144, 149] In dilute solutions (10^{-5} M) of apolar solvents, BTAs form long helical polymers with a high DP due to their large association constant (3×10^7 M^{-1}). The intermolecular hydrogen bonds disappear in more polar solvents like chloroform or methanol.[143, 150] Moreover, in apolar solvents the propensity to form columnar helical stacks is significantly lowered when changing one alkyl side chain in a BTA to an oligo(ethylene oxide) side chain, due to a dramatic reduction of the association constant (20 M^{-1}) caused by backfolding of the oligo(ethylene oxide) side chain.[148, 151] This means that the self-assembly of BTAs into helical aggregates not only depends on the solvent polarity but also on the micro-environment of the BTA. BTAs are one of the simplest and most studied supramolecular motifs and have great potential to be used in various applications.

1.7 Tuning the size and shape of supramolecular polymers

Researchers have been intrigued by the development of supramolecular assemblies that are defined in size and shape.[152-158] Such assemblies resemble the well-defined structures of many biomacromolecules. In addition, these assemblies can bear functionality or can be used to study folding processes of natural polymers. In general, three approaches can be used to form supramolecular assemblies that are limited in size; the use of bulky substituents to induce steric constraints, the use of preorganized rigid building blocks, and finally the use of multiple non-covalent interactions that form preferentially intramolecular bonds due to specific placement or specific conditions. Bulky substituents can induce steric constraints to supramolecular assemblies. Well-known examples of natural systems in which the supramolecular organization is determined by steric constraints are the icosahedral capsid viruses.[159] They consist of a RNA strand coated with proteins in a perfectly defined ordered structure. The group of Percec has developed synthetic systems that show great similarities with icosahedral capsid viruses when they introduced branched side groups (protein equivalent) to a single string of polymer (RNA equivalent).[79, 160] In our group, Besenius *et al.* introduced a system based on self-assembling discotic amphiphiles that formed chiral columnar aggregates.[161] By balancing out attractive non-covalent interactions within a hydrophobic core with repulsive electrostatic interactions in the periphery, control was gained over stack length and shape of the supramolecular assembly (Figure 1.12).
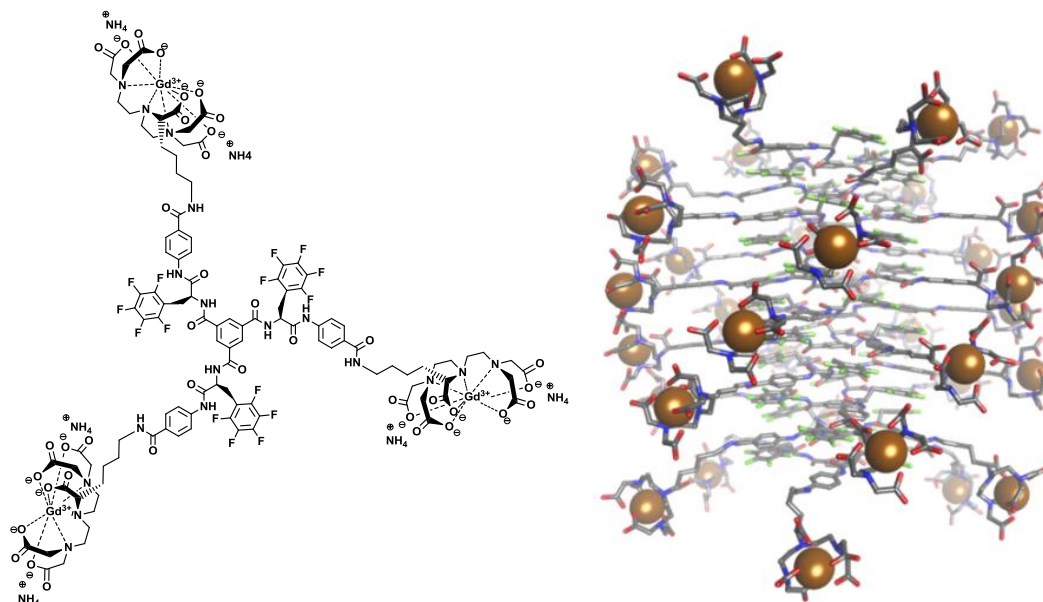
Figure 1.12 Molecular structure of a discotic amphiphile (left) that forms a stack with a controlled length (right).

By using rigid building blocks, more control in the directionality of non-covalent interactions is obtained. As observed in liquid crystalline supramolecular polymers (*vide supra*), the increase in directionality leads to an increase in anisotropy resulting in stronger binding. In addition, the careful placement of multiple binding interactions generates more strength due to an increase of the effective concentration. This approach was successfully shown by the group of Reinhoudt[162, 163] and others.[164-166] They prepared a library of compounds that form very stable dimers based on calixarenes and resorcinarenes. Dimeric complexes were able to selectively bind small guest molecules. This approach was expanded by the group of Rebek by increasing the distance between glycoluril hydrogen bonding motifs.[167-169] Depending on the spacer employed, spherical objects were obtained that show structural similarities with tennis- or softballs (Figure 1.13A) These objects bound small guest molecules and showed enantiomeric selective binding.

A)
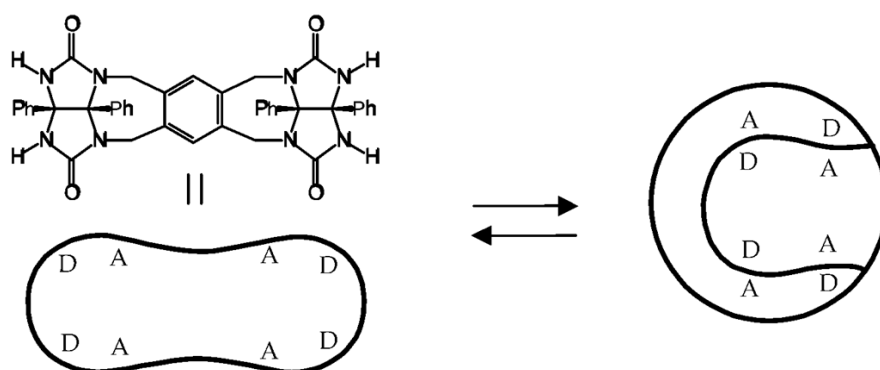
B)
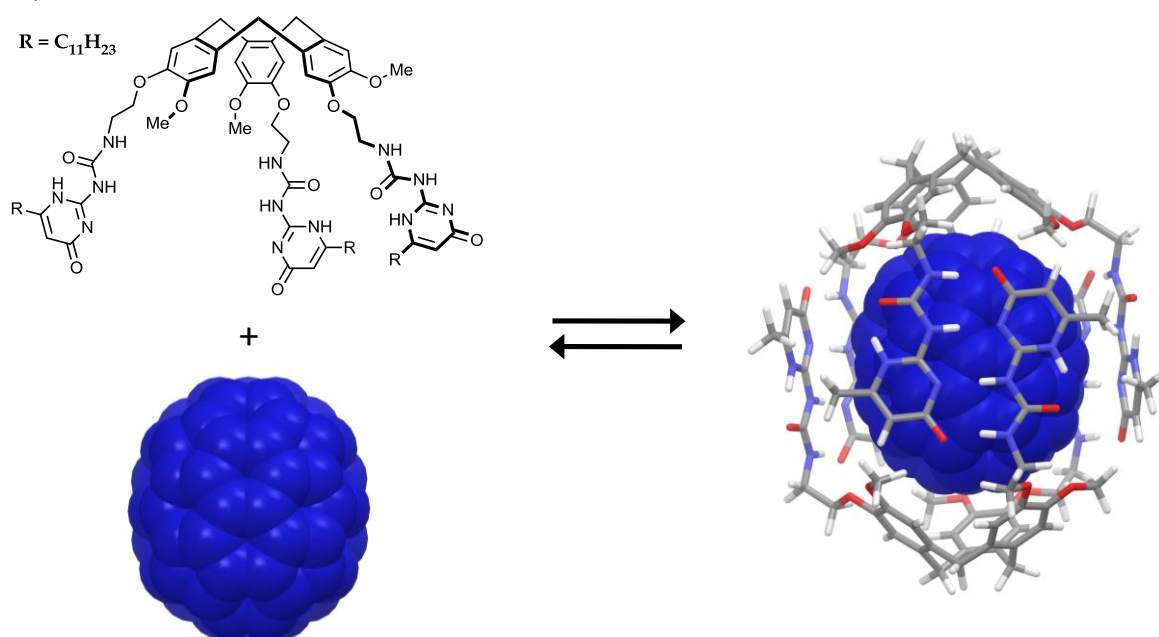
Figure 1.13 A) A "tennis ball" formed via dimerization of a glycoluril derivative. B) Encapsulation of a fullerene in a dimer of cyclotriveratrylenes functionalized with UPys.

Huerta *et al*. developed a system based on cyclotriveratrylenes functionalized with UPy groups that can encapsulate fullerenes via π-π interactions and subsequent dimerization via hydrogen bonding.[170, 171] The rigidity of the core is increased upon complexation with a fullerene molecule leading to the formation of dimeric species. Since the association strength is determined by the efficiency of filling of the cavity, selective binding of fullerene analogs was obtained. These systems are successfully employed in the separation and isolation of fullerenes due to their size selective and reversible binding properties (Figure 1.13B).[172]

The specific placement of multiple interacting motifs can lead to a variety of supramolecular assemblies including linear and other geometrical shapes. Natural systems often use multiple interacting groups, which bind to a specific counterpart within the same molecule. Due to the site-specific intramolecular binding in proteins, an endless variety of perfectly ordered structures is obtained. Synthetic analogies, which mimic structural order of proteins by intramolecular interactions at specific locations can be found in the field of dendrimers and foldamers. The group of Parquette developed a series of monodisperse dendritic structures that exhibited an ordered chiral arrangement via intramolecular hydrogen bonding. These structures show enantioselective catalysis and others possessed the ability to change their conformation using light.[173-175] In contrast to dendritic structures, foldamers possess more structural similarity with proteins since they are built from a single or multiple linear chains. Foldamers are an especially valuable class of supramolecular polymers because the formation of assemblies (folding process) might provide insights into the (mis) folding of proteins and into the formation of the structure of DNA and RNA.[26, 28, 176] Foldamers can be based on a number of different backbones and non-covalent interactions. However, the most popular foldamers are based on poly-β-peptides due to their structural and chemical similarities with natural polymers. The group of Gellman[27, 177] and the group of Seebach[178, 179] have been the most active in the exploration of short β-peptides that form helical folded objects via intramolecular hydrogen bonding (Figure 1.14).
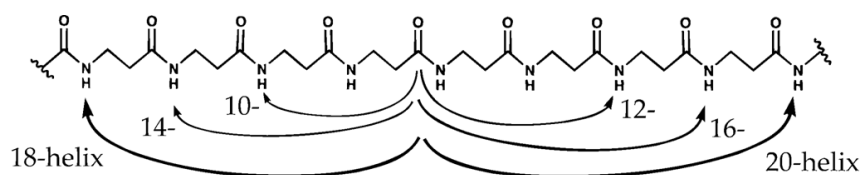
Figure 1.14 Poly(β-amino acid) backbone. The arrows show all possible helical conformations in short β-peptides.

Hydrogen bonding interactions have also been used in combination with π-π interactions of aromatic rings in oligomer systems.[180, 181] A common motif in this research is the use of aryl amides. In contrast to polypeptides, these oligomers make only use of interactions between adjacent monomer units. These chain conformations can behave cooperatively or as

a collection of independent units. The group of Hamilton reported on a class of foldamers exhibiting a helical conformation based on oligoanthranilamides.[182, 183] The system is based on the intramolecular hydrogen bonding and π-π interactions of anthranilamide and 2,6-pyridinedicarboxamide (Figure 1.15). These structures form very stable helical structures in the solid state and in chloroform solutions.
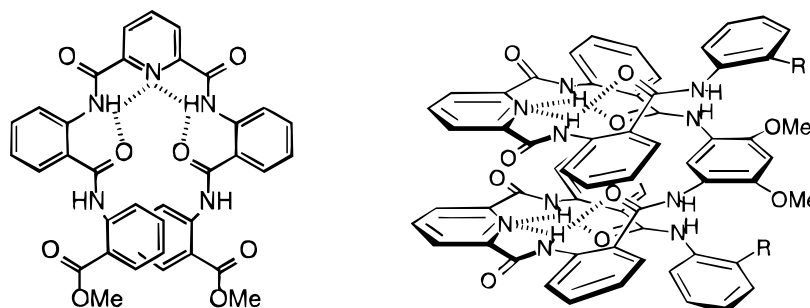
Figure 1.15 Folded conformation of oligoanthranilamides by intramolecular hydrogen bonding and π-π interaction.

On one hand, foldamers possess a secondary structure, and in this sense, they partially mimic the structure of biomacromolecules. On the other hand, the molecular weight is rather low and therefore they are not very good mimics for natural polymers. The development of higher molecular weight foldamers is limited because of the synthetic challenge.

Recently, considerable effort has been put in the development of a novel class of nanometer-sized supramolecular assemblies, namely, single-chain polymeric nanoparticles (SCPNs). SCPNs consist of linear polymeric chains with side groups that have the ability to form intramolecular bonds. Initially, SCPNs were developed that were formed by intramolecular covalent bonds.[184-188] Later, SCPNs were developed, which contain side groups that have the ability to form non-covalent bonds. In the right circumstances, these polymer chains collapse, via non-covalent interactions, into a single-chain polymeric nanoparticle. SCPN based on non-covalent interactions are reversible and can therefore change their conformation by using external stimuli. This approach has been successfully introduced by our[189-191] and other groups[125, 192] using hydrogen bonding motifs. Foster *et al*. developed polynorbornenes side-functionalized with UPy groups (Figure 1.16). The UPy groups were equipped with a photolabile protecting group that prevented dimerization. Upon photoirradiation, the protecting group was cleaved allowing UPy dimerization. In dilute condition, only intramolecular hydrogen bonds are formed leading to the formation of nanoparticles consisting of single polymeric chains. Gel permeation chromatography was used to visualize the corresponding decrease of the hydrodynamic volume. Atomic force

microscopy showed the presence of nanometer-sized particles that were approximately similar in size and presumably consist of one single polymer chain.
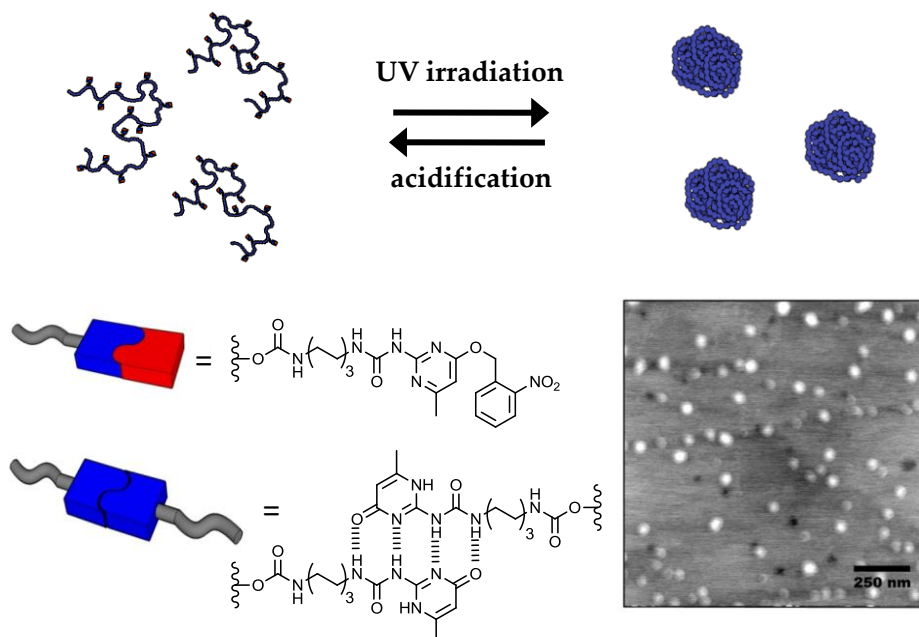
Figure 1.16 Nanoparticle fabrication; the collapse by UV irradiation and expansion on the addition of acid. AFM height image of nanoparticles (right, down).

1.8 Aim and outline

As described in this introductory chapter, the self-assembly of small and relatively simple molecules is a powerful tool to develop complex supramolecular nanostructures of defined size and shape. Supramolecular chemistry initially focused on the development of well-defined supramolecular assemblies based on small molecules. However, due to the increased knowledge of the reversible non-covalent interactions involved in these systems, also polymeric aggregates have become a research aim.

The aim of this thesis is to prepare and characterize supramolecular polymers based on benzene-1,3,5-tricarboxamides (BTAs) in order to gain a better understanding on the formation and the remarkable properties of supramolecular materials. BTAs comprising alkyl side chains form supramolecular polymers in dilute solution and in the solid state as a result of the threefold helical arrangement of the intermolecular hydrogen bonds. It is expected that the self-assembly properties of BTAs combined with traditional polymers give rise to novel supramolecular polymers. Because the chirality of monomeric BTAs can be expressed at the supramolecular level, this system allows the use of a wide range of spectroscopic techniques to study the self-assembly. As a result, valuable insights into the formation and supramolecular structure of the resulting polymers can be attained, which are crucial to further develop the field of supramolecular polymers.

Chapter 2 investigates the self-assembly of BTAs into helical aggregates when end-capped to or copolymerized with low molecular weight poly(ethylene-*co*-butylene) in solution and in the solid state. Self-assembly is evaluated with a variety of spectroscopic techniques such as CD, UV and IR. Gratifyingly, the introduction of BTAs leads to drastic improvements of the material properties, as revealed by tensile testing and oscillating shear measurements.

Chapter 3 presents a systematic study on the role of polarity on the self-assembly of BTAs in solution and on their ability to phase segregate in the solid state. In dilute solution, the polarity was varied by mixing polar and apolar solvents. In the solid state, a wide range of backbone polarities is covered by end-capping of telechelics of varying polarity with the BTA motif. In both cases, an increase of polarity leads to a significant decrease of the stability of BTA aggregates, which eventually results in the loss of nanorod formation. This study gives us a detailed understanding of the scope and limitations to use BTA based polymers in various applications.

Chapter 4 explores the use of BTA functionalized polymers as hydrogelators. BTAs equipped with aliphatic side tails are end-capped to polyethylene glycol via a short apolar spacer. In water, long entangled nanorods are formed as a result of intermolecular hydrogen bonding stabilized by hydrophobic interactions. At higher concentrations, strong and transparent gels are obtained. The supramolecular structure and the material properties of the gel are determined with CD spectroscopy and with oscillating shear measurements.

Chapter 5 introduces a supramolecular polymer system that consists of a mixture of BTAs and UPys, end-capped to monofunctional polymers. Both supramolecular motifs self-assemble in an orthogonal fashion in two separate types of phase segregated nanorods. We added an α, ω-telechelic polymer containing both the BTA and UPy motif (compatibilizer) to this system to cross-link the separate nanorods. The addition of only a small amount transforms a viscous sticky liquid into a solid material with elastomeric properties, showing the potential of orthogonal self-assembly based on hydrogen bonding motifs.

Finally, Chapter 6 investigates the ability of BTAs grafted to the side chain of polymethacrylate to form well-defined nanometer-sized objects comprising an internal helical architecture. We have been able to follow and control the folding of polymers into ordered chiral single-chain polymeric nanoparticles by making use of photolabile deprotection chemistry and with the aid of heating and cooling steps. The high stability and chiral conformation of the folded particles make them excellent candidates for compartmentalized catalytic systems.

1.9 References

[1]   H. Staudinger, *Ber. Deut. Chem. Ges.* **1920**, *53*, 1073.

[2]   L. Stryer, in *Biochemistry*, W.H. Freeman, New York, **2002**.

[3]   A. Ciferri, *Supramolecular Polymers*, New York, **2000**.

[4]   N. Zimmerman, J. S. Moore, S. C. Zimmerman, *Chem. Ind.* **1998**, 604.

[5]   L. Brunsveld, B. J. Folmer, E. W. Meijer, R. P. Sijbesma, *Chem. Rev.* **2001**, *101*, 4071.

[6]   L. Brunsveld, B. J. B. Folmer, E. W. Meijer, *MRS Bulletin* **2000**, *25*, 49.

[7]   J.-M. Lehn, *Angew. Chem., Int. Ed.* **1988**, *27*, 89.

[8]   J.-M. Lehn, *Chem. Soc. Rev.* **2007**, *36*, 151.

[9]   D. J. Cram, J. M. Cram, *Science* **1974**, *183*, 803.

[10]   D. J. Cram, *Angew. Chem., Int. Ed.* **1988**, *27*, 1009.

[11]   B. Dietrich, J. M. Lehn, J. P. Sauvage, *Tetrahedron Lett.* **1969**, *10*, 2889.

[12]   B. Dietrich, J. M. Lehn, J. P. Sauvage, J. Blanzat, *Tetrahedron* **1973**, *29*, 1629.

[13]   C. J. Pedersen, *Angew. Chem., Int. Ed.* **1988**, *27*, 1021.

[14]   C. J. Pedersen, *J. Am. Chem. Soc.* **1967**, *89*, 7017.

[15]   C. J. Pedersen, *J. Am. Chem. Soc.* **1967**, *89*, 2495.

[16]   P. Y. W. Dankers, M. C. Harmsen, L. A. Brouwer, M. J. A. van Luyn, E. W. Meijer, *Nat. Mater.* **2005**, *4*, 568.

[17]   M. Burnworth, L. Tang, J. R. Kumpfer, A. J. Duncan, F. L. Beyer, G. L. Fiore, S. J. Rowan, C. Weder, *Nature* **2011**, *472*, 334.

[18]   S. D. Bergman, F. Wudl, *J. Mater. Chem.* **2008**, *18*, 41.

[19]   S. Burattini, B. W. Greenland, D. H. Merino, W. Weng, J. Seppala, H. M. Colquhoun, W. Hayes, M. E. Mackay, I. W. Hamley, S. J. Rowan, *J. Am. Chem. Soc.* **2010**, *132*, 12051.

[20]   P. Cordier, F. Tournilhac, C. Soulié-Ziakovic, L. Leibler, *Nature* **2008**, *451*, 977.

[21]   J. D. Hartgerink, E. Beniash, S. I. Stupp, *Science* **2001**, *294*, 1684.

[22]   S. Kyle, A. Aggeli, E. Ingham, M. J. McPherson, *Biomaterials* **2010**, *31*, 9395.

[23]   D. Wu, W. Pisula, V. Enkelmann, X. Feng, K. Müllen, *J. Am. Chem. Soc.* **2009**, *131*, 9620.

[24]   Z. Chen, A. Lohr, C. R. Saha-Möller, F. Würthner, *Chem. Soc. Rev.* **2009**, *38*, 564.

[25]   J. P. Hill, W. Jin, A. Kosaka, T. Fukushima, H. Ichihara, T. Shimomura, K. Ito, T. Hashizume, N. Ishii, T. Aida, *Science* **2004**, *304*, 1481.

[26]   S. H. Gellman, *Acc. Chem. Res.* **1998**, *31*, 173.

[27]   D. H. Appella, L. A. Christianson, D. A. Klein, D. R. Powell, X. Huang, J. J. Barchi, S. H. Gellman, *Nature* **1997**, *387*, 381.

[28]   D. J. Hill, M. J. Mio, R. B. Prince, T. S. Hughes, J. S. Moore, *Chem. Rev.* **2001**, *101*, 3893.

[29]   J. Rebek, Jr., *Chem. Commun.* **2000**, 637.

[30]   D. Sievers, G. von Kiedrowski, *Nature* **1994**, *369*, 221.

[31]   S. Labeit, D. P. Barlow, M. Gautel, T. Gibson, J. Holt, C. L. Hsieh, U. Francke, K. Leonard, J. Wardale, A. Whiting, J. Trinick, *Nature* **1990**, *345*, 273.

[32]   S. Labeit, B. Kolmerer, *Science* **1995**, *270*, 293.

[33]   G. Bhat, S. Chand, S. Yakopson, *Thermochim. Acta* **2001**, *367-368*, 161.

[34]   M. Reisch, *Chem. Eng. News* **1999**, *77*, 70.

[35]   C.-A. Fustin, P. Guillet, U. S. Schubert, J.-F. Gohy, *Adv. Mater.* **2007**, *19*, 1665.

[36]   B. J. B. Folmer, R. P. Sijbesma, R. M. Versteegen, J. A. J. van der Rijt, E. W. Meijer, *Adv. Mater.* **2000**, *12*, 874.

[37]   D. J. M. van Beek, M. A. J. Gillissen, B. A. C. van As, A. R. A. Palmans, R. P. Sijbesma, *Macromolecules* **2007**, *40*, 6340.

[38]   V. G. H. Lafitte, A. E. Aliev, P. N. Horton, M. B. Hursthouse, K. Bala, P. Golding, H. C. Hailes, *J. Am. Chem. Soc.* **2006**, *128*, 6544.

[39]   J. M. J. Paulusse, R. P. Sijbesma, *Angew. Chem., Int. Ed.* **2004**, *43*, 4460.

[40]   C.-F. Chow, S. Fujii, J.-M. Lehn, *Angew. Chem., Int. Ed.* **2007**, *46*, 5007.

[41]   J. D. Fox, S. J. Rowan, *Macromolecules* **2009**, *42*, 6823.

[42]   H. M. Keizer, R. v. Kessel, R. P. Sijbesma, E. W. Meijer, *Polymer* **2003**, *44*, 5505.

[43]   W. H. Binder, S. Bernstorff, C. Kluger, L. Petraru, M. J. Kunz, *Adv. Mater.* **2005**, *17*, 2824.

[44]   W. H. Binder, M. J. Kunz, C. Kluger, G. Hayn, R. Saf, *Macromolecules* **2004**, *37*, 1749.

[45]   T. Park, S. C. Zimmerman, *J. Am. Chem. Soc.* **2006**, *128*, 13986.

[46]   T. Park, S. C. Zimmerman, *J. Am. Chem. Soc.* **2006**, *128*, 14236.

[47]   T. F. A. de Greef, M. M. J. Smulders, M. Wolffs, A. P. H. J. Schenning, R. P. Sijbesma, E. W. Meijer, *Chem. Rev.* **2009**, *109*, 5687.

[48]   R. P. Sijbesma, F. H. Beijer, L. Brunsveld, B. J. B. Folmer, J. H. K. K. Hirschberg, R. F. M. Lange, J. K. L. Lowe, E. W. Meijer, *Science* **1997**, *278*, 1601.

[49]   A. Ciferri, *J. Macromol. Sci-Pol. R.* **2003**, *C43*, 271.

[50]   F. Oosawa, *Biophys. Chem.* **1993**, *47*, 101.

[51]   L. Brunsveld, E. W. Meijer, R. B. Prince, J. S. Moore, *J. Am. Chem. Soc.* **2001**, *123*, 7978.

[52]   C. Nuckolls, T. J. Katz, G. Katz, P. J. Collings, L. Castellanos, *J. Am. Chem. Soc.* **1999**, *121*, 79.

[53]   D. Zhao, J. S. Moore, *Org. Biomol. Chem.* **2003**, *1*, 3471.

[54]   L. J. Prins, D. N. Reinhoudt, P. Timmerman, *Angew. Chem., Int. Ed.* **2001**, *40*, 2382.

[55]   G. A. Jeffrey, *An Introduction to Hydrogen Bonding*, Oxford press, New York, **1997**.

[56]   J. Emsley, *Chem. Soc. Rev.* **1980**, *9*, 91.

[57]   C. A. Hunter, *Angew. Chem., Int. Ed.* **2004**, *43*, 5310.

[58]   D. C. Sherrington, K. A. Taskinen, *Chem. Soc. Rev.* **2001**, *30*, 83.

[59]   R. P. Sijbesma, E. W. Meijer, *Chem. Commun.* **2003**, 5.

[60]   H. Zeng, H. Ickes, R. A. Flowers, B. Gong, *J. Org. Chem.* **2001**, *66*, 3574.

[61]   P. S. Corbin, S. C. Zimmerman, *J. Am. Chem. Soc.* **2000**, *122*, 3779.

[62]   W. L. Jorgensen, J. Pranata, *J. Am. Chem. Soc.* **1990**, *112*, 2008.

[63]   J. Pranata, S. G. Wierschke, W. L. Jorgensen, *J. Am. Chem. Soc.* **1991**, *113*, 2810.

[64]   T. J. Murray, S. C. Zimmerman, *J. Am. Chem. Soc.* **1992**, *114*, 4010.

[65]   J. Sartorius, H.-J. Schnneider, *Chem. Eur. J.* **1996**, *2*, 1446.

[66]   B. A. Blight, C. A. Hunter, D. A. Leigh, H. McNab, P. I. T. Thomson, *Nat. Chem.* **2011**, *3*, 244.

[67]   F. H. Beijer, H. Kooijman, A. L. Spek, R. P. Sijbesma, E. W. Meijer, *Angew. Chem., Int. Ed.* **1998**, *37*, 75.

[68]   F. H. Beijer, R. P. Sijbesma, H. Kooijman, A. L. Spek, E. W. Meijer, *J. Am. Chem. Soc.* **1998**, *120*, 6761.

[69]   S. H. M. Söntjens, R. P. Sijbesma, M. H. P. van Genderen, E. W. Meijer, *J. Am. Chem. Soc.* **2000**, *122*, 7487.

[70]   T. F. A. Greef, G. Ercolani, G. B. W. L. Ligthart, E. W. Meijer, R. P. Sijbesma, *J. Am. Chem. Soc.* **2008**, *130*, 13755.

[71]   P. S. Corbin, S. C. Zimmerman, *J. Am. Chem. Soc.* **1998**, *120*, 9710.

[72]   C. Fouquey, J.-M. Lehn, A.-M. Levelut, *Adv. Mater.* **1990**, *2*, 254.

[73]   J. M. Lehn, *Makromol. Chem., Macromol. Symp.* **1993**, *69*, 1.

[74]   U. Kumar, T. Kato, J. M. J. Frechet, *J. Am. Chem. Soc.* **1992**, *114*, 6630.

[75]   T. Kato, H. Kihara, U. Kumar, T. Uryu, J. M. J. Fréchet, *Angew. Chem., Int. Ed.* **1994**, *33*, 1644.

[76]   M. Lee, B.-K. Cho, Y.-S. Kang, W.-C. Zin, *Macromolecules* **1999**, *32*, 8531.

[77]   G. Ungar, Y. Liu, X. Zeng, V. Percec, W.-D. Cho, *Science* **2003**, *299*.

[78]   C. B. St.Pourcain, A. C. Griffin, *Macromolecules* **1995**, *28*, 4116.

[79]   V. Percec, C.-H. Ahn, T. K. Bera, G. Ungar, D. J. P. Yeardley, *Chem. Eur. J.* **1999**, *5*, 1070.

[80]   H. Kihara, T. Kato, T. Uryu, J. M. J. Fréchet, *Chem. Mater.* **1996**, *8*, 961.

[81]   C. P. Lillya, R. J. Baker, S. Hutte, H. H. Winter, Y. G. Lin, J. Shi, L. C. Dickinson, J. C. W. Chien, *Macromolecules* **1992**, *25*, 2076.

[82]   S. Abed, S. Boileau, L. Bouteiller, *Macromolecules* **2000**, *33*, 8479.

[83]   S. Sivakova, D. A. Bohnsack, M. E. Mackay, P. Suwanmala, S. J. Rowan, *J. Am. Chem. Soc.* **2005**, *127*, 18202.

[84]   H. Kautz, D. J. M. van Beek, R. P. Sijbesma, E. W. Meijer, *Macromolecules* **2006**, *39*, 4265.

[85]   J. B. Beck, J. M. Ineman, S. J. Rowan, *Macromolecules* **2005**, *38*, 5060.

[86]   D. Duweltz, F. Lauprêtre, S. Abed, L. Bouteiller, S. Boileau, *Polymer* **2003**, *44*, 2295.

[87]   O. Colombani, C. Barioz, L. Bouteiller, C. Chaneac, L. Fomperie, F. Lortie, H. Montes, *Macromolecules* **2005**, *38*, 1752.

[88]   A. J. Kirby, *Adv. Phys. Org. Chem.* **1980**, *17*, 183.

[89]   C. Hilger, R. Stadler, *Macromolecules* **1990**, *23*, 2095.

[90]   C. Hilger, R. Stadler, F. De Lucca, L. Liane, *Polymer* **1990**, *31*, 818.

[91]   C. Hilger, R. Stadler, *Macromolecules* **1992**, *25*, 6670.

[92]   L. Brunsveld, B. G. G. Lohmeijer, J. A. J. M. Vekemans, E. W. Meijer, *Chem. Commun.* **2000**, 2305.

[93]   E. Obert, M. Bellot, L. Bouteiller, F. Andrioletti, C. Lehen-Ferrenbach, F. Boue, *J. Am. Chem. Soc.* **2007**, *129*, 15601.

[94]   K. J. C. van Bommel, C. van der Pol, I. Muizebelt, A. Friggeri, A. Heeres, A. Meetsma, B. L. Feringa, J. van Esch, *Angew. Chem., Int. Ed.* **2004**, *43*, 1663.

[95]   I. Yoshikawa, J. Sawayama, K. Araki, *Angew. Chem., Int. Ed.* **2008**, *47*, 1038.

[96]   M. Merschky, M. Wyszogrodzka, R. Haag, C. Schmuck, *Chem. Eur. J.* **2010**, *16*, 14242.

[97]   E. Wisse, R. A. E. Renken, J. R. Roosma, A. R. A. Palmans, E. W. Meijer, *Biomacromolecules* **2007**, *8*, 2739.

[98]   P. Y. W. Dankers, J. M. Boomker, A. Huizinga-van der Vlag, E. Wisse, W. P. J. Appel, F. M. M. Smedts, M. C. Harmsen, A. W. Bosman, W. Meijer, M. J. A. van Luyn, *Biomaterials* **2011**, *32*, 723.

[99]   J.-L. Wietor, A. Dimopoulos, L. E. Govaert, R. A. T. M. van Benthem, G. de With, R. P. Sijbesma, *Macromolecules* **2009**, *42*, 6640.

[100]   A. W. Bosman, R. P. Sijbesma, E. W. Meijer, *Mater. Today* **2004**, *7*, 34.

[101]   A R. Hirst, B. Escuder, J F. Miravet, D K. Smith, *Angew. Chem., Int. Ed.* **2008**, *47*, 8002.

[102]   F. van de Manakker, L. M. J. Kroon-Batenburg, T. Vermonden, C. F. van Nostrum, W. E. Hennink, *Soft Matter* **2010**, *6*, 187.

[103]   N. E. Botterhuis, K. Sivasubramanian, D. Veldman, S. C. J. Meskers, R. P. Sijbesma, *Chem. Commun.* **2008**, 3915

[104]   L. Bouteiller, O. Colombani, F. Lortie, P. Terech, *J. Am. Chem. Soc.* **2005**, *127*, 8893.

[105]   B. D. Mather, M. B. Baker, F. L. Beyer, M. A. G. Berg, M. D. Green, T. E. Long, *Macromolecules* **2007**, *40*, 6834.

[106]   J. H. Hirschberg, L. Brunsveld, A. Ramzi, J. A. Vekemans, R. P. Sijbesma, E. W. Meijer, *Nature* **2000**, *407*, 167.

[107]   R. M. Versteegen, R. P. Sijbesma, E. W. Meijer, *Macromolecules* **2005**, *38*, 3176.

[108]   R. M. Versteegen, R. Kleppinger, R. P. Sijbesma, E. W. Meijer, *Macromolecules* **2006**, *39*, 772.

[109]   R. J. Thibault, P. J. Hotchkiss, M. Gray, V. M. Rotello, *J. Am. Chem. Soc.* **2003**, *125*, 11249.

[110]   G. Cooke, V. M. Rotello, *Chem. Soc. Rev.* **2002**, *31*, 275.

[111]   J. M. Pollino, M. Weck, *Chem. Soc. Rev.* **2005**, *34*, 193.

[112]   K. P. Nair, V. Breedveld, M. Weck, *Macromolecules* **2008**, *41*, 3429.

[113]   C. R. South, C. Burd, M. Weck, *Acc. Chem. Res.* **2007**, *40*, 63.

[114]   W. H. Binder, R. Zirbs, *Adv. Pol. Sci.* **2007**, *207*, 1.

[115]   T. Park, S. C. Zimmerman, *J. Am. Chem. Soc.* **2006**, *128*, 11582.

[116]   L. R. Rieth, R. F. Eaton, G. W. Coates, *Angew. Chem., Int. Ed.* **2001**, *40*, 2153.

[117]   C. L. Elkins, T. Park, M. G. McKee, T. E. Long, *J. Polym. Sci. Part A: Polym. Chem.* **2005**, *43*, 4618.

[118]   K. Hanabusa, A. Kawamaki, M. Kimura, H. Shirai, *Chem. Lett.* **1997**, 191.

[119]   Y. Yasuda, Y. Takebe, M. Fukumoto, H. Inada, Y. Shirota, *Adv. Mater.* **1996**, *8*, 740.

[120]   I. YiIgör, A. K. Sha'aban, W. P. Steckle Jr, D. Tyagi, G. L. Wilkes, J. E. McGrath, *Polymer* **1984**, *25*, 1800.

[121]   O. Colombani, L. Bouteiller, *New J. Chem.* **2004**, *28*, 1373.

[122]   J. Ruokolainen, R. Makinen, M. Torkkeli, T. Makela, R. Serimaa, G. Ten Brinke, O. Ikkala, *Science* **1998**, *280*, 557.

[123]   A. K. Boal, F. Ilhan, J. E. DeRouchey, T. Thurn-Albrecht, T. P. Russell, V. M. Rotello, *Nature* **2000**, *404*, 746.

[124]   R. J. Thibault, T. H. Galow, E. J. Turnberg, M. Gray, P. J. Hotchkiss, V. M. Rotello, *J. Am. Chem. Soc.* **2002**, *124*, 15249.

[125]   R. Deans, F. Ilhan, V. M. Rotello, *Macromolecules* **1999**, *32*, 4956.

[126]   J. M. Pollino, M. Weck, *Chem. Soc. Rev.* **2005**, *34*, 193.

[127]   C. Burd, M. Weck, *Macromolecules* **2005**, *38*, 7225.

[128]   J. M. Pollino, L. P. Stubbs, M. Weck, *J. Am. Chem. Soc.* **2003**, *126*, 563.

[129]   K. P. Nair, V. Breedveld, M. Weck, *Macromolecules* **2011**, *44*, 3346.

[130]   J. Wu, W. Pisula, K. Müllen, *Chem. Rev.* **2007**, *107*, 718.

[131]   T. Haino, M. Tanaka, Y. Fukazawa, *Chem. Commun.* **2008**, 468.

[132]   M. Peterca, V. Percec, M. R. Imam, P. Leowanawat, K. Morimitsu, P. A. Heiney, *J. Am. Chem. Soc.* **2008**, *130*, 14840.

[133]   R. F. Pasternack, P. R. Huber, P. Boyd, G. Engasser, L. Francesconi, E. Gibbs, P. Fasella, G. Cerio Venturo, L. d. Hinds, *J. Am. Chem. Soc.* **1972**, *94*, 4511.

[134]   D. Demus, *Vol. VI* (Eds.: D. Demus, J. Goodby, G. W. Gray, H. W. Spiess, V. Vill), Wiley-VCH, Weinheim, **1998**, pp. 146.

[135]   K. Hanabusa, C. Koto, M. Kimura, H. Shirai, A. Kakehi, *Chem. Lett.* **1997**, 429.

[136]   A. Sakamoto, D. Ogata, T. Shikata, K. Hanabusa, *Macromolecules* **2005**, *38*, 8983.

[137] E. Fan, J. Yang, S. J. Geib, T. C. Stoner, M. D. Hopkins, A. D. Hamilton, *Chem. Commun.* **1995**, 1251.

[138] J. Boekhoven, A. M. Brizard, P. van Rijn, M. C. A. Stuart, R. Eelkema, J. H. van Esch, *Angew. Chem., Int. Ed.* **2011**, DOI: 10.1002/anie.201102364.

[139] J. Boekhoven, P. van Rijn, A. M. Brizard, M. C. A. Stuart, J. H. van Esch, *Chem. Commun.* **2010**, *46*, 3490.

[140] K. J. C. Van Bommel, M. C. A. Stuart, B. L. Feringa, J. Van Esch, *Org. Biomol. Chem.* **2005**, *3*, 2917.

[141] Y. Matsunaga, Y. Nakayasu, S. Sakai, M. Yonenaga, *Mol. Cryst. Liq. Cryst.* **1986**, *141*, 327.

[142] Y. Matsunaga, N. Miyajima, Y. Nakayasu, S. Sakai, M. Yonenaga, *Bull. Chem. Soc. Jpn.* **1988**, *61*, 207.

[143] L. Brunsveld, A. P. H. J. Schenning, M. A. C. Broeren, H. M. Janssen, J. A. J. M. Vekemans, E. W. Meijer, *Chem. Lett.* **2000**, 292.

[144] M. M. J. Smulders, A. P. H. J. Schenning, E. W. Meijer, *J. Am. Chem. Soc.* **2008**, *130*, 606.

[145] M. P. Lightfoot, F. S. Mair, R. G. Pritchard, J. E. Warren, *Chem. Commun.* **1999**, 1945.

[146] T. Shikata, D. Ogata, K. Hanabusa, *J. Phys. Chem. B* **2004**, *108*, 508.

[147] T. Shikata, Y. Kuruma, A. Sakamoto, K. Hanabusa, *J. Phys. Chem. B* **2008**, *112*, 16393.

[148] P. J. M. Stals, J. F. Haveman, R. Martín-Rapún, C. F. C. Fitié, A. R. A. Palmans, E. W. Meijer, *J. Mater. Chem.* **2009**, *19*, 124.

[149] P. Jonkheijm, P. van der Schoot, A. P. H. J. Schenning, E. W. Meijer, *Science* **2006**, *313*, 80.

[150] P. J. M. Stals, M. M. J. Smulders, R. Martín-Rapún, A. R. A. Palmans, E. W. Meijer, *Chem. Eur. J.* **2009**, *15*, 2071.

[151] T. F. A. de Greef, M. M. L. Nieuwenhuizen, P. J. M. Stals, C. F. C. Fitié, A. R. A. Palmans, R. P. Sijbesma, E. W. Meijer, *Chem. Commun.* **2008**, 4306.

[152] S. I. Stupp, V. LeBonheur, K. Walker, L. S. Li, K. E. Huggins, M. Keser, A. Amstutz, *Science* **1997**, *276*, 384.

[153] H. Dong, S. E. Paramonov, L. Aulisa, E. L. Bakota, J. D. Hartgerink, *J. Am. Chem. Soc.* **2007**, *129*, 12468.

[154] M. C. O'Sullivan, J. K. Sprafke, D. V. Kondratuk, C. Rinfray, T. D. W. Claridge, A. Saywell, M. O. Blunt, J. N. O'Shea, P. H. Beton, M. Malfois, H. L. Anderson, *Nature* **2011**, *469*, 72.

[155] P. G. A. Janssen, J. Vandenbergh, J. L. J. van Dongen, E. W. Meijer, A. P. H. J. Schenning, *J. Am. Chem. Soc.* **2007**, *129*, 6078.

[156] S. R. Bull, L. C. Palmer, N. J. Fry, M. A. Greenfield, B. W. Messmore, T. J. Meade, S. I. Stupp, *J. Am. Chem. Soc.* **2008**, *130*, 2742.

[157] F. Lortie, S. Boileau, L. Bouteiller, C. Chassenieux, F. Lauprêtre, *Macromolecules* **2005**, *38*, 5283.

[158] M. M. J. Smulders, M. M. L. Nieuwenhuizen, M. Grossman, I. A. W. Filot, C. C. Lee, T. F. A. de Greef, A. P. H. J. Schenning, A. R. A. Palmans, E. W. Meijer, *Macromolecules* **2011**, *44*, 6581.

[159] J. Lidmar, L. Mirny, D. R. Nelson, *Phys. Rev. E* **2003**, *68*, 051910.

[160] V. Percec, C. H. Ahn, G. Ungar, D. J. P. Yeardley, M. Moller, S. S. Sheiko, *Nature* **1998**, *391*, 161.

[161] P. Besenius, G. Portale, P. H. H. Bomans, H. M. Janssen, A. R. A. Palmans, E. W. Meijer, *Proc. Natl. Acad. Sci. USA* **2010**, *107*, 17888.

[162] J.-D. van Loon, R. G. Janssen, W. Verboom, D. N. Reinhoudt, *Tetrahedron Lett.* **1992**, *33*, 5125.

[163] R. H. Vreekamp, J. P. M. van Duynhoven, M. Hubert, W. Verboom, D. N. Reinhoudt, *Angew. Chem., Int. Ed.* **1996**, *35*, 1215.

[164] C. Jaime, J. De Mendoza, P. Prados, P. M. Nieto, C. Sanchez, *J. Org. Chem.* **1991**, *56*, 3372.

[165] S. Shinkai, *Tetrahedron* **1993**, *49*, 8933.

[166] K. D. Shimizu, J. Rebek Jr., *P. Natl. Acad. Sci. USA* **1995**, *92*, 12403.

[167] F. Hof, S. L. Craig, C. Nuckolls, J. J. Rebek, *Angew. Chem., Int. Ed.* **2002**, *41*, 1488.

[168] R. S. Meissner, J. Rebek, J. de Mendoza, *Science* **1995**, *270*, 1485.

[169] R. Wyler, J. de Mendoza, J. Rebek, *Angew. Chem., Int. Ed.* **1993**, *32*, 1699.

[170] E. Huerta, G. A. Metselaar, A. Fragoso, E. Santos, C. Bo, J. de Mendoza, *Angew. Chem., Int. Ed.* **2007**, *46*, 202.

[171] E. Huerta, E. Cequier, J. de Mendoza, *Chem. Commun.* **2007**, 5016.

[172] J. de Mendoza, E. M. Huerta, G. Metselaar, **2008**, patent US20080025904A1.

[173] C. J. Gabriel, J. R. Parquette, *J. Am. Chem. Soc.* **2006**, *128*, 13708.

[174] A. L. Hofacker, J. R. Parquette, *Angew. Chem., Int. Ed.* **2005**, *44*, 1053.

[175] J. F. Yu, T. V. RajanBabu, J. R. Parquette, *J. Am. Chem. Soc.* **2008**, *130*, 7845.

[176] J. C. Nelson, J. G. Saven, J. S. Moore, P. G. Wolynes, *Science* **1997**, *277*, 1793.

[177] D. H. Appella, L. A. Christianson, I. L. Karle, D. R. Powell, S. H. Gellman, *J. Am. Chem. Soc.* **1996**, *118*, 13071.

[178] D. Seebach, M. Overhand, F. N. M. Kühnle, B. Martinoni, L. Oberer, U. Hommel, H. Widmer, *Helv. Chim. Acta* **1996**, *79*, 913.

[179] D. Seebach, P. E. Ciceri, M. Overhand, B. Jaun, D. Rigo, L. Oberer, U. Hommel, R. Amstutz, H. Widmer, *Helv. Chim. Acta* **1996**, *79*, 2043.

[180] R. W. Sinkeldam, M. H. C. J. van Houtem, K. Pieterse, J. A. J. M. Vekemans, E. W. Meijer, *Chem. Eur. J.* **2006**, *12*, 6129.

[181] R. W. Sinkeldam, M. H. C. J. van Houtem, G. Koeckelberghs, J. A. J. M. Vekemans, E. W. Meijer, *Org. Lett.* **2006**, *8*, 383.

[182] Y. Hamuro, S. J. Geib, A. D. Hamilton, *Angew. Chem., Int. Ed.* **1994**, *33*, 446.

[183] Y. Hamuro, S. J. Geib, A. D. Hamilton, *J. Am. Chem. Soc.* **1997**, *119*, 10587.

[184] A. E. Cherian, F. C. Sun, S. S. Sheiko, G. W. Coates, *J. Am. Chem. Soc.* **2007**, *129*, 11350.

[185] J. B. Beck, K. L. Killops, T. Kang, K. Sivanandan, A. Bayles, M. E. Mackay, K. L. Wooley, C. J. Hawker, *Macromolecules* **2009**, *42*, 5629.

[186] E. Harth, B. Van Horn, V. Y. Lee, D. S. Germack, C. P. Gonzales, R. D. Miller, C. J. Hawker, *J. Am. Chem. Soc.* **2002**, *124*, 8653.

[187] T. A. Croce, S. K. Hamilton, M. L. Chen, H. Muchalski, E. Harth, *Macromolecules* **2007**, *40*, 6028.

[188] C. T. Adkins, H. Muchalski, E. Harth, *Macromolecules* **2009**, *42*, 5786.

[189] E. B. Berda, E. J. Foster, E. W. Meijer, *Macromolecules* **2010**, *43*, 1430.

[190] E. J. Foster, E. B. Berda, E. W. Meijer, *J. Am. Chem. Soc.* **2009**, *131*, 6964.

[191] E. J. Foster, E. B. Berda, E. W. Meijer, *J. Polym. Sci. Part A: Polym. Chem.* **2011**, *49*, 118.

[192] M. Seo, B. J. Beck, J. M. J. Paulusse, C. J. Hawker, S. Y. Kim, *Macromolecules* **2008**, *41*, 6413.

2

Supramolecular materials from benzene-1,3,5-tricarboxamide-based nanorods

Abstract. Benzene-1,3,5-tricarboxamides (BTAs) comprising alkyl side chains form supramolecular polymers in dilute solution and in the solid state as a result of the threefold helical arrangement of the intermolecular hydrogen bonds. In this chapter, the self-assembly properties of BTAs, with one or more low molecular weight telechelic poly(ethylene-*co*-butylene) (pEB) covalently attached, are investigated. We have observed a pronounced tendency to form helical aggregates in the dilute condition and in the solid state. However, in dilute conditions, the association constant of BTAs is reduced with increasing number of pEB side chains, due to steric crowding of pEB. The functionalization of telechelic pEB (end-capped or copolymerized) with the BTA moiety leads to the formation of supramolecular materials. The intrinsic phase segregation of BTA nanorods with the amorphous pEB, which is visualized with atomic force microscopy, results in thermoplastic elastomeric behavior. Polarized optical microscopy, differential scanning calorimetry, variable temperature infrared spectroscopy and X-ray scattering techniques confirm the presence of aggregated BTAs embedded in the pEB matrix.

2.1 Introduction

The field of supramolecular polymeric materials has grown rapidly over the last decade[1-9] It has passed the stage of scientific curiosity to become industrially relevant.[10] The potential of supramolecular polymers arises from their tunable thermal and mechanical properties, combined with a highly dynamic and reversible character.[11-14] This facilitates processing and gives rise to new and unique material properties with applications envisioned in biomaterials,[15-17] self-healing materials,[10, 18-23] hydrogels[24-27] and optoelectronic devices.[28-30] Under suitable conditions, these supramolecular polymers display macroscopic material properties comparable to high molecular weight macromolecules. The non-covalent interactions that are responsible for the reversible bonds can be based on hydrogen bonding, $\pi-\pi$ interactions, dipole interactions, metal-ligand complexation, hydrophobic or solvophobic interactions and combinations thereof. A particularly interesting class of supramolecular polymers is that of polymer chains based on low molar mass monomers end-capped with multiple hydrogen bonding units.[12, 31-40] Besides the strength of the hydrogen bonding, also the propensity to phase segregate was found to be important for the polymer properties as convincingly shown by Stadler and Rowan.[8, 41-44] This phase segregation results in strong multiple physical cross-linking points in two or three dimensions within the soft polymer matrix. These cross-links eventually result in thermoplastic elastomeric properties.

In the past, our group has successfully employed the quadruple hydrogen bonding ureidopyrimidinone (UPy) unit to prepare supramolecular thermoplastic elastomers. It was observed that thermoplastic elastomeric properties were only obtained when, next to the dimerization of the UPys by hydrogen bonding, additional lateral interactions were present. The latter ensured the formation of columnar structures resulting in phase segregation between the hard rods and the soft polymer.[13, 45] We here propose the benzene-1,3,5-tricarboxamide (BTA) motif for supramolecular materials based on phase segregated nanorods in a polymer matrix. The BTA motif has successfully been employed in thermotropic liquid crystals, in organogelators, as a nucleating agent for *iso*-tactic polypropylene and also as MRI contrast agents.[46-54] BTA motifs form a one dimensional supramolecular polymer in solution and in the solid state, as a result of the threefold α-helix type arrangement of the intermolecular hydrogen bonds.[55-58] Circular dichroism (CD) spectroscopy revealed that the introduction of chiral side chains results in columnar structures with a preferred helicity.[57] Since the lateral interactions in BTAs suffice to form a columnar structure, we anticipate that end capping or copolymerizing low molecular weight telechelic polymers with BTAs results in supramolecular thermoplastic elastomeric materials. With the BTA motif inducing physical cross-linking via the formation of nanorods, elastomeric properties can be expected in these supramolecular materials. A schematic

representation of phase segregated BTA nanorods embedded in a soft polymeric matrix is given in Figure 2.1.
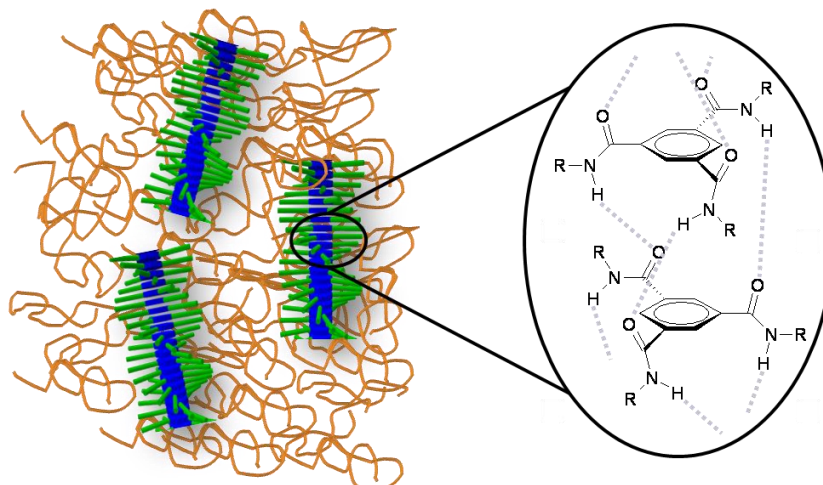
Figure 2.1 Schematic representation of BTA nanorods embedded in a polymer matrix.

2.2 Synthesis

We synthesized various bifunctional and monofunctional low molecular weight polymer backbones bearing BTAs, end capped to or in the main chain of the polymer. As the soft polymer matrix, we selected the apolar and amorphous, easily accessible amine-functional telechelic poly(ethylene-*co*-butylene) (pEB) and mono functional amino pEB with molecular weights of ~3500 g/mol. PEB is a copolymer made by the hydrogenation of polybutadiene. The ratio of ethylene/butylene in pEB depends on the number of the 1,2 and 1,4 additions during the polymerization of butadiene. The ratio of ethylene/butylene is 45/55, which was determined with ^{1}H-NMR. These telechelic polymers were subsequently coupled to, or copolymerized with, various BTA precursors affording compounds **1**-**4** (Scheme 2.1). All compounds were obtained in high purity as evidenced with NMR and GPC. As a reference compound, the chiral disc-shaped BTA **5** bearing three *R*-3,7-dimethyloctyl side chains was selected.

Scheme 2.1 Overview of the BTA functionalized polymers **1**-**4** and BTA **5**.
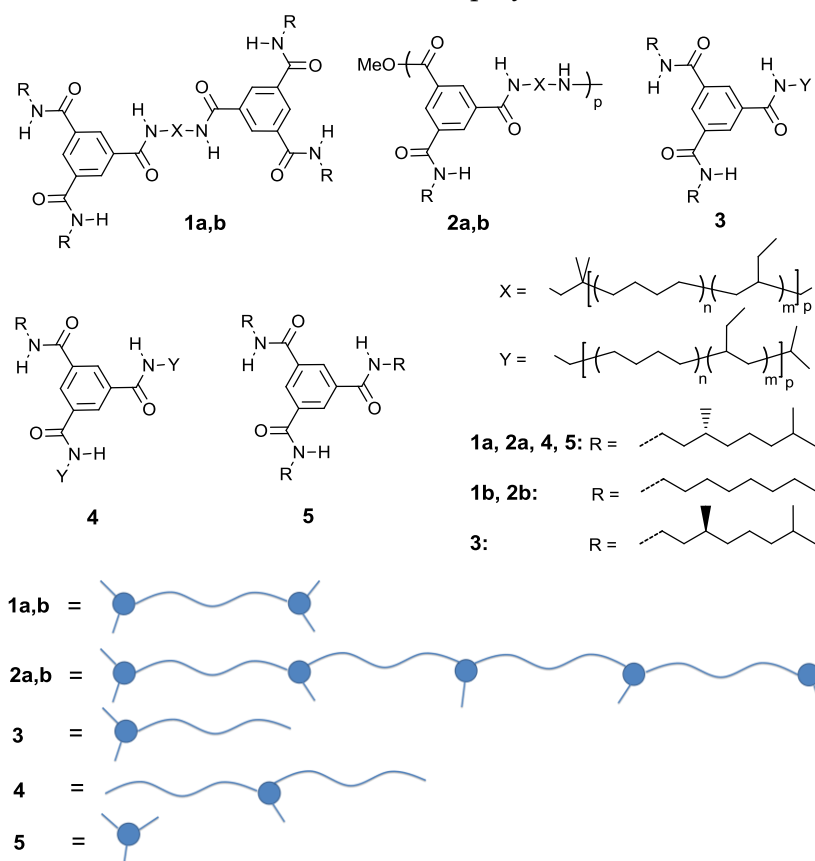
Table 2.1 Summary of NMR, GPC and DSC data of compounds **1**-**5**.

Compound	Configuration	M_n^a	M_n^b	PDI^b	T_g^c	T_m^c	ΔH^c	ΔH^c
		[kg/mol]	[kg/mol]	[-]	[°C]	[°C]	[J/g]	[kJ/mol]
1a	R	4.47	6.23	1.08	-60	205	2.63	11.76
1b	-	4.36	6.72	1.08	-60	205	2.79	12.16
2a	R	20.0	32.7	1.7	-59	185	1.87	7.14
2b	-	17.9	27.7	1.7	-59	185	2.12	8.16
3	S	4.00	7.6	1.05	-60	192	4.09	16.36
4	R	7.35	13.5	1.10	-60	157	1.17	8.60
5	R	0.63	n.a.	1.0	n.d.	119/236	25.5/33.4	16/21

n.a. = not applicable, n.d. = not determined. [a] Theoretical molecular weight. [b] Determined by GPC in chloroform. [c] Derived from the third heating run (40 K min⁻¹).

Scheme 2.2 Synthesis of compounds **1a,b**.
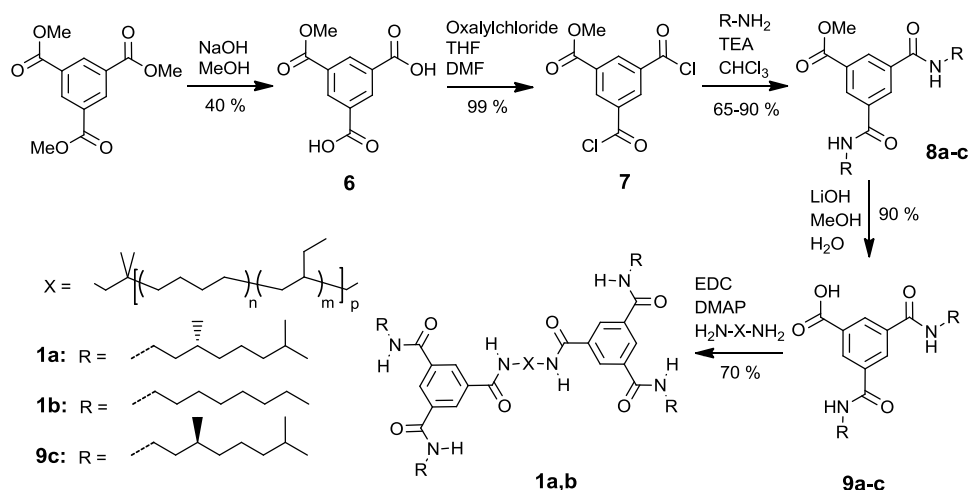
Trimethyl benzene-1,3,5-tricarboxylate was partially hydrolyzed to the dicarboxylic acid monomethyl carboxylate (**6**) using sodium hydroxide. Compound **6** was converted to the corresponding acid chloride (**7**), which was subsequently coupled to the chiral and achiral amines yielding the dicarboxamide monomethyl carboxylates (**8a-c**). The methyl carboxylates were hydrolyzed at room temperature yielding the BTA precursors **9a-c**. In the final step, the precursors were coupled to diamino-functional telechelic pEB yielding the dumbbell shaped polymers (**1a,b**). The low overall yield of ~20% was mainly the result of the poor yield of the hydrolysis of trimethyl benzene-1,3,5-tricarboxylate.

Scheme 2.3 Synthesis of compounds **2a,b**.
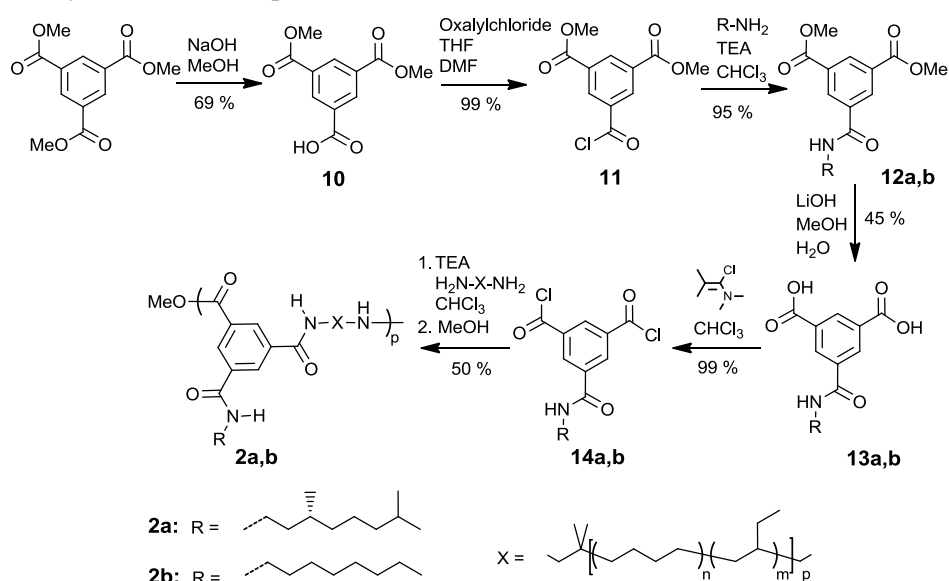
Copolymers **2a,b** were synthesized in an almost identical approach as was used for the synthesis of compounds **1a,b**. Trimethyl benzene-1,3,5-tricarboxylate was partially

hydrolyzed to the monocarboxylic acid dimethyl carboxylate (**10**) using sodium hydroxide. Compound **10** was converted in the corresponding acid chloride (**11**), which was subsequently coupled to the chiral and achiral amines yielding the monocarboxamide dimethyl carboxylates (**12a,b**). The dimethyl carboxylates were hydrolyzed at room temperature yielding the BTA precursors **13a,b**. In the final step, the precursors were polymerized with diamino-functional telechelic pEB yielding the copolymers (**2a,b**). Polymers **2a,b** were purified by precipitation in methanol, which leads to the formation of methyl ester end-groups. The copolymers demonstrated molecular masses in the range of 27-33 kg/mol corresponding to degrees of polymerizations of around 5 (Table 2.1). This leads to an average methylester/amide substitution of 1/7 that could influence the stability of BTA aggregates.

Scheme 2.4 Synthesis of compound **3** (A) and **4** (B).
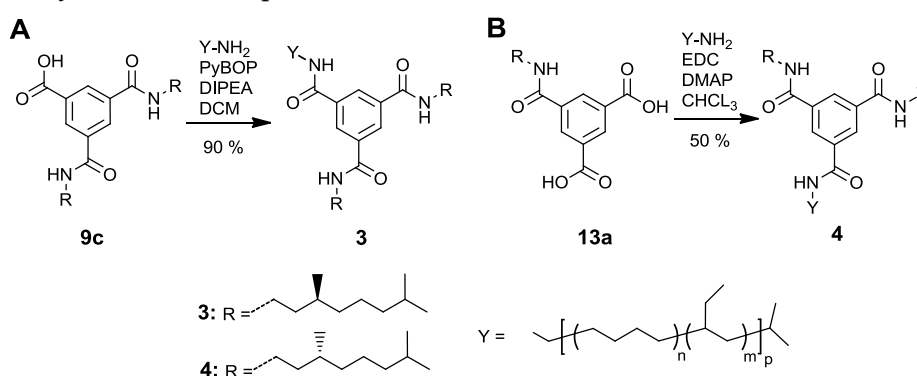
Finally, compound **3** was synthesized by a PyBOP coupling of precursor **9c** to mono amino functionalized pEB. Compound **4** was synthesized by a coupling of the diacid carboxylic acid BTA precursor (**13a**) with mono amino functionalized pEB using EDC and DMAP.

2.3 Self-assembly in dilute solution

Aggregates of BTA (**5**) in alkane solvents are characterized by a λ_{max} of 192 nm in ultraviolet (UV) spectroscopy and a Cotton effect at 223 nm with a molar ellipticity ($\Delta\varepsilon$) of $|\Delta\varepsilon|$ = 43 L/mol cm.[57] In acetonitrile, a red shift in UV to 208 nm with a corresponding disappearance of the Cotton effect was attributed to the loss of intermolecular hydrogen bonds. Temperature-dependent CD and UV measurements showed that BTAs self-assemble in a cooperative fashion and follow a nucleation-elongation growth mechanism. The transition from the molecularly dissolved state to the aggregated state, indicated by the temperature of elongation T_e, is abrupt and highly concentration dependent.[57, 59] While the mechanistic aspects of the self-assembly behavior of single BTAs have been studied in great detail, the self-assembly of BTAs connected to a polymer backbone is unexplored. Therefore, we

studied the self-assembly of **1a**, **3**, **4** with circular dichroism (CD) spectroscopy in dilute conditions in apolar solvents.

We selected dodecane as the solvent of choice because of its capability to stabilize hydrogen bonds. Copolymer **2a** could not be measured in dodecane solutions as a result of its poor solubility. CD spectroscopy measurements were performed on solutions of **1a**, **3**, **4** (**1a**: c_{BTA} = 8 x 10^{-6} M, l = 1 cm; **3** and **4**: c_{BTA} = 4.8 x 10^{-4} M, l = 1 mm) at 20 °C and the results were compared to those of compound **5**.
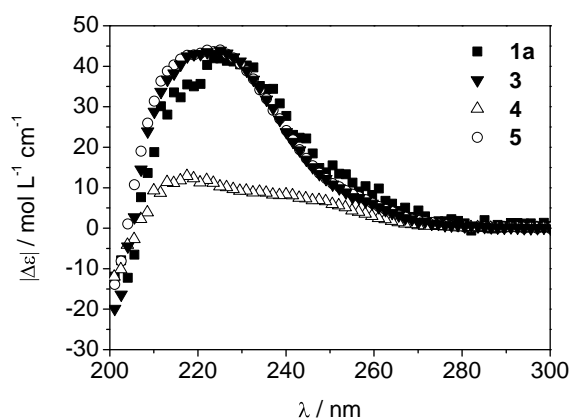
Figure 2.2 CD spectra of **1a**, **3**, **4** and **5** at 20 °C (**1a**: c_{BTA} = 8 x 10^{-6} M in dodecane, l = 1 cm; **3** and **4**: c_{BTA} = 4.8 x 10^{-4} M in dodecane, l = 1 mm and **5**: c_{BTA} = 1.4 x 10^{-5} M in heptane).

All polymers show a Cotton effect at 20 °C indicative for the presence of BTAs aggregated in a helical fashion (Figure 2.2). The $\Delta\varepsilon$ at 223 nm for **1a**, **3** and **4** is 41, -42, and 12 L/mol cm, respectively. The sign of the Cotton effect is in agreement with the configuration of the methyl group on the side chain. Polymer **4** shows a small difference in the shape of the Cotton effect compared to that of BTA **5**. This probably originates from a small difference in packing due to a different angle of the amide bonds with respect to the benzene core.[60] The $\Delta\varepsilon$ of **4**, which contains two pEB side chains and one *R*-3,7-dimethyloctyl side chain, is 3.5 times lower than the other compounds.
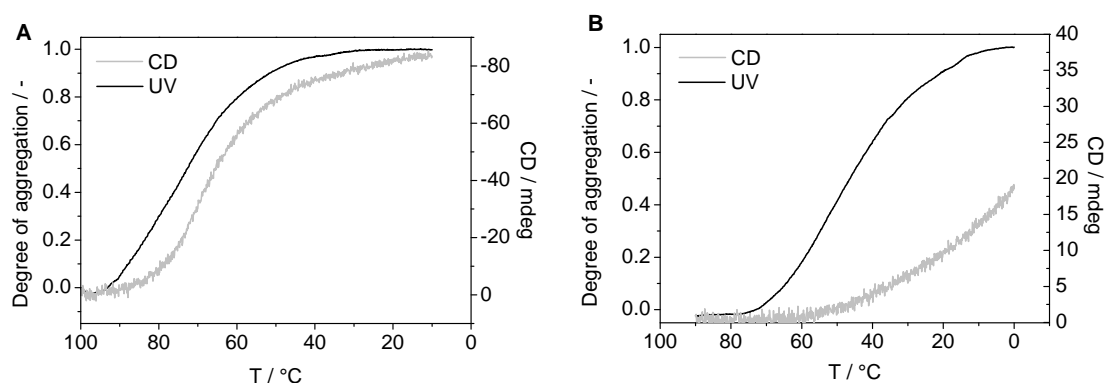
Figure 2.3 CD and degree of aggregation (based on UV absorption) versus temperature of **3** (A) and **4** (B) (λ = 223 nm, c_{BTA} = 4.8 x 10^{-4} M in dodecane, cooling rate = 1 K min^{-1}, l = 1 mm).

To investigate the origin of the small $\Delta\varepsilon$ in **4**, we performed temperature-dependent CD and UV spectroscopy (Figure 2.3). Compounds **3** and **4** were dissolved in dodecane (c_{BTA} = 4.8 x 10^{-4} M, l = 1 mm) and heated to 90-95 °C. At this temperature, compounds **3** and **4** showed no Cotton effect and the λ_{max} was 208 nm indicating that they are molecularly dissolved. Subsequently, the solutions were slowly cooled (1 K min^{-1}) to 0-10 °C. We followed the Cotton effect and UV absorption at λ = 223 nm upon cooling. The degree of aggregation was derived from the UV data by assuming a molecularly dissolved state at high temperatures and a fully aggregated state at low temperatures. Quantitative data on the self-assembly process were obtained by fitting the temperature-dependent UV data to a nucleation-elongation model developed by van der Schoot:[57, 59]

$$UV(T) = UV_{SAT}\left[1 - \exp\left(\frac{-h_e}{RT_e^2}(T - T_e)\right)\right] \tag{2.1}$$

where UV_{SAT} is the maximal UV intensity at low temperature and corresponds to fully aggregated state, h_e is the enthalpy release upon elongation, T_e is the elongation temperature, T is the temperature and R is gas constant. The temperature-dependent UV data were then normalized by dividing the UV value by UV_{SAT}, yielding $\phi = UV(T) / UV_{SAT}$ as the dimensionless y-axis. According to UV, the aggregation of compounds **3** and **4** is cooperative as illustrated by a sudden change in UV. The T_e for **3** and **4** was 95 and 75 °C, respectively. The enthalpy change upon elongation h_e, for **3** and **4** is -66 and -39 kJ/mol. The corresponding association constant, K_E, for **3** and **4** is derived using an equilibrium model recently developed by Markvoort *et al.* and is 2 x 10^5 and 1.5 x 10^4 M^{-1}, respectively.[61]

The appearance of a Cotton effect for **3** and **4** started at 87 and 60 °C, respectively. The difference between the change in UV and the appearance of a Cotton effect clearly shows that the chirality in BTA aggregates is not expressed in the same way as in the aggregation of BTAs. This phenomenon is more pronounced in compound **4**, which contains one chiral dimethyloctyl side chain and two pEB side chains. The presence of branching groups with the opposite stereoconfiguration close to the BTA and the presence of linear achiral pEB ends presumably reduce the tendency of BTAs to form helical aggregates that contain only one handedness and cause the small $\Delta\varepsilon$ at room temperature. The reduction of the T_e, h_e and K_e with increasing amount of pEB side chains is probably a result of the steric crowding of the pEB backbone.[62, 63] Alternatively, the bias for one helical sense may be reduced by the pEB side chains. The stereogenic centers of the butylene branches in pEB are racemic. The configuration of the butylene branching group, which is located at the second carbon from the BTA amide bond, can influence the helical arrangement of the aggregates. Although, the number of stereogenic centers close to the BTA with the opposite configuration is limited due to the 45/55 ratio of ethylene/butylene endgroups in monofunctional pEB and 50/22/28 ratio of neopentyl/ethylene/butylene endgroups in the difunctional pEB, some BTAs will consist of

mixed chiral and achiral side chains. Ogata *et al*. demonstrated that BTAs consisting of racemic 3,7-dimethyloctyl side chains show different helical sense behavior compared to achiral BTAs upon the addition of homochiral BTAs.[56, 64] Therefore, this behavior might lead to a situation in which the degree of aggregation is not coupled to the net helicity of BTA aggregates. A similar phenomenon was also observed in BTAs in which the chiral information is introduced via deuterium/hydrogen isotope substitution.[65] Chirality arising from this substitution in BTA based supramolecular polymers still results in a preference for one helical conformation. However, the energy difference of the stability between left- and right-handed helical supramolecular polymers is very small. This results in the formation of helices with both handedness in which the ratio of P and M is dependent on temperature and the nature of the solvent. This is in sharp contrast to the chiral methyl-substituted BTA (**5**), where CD and UV cooling curves are superimposable and the degree of aggregation is coupled to the net helicity.[57] Thus pEB not only reduces K_e as a result of steric crowding but also diminishes the bias for one helicity.

2.4 Self-assembly in the solid state

2.4.1 Differential scanning calorimetry

While amine telechelic pEB is a viscous liquid at room temperature, **1a,b** and **2a,b** were obtained as transparent, elastic solids. As an example, the significant visual change in properties of pEB and BTA end-capped pEB (compound **1b**) is shown in Figure 2.4. Compounds **3** and **4** are both sticky viscous liquids and do not show a significant change of the material properties.
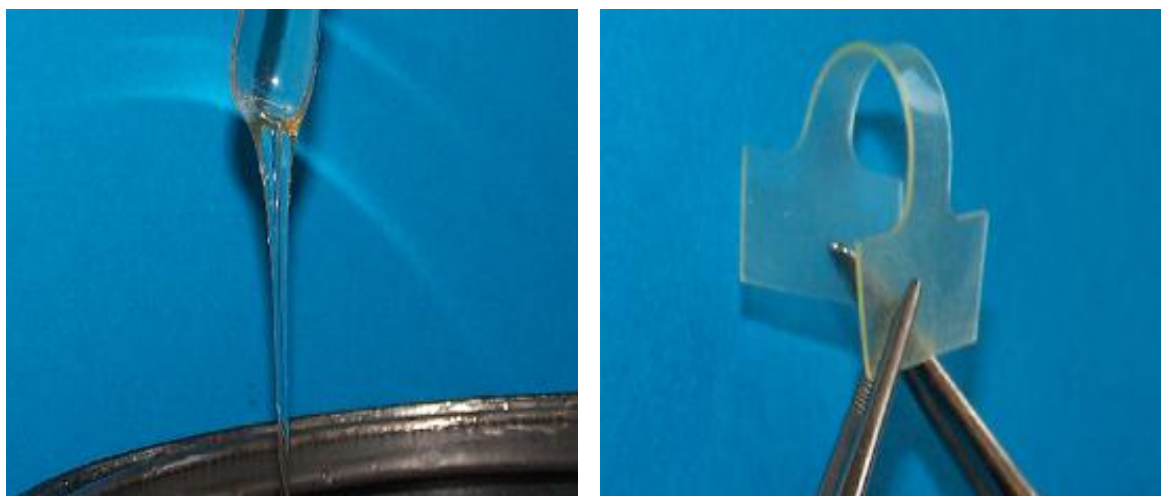
Figure 2.4 Amine telechelic pEB before (left) and after (right, compound **1b**) functionalization with the BTA motif.

The origin of these changes in phase behavior was investigated with differential scanning calorimetry (DSC) and polarized optical spectroscopy (POM) (Table 2.1). The phase transitions and the corresponding enthalpy changes were derived from the third heating run (40 k min^{-1}). DSC of **1a** showed a T_g at -60 °C and a small transition around 205 °C (ΔH = 11.76 kJ/mol for **1a**, ΔH = 12.16 kJ/mol for **1b**). With POM, we observed a mobile, birefringent texture typical for a nematic phase starting from 60 °C up to the clearing temperature around 200 °C. DSC traces for the copolymers **2a,b** revealed a T_g at -57 °C and a small transition at around 185 °C (ΔH = 7.14 kJ/mol for **2a** and 8.16 kJ/mol for **2b**). In this case, no liquid crystalline phase was observed with POM. Compound **3** showed a T_g at -60 °C and a small transition at around 192 °C (ΔH = 16.36 kJ/mol). POM revealed an unidentified mobile birefringent texture starting from room temperature up to the clearing temperature around 190 °C. Compound **4** revealed a T_g at -59 °C and a small transition around 157 °C (ΔH = 8.60 kJ/mol). POM did not show the presence of a liquid crystalline phase. Compound **5** has a crystalline to liquid crystalline transition at 119 °C (ΔH = 16.0 kJ/mol) and a transition into the isotropic state at 236 °C (ΔH = 21.0 kJ/mol).[56]

2.4.2 Circular dichroism spectroscopy

Since BTAs attached to pEB form helical stacks with a preferred helicity in dilute solution, we wondered if the propensity to form helical stacks is retained in the solid state when BTAs are embedded in a polymer matrix. We studied chiral polymer **2a** and achiral polymer **2b** with CD spectroscopy to verify the presence of columnar helical structures as found for **1a**, **3**, **4** and **5** in dilute solution. It is expected that chiral **2a** shows a Cotton effect in contrast to achiral **2b** in which no preferred helical sense is present. Since **2a,b** were insoluble in apolar solvents, we spin-coated CHCl$_3$ solutions of **2a,b** on quartz plates and measured CD of the obtained films (thickness = ~440 nm) (Figure 2.5A). As expected, the achiral polymer **2b** did not show any CD effect. A clear CD effect was observed for **2a**, similar in shape as observed for **1a**, **3** and **5**. The CD effect was independent of the orientation of the quartz slide with respect to the beam, and no linear dichroism effects were present. This suggests that the columnar helical order present in solution is retained in the solid state.
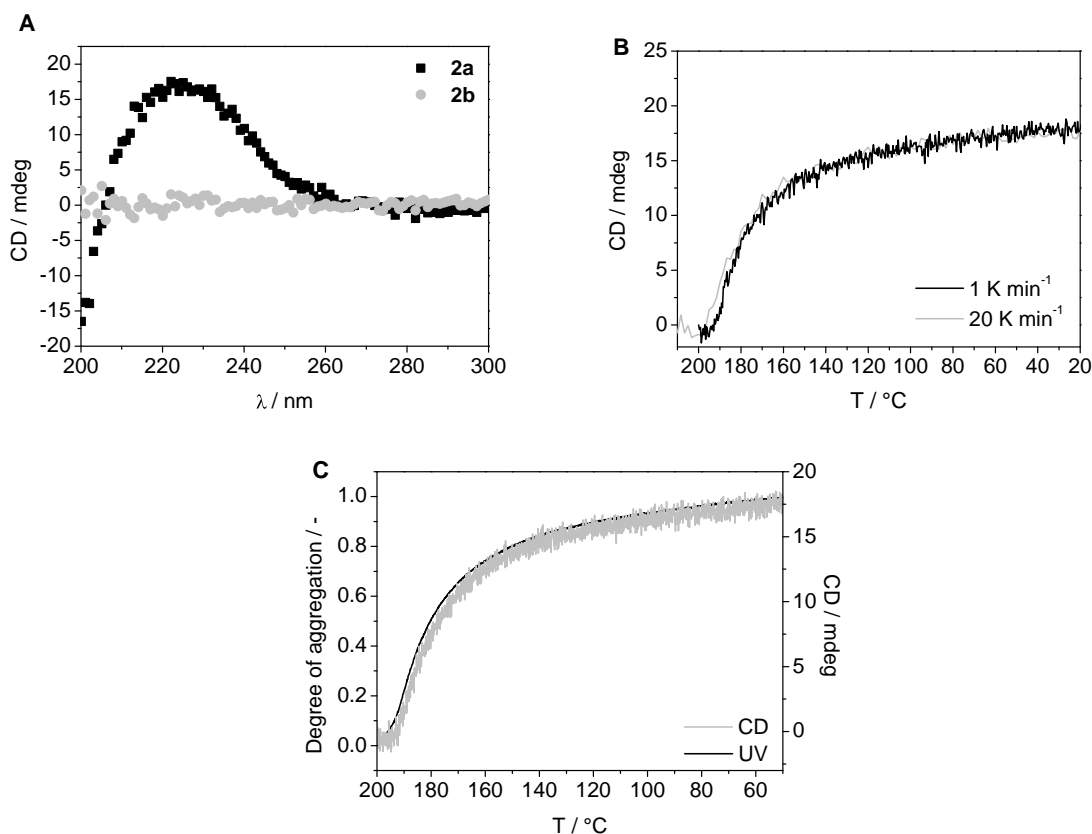
Figure 2.5. A) CD spectra of spin-coated films of **2a,b**. Film thickness of **2a,b** is 440 nm and 450 nm, respectively (at room temperature). B) CD absorption at $\lambda = 225$ nm versus temperature of a spin-coated film of **2a**. The sample was cooled from 210 °C with a rate of 1 or 20 K min^{-1}. C) CD and the degree of aggregation (based on UV absorption) at $\lambda = 225$ nm versus temperature of a spin-coated film of **2a** (rate = 1 K min^{-1}, thickness = 440 nm).

DSC and POM of **2a,b** showed a phase transition into the isotropic state around 185 °C. This is presumably connected to the loss of hydrogen bonding in BTA aggregates. To investigate if the helical arrangement of BTAs is still present at high temperature, we performed temperature-dependent CD spectroscopy on the spin-coated film of **2a**. The film was cooled from 210 °C to 20 °C at a rate of 1 K min^{-1} or 20 K min^{-1}, respectively. The CD effect was monitored upon cooling at $\lambda = 225$ nm and plotted versus temperature (Figure 2.5B). At 200 °C no Cotton effect was visible however, upon cooling **2a** showed a sudden appearance of a Cotton effect starting at around 190 °C. The sudden appearance of a Cotton effect is typical for a nucleation-elongation type self-assembly process, which is also observed for compound **5** in dilute conditions.[57] Furthermore, the shape and size of the curve was not affected by the cooling rate, meaning that self-assembly is under thermodynamic control. We also followed the Cotton effect and UV absorption at $\lambda = 223$ nm upon cooling (Figure 2.5C). The degree of aggregation was derived from the UV data by

assuming the presence of a molecularly dissolved state at high temperatures and a fully aggregated state at low temperatures. The cooling curves are superimposable and indicating that the degree of aggregation is coupled to the net helicity. This is in contrast to the solution studies on compounds **3** and **4** in which pEB diminished the bias for one helicity (Figure 2.3). Surprisingly, the slopes of the UV cooling curves of **3** and **4** in solution, which reflect the degree of aggregation, are less steep than that of **2a** in the solid state. It seems that the formation of BTA aggregates in the solid state is a more cooperative process than in solution. An explanation for this can be the presence of phase segregation even in the isotropic state. Phase segregation results in a higher effective concentration of BTAs. Phase segregation is connected to the degree of aggregation of BTAs and is temperature-dependent as well. This means that the effective concentration of BTAs depends on the temperature. Phase segregation can therefore be seen as a temperature-dependent additional interaction that favors BTA self-assembly, which results in a more cooperative self-assembly process and certainly explains the relative high values of the T_e found for the solid state polymer materials.

2.4.3 Infrared spectroscopy

Temperature-dependent CD spectroscopy in the solid state suggests that the mesophase to isotropic transition observed in compounds **2a** is connected to the loss of the intermolecular hydrogen bonds and the helical arrangement of aggregated BTAs. To investigate this in more detail, we performed infrared (IR) measurements on polymers **1**-**4**, since this is a sensitive technique to investigate hydrogen bonding in the solid state.[56, 58] BTA amides, involved in a threefold α–helical type of hydrogen bonding, show vibrations at characteristic wavenumbers (ν(N-H) 3226 cm^{-1}, ν(amide I) 1637 cm^{-1} and ν(amide II) 1563 cm^{-1}). The vibrations are visible at different wavenumbers in a non-hydrogen bonded α–helical type arrangement (ν(N-H) 3334 cm^{-1}, ν(amide I) 1656 cm^{-1} and ν(amide II) 1537 cm^{-1}).

Table 2.2 Summary of the IR spectroscopy data of compounds **1**-**5**. Determined at 20 °C in the solid state.

Compound	ν (N-H) [cm^{-1}]	ν (amide I) [cm^{-1}]	ν (amide II) [cm^{-1}]
1a	3240	1642	1562
1b	3241	1642	1561
2a	3265	1644	1550
2b	3252	1644	1552
3	3254	1634	1562
4	3241	1643	1560
5	3226	1637	1563

IR spectra in the solid state of **1**-**4** showed vibrations at positions typical for amides involved in threefold α–helical type hydrogen bonding, as evidenced by comparison with compound **5**. However, small differences are visible in the positions of the vibrations in **1**-**4**. For example, **2a**,**b** showed vibrations at wavenumbers closer to those of amides involved in non-hydrogen bonded fashion than those of **1a**,**b**. This suggests that relatively less BTAs are aggregated in a helical fashion in the copolymers (**2a**,**b**) than in BTA end-capped pEB (**1a**,**b**). The lower degree of aggregation of BTAs in the copolymers is probably a result of the reduction of the freedom of BTAs due to the high degree of physical cross-linking. As a result, more BTAs are trapped in the cross-linked network and cannot participate in hydrogen bonding. Also the presence of the small number of methylesters in **2a**,**b** can cause destabilization of the BTA aggregates. Next, we performed variable temperature IR on compound **1a**. The position of the NH stretch and amide II vibration versus temperature is plotted in Figure 2.6. Variable temperature IR revealed a gradual shifting of the characteristic vibrations starting from room temperature up to the clearing temperature and allowed us to attribute the transitions at 205 °C, observed in DSC and POM, to the loss of threefold helical arrangement of hydrogen bonds.
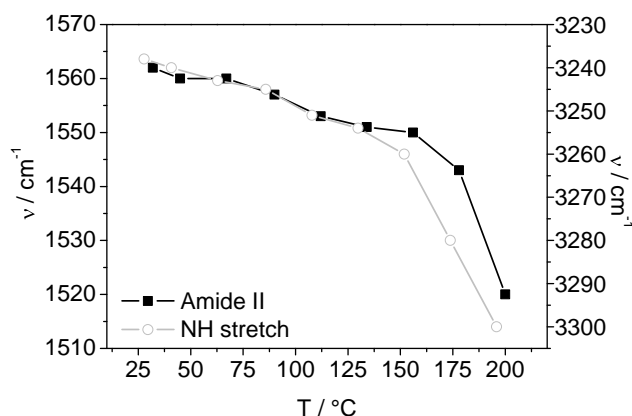
Figure 2.6 Infrared spectroscopy of **1a**. Position of the NH-stretch and amide II vibration versus temperature.

2.4.4 Correlation of phase behavior with self-assembly

The solid state phase behavior of compounds **1**-**4** is directly connected to BTA aggregation according to IR and CD spectroscopy. The melting temperature and the corresponding change of enthalpy of the hard phase formed by the supramolecular polymers are determined by the strength of the interaction and the domain size[66] of the phase segregated supramolecular motif. Correlating the phase behavior to BTA self-assembly may give insights into the structure and formation process of BTA aggregates.

The melting points of **1**-**5** occur at different temperatures and appear to be related to the mass fraction of BTAs in the pEB matrix. BTA (**5**), which is not connected to a pEB backbone,

has the highest melting point (Table 2.1). The melting points of **1**-**4** decrease with increasing amount of pEB. This phenomenon is also observed in dilute condition, in which the temperature of elongation (T_e) highly depends on the concentration of BTAs in solution.[57] The temperature-dependent CD and UV spectroscopy of **2a** in the solid state showed a T_e of 190 °C and compound **2a** also showed a melting point in DSC around the same temperature. As a result, these two phenomena appeared to be connected. This prompted us to plot the natural logarithm of the dimensionless BTA mol fraction in **1**-**5** (the BTA mass fraction in the BTA/pEB compounds) versus the reciprocal T_m (observed with DSC) (Van 't Hoff plot, Figure 2.7). We neglected steric limitations on aggregate growth and assumed that the degree of aggregation is only determined by the concentration.
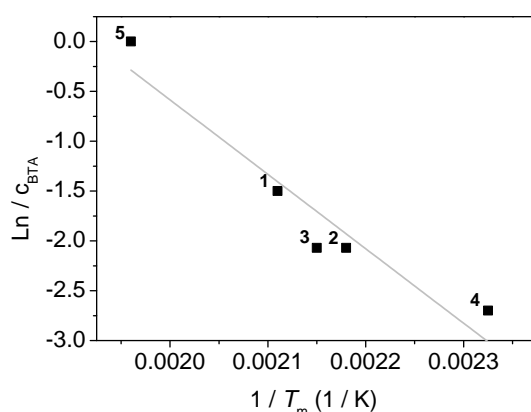
Figure 2.7 The natural logarithm of the BTA mass fraction in **1**-**5** versus the reciprocal T_m for **1**-**5**. The line represent a linear fit of the data points, which slope is proportional to the enthalpy change h_e.

A linear relationship is observed between the concentration of BTAs and the reciprocal melting temperatures of compounds **1**-**5**. We derived an enthalpy change upon elongation (h_e) of -61 kJ/mol. The negative value for h_e shows that the supramolecular polymerization is enthalpy driven. Furthermore, the value of h_e is close to the enthalpic change of BTAs upon elongation in dilute solutions of apolar solvents.[57] Since pEB is of comparable low polarity, we can conclude that BTAs form similar types of aggregates in the solid state as in dilute solutions.

2.5 Material morphology

2.5.1 Atomic force microscopy

Atomic force microscopy (AFM) of compound **1a** displayed a fibrillar structure, which is indicative for phase segregation between the pEB soft phase and the BTA columnar aggregates (Figure 2.8, left). The diameter of the fibrils was estimated around 6 nm and their length was 500-800 nm. This shows that nanorods are indeed present in the soft polymer matrix. Since the average diameter of columnar aggregates of single BTAs in the liquid

crystalline state is ~1.6 nm, the diameter of 6 nm suggests that the nanorods consist of bundles of BTA aggregates.[67] However, an accurate size of the fibrils cannot be determined due to the limitations of the resolution as a result of the AFM tip size. The morphology is reminiscent of the morphologies previously observed for UPy-urea modified pEB, although the dimensions are smaller in the case of **1a**.[13] AFM of copolymer **2b** shows a less developed morphology than the one observed for **1a** (Figure 2.8, right). Although phase segregation is clearly present in the morphology of **2b**, a more rod-like structure was observed with a diameter of 6 nm, but with much shorter length (20-30 nm) indicating that the aspect ratio is significantly lower than the aspect ratio observed for **1a**. The reduction in length is probably a result of the higher degree of cross-linking in the copolymer that reduces the freedom of BTAs to form long elongated nanorods. This corresponds well with IR measurements of **2b** in which the vibrations of BTA amides occurred at positions more closer to those of BTAs involved in a non-hydrogen bonded fashion, suggesting that not all BTAs are aggregated. AFM measurements on compounds **3**-**4** were not successful due to the viscous and sticky material properties.
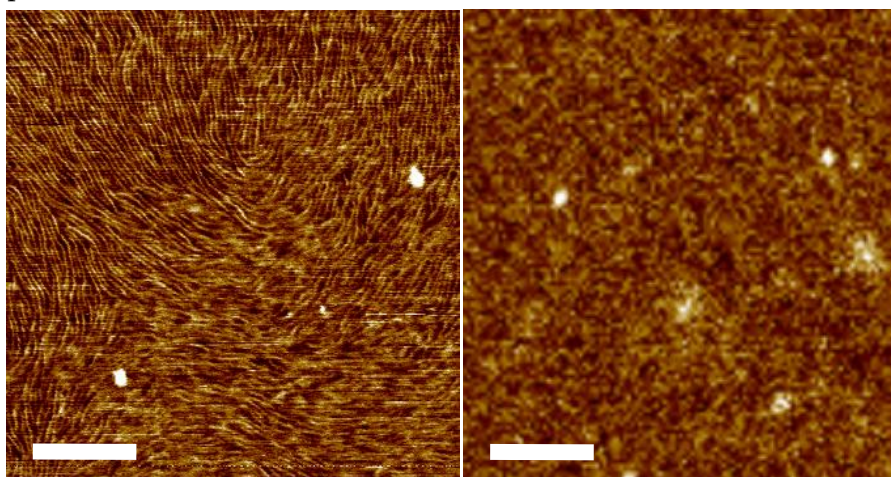
Figure 2.8 AFM phase images of **1a** (left) and **2a** (right). The scale bar is 100 nm.

2.5.2 X-ray scattering

WAXS and SAXS measurements were performed on compound **1a** to reveal the long range ordering of the phase segregated nanorods. The WAXS profile is dominated by a broad amorphous halo, however, two weak reflections were visible at q = 8.8 nm^{-1} and at q = 18 nm^{-1} (Figure 2.9A). The corresponding *d*-spacings are 7.1 Å and 3.5 Å, respectively. The *d*-spacing of 3.5 Å corresponds with the inter-disc distance observed in single crystal X-ray measurements and in BTAs in the liquid crystalline state. The origin of the reflection at 8.8 nm^{-1} is probably related to the periodicity of the helix.[67] In SAXS one reflection, which is visible at q = 1.2 nm^{-1}, corresponding to a *d*-spacing of 5.3 nm (Figure 2.9B). This distance is probably related to the fibril width since this distance was also observed in AFM measurements.
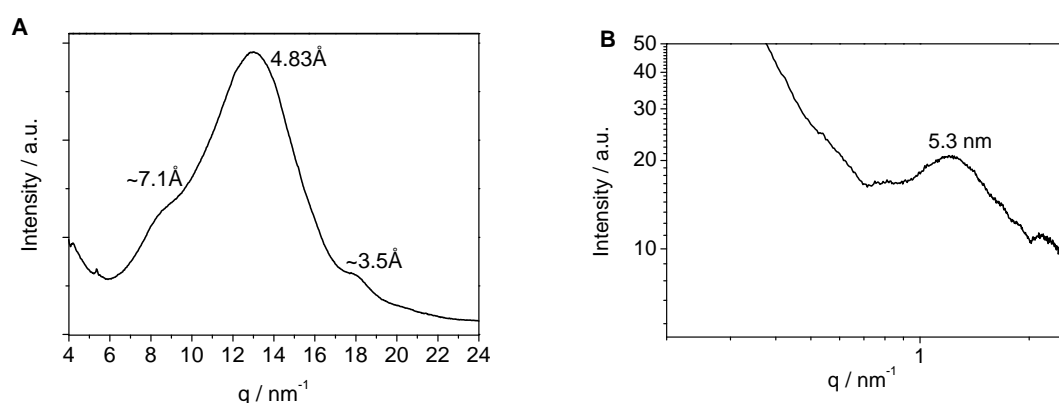
Figure 2.9 A) WAXS profile of **1a** at 25 °C. B) SAXS profile of **1a** at 25 °C.

2.6 Mechanical properties

The dumbbell shaped BTAs **1a,b** appeared as elastic solids, however, the material properties were not sufficient to allow tensile testing to be performed. Gratifyingly, the elasticity in copolymers **2a,b** was more pronounced than the elasticity (visually) observed for **1a,b**. Therefore, we performed tensile tests on **2b**. The stress-strain curve was typical for a thermoplastic elastomer (Figure 2.10A). The *E*-modulus was 3.4 ± 0.2 MPa, indicative for a soft rubber. The yield stress and the strain at break were 1.42 ± 0.07 MPa and 497±43%, respectively. These values compare well with the relatively low molecular weight UPy-urea functionalized blockcopolymers,[68] poly(urea EB)[69] analogues or bis-urea grafted poly(dimethylsiloxane)[14] but are significantly lower compared to large and highly ordered supramolecular segmented copolymers or industrial thermoplastic elastomers.
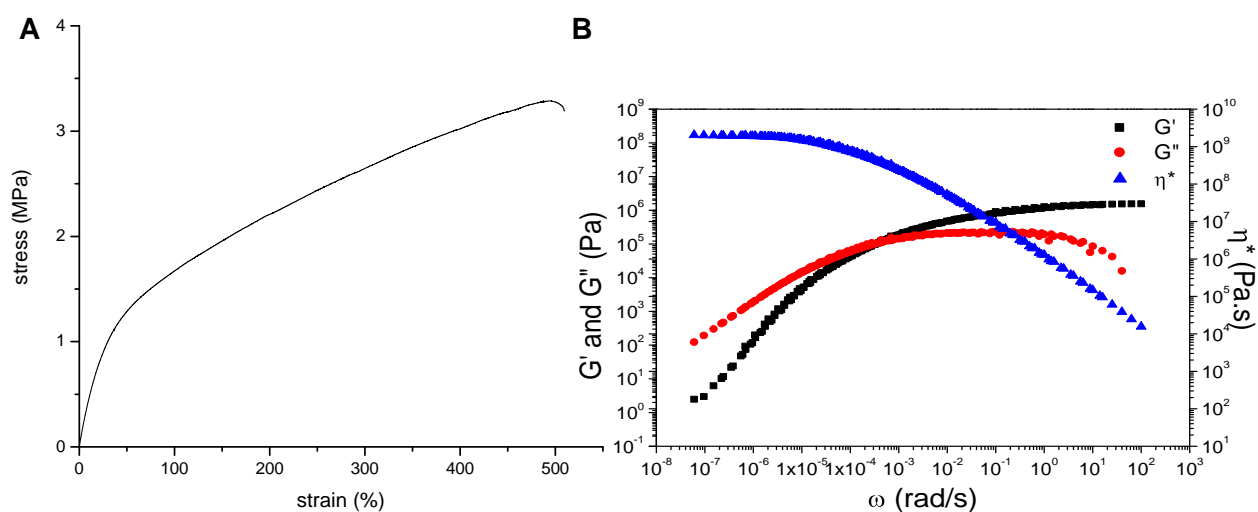
Figure 2.10 A) Stress strain curve for polymer **2b**. B) Master curve of storage (G′) and loss (G″) moduli and the complex viscosity (η*) of **2b**.

The elasticity of the copolymer **2b** was further investigated by dynamic oscillatory shear measurements. Figure 2.10B shows the master curves of the storage (G′), loss modulus (G″) and the complex viscosity (η^*) of **2b** at 40 °C. Both moduli and the complex viscosity show frequency-dependent behavior indicative for visco-elastic behavior. The zero-shear viscosity, at low frequencies, is determined at 10^9 Pa.s. The viscosity is frequency dependent at higher frequencies with a slope of -1. A rubber plateau is visible at high frequencies with a storage modulus of 10^6 Pa. A visco-elastic transition towards the terminal flow regime is visible at lower frequencies. The storage modulus (G′) is proportional to the square root of the frequency and the loss modulus (G″) is proportional to the frequency. Unfunctionalized pEB has a viscosity of 10 Pa, which is frequency independent.[70] Also the loss modulus (G″) is proportional to the frequency without showing a visco-elastic transition. The significant difference of the viscosity and the loss modulus between **2b** and pure pEB, clearly shows the increase in the virtual molecular weight and the effect of the physical cross-links formed by BTA phase segregated nanorods.

2.7 Conclusions

We have shown the potential of BTAs attached to pEB chains to induce physical cross-linking and thereby generating supramolecular materials with elastomeric properties. The propensity of BTAs to form supramolecular polymers, when end-capped to or copolymerized with telechelic pEB, is retained in dilute solution and in the solid state, as evidenced by CD spectroscopy. In solution, the pEB polymer backbone influences the degree of aggregation and the expression of chirality in aggregated BTAs. This was deduced from a decrease of the temperature of aggregation with increasing amounts of pEB and a difference in shape between the UV and CD cooling curves. These phenomena are attributed to solvent effects since they were less pronounced in the solid state. DSC and POM of BTA functionalized pEB showed additional phase transitions around 150-200 °C. Temperature-dependent CD and IR spectroscopy showed that these phase transitions originates from the loss of intermolecular hydrogen bonds between BTAs. The melting points observed in DSC were correlated to the concentration of BTAs in the polymer matrix. Plotting the BTA mass fraction versus the reciprocal melting temperatures allowed us to estimate an enthalpy change for the aggregation process of -60 kJ/mol. This value is similar as the enthalpy change determined for BTAs in dilute solutions of apolar solvents suggesting that similar types of aggregates are formed in the solid state. The physical appearance of pEB changed after end-capping or copolymerizing with BTAs from a viscous liquid to an elastic solid. AFM showed the presence of phase segregated nanorods with a diameter of 6 nm and a length of 500-800 nm for the end-capped polymer and 30 nm for the copolymer. The smaller rod length in the copolymers is probably a result of a reduced mobility of BTAs due to steric hindrance. SAXS and WAXS showed *d*-spacings of 3.5 Å and 5.3 nm that correspond with the inter disc

distance and the fibril width, respectively. The distances, observed with AFM and X-ray measurements, suggest that nanorods consist of bundles of BTA aggregates. Thermoplastic elastomeric behavior of the BTA copolymers was demonstrated by the presence of frequency-dependent moduli and a dynamic viscosity as observed with oscillating shear measurements. Furthermore, stress-strain curves showed an *E*-modulus of 3.4 MPa, which is characteristic for a soft rubber.

Functionalization of low molecular weight pEB with the BTA motif results in a remarkable improvement of the material properties. The obtained material properties are comparable to those of soft natural rubbers. The need for multiple synthetic steps to obtain these materials makes them not yet applicable for general use on an industrial scale. The true strength of BTA based supramolecular polymers lays in the chiral helical arrangement of the supramolecular structure. This enables the use of various spectroscopic techniques to study the self-assembly process, resulting in a detailed understanding of the supramolecular structure. Supramolecular polymers based on the BTA motif are therefore excellent candidates to reveal insights into the formation and structure of supramolecular polymers in general.

2.8 Experimental

Materials

Compound **5** was synthesized according to previously published procedures. (*R*)-(+)-citronellal (ABCR, ee = 79%) and (*S*)-(-)-citronellol (Takasago, ee = 99%) was used as the chiral synthon. Kraton L2203 and Kraton L-1203 were kindly provided by Kraton Polymers Research. Solvents were dried by distillation from molsieves or by a solvent purification system and used immediately. All other chemicals were used as received.

Instrumentation and Analysis

CD and UV spectra were recorded on a Jasco J-815 CD spectrometer equipped with a Jasco PTC-348 WI temperature controller. Experiments were conducted using spectroscopic grade heptane or dodecane as the solvent. Cells with an optical path length of 1 cm (for ~10^{-5} M solutions) or quartz plates (for spin coated films) were employed.

Spin coated films of **2a,b** were prepared by dropping a solution of **2a,b** (21 mg/mL CHCl$_3$) onto a quartz plate (cleaned by sonicating in acetone for 45 min) and spin coating the solution at 800 rpm (total volume ~1.3 mL). The film thickness was determined with a Tencor P-10 surface profiler. The concentration independent value for the Cotton effect, the molar ellipticity ($\Delta\varepsilon$), was calculated as $\Delta\varepsilon$ = CD-effect/(32980xcxl) where c is the concentration in mol/L and l = the optical path length in cm. The CD spectra of the films were checked for the presence of linear dichroism, which was not observed. ^{1}H-NMR and ^{13}C-NMR spectra were recorded on a Varian Gemini 400 MHz NMR (400 MHz for ^{1}H-NMR and 100 MHz for ^{13}C-

NMR). Proton chemical shifts are reported in ppm downfield from tetramethylsilane (TMS). Carbon chemical shifts are reported downfield from TMS using the resonance of the deuterated solvent as the internal standard. IR spectra were recorded on a Perkin Elmer 1600 FT-IR. Temperature variable IR spectra were recorded on an Excalibur FTS 3000 MX FT-IR from Biorad. MALDI-ToF mass spectrometry has been performed using a PerSeptive Biosystems Voyager DE PRO Spectrometer. POM measurements were performed using a Jenaval polarisation microscope equipped with a Linkam THMS 600 heating device, with crossed polarisers. The thermal transitions were determined with DSC using a Perkin-Elmer DSC–7 under a nitrogen atmosphere with heating and cooling rates of 40 K/min (3rd heating run). GPC measurements were performed on a Resi Pore column with chloroform as the eluent (flow = 1 mL/min) and employing a UV detector (λ = 254 nm). The molecular weights were determined using the polystyrene calibration method.

Tensile tests and dynamic oscillating shear measurements

Uniaxial tensile tests were performed on solvent cast films. Films were cast from $CHCl_3$ solutions in a Teflon mould. After slow evaporation of the solvent, the films were subjected to a vacuum at 30-40 °C for 18 hours. Tensile bars were punched from the films. Tensile properties were measured according to ASTM D 1708-96 on a Zwick Z010 equipped with a 20N load cell applying a crosshead speed of 20 mm/min. Grip to grip separation was 18-22 mm. The width of the test section was 5 mm, the thickness of the films was 0.2-0.3 mm. Samples that failed at the clamps were not included. Yield stresses were determined by determining the intersection point of the two tangents to the initial and final parts of the load elongation curves around the yield point. An indicative Young's modulus was determined by calculating the slope of the stress-strain curve via E [MPa] = $(\sigma_2 - \sigma_1) / (\varepsilon_2 - \varepsilon_1)$, ε_2 = 0.0005 and ε_1 = 0.0025.

Dynamic mechanical measurements were performed on a Rheometrics RMS 800 in a cone-plate geometry (25 mm). Strain amplitudes up to 30% were used, which were all within the viscoelastic range.

X-Ray Scattering

SAXS and WAXS experiments were performed at the DUBBLE beamline (BM26B) at the European Synchrotron Radiation Facility (ESRF) in Grenoble (France). The data were collected using a 2D multiwire gas-filled detector with pixel array dimensions of 512 x 512. The pixel size was 260 x 260 μm^2. The SAXS detector was positioned at 3 m from the sample and the q-scale was calibrated using the position of diffracted peaks from a standard silver behenate powder. The exposure time for each sample was varied from 30 to 60 s and a wavelength of 1.24 Å was used. The WAXS data were acquired using a Photonic Science CCD camera with pixel dimension of 22 μm^2 and with a sample-to-detector distance of

95mm. The experimental data were corrected for background scattering, i.e., subtraction of instrumental errors. The SAXS and WAXS scattered intensities were integrated after background subtraction and plotted against the scattering vector, $q = (4\pi/\lambda) \sin\theta$ where 2θ is the scattering angle.

AFM Measurements

Thin copolymer films were cast on glass substrates (cleaned by sonicating in acetone for 15 min and dried for 1 hour at 40 °C *in vacuo*) from dilute solutions in $CHCl_3$ (1 mg/ml). The final film thickness was *ca.* 440 nm. This value is larger than the intrinsic pattern period observed in the materials, which ensures that the morphology is not driven by the assembly on the substrate. The films were annealed at 100 °C *in vacuo* for 18 hours before AFM observation. All the AFM images were recorded with a Nanoscope IV microscope from Veeco Inc. (Santa Barbara, California) in the Tapping Mode (25 °C, in air). Microfabricated cantilevers were used with a resonance frequency of 300 kHz spring constant of 40 Nm^{-1}. The working frequency was chosen slightly below the resonance frequency to be sure to be in the repulsive regime. The instrument measured simultaneously height and phase cartography. Images of different areas of each sample were recorded. For image analysis, the Nanoscope image processing software was used.

Synthesis

Kraton bisamine. HO-PEB-OH (Kraton L2203; M_n = 3500 g/mol and M_w/M_n = 1.08) (41 g, 11.7 mmol) was dissolved in 200 mL THF. Then, triphenylphosphine (7.7 g, 29.2 mmol) and phthalimide (4.3 g, 29.2 mmol) were added. The solution was cooled with an ice bath. Diisopropyl azodicarboxylate (DIAD) (5.9 g, 29.2 mmol) was dissolved in 10 mL THF and added drop wise to the cooled solution. The mixture was stirred for 48 hours. The resulting clear yellow solution was evaporated *in vacuo*. After addition of 500 mL hexane a white solid was filtrated off. The remaining solution was subjected to silica filtration twice, with hexane as eluent. Kraton bisphthalimide was obtained as a viscous oil after evaporation *in vacuo* in a 22% yield. ^{1}H-NMR (400 MHz, $CDCl_3$, δ): 7.87 (m, 4H, Ar-H), 7.72 (m, 4H, Ar-H), 3.71 (t, 2H, CH_2-C$\underline{H}_2$-N), 3.55 (s, 2H, C-CH_2-N), 2.00 - 0.84 ppm (m, ~600H, alkyl). Kraton bis phthalimide (9.47 g, 2.46 mmol) was dissolved in 150 mL tetrahydrofuran. After addition of hydrazine monohydrate (4.0 g, 124.8 mmol), the solution was stirred under reflux for 48 hours. After addition of 250 mL hexane, the mixture was washed twice with 200 mL water and twice with brine (200 mL). The organic phase was dried over Na_2SO_4. After filtration and evaporation *in vacuo*, Kraton bisamine was obtained as a slightly yellow oil. Yield = 30 g, 74%. ^{1}H-NMR (400 MHz, $CDCl_3$, δ): 2.70 (t, 2H, CH_2-C$\underline{H}_2$-NH_2), 2.44 (s, 2H, C-C$\underline{H}_2$-NH_2), 2.00 - 0.84 ppm (m, ~600H, alkyl). ^{13}C-NMR (200 MHz, $CDCl_3$): δ = 52.9, 38.9, 38.4, 37.9, 36.1, 33.5, 33.3, 32.0, 30.7 30.2, 29.8, 29.1, 26.8, 26.6, 26.5, 26.2, 26.1 26.0, 25.9, 22.7, 14.1, 10.9, 10.7, 10.6.

Kraton monoamine. PEB-OH (Kraton L-1203, M_w = 3500 g/mol, *PDI* = 1.03) (0.5 g, 0.14 mmol) was was dissolved in 10 mL THF. Then triphenylphosphine (39.6 mg, 0.154 mmol) and phthalimide (22 mg, 0.154 mmol) were added. The solution was cooled with an ice bath. DIAD (30.8 mg, 0.154 mmol) was dissolved in 2 mL THF and added drop wise to the cooled solution. The mixture was stirred for 48 hours. The resulting clear yellow solution was concentrated and precipitated twice in methanol. The product was obtained as a viscous, sticky oil in a 95% yield. ^{1}H NMR (400 MHz, CDCl$_3$, δ): 7.87 (m, 2H, Ar-H), 7.72 (m, 2H, Ar-H), 3.71 (t, 2H, CH$_2$-C$\underline{H}_2$-N), 1.7-0.8 (alkyl). Kraton-phthalimide was dissolved in 20 mL THF. After the addition of hydrazine monohydrate (150 mg, 3 mmol), the solution was stirred under reflux for 48 hours. THF was removed *in vacuo*. Subsequently 50 mL of chloroform was added. The organic phase was washed with NaOH (2 x 50 mL) and with brine (50 mL), respectively. After removal of chloroform in vacuo Kraton monoamine was obtained as a sticky oil. Yield = 0.48 g, 99%. ^{1}H-NMR (400 MHz, CDCl$_3$, δ): 2.65 (t, 2H, -C$\underline{H}_2$-NH$_2$) 1.7-0.8 (m, ~600H, alkyl).

5-Methoxycarbonyl-benzene-1,3-dicarboxylic acid (**6**). Trimethyl benzene-1,3,5-tricarboxylate (39.65 mmol, 10 gram) was dissolved in MeOH, 350 mL NaOH (86.71 mmol, 3.47 gram) was added to the solution. The solution was boiled under reflux at 85 °C for 12 hours. The solution was poured into 800 mL H$_2$O. The aqueous phase was acidified to pH 1 with 5 % hydrochloric acid and washed three times with diethyl ether (250 mL). The organic layers were separated making use of a separation funnel and dried over MgSO$_4$. The organic solvents were removed *in vacuo*. The product was recrystallized twice from ethyl acetate and obtained as a white solid. Yield = 3.56 g, 40%. ^{1}H-NMR (400 MHz, DMSO-d^6, δ): 8.78 (d, 1H, ArH), 8.76 (d, 2H, ArH), 3.95 (s, 3H, OCH$_3$).

Methyl 3,5-bis-chlorocarbonyl-benzoate (**7**). Compound **6** (6.47 mmol, 1.45 gram) was dissolved in 40 mL dry THF under an argon atmosphere. A catalytic amount of DMF (two droplets) was added to the solution. Oxalyl chloride (14.23 mmol, 1.81 gram) was dissolved in 20 mL dry THF and added dropwise to this solution. The solution was stirred for 1.5 hour at room temperature. THF was removed *in vacuo* and a yellowish suspension was obtained. The excess of oxalyl chloride was removed by co-evaporation with toluene. The product was obtained as a yellowish solid in a quantitative yield. ^{1}H-NMR (400 MHz, CDCl$_3$, δ): 9.00 (d, 2H, ArH), 8.95 (d, 1H, ArH), 4.00 (s, 3H, OCH$_3$).

General procedure for the synthesis of BTA end-functionalized poly(ethylene-co-butylene). The following procedures were used for all BTA end-functionalized poly(ethylene-*co*-butylene) (**1a**,**b**) using the same reaction conditions as described for the synthesis of compound **8a**, **9a** and **1a**.

Methyl 3,5-bis-(3R)-(3,7-dimethyl-octylaminocarbonyl)-benzoate (**8a**). Compound **7** (6.47 mmol, 1.69 gram) was dissolved in 40 mL dry CHCl₃ under an argon atmosphere. To this stirred solution, a solution of (3R)-3,7-dimethyloctylamine (14.23 mmol, 2.24 gram) and triethylamine (25.9 mmol, 2.62 gram) in dry CHCl₃ (20 mL) was added dropwise. After 24 hours the organic layer was washed three times with HCl (1 M, 50 mL) solution and two times with NaCl$_{aq}$ (saturated, 50 mL). The organic layer was separated and dried over MgSO₄. CHCl₃ was removed *in vacuo*. The product was isolated from the excess of (3R)-3,7-dimethyloctylamine by recrystallization from ethyl acetate and obtained as a white solid. Yield = 3.1 g, 90%. ¹H-NMR (400 MHz, CDCl₃, δ): 8.52 (d, 2H, ArH), 8.40 (d, 1H, ArH), 6.79 (t, 2H, NH), 3.95 (s, 3H, OCH₃), 3.49 (m, 4H, CONHC$\underline{H}$₂), 1.15-1.64 (20H, alkyl), 0.94 (d, 6H, CH₃), 0.86 (d, 12H, CH(C$\underline{H}$₃)₂).

Methyl 3,5-Bis-octylaminocarbonyl-benzoate (**8b**). Yield = 3.2 g, 40%. ¹H-NMR (400 MHz, CDCl₃, δ): 8.52 (s, 2H, ArH), 8.40 (s, 1H, ArH), 6.79 (t, 2H, NH), 3.95 (s, 3H, OCH₃), 3.49 (m, 4H, CONHC$\underline{H}$₂), 1.15-1.64 (24H, alkyl), 0.94 (t, 6H, CH₃).

Methyl 3,5-bis-(3S)-(3,7-dimethyl-octylaminocarbonyl)-benzoate (**8c**). Yield = 3.0 g, 88%. ¹H-NMR (400 MHz, CDCl₃, δ): 8.54 (d, 2H, ArH), 8.42 (d, 1H, ArH), 6.49 (t, 2H, NH), 3.98 (s, 3H, OCH₃), 3.49 (m, 4H, CONHC$\underline{H}$₂), 1.15-1.64 (20H, alkyl), 0.94 (d, 6H, CH₃), 0.86 (d, 12H, CH(C$\underline{H}$₃)₂).

3,5-Bis-(3R)-(3,7-dimethyl-octylaminocarbonyl)-benzoic acid (**9a**). Compound **6a** (4.97 mmol, 2.5 gram) was dissolved in MeOH, 60 mL. LiOH (11 mmol, 0.26 gram) and 3 mL H₂O were added to the solution. The solution was stirred at room temperature for 24 hours. Then the solution was poured in H₂O (pH < 1, 500 mL). A white powder precipitated and was isolated by filtration. The product was dried *in vacuo* at 40 °C. Yield = 1.95 g, 65%. ¹H-NMR (400Mhz, CDCl₃/MeOH-*d*⁴ 99/1, δ): 8.55 (d, 2H, ArH), 8.35 (d, 1H, ArH), 7.4 (t, 2H, NH), 3.49 (m, 4H, CONHC$\underline{H}$₂), 1.64-1.15 (20H, alkyl), 0.94 (d, 6H, CH₃), 0.86 (d, 12H, CH(C$\underline{H}$₃)₂).

3,5-Bis-octylaminocarbonyl-benzoic acid (**9b**). Yield = 2.2 g, 68%. ¹H-NMR (400Mhz, CDCl₃/MeOH-*d*⁴ 99/1, δ): 8.55 (s, 2H, ArH), 8.35 (s, 1H, ArH), 7.4 (t, 2H, NH), 3.49 (m, 4H, CONHC$\underline{H}$₂), 1.64-1.15 (24H, alkyl), 0.94 (t, 6H, CH₃).

3,5-Bis-(3S)-(3,7-dimethyl-octylaminocarbonyl)-benzoic acid (**9c**). Yield = 1.95 g, 65%. ¹H-NMR (400Mhz, CDCl₃/MeOH-*d*⁴ 99/1, δ): 8.55 (d, 2H, ArH), 8.35 (d, 1H, ArH), 7.4 (t, 2H, NH), 3.49 (m, 4H, CONHC$\underline{H}$₂), 1.64-1.15 (20H, alkyl), 0.94 (d, 6H, CH₃), 0.86 (d, 12H, CH(C$\underline{H}$₃)₂).

Kraton bis-BTA (**1a**). A solution of *N*-(3-dimethylaminopropyl)-*N'*-ethylcarbodiimide hydrochloride (0.215 mmol, 41 mg) in 5 mL dry CHCl₃ was added to an ice cooled stirred solution of compound **9a** (0.16 mmol, 77 mg), 4-dimethylaminopyridine (0.215 mmol, 26 mg) and Kraton bisamine (0.071 mmol, 250 mg) in 25 mL dry CHCl₃. The reaction mixture was allowed to warm to room temperature and stirred overnight. Then the mixture was diluted

with CHCl$_3$ (50 mL) and washed successively with HCl (1 M, 50 mL), NaHCO$_3$ (10%, 20 mL) and NaCl$_{aq}$ (saturated, 20 mL). The CHCl$_3$ layer was separated and the CHCl$_3$ was removed *in vacuo*. The product was precipitated from heptane and methanol, respectively, and obtained as a white solid. Yield = 184 mg, 59%. ^{1}H-NMR (400 MHz, CDCl$_3$, δ): 8.38 (s, 6H, ArH), 6.43 (b, 6H, NH), 3.5 and 3.3 (m, 10H + 2H, CONHC$\underline{H}_2$), 1.85-0.8 (~600H, alkyl). ^{13}C-NMR (CDCl$_3$): δ = 165.6, 134.8, 127.8, 40.4, 38.9, 37.9, 36.2, 33.5, 33.3, 31.8, 30.7, 30.2, 29.7, 29.3, 27.0, 26.8, 26.6, 26.2, 26.1, 25.8, 25.0, 22.7, 14.2, 10.9, 10.9, 10.6, 10.7. IR at 20 °C: ν (cm^{-1}): 3240 (N-H), 1642 (Amide I), 1563 (Amide II). M_n (calculated from ^{1}H-NMR) = 4.450 kg/mol. M_n (SEC) = 6.23 kg/mol, *PDI* = 1.13. DSC: T_g = -60 °C, T_m = 195-215 °C (ΔH = 2.68 J/g).

Kraton bis-BTA (**1b**). Yield = 720 mg, 68%. ^{1}H-NMR (400 MHz, CDCl$_3$, δ): 8.40 (s, 6H, ArH), 6.45 (b, 6H, NH), 3.52 and 3.34 (m, 10H + 2H, CONHC$\underline{H}_2$), 1.85-0.81 (~600H, alkyl). ^{13}C-NMR (CDCl$_3$): δ = 165.6, 134.8, 127.8, 40.4, 38.9, 37.9, 36.2, 33.5, 33.3, 31.8, 30.7, 30.2, 29.8, 29.3, 27.0, 26.8, 26.6, 26.2, 26.1, 25.8, 25.0, 22.7, 14.2, 10.9, 10.9, 10.6, 10.7. IR at 20 °C: ν (cm^{-1}): 3239 (N-H), 1642 (Amide I), 1562 (Amide II). M_n (calculated from ^{1}H-NMR) = 4.380 kg/mol. M_n (SEC) = 6.72 kg/mol, *PDI* = 1.12. DSC: T_g = -60 °C, T_m = 195-215 °C (ΔH = 2.79 J/g).

Benzene-1,3,5-tricarboxylic acid 1,3-dimethylester (**10**). Benzene-1,3,5-tricarboxylic acid trimethylester (2.0 g, 7.93 mmol) and NaOH (0.32 g, 7.93 mmol) were dissolved in methanol (70 mL) and refluxed for 12 hours. The reaction mixture was poured into water (200 mL), and the solution washed with diethyl ether (3 x 100 mL). The aqueous phase was acidified to pH 1 with 5% hydrochloric acid and extracted with diethyl ether (3 × 100 mL). The combined organic layers were dried over MgSO$_4$, and concentrated *in vacuo* to give the desired product. Yield = 1.3 g, 69%. ^{1}H-NMR (400 MHz, DMSO-d^6, δ): 8.44 (s, 2H, Ar-H), 8.35 (s, 1H, Ar-H), 3.88 (s, 6H, -OCH$_3$); ^{13}C-NMR (100 MHz, DMSO-d^6, δ): 165.5, 164.6, 133.5, 132.9, 132.2, 130.5, 52.7.

Dimethyl 5-(chlorocarbonyl) isophthalate (**11**). Benzene-1,3,5-tricarboxylic acid 1,3-dimethylester **8** (8,0 g, 33.59 mmol) was dissolved in 250 mL dry chloroform. After addition of one drop of DMF, oxalyl chloride (4.7 g, 37.04 mmol) in 50 mL dry chloroform was added drop-wise in a period of 10 minutes. After stirring for 2 hours, the excess of oxalyl chloride and chloroform were removed *in vacuo*. The remaining solid was co-evaporated twice with 100 mL toluene to ensure the removal of oxalyl chloride. The product was obtained in a quantitative yield, and directly used for further synthesis. ^{1}H-NMR (400 MHz, CDCl$_3$, δ): 8.93 (s, 1H, Ar-H), 8.92 (s, 2H, Ar-H), 4.02 (s, 6H, -OCH$_3$); ^{13}C-NMR (100 MHz, CDCl$_3$, δ): 167.0, 164.5, 136.3, 135.6, 134.1, 131.8, 52.8.

General procedure for the synthesis of BTA / poly(ethylene-co-butylene) copolymers The following procedures were used for all BTA / poly(ethylene-*co*-butylene) copolymers (**2a,b**) using the same reaction conditions as described for the synthesis of compound **12a**, **13a**, **14a** and **2a**.

Dimethyl 5-[(octylamino)carbonyl] isophthalate (**12b**). Dimethyl 5-(chlorocarbonyl) isophthalate **9** (33.59 mmol) was dissolved in 150 mL dry chloroform. *n*-Octyl amine (5.2 g., 40.3 mmol and triethylamine (6.8 g, 67.1 mmol) were added dropwise over a period of 10 minutes. After 18 hours the solvent was removed *in vacuo*. The remaining residue was dissolved in 300 mL chloroform and subsequently washed with 1 M HCl (2 x 150 mL.) and brine (1 x 150 mL.). The organic phase was dried over Na_2SO_4. The product was obtained after removal of $CHCl_3$ *in vacuo*. Yield = 6.2 g, 96%. ^{1}H-NMR (400 MHz, $CDCl_3$, δ): δ 8.76 (s, 1H, Ar-H), 8.61 (s, 2H, Ar-H), 6.48 (t, 1H, NH), 3.97 (s, 6H, OCH_3), 3.50 (m, 2H, CONHC$\underline{H}_2$), 1.64 (m, 2H, CONHCH$_2$C$\underline{H}_2$), 1.28, (m, 10H, alkyl), 0.88 (t, 3H, CH_2C$\underline{H}_3$). ^{13}C-NMR (100 MHz, $CDCl_3$): δ = 165.5, 165.1, 135,5, 132.4, 131.9 130.4, 52.1, 40.2, 31.5, 29.2, 29.0, 28.9 26.8, 22.3, 13.7.

N-((R)-3,7-dimethyloctyl)-3,5-bis(methoxycarbonyl)benzamide (**12a**). Compound **12a** was synthesized with the same conditions as **12b**. ^{1}H-NMR (400 MHz, $CDCl_3$, δ): 8.73 (s, 1H, Ar-H), 8.59 (s, 2H, Ar-H), 6.65 (t, 1H, NH), 3.91 (s, 6H, OCH_3), 3.49 (m, 4H, CONHC$\underline{H}_2$), 1.66 (m, 3H, alkyl), 1.30 (m, 7H, alkyl), 0.93 (d, 3H, CH_3), 0.86 (d, 6H, CH(C$\underline{H}_3$)$_2$). ^{13}C-NMR (100 MHz, $CDCl_3$, δ): 165.5, 165.4, 135.6, 132.8, 132.0, 130.9, 52.5, 39.1, 38.5, 37.0, 36.6, 30.7, 27.8, 24.5, 22.6, 22.5, 19.4.

5,N-((R)-3,7-dimethyloctylamino)carbonyl] isophthalic acid (**13a**). N-((R)-3,7-dimethyloctyl)-3,5-bis(methoxycarbonyl)benzamide **12a** (1.98 g, 5.76 mmol) was dissolved in methanol (40 mL). LiOH (0.54 mg, 22.6 mmol) and 5 mL of distilled water was added. After 18 hours, the reaction mixture was poured in 500 mL distilled water. A HCl solution (1 M) was added until the pH was 1. The precipitated product was collected by filtration and dissolved in 150 mL acetone. This solution was dried over Na_2SO_4. A white powder was obtained after concentration in vacuo. The product was recrystallized from ethylacetate and obtained in a white solid. Yield = 800 mg, 40%. ^{1}H-NMR (200 MHz, DMSO-d^6, δ): 13.40 (b, 2H, (C=O)-OH), 8.85 (t, 1H, NH), 8.61 (s, 2H, Ar-H), 8.55 (s, 1H, Ar-H), 3.24 (m, 2H, CONHC$\underline{H}_2$), 1.51 (m, 2H, CONHCH$_2$C$\underline{H}_2$), 1.23 (m, 10H, alkyl), 0.88 (t, 3H, CH_2C$\underline{H}_3$). ^{13}C-NMR (50 MHz, DMSO-d^6, δ): 167.5, 166.8, 135.1, 131.4, 131.0, 129.8, 39.2, 38.7, 37.2, 36.5, 30.3, 28.0, 24.4, 22.3, 19.3.

5-[(Octylamino)carbonyl]isophthalic acid (**13b**). 5-[(Octylamino)carbonyl] isophthalic acid **12b** was synthesized with the same conditions as **13a**. ^{1}H-NMR (200 MHz, DMSO-d^6, δ): 13.40 (b, 2H, (C=O)-OH), 8.85 (t, 1H, NH), 8.61 (s, 2H, Ar-H), 8.55 (s, 1H, Ar-H), 3.24 (m, 2H, CONHC$\underline{H}_2$), 1.51 (m, 2H, CONHCH$_2$C$\underline{H}_2$), 1.23 (m, 10H, alkyl), 0.88 (t, 3H, CH_2C$\underline{H}_3$). ^{13}C-NMR (50 MHz, DMSO-d^6, δ): 166.3, 164.5, 135.6, 132.2, 132.0, 131.7, 31.3, 29.0, 28.8, 26.6, 22.2, 14.0.

5,N-((R)-3,7-dimethyloctylamino)carbonyl] isophthaloyl chloride (**14a**). 5,N-((R)-3,7-dimethyloctylamino)carbonyl] isophthalic acid **13a** (47.7 mg, 0.137 mmol) was suspended in 4 mL freshly distilled dichloromethane under argon atmosphere. After addition of 1-chloro-*N*,*N*,2-trimethyl-1-propenylamine (136.7 mg, 1.02 mmol), the suspension was stirred for 18 hours. Subsequently, the resulting clear solution was evaporated. The residue was dried thoroughly using high vacuum to assure removal of the excess of 1-chloro-*N*,*N*,2-trimethyl-1-propenylamine. The presence of the desired product was confirmed with ^{1}H-NMR, but no further characterization was performed. The resulting product was directly used in further synthesis.

5-[(Octylamino)carbonyl]isophthaloyl chloride (**14b**). Compound **14b** was synthesized using the same conditions as **14a**.

BTA / poly(ethylene-co-butylene) copolymer (**2a**). 5,N-((R)-3,7-dimethyloctylamino)carbonyl] isophthaloyl chloride (**14a**) (0.137 mmol) was dissolved in 10 mL dry chloroform directly after synthesis, and added via a cannula to a stirred solution of Kraton bisamine (519 mg, 0.137 mmol) and triethylamine (55 mg, 0.55 mmol) in 24 mL dry chloroform. After complete addition the temperature was raised to 50 °C and stirred for 48 hours. The reaction product was evaporated to dryness and subsequently precipitated in cold pentane and cold methanol from chloroform solutions and obtained as a transparent solid. Yield = 300 mg, 49%. ^{1}H-NMR (400 MHz, CDCl$_3$, δ): 8.34 (s, 3H, Ar-H), 6.39 (m, 3H, NH), 3.49 (m, 2H, CH$_2$-C$\underline{H}_2$-NH), 3.31 (m, 2H, C-C$\underline{H}_2$-NH), 2.00 - 0.84 ppm (m, ~600H, alkyl). ^{13}C-NMR (100 MHz, CDCl$_3$, δ): 167.1, 166.9, 136.1, 135.9, 128.5, 50.8, 39.5, 39.0, 38.5, 36.7, 34.1, 33.9, 31.3, 30.8, 30.3, 27.4, 27.2, 26.7, 26.5, 11.5, 11.3. M_n (SEC) = 32.7 kg/mol, *PDI* = 1.7. DSC: T_m = 186 °C (ΔH = 1.87 J/g), T_g = -56 °C. IR at 20 °C: ν (cm^{-1}): 3244 (N-H stretch), 1644 (Amide I), 1562 (Amide II).

BTA / poly(ethylene-co-butylene) copolymer (**2b**). Polymer **2b** was synthesized using the same procedure as used for **2a**. ^{1}H-NMR (400 MHz, CDCl$_3$, δ): 8.34 (s, 3H, Ar-H), 6.44 (m, 3H, NH), 3.46 (m, 2H, CH$_2$-C$\underline{H}_2$-NH), 3.32 (m, 2H, C-C$\underline{H}_2$-NH), 2.00 - 0.84 ppm (m, ~600H, alkyl). ^{13}C-NMR (100 MHz, CDCl$_3$, δ): 165.9, 165.7, 135.4, 135.3, 127.9, 50.2, 38.9 38.4, 37.9, 36.1, 33.6, 33.5, 33.4, 33.3, 30.6, 30.2, 29.7, 26.8, 26.6, 26.4, 26.1, 26.1, 26.0, 25.9 10.9, 10.7, 10.6. M_n (SEC) = 27.7 kg/mol, *PDI* = 1.5. DSC: T_m = 182 °C (ΔH = 2.12 J/g), T_g = -56 °C. IR at 20 °C: ν (cm^{-1}): 3241 (N-H stretch), 1644 (Amide I), 1561 (Amide II).

Kraton mono BTA (**3**). Kraton monoamine (0.46 g, 0.13 mmol) and 3,5-bis((3S)-3,7-dimethyloctylcarbamoyl)benzoic acid (**9c**) (69 mg, 0.145 mmol) were dissolved in 10 mL dry dichloromethane. PyBOP (101.4 mg, 0.195 mmol) and DIPEA (25.3 mg, 0.195 mmol) were added to the solution. The solution was stirred for 12 hours at room temperature. Dichloromethane was removed *in vacuo*. Subsequently, 50 mL of chloroform was added. The originating precipitates were removed by filtration. The solution was concentrated *in vacuo*

and precipitated in methanol (three times). The product was obtained as a sticky oil. Yield = 0.5 g, 95%. GPC (Polystyrene standards): M_n = 7.6 kg/mol, M_w = 7.8 kg/mol, PDI = 1.03. ^{1}H-NMR (400 MHz, CDCl$_3$, δ): 8.38 (s, 3H, Ar-H), 6.49 (t, 3H, NHC=O), 3.50 (q, 6H, CH$_2$-NHC=O), 1.7-0.8 (alkyl). ^{13}C-NMR (100 MHz, CDCl$_3$, δ): 165.4, 136.8, 127.7, 40.2, 39.2, 38.8, 38.4, 37.9, 36.8, 36.1, 34.4, 33.5, 33.2, 31.8, 30.7, 30.3, 29.7, 29.5, 29.3, 27.0, 26.8, 26.6, 26.5, 26.3, 26.2, 26.1, 25.8, 25.0, 22.7, 14.2, 10.9, 10.9, 10.6, 10.7. IR at 20 °C: ν (cm^{-1}): 3254 (N-H), 1634 (Amide I), 1562 (Amide II). M_n (SEC) = 7.6 kg/mol, PDI = 1.05. DSC: T_g = -60 °C, T_m = 192 °C (ΔH = 4.09 J/g).

Bis Kraton mono BTA (**4**). A solution of *N*-(3-dimethylaminopropyl)-*N′*-ethylcarbodiimide hydrochloride (0.3 mmol, 57 mg) in 5 mL dry CHCl$_3$ was added to an ice cooled stirred solution of Kraton monoamine (1.05 g, 0.3 mmol) 5,*N*-((*R*)-3,7-dimethyloctylamino)carbonyl] isophthalic acid (**13a**) (47 mg, 0.136 mmol) and 4-dimethylaminopyridine (0.3 mmol, 36 mg) in 30 mL CHCl$_3$. The reaction mixture was allowed to warm to room temperature and stirred overnight. Then the mixture was diluted with CHCl$_3$ (50 mL) and washed successively with HCl (1 M, 50 mL), NaHCO$_3$ (10%, 20 mL) and NaCl$_{aq}$ (saturated, 20 mL). The CHCl$_3$ layer was separated and the CHCl$_3$ was removed *in vacuo*. The product was precipitated from heptane and methanol, respectively, and obtained as a colorless oil. Yield = 500 mg, 50%. ^{1}H-NMR (400 MHz, CDCl$_3$, δ): 8.34 (Ar-H, s, 6H), 6.42 (NH, b, 6H), 3.43 (CONHCH$_2$, q, 4H), 1.85-0.8 (alkyl, ~600H). ^{13}C-NMR (100 MHz, CDCl$_3$, δ): 165.5, 136.8, 127.8, 40.4, 39.1, 38.9, 38.4, 37.9, 36.8, 36.6, 36.1, 34.4, 33.5, 33.3, 31.8, 30.7, 30.2, 29.7, 29.5, 29.3, 27.0, 26.8, 26.6, 26.5, 26.3, 26.2, 26.1, 25.8, 25.0, 22.7, 14.2, 10.9, 10.9, 10.6, 10.7. IR at 20 °C: ν (cm^{-1}): 3241 (N-H), 1643 (Amide I), 1560 (Amide II). M_n (SEC) = 13.5 kg/mol, PDI = 1.10. DSC: T_g = -60 °C, T_m = 157 °C (ΔH = 1.17 J/g).

2.9 References

[1]   A. Ciferri, *Supramolecular Polymers*, New York, **2000**.
[2]   J.-M. Lehn, *Polym. Int.* **2002**, *51*, 825.
[3]   A. W. Bosman, L. Brunsveld, B. J. B. Folmer, R. P. Sijbesma, E. W. Meijer, *Macromol. Symp.* **2003**, *201*, 143.
[4]   L. Brunsveld, B. J. B. Folmer, E. W. Meijer, R. P. Sijbesma, *Chem. Rev.* **2001**, *101*, 4071.
[5]   A. Ciferri, *Macromol. Rapid Comm.* **2002**, *23*, 511.
[6]   U. Velten, M. Rehahn, *Chem. Commun.* **1996**, 2639.
[7]   H. Hofmeier, R. Hoogenboom, M. E. L. Wouters, U. S. Schubert, *J. Am. Chem. Soc.* **2005**, *127*, 2913.
[8]   C. Hilger, R. Stadler, *Macromolecules* **1990**, *23*, 2095.
[9]   T. F. A. de Greef, M. M. J. Smulders, M. Wolffs, A. P. H. J. Schenning, R. P. Sijbesma, E. W. Meijer, *Chem. Rev.* **2009**, *109*, 5687.
[10]   A. W. Bosman, R. P. Sijbesma, E. W. Meijer, *Mater. Today* **2004**, *7*, 34.
[11]   D. J. M. Van Beek, M. A. J. Gillissen, B. A. C. van As, A. R. A. Palmans, R. P. Sijbesma, *Macromolecules* **2007**, *40*, 6340.
[12]   B. J. B. Folmer, R. P. Sijbesma, R. M. Versteegen, J. A. J. van der Rijt, E. W. Meijer, *Adv. Mater.* **2000**, *12*, 874.
[13]   H. Kautz, D. J. M. van Beek, R. P. Sijbesma, E. W. Meijer, *Macromolecules* **2006**, *39*, 4265.
[14]   O. Colombani, C. Barioz, L. Bouteiller, C. Chaneac, L. Fomperie, F. Lortie, H. Montes, *Macromolecules* **2005**, *38*, 1752.

[15] P. Y. W. Dankers, M. C. Harmsen, L. A. Brouwer, M. J. A. van Luyn, E. W. Meijer, *Nat. Mater.* **2005**, *4*, 568.

[16] E. Wisse, R. A. E. Renken, J. R. Roosma, A. R. A. Palmans, E. W. Meijer, *Biomacromolecules* **2007**, *8*, 2739.

[17] P. Y. W. Dankers, J. M. Boomker, A. Huizinga-van der Vlag, E. Wisse, W. P. J. Appel, F. M. M. Smedts, M. C. Harmsen, A. W. Bosman, W. Meijer, M. J. A. van Luyn, *Biomaterials* **2011**, *32*, 723.

[18] M. Burnworth, L. Tang, J. R. Kumpfer, A. J. Duncan, F. L. Beyer, G. L. Fiore, S. J. Rowan, C. Weder, *Nature* **2011**, *472*, 334.

[19] J.-L. Wietor, A. Dimopoulos, L. E. Govaert, R. A. T. M. van Benthem, G. de With, R. P. Sijbesma, *Macromolecules* **2009**, *42*, 6640.

[20] S. D. Bergman, F. Wudl, *J. Mater. Chem.* **2008**, *18*, 41.

[21] S. Burattini, B. W. Greenland, D. H. Merino, W. Weng, J. Seppala, H. M. Colquhoun, W. Hayes, M. E. Mackay, I. W. Hamley, S. J. Rowan, *J. Am. Chem. Soc.* **2010**, *132*, 12051.

[22] P. Cordier, F. Tournilhac, C. Soulié-Ziakovic, L. Leibler, *Nature* **2008**, *451*, 977.

[23] J.-L. Wietor, D. J. M. van Beek, G. W. Peters, E. Mendes, R. P. Sijbesma, *Macromolecules* **2011**, *44*, 1211.

[24] A R. Hirst, B. Escuder, J F. Miravet, D K. Smith, *Angew. Chem., Int. Ed.* **2008**, *47*, 8002.

[25] J. D. Hartgerink, E. Beniash, S. I. Stupp, *Science* **2001**, *294*, 1684.

[26] S. Kyle, A. Aggeli, E. Ingham, M. J. McPherson, *Biomaterials* **2010**, *31*, 9395.

[27] F. van de Manakker, L. M. J. Kroon-Batenburg, T. Vermonden, C. F. van Nostrum, W. E. Hennink, *Soft Matter* **2010**, *6*, 187.

[28] D. Wu, W. Pisula, V. Enkelmann, X. Feng, K. Müllen, *J. Am. Chem. Soc.* **2009**, *131*, 9620.

[29] Z. Chen, A. Lohr, C. R. Saha-Möller, F. Würthner, *Chem. Soc. Rev.* **2009**, *38*, 564.

[30] J. P. Hill, W. Jin, A. Kosaka, T. Fukushima, H. Ichihara, T. Shimomura, K. Ito, T. Hashizume, N. Ishii, T. Aida, *Science* **2004**, *304*, 1481.

[31] J. D. Fox, S. J. Rowan, *Macromolecules* **2009**, *42*, 6823.

[32] Z. Guan, J. T. Roland, J. Z. Bai, S. X. Ma, T. M. McIntire, M. Nguyen, *J. Am. Chem. Soc.* **2004**, *126*, 2058.

[33] N. E. Botterhuis, S. Karthikeyan, D. Veldman, S. C. J. Meskers, R. P. Sijbesma, *Chem. Commun.* **2008**, 3915.

[34] R. M. Versteegen, R. P. Sijbesma, E. W. Meijer, *Macromolecules* **2005**, *38*, 3176.

[35] J. H. Hirschberg, L. Brunsveld, A. Ramzi, J. A. Vekemans, R. P. Sijbesma, E. W. Meijer, *Nature* **2000**, *407*, 167.

[36] R. P. Sijbesma, F. H. Beijer, L. Brunsveld, B. J. B. Folmer, J. H. K. K. Hirschberg, R. F. M. Lange, J. K. L. Lowe, E. W. Meijer, *Science* **1997**, *278*, 1601.

[37] F. H. Beijer, R. P. Sijbesma, H. Kooijman, A. L. Spek, E. W. Meijer, *J. Am. Chem. Soc.* **1998**, *120*, 6761.

[38] R. M. Versteegen, R. Kleppinger, R. P. Sijbesma, E. W. Meijer, *Macromolecules* **2006**, *39*, 772.

[39] J. H. K. K. Hirschberg, R. A. Koevoets, R. P. Sijbesma, E. W. Meijer, *Chem. Eur. J.* **2003**, *9*, 4222.

[40] G. M. Whitesides, E. E. Simanek, J. P. Mathias, C. T. Seto, D. Chin, M. Mammen, D. M. Gordon, *Acc. Chem. Res.* **1995**, *28*, 37.

[41] S. Sivakova, D. A. Bohnsack, M. E. Mackay, P. Suwanmala, S. J. Rowan, *J. Am. Chem. Soc.* **2005**, *127*, 18202.

[42] S. J. Rowan, P. Suwanmala, S. Sivakova, *J. Polym. Sci. Part A: Polym. Chem.* **2003**, *41*, 3589.

[43] C. P. Lillya, R. J. Baker, S. Hutte, H. H. Winter, Y. G. Lin, J. Shi, L. C. Dickinson, J. C. W. Chien, *Macromolecules* **1992**, *25*, 2076.

[44] D. Duweltz, F. Lauprêtre, S. Abed, L. Bouteiller, S. Boileau, *Polymer* **2003**, *44*, 2295.

[45] N. E. Botterhuis, D. J. M. van Beek, G. M. L. van Gemert, A. W. Bosman, R. P. Sijbesma, *J. Polym. Sci. Part A: Polym. Chem.* **2008**, *46*, 3877.

[46] M. Blomenhofer, S. Ganzleben, D. Hanft, H.-W. Schmidt, M. Kristiansen, P. Smith, K. Stoll, D. Maeder, K. Hoffmann, *Macromolecules* **2005**, *38*, 3688.

[47] Y. Matsunaga, N. Miyajima, Y. Nakayasu, S. Sakai, M. Yonenaga, *Bull. Chem. Soc. Jpn.* **1988**, *61*, 207.

[48] K. Hanabusa, C. Koto, M. Kimura, H. Shirai, A. Kakehi, *Chem. Lett.* **1997**, 429.

[49] Y. Yasuda, E. Iishi, H. Inada, Y. Shirota, *Chem. Lett.* **1996**, 575.

[50] A. Sakamoto, D. Ogata, T. Shikata, K. Hanabusa, *Macromolecules* **2005**, *38*, 8983.

[51] T. Shikata, Y. Kuruma, A. Sakamoto, K. Hanabusa, *J. Phys. Chem. B* **2008**, *112*, 16393.

[52] M. De Loos, J. H. Van Esch, R. M. Kellogg, B. L. Feringa, *Tetrahedron* **2007**, *63*, 7285.

[53] N. Mohmeyer, N. Behrendt, X. Zhang, P. Smith, V. Altstädt, G. M. Sessler, H.-W. Schmidt, *Polymer* **2007**, *48*, 1612.

[54] P. Besenius, G. Portale, P. H. H. Bomans, H. M. Janssen, A. R. A. Palmans, E. W. Meijer, *Proc. Natl. Acad. Sci. USA* **2010**, *107*, 17888.

[55]   M. P. Lightfoot, F. S. Mair, R. G. Pritchard, J. E. Warren, *Chem. Commun.* **1999**, 1945.

[56]   L. Brunsveld, A. P. H. J. Schenning, M. A. C. Broeren, H. M. Janssen, J. A. J. M. Vekemans, E. W. Meijer, *Chem. Lett.* **2000**, 292.

[57]   M. M. J. Smulders, A. P. H. J. Schenning, E. W. Meijer, *J. Am. Chem. Soc.* **2008**, *130*, 606.

[58]   P. J. M. Stals, J. F. Haveman, R. Martín-Rapún, C. F. C. Fitié, A. R. A. Palmans, E. W. Meijer, *J. Mater. Chem.* **2009**, *19*, 124.

[59]   P. Jonkheijm, P. van der Schoot, A. P. H. J. Schenning, E. W. Meijer, *Science* **2006**, *313*, 80.

[60]   Y. Nakano, T. Hirose, P.J.M. Stals, E.W. Meijer, A.R.A. Palmans, *Chem. Science*, DOI: 10.1039/C1SC00547B.

[61]   A.J. Markvoort, H.M.M. ten Eikelder, P.A.J. Hilbers T.F.A. de Greef, E.W. Meijer. *Nat. Commun.* accepted

[62]   F. Ilhan, M. Gray, V. M. Rotello, *Macromolecules* **2001**, *34*, 2597.

[63]   S. Chen, A. Bertrand, X. Chang, P. Alcouffe, C. Ladavière, J.-F. Gérard, F. Lortie, J. Bernard, *Macromolecules* **2010**, *43*, 5981.

[64]   D. Ogata, T. Shikata, K. Hanabusa, *J. Phys. Chem. B* **2004**, *108*, 15503.

[65]   S. Cantekin, D. W. R. Balkenende, M. M. J. Smulders, A. R. A. Palmans, E. W. Meijer, *Nat. Chem.* **2011**, *3*, 42.

[66]   Y. Wang, S. Ge, M. Rafailovich, J. Sokolov, Y. Zou, H. Ade, J. Lüning, A. Lustiger, G. Maron, *Macromolecules* **2004**, *37*, 3319.

[67]   P. J. M. Stals, M. M. J. Smulders, R. Martín-Rapún, A. R. A. Palmans, E. W. Meijer, *Chem. Eur. J.* **2009**, *15*, 2071.

[68]   S. H. M. Söntjens, R. A. E. Renken, G. M. L. van Gemert, T. A. P. Engels, A. W. Bosman, H. M. Janssen, L. E. Govaert, F. P. T. Baaijens, *Macromolecules* **2008**, *41*, 5703.

[69]   D. B. Klinedinst, E. Yilgör, I. Yilgör, F. L. Beyer, G. L. Wilkes, *Polymer* **2005**, *46*, 10191.

[70]   PhD Thesis, Brigitte Folmer. **2000**.

3

Effect of polarity on the self-assembly of benzene-1,3,5-tricarboxamides

Abstract. Benzene-1,3,5-tricarboxamides (BTAs) comprising alkyl side chains form supramolecular polymers in dilute solution and in the solid state as a result of the threefold helical arrangement of the intermolecular hydrogen bonds. We investigated systematically the role of polarity on the self-assembling behavior of BTAs in dilute solution and, when incorporated in polymeric materials, on their ability to phase segregate. In dilute solutions, the polarity was gradually increased by mixing in methyl *tert*-butyl ether (in which BTAs are molecularly dissolved) into methylcyclohexane (in which BTAs form stable helical aggregates). We observed a significant decrease in the stability of BTA aggregates after the addition of small amounts of ether. This strong dependence on the polarity of the environment was also found in the solid state. By end-capping telechelics of varying polarity with the BTA motif, a wide range of backbone polarities was covered. Commercially available polymers as well as polymers that were synthesized via ring-opening metathesis polymerization were evaluated. BTA motifs connected to apolar telechelics formed stable phase segregated nanorods. Increasing the polarity resulted in a decrease of the stability, and this eventually resulted in the loss of nanorod formation. This systematic study on the influence of polarity on self-assembly gives us a detailed understanding of the potential to use BTAs as functional nanorods in various applications.

3.1 Introduction

Benzene-1,3,5-tricarboxamides (BTAs) have been studied in detail as liquid crystals, organogelators and nucleating agents for poly(propylene).[1-7] A threefold helical arrangement of the intermolecular hydrogen bonds stabilizes the columnar packing of the BTA discs in the solid state and in dilute heptane solution.[8, 9] Circular dichroism (CD) spectroscopy showed that the introduction of homochiral side chains results in columnar structures with a preferred helicity.[10] In Chapter 2, we described that BTA motifs end-capped to or copolymerized with poly(ethylene-*co*-butylene) (pEB) induced physical cross-linking via the formation of nanorods in solution and in the solid state as evidenced by UV, CD and IR spectroscopy.[11] A distinct fibrillar structure was observed with atomic force microscopy which is indicative for phase segregation between the pEB soft phase and the BTA columnar aggregates. This intrinsic phase segregation of BTA nanorods with an amorphous polymer resulted in thermoplastic elastomeric behavior.

In solution, self-assembly based on hydrogen bonding is highly affected by the choice of solvent. Typically, low-polarity solvents are used to enhance the formation of hydrogen bonds or, alternatively, a hydrophobic shell is introduced to shield the hydrogen bonds from polar environments.[12-15] While BTAs form helical stacks in dilute solutions of apolar alkane solvents as a result of a high association constant (3×10^7 M^{-1}), the intermolecular hydrogen bonds disappear in more polar solvents like chloroform or methanol.[9, 10, 16] Moreover, in apolar solvents the propensity to form columnar helical stacks is significantly lowered when changing one alkyl side chain in a BTA to an oligo(ethylene oxide) side chain, due to a dramatic reduction of the association constant (20 M^{-1}) caused by backfolding of the oligo(ethylene oxide) side chain.[16, 17] This means that the self-assembly of BTAs into helical aggregates not only depends on the solvent polarity but also on the micro-environment of the BTA. The latter may have a significant impact on the material properties when designing biocompatible and biodegradable polymers end-capped with the BTA motif.

In this chapter, we investigate in detail the influence of the environment's polarity on the self-assembly behavior of BTAs in the solid state and in dilute solution. The ability of BTAs to form helical aggregates in dilute solution was taken as an indication for its tendency to phase segregate when incorporated in a polymer matrix. We first performed CD measurements on dilute solutions of BTA **1** (Scheme 3.1) in alkane/ether mixtures (c = 10^{-5} M), which allows us to investigate systematically the self-assembly of BTAs as a function of solvent polarity. Polarity effects in the solid state, and their influence on BTA nanorod formation, were evaluated by functionalizing telechelic polymers **4a-c** of varying polarity with a BTA precursor (Scheme 3.1). We selected three easily accessible amine-functional telechelic apolar pEB, polar poly-ε-caprolactone (pCL), and medium polar polytetrahydrofuran (pTHF), and subsequently end-capped these polymers with BTA

precursor **2** (Scheme 3.2). In addition, we gradually altered the polymer backbone's polarity by preparing copolymers **4d**-**g** of cyclooctene (CO) and the more polar 5-ethoxy cyclooctene (ECO) via ring opening metathesis polymerization (ROMP) (Scheme 3.3). Cyclooctene based monomers were selected because of their well-known reactivity in ROMP. We assumed that the difference in ring-strain between the two monomers is negligible and therefore leads to statistical copolymers. The telechelic amine polymers are readily accessible by using a protected amine as a chain transfer agent (CTA) during ROMP. The solid state properties of these polymers with a varying backbone polarity were investigated with CD spectroscopy, IR spectroscopy and differential scanning calorimetry (DSC) with the aim to relate backbone polarity to BTA nanorod formation and, ultimately, polymer properties.

Scheme 3.1. Chemical structures of compound **1** and BTA end-capped polymers **4a**-**g**.
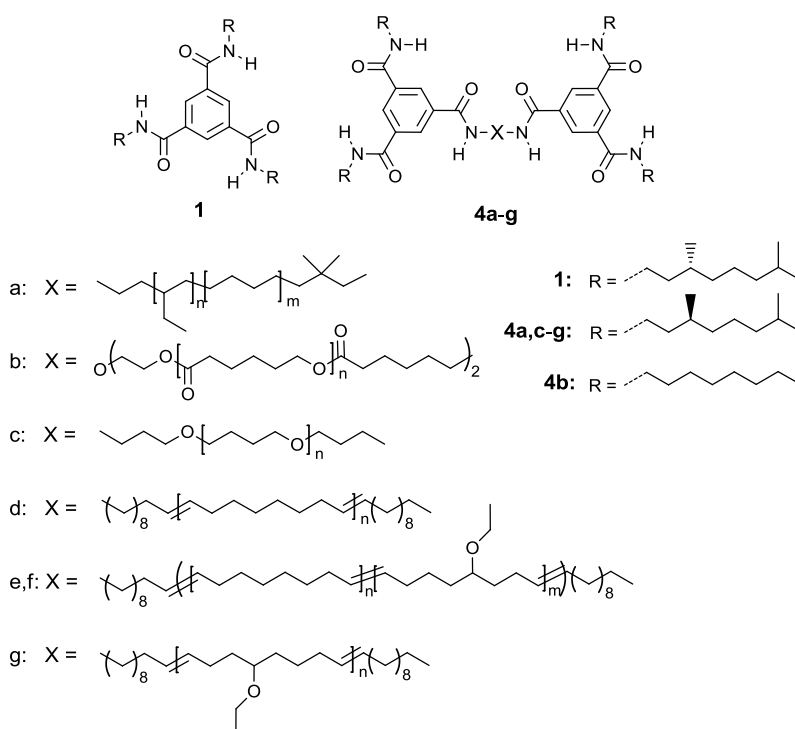
3.2 Polarity effects in dilute solutions of (*R*)-1

The self-assembly of BTA (*R*)-**1** in dilute solutions was previously studied in great detail.[10] In heptane, the formation of helical columnar aggregates is characterized by a λ_{max} of 192 nm in UV and a strong Cotton effect at 223 nm with $\Delta\varepsilon$ = +43 L/mol cm.[10, 18] In acetonitrile, a red shift in UV to 208 nm with a corresponding disappearance of the Cotton effect was attributed to the loss of intermolecular hydrogen bonds. Moreover, temperature-dependent CD measurements showed that the temperature-dependent aggregation could be described by a nucleation-elongation mechanism.[10, 19] In a nucleation-elongation mechanism, polymerization can only occur after nucleation (activation) of the monomer. This relatively

unfavorable nucleation step precedes the elongation regime of the polymerization and is governed by a dimensionless activation constant, K_a. A smaller K_a value corresponds to a higher degree of cooperativity. The addition of the monomer to the growing chain in the elongation regime is governed by an equilibrium constant K_e, which can be expressed as function of an elongation enthalpy, h_e, and an elongation temperature, T_e. This T_e separates the two polymerization regimes (*i.e.* the nucleation and elongation regime), while the elongation enthalpy is the enthalpy that is released due to the formation of non-covalent intermolecular interactions during the elongation phase. Quantitative data on the self-assembly process were obtained by fitting the temperature-dependent CD data to a nucleation-elongation model developed by van der Schoot:[10, 19]

$$CD(T) = CD_{SAT}\left[1 - \exp\left(\frac{-h_e}{RT_e^2}(T - T_e)\right)\right] \tag{3.1}$$

where CD_{SAT} is the maximal CD intensity at low temperature, h_e is the enthalpy release upon elongation, T_e is the elongation temperature, T is the temperature and R is gas constant. The temperature-dependent CD data were then normalized by dividing the CD value by CD_{SAT}, yielding the net helicity; $\phi = CD(T) / CD_{SAT}$ as the dimensionless y-axis.

We selected methyl *tert*-butyl ether (MTBE) as a solvent capable of interfering with the intermolecular hydrogen bonds because of its low UV cutoff and boiling point of 55 °C. We anticipated that the addition of small amounts of MTBE to methylcyclohexane (MCH), in which (R)-**1** forms long stable aggregates, reduces the average aggregate size and increases the fraction of (R)-**1** in the monomeric form.[18] CD spectroscopy on (R)-**1** in mixtures of MCH and MTBE was performed while the amount of MTBE was increased from 0% to 7.5% v/v. The concentration was kept constant at 10 μM. At room temperature, a linear decrease of the molar ellipticity at 223 nm was observed with increasing the amount of MTBE (Figure 3.1A). After the addition of 7.5% v/v MTBE, the CD effect was completely lost, which indicates that this solvent mixture is unable to stabilize the threefold hydrogen bonds required for the helical aggregate formation.

We then performed temperature-dependent CD spectroscopy measurements of (R)-**1** in mixtures of MCH and MTBE. Probing the CD effect at 223 nm, showed the sudden appearance of a CD effect upon cooling the solutions from 60 °C, at which (R)-**1** was molecularly dissolved, to 10 °C (cooling rate = 5 K min⁻¹) as is visible in Figure 3.1B. Non-sigmoidal curves were found for all mixtures, indicating a nucleation-elongation type self-assembly process, even when significant amounts of MTBE were added. The elongation temperature, T_e, is lowered and the slope of the curve (at the T_e), which is proportional to h_e, is decreased upon increasing the amount of MTBE.
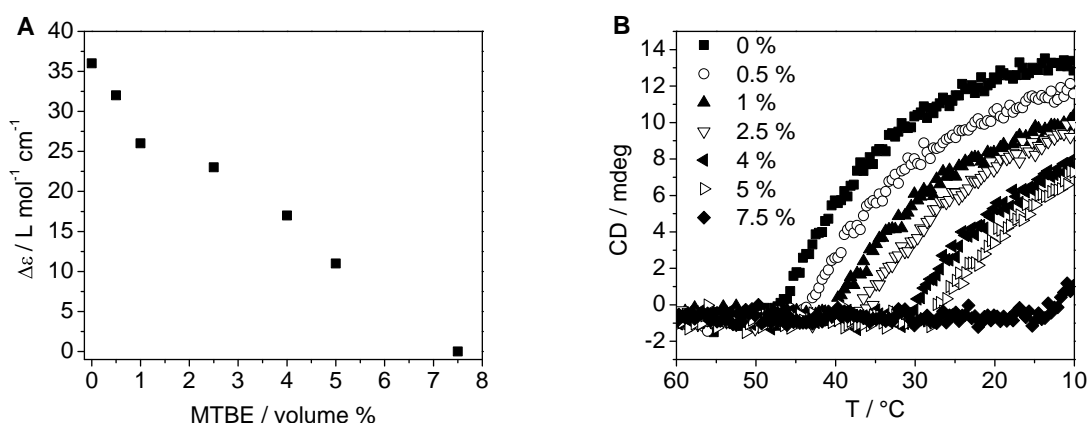
Figure 3.1. A) Decrease of $\Delta\varepsilon$ as a function of the amount of MTBE added (at 20 °C). B) CD cooling curves of (R)-**1** in MTBE/MCH mixtures at c = 10 µM.

Fitting the CD cooling curves to equation 3.1 allows deriving T_e and h_e values as a function of the amount of MTBE added. The data are summarized in Table 3.1. As expected, both T_e and h_e decrease. In fact, h_e is reduced to less than half of its original value when 7.5% of MTBE is added meaning that less enthalpy is released when aggregates are formed in more polar media because a larger number of BTAs is still in the monomeric form. The reduction of the T_e is a result of the solvent composition, which possesses better solvability properties upon the addition of MTBE. Therefore, a lower temperature is needed to form and stabilize aggregates.

Table 3.1. Thermodynamic parameters for the self-assembly of (R)-**1** in mixtures of MTBE/MCH (c = 10 µM).

MTBE in MCH [vol%]	0	0.5	1	2.5	4	5	7.5
h_e [kJ/mol]	-64.4	-58.8	-53.3	-47.5	-46.7	-36.6	-28.0
T_e [°C]	48	45	41	36	33	28	10

3.3 BTA end-capped polymers of different polarity

3.3.1 Synthesis

From our solution studies, we observed that a more polar environment causes a decrease in the stability of aggregates resulting in smaller values for the degree of aggregation, a lower h_e, and a lower T_e. As this may have dramatic effects on the properties of functional polymers end-capped with a BTA unit, we systematically varied the polymer backbone polarity to study its effect on the formation of BTA aggregates in the solid state. We first selected readily accessible polymers such as apolar pEB, medium polar pTHF and polar pCL, all

commercially available as hydroxy telechelic polymers. Both pEB —an amorphous apolar polymer— and pTHF —a semi-crystalline polyether— were chosen because of their promising ability to behave as the soft part in supramolecular thermoplastic elastomers.[20-22] PCL is a particularly interesting backbone because of its biocompatible and biodegradable character.[23] Amine telechelics **3a-c** were readily accessible via standard synthetic procedures and were subsequently coupled to BTA precursors (**2a-b**) using EDC as the coupling agent in the presence of DMAP (Scheme 3.2).

Scheme 3.2. Synthesis of pEB-bisBTA **4a**, pTHF-bisBTA **4b** and pCL-bisBTA **4c**.
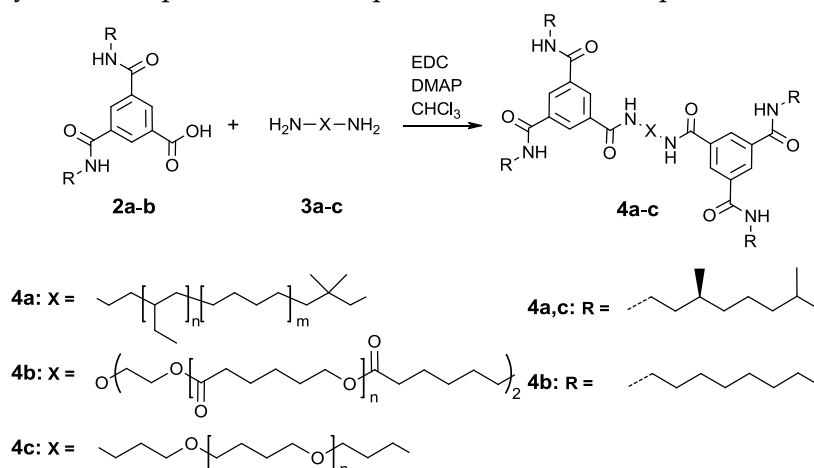
Polymers **4a-c** were obtained in an average yield of 60% and isolated in high purity as evidenced by ^{1}H-NMR and ^{13}C-NMR. GPC traces (polystyrene calibrated) showed molecular weights of 6.2, 12.4 and 4.2 kg/mol for **4a**, **4b** and **4c**, respectively, and low polydispersity indexes for all three polymers (Table 3.2). In order to systematically tune the polarity of the polymer backbone, we also designed amine telechelic polymers **3d-g** (Scheme 3.3). Here, the polarity of the backbone is varied by copolymerizing two monomers namely cyclooctene (CO) and the more polar racemic 5-ethoxycyclooctene (ECO) **6**. The latter is accessible in a one-step synthesis starting from 1,5-cyclooctadiene. The ether group in ECO not only increases the polarity but also acts as a hydrogen bond acceptor that might destabilize BTA aggregates, similarly to the effect of MTBE in the aggregation of *(R)*-**1** (*vide supra*). The monomers CO and ECO were selected because of their well-known reactivity in ROMP.[24] Moreover, similar ring strains were expected, which will result in the formation of random copolymers. The BTA end-groups were introduced by using a phthalimide based bifunctional chain transfer reagent (CTA) (Scheme 3.3). Conceptually, ROMP of a cyclic olefin in the presence of a symmetric CTA agent with two functional groups can be viewed as growing a polymer in between these groups. The phthalimide based CTA (**7**) was used for two reasons: (*i*) the phthalimide groups do not interfere with the ruthenium catalyst during polymerization, in contrast to BTA functionalized CTAs,[25] and (*ii*) phthalimide groups give easy access to amine end-groups (Scheme 3.3).

Four different phthalimide end-capped polymers were synthesized using CO and ECO as monomers namely p(CO) **8d**, p(CO-*co*-25%ECO) **8e**, p(CO-*co*-50%ECO) **8f** and p(ECO) **8g** (Scheme 3.3). All polymerizations were performed in dry toluene for 18 hours at 55 °C under an argon atmosphere. A monomer:initiator ratio of 5,000:1 was used with concentrations of about 2 M, allowing the end-group functionality to be >99%.[26, 27] According to ^{1}H-NMR, the observed ratio of CO:ECO in polymers **4e,f** is identical to the feed ratio, suggesting that the reactivity of both monomers is indeed equal (Table 3.2). Subsequently, the phthalimide groups were reduced to amines in a solution of hydrazine monohydrate in THF at reflux temperature. Telechelics **3d**-**g** were then coupled to the chiral BTA precursor **2a** to form BTA end-capped polymers **4d**-**g**. Polymers **4d**-**4f** were synthesized using *N,N'*-dicyclohexylcarbodiimide (DCC) as peptide coupling agent and 4-dimethylaminopyridine *para*-toluenesulfonate (DPTS) as the catalyst. Polymers **4d**-**4f** were purified by precipitation in methanol twice. Polymer **4g** was synthesized using *N*-(3-dimethylaminopropyl)-*N'*-ethylcarbodiimide hydrochloride (EDC) as the coupling agent in the presence of 4-dimethylaminopyridine (DMAP) for a more convenient work-up. Polymers **4d**-**g** were obtained in high yield and characterized with ^{1}H-NMR, ^{13}C-NMR and GPC. The results are summarized in Table 3.2.

Scheme 3.3. Synthetic approach to polymers **4d**-**g** with tunable polymer's backbone polarity.

According to ^{1}H-NMR and GPC all polymers had a similar molecular weight of around 4 kg/mol with a relatively low polydispersity of 1.4 (Table 3.2). The molecular weight of polymers **4a-g** was also easily estimated with ^{1}H-NMR by comparing signals from the aromatic BTA motif and various signals from the repeating unit. The degree of polymerization was around 20, which resulted in similar molecular weights compared to the functionalized commercially available telechelics (**4a-c**). Therefore, we can easily assess the influence of backbone polarity on the properties of BTA end-capped polymers and exclude effects of molecular weight.

Table 3.2 Summary of the ^{1}H-NMR, GPC and DSC data of polymers **4a-g**.

Polymer	backbone	Obs. ratio		Yield	M_n^a	M_n^b	PDI^b	T_g^c	T_{m1}^c	ΔH_1^c	T_{m2}^c	ΔH_2^c
		n	m	[%]	[kg/mol]	[kg/mol]	[-]	[°C]	[°C]	[J/g]	[°C]	[J/g]
		[%]	[%]									
4a	pEB	*n.a.*		60	4.4	6.2	1.12	-60	-	-	210	2.63
4b	pCL	*n.a*		60	5.8	12.4	1.15	-	44	58	-	-
4c	pTHF	*n.a.*		50	3.9	4.1	1.7	-	-	-	122	1.89
4d	pCO	100	0	85	3.8	5.5	1.25	-80	45	24	190	3.3
4e	p(CO-co-25%ECO)	75	25	75	3.6	6.5	1.55	-70	25	8	165	0.9
4f	p(CO-co-50%ECO)	50	50	70	3.6	8.0	1.87	-	-	-	150	0.6
4g	pECO	0	100	80	3.3	6.7	1.32	-	-	-	130	0.34

n.a. = not applicable. [a] Determined by ^{1}H-NMR. [b] Determined by GPC. [c] Derived from the third heating run (40 K min^{-1})

3.3.2 Thermal properties

As observed in Chapter 2, pEB —a viscous liquid at room temperature— became a solid after functionalization with two BTA units, and showed material properties similar to that of a soft rubber.[11] In contrast, pCL and pTHF did not show any remarkable changes in material properties after functionalization with the BTA unit. BTA functionalized telechelics **4d-e** did also not show any significant change in their physical appearance compared to **3d-e**. In contrast, amorphous polymers **4f-g** did change after functionalization from sticky viscous fluids to elastic solids. This change in physical appearance is indicative for the presence of phase segregated nanorods that act as physical cross-linkers.

To rationalize the differences, we performed DSC and polarization optical microscopy (POM) measurements on samples of BTA endcapped polymers **4a-g**. The DSC data of all polymers were derived from the third heating run (40 K/min) and summarized in Table 3.2. The DSC trace of pEB-bisBTA showed a T_g at -60 °C and a small transition around 195-215 °C

(ΔH = 2.63 J/g). With POM, we observed a mobile, birefringent texture typical for a nematic phase starting from 60 °C up to the clearing temperature around 200 °C, allowing us to attribute the transition at 195-215 °C to a transition into the isotropic state. In contrast, the DSC trace of pCL-bisBTA (**4b**) showed only one phase transition at 44 °C (ΔH = 58 J/g). This transition is related to the melting of the pCL backbone. The DSC trace of pTHF-bisBTA (**4c**) showed a small transition around 115-125 °C. Remarkably, no phase transition was observed that could be attributed to the melting of the pTHF backbone, typically found at 23 °C (for pTHF diol, M_n = 3000 g/mol).[28] This indicates that the presence of the BTA motifs hinders the crystallization of the pTHF backbone. With POM, we observed a mobile, birefringent texture indicative for a nematic phase starting from around 50 °C up to the clearing temperature around 120 °C.

In terms of backbone polarity, pEB-bisBTA (**4a**) and pCO-bisBTA (**4d**) are very similar, *i.e.* non-polar, although pCO is a semi-crystalline polymer (T_m = 50 °C, T_g = -90 °C) while pEB is amorphous. If the formation of BTA aggregates in the solid state is primarily governed by polarity effects, similar thermal properties could be expected for **4a** and **4d**. Indeed, the DSC trace of **4d** showed a T_g at -80 °C, a phase transition around 45 °C (ΔH = 24 J/g) corresponding to the melting of the pCO polymer and a small transition around 190 °C (ΔH = 3.3 J/g). With POM, we observed a mobile, birefringent texture typical for a nematic phase starting from 80 °C up to the clearing temperature around 190 °C. Clearly, the mobile birefringent phase and an isotropic transition around 190-210 °C for **4a**,**d** show the similarities of these polymer's thermal behavior. Moreover, pECO-bisBTA **4g** resembles pTHF-bisBTA **4c** with regard to its backbone polarity and also in this case the thermal behavior is rather similar. The DSC trace of compound **4g** showed a small phase transition at 130 °C (ΔH = 0.34 J/g), and POM revealed a mobile birefringent texture starting from around room temperature up to its clearing temperature of 130 °C, which is close to the clearing temperature of 120 °C found for pTHF-bisBTA **4c**.
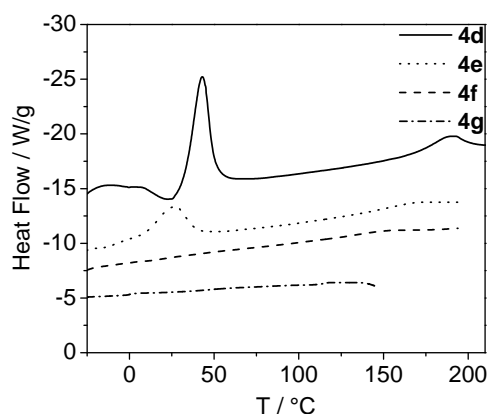
Figure 3.2. DSC traces of polymers **4d**-**g**.

As expected, copolymers p(CO-*co*-25%ECO)-bisBTA (**4e**) and p(CO-*co*-50%ECO)-bisBTA (**4f**) show a thermal behavior that is intermediate to that of **4d** and **4g** (Figure 3.2). P(CO-*co*-25%ECO)-bisBTA showed a T_g at -70 °C, a phase transition around 25 °C (ΔH = 8 J/g) and a small transition around 165 °C (ΔH = 0.9 J/g). POM showed a mobile birefringent texture starting from 50 °C up to clearing temperature of 165 °C. The DSC trace of compound **4f** showed a small phase transition at 150 °C (ΔH = 0.6 J/g) and POM revealed a mobile birefringent texture starting from around room temperature up to its clearing temperature at 150 °C. In fact, an interesting trend in the thermal behavior of **4d**-**4g** can be distinguished: polymers containing more ECO monomer are less crystalline and the liquid crystalline to isotropic phase transition temperature decreases.

3.3.3 CD spectroscopy in the solid state

Since BTAs form helical stacks with a preferred helicity in dilute solution, we wondered if the propensity to form helical stacks is retained when BTAs are embedded in a polymer matrix. We studied chiral polymers **4a**,**c**-**g** with CD spectroscopy to verify the presence of columnar helical structures as found for (*R*)-**1** in dilute solution. PCL (**4b**) was not functionalized with chiral side chains because the BTA motif is unable to form helical structures when embedded in a pCL matrix. Films of **4a**,**c**-**g** with a thickness of 250-650 nm were spin-coated from a CHCl₃ solution on quartz plates. CD spectra were recorded at room temperature and are shown in Figure 3.3. A clear Cotton effect was observed for **4a**,**c**-**g**, similar in shape and opposite in sign as observed for **1**. The latter was expected since an *R*-configuration was used for **1** while the polymers were functionalized with BTA precursors comprising the *S*-configuration. Moreover, the chirality of the BTA determines the helicity in the stacks as seen with BTAs in solution.[18] The CD effect was independent of the orientation of the quartz plate with respect to the beam, excluding linear dichroism effects. This suggests that the helical order present in a dilute solution of **1** is also present in the solid state of **4a**,**c**-**g**. The CD-effect of pCO-bisBTA (**4d**) is about twice as large compared to that of p(CO-*co*-50%ECO)-bisBTA (**4f**) and pECO-bisBTA (**4g**) (Figure 3.3A). This suggests that the BTA motifs in polar polymers **4f**,**g** are relatively more present in the monomeric form instead of in the aggregated form, leading to the formation of smaller or fewer stacks.
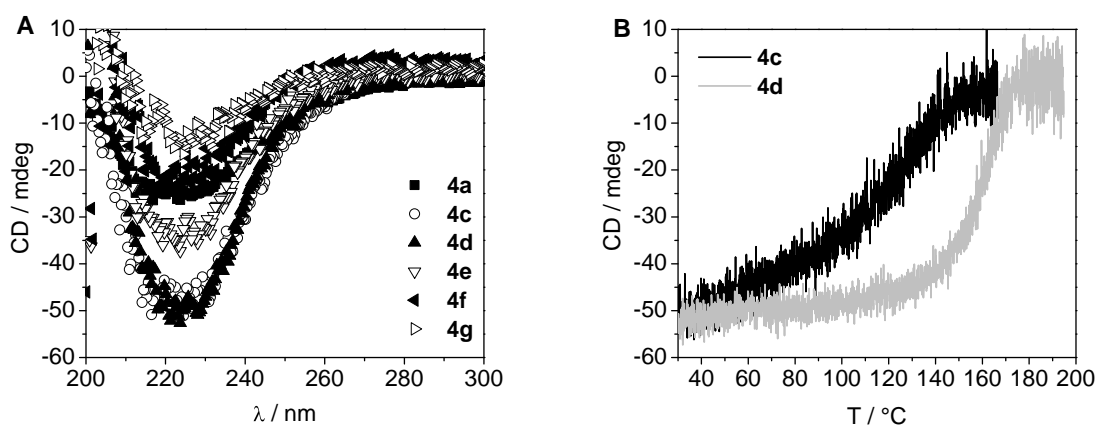
Figure 3.3. A) CD spectra of spin-coated films of **4a,c-g**. Film thickness of **4a,c-g** is 320 nm, 650 nm, 600 nm, 550 nm, 500 nm and 260 nm, respectively (at room temperature). B) CD absorption at $\lambda = 225$ nm versus temperature of spin-coated films of **4c,d**.

DSC and POM results of polymers **4a,c-g** showed a decrease of the solid to isotropic phase transitions with increasing polarity. Temperature dependent CD measurements on polymers **4a,c-g** can elucidate if this difference in thermal behavior is related to the helical aggregation of BTAs embedded in the polymer matrix. We selected pTHF-bisBTA (**4c**) and pCO-bisBTA (**4d**) because of their large difference in polarity and their similar film thicknesses. The temperature was increased from 30 °C to 200 °C with a rate of 5 K min^{-1}. The CD effect was monitored upon heating at $\lambda_{max} = 225$ nm and plotted versus temperature (Figure 3.3B).

Both polymers showed a decrease of the CD effect upon heating. The CD effect of pTHF-bisBTA (**4c**) decreased gradually and was completely absent above 140 °C. Apolar polymer pCO-bisBTA (**4d**) showed a more sudden decrease of the CD effect and the decrease started at a higher temperature and disappeared at around 180 °C. The CD effects of pTHF-bisBTA and pCO-bisBTA disappeared at similar temperatures at which the mesophase to isotropic transition was observed in DSC and POM (120 °C and 190 °C, respectively). This indicates that indeed this phase transition is related to the disappearance of the helical arrangement of BTAs in the polymer matrix.

In addition to the differences of the temperature at which the CD effects disappear, we also observe a difference in the slope of the CD effect upon heating (Figure 3.3B). Interestingly, the slope of **4d** is steeper compared to the slope of the more polar polymer **4c**. A similar difference in the slope is observed in cooling experiments of the monomeric BTA (**1**) dissolved in mixtures of MCH and MTBE (*vide supra*). With increasing concentration of MTBE and thus polarity, the slope of the CD effect upon cooling becomes less steep. The slope is related to the enthalpy change upon aggregation (h_e), which reflects the amount of energy that is released during the formation of hydrogen bonds. Assuming that the disassembly of BTAs in **4c,d** upon heating (5 K min^{-1}) occurs under thermodynamic

conditions, a less steep slope indicates that less hydrogen bonds are formed in the more polar pTHF-bisBTA compared to the apolar pCO-bisBTA. In addition, the steepness of the slope of the Cotton effect versus temperature when altering the polarity, is higher in spin-coated films of **4c,d** compared to the steepness of the slope of **1** in dilute solutions. This observation is presumably related to the presence of phase segregation in the solid films of **4c,d**. In Chapter 2, we proposed that phase segregation is an additional interaction that drives the self-assembly of BTAs and the degree of phase segregation depends on the temperature. Phase segregation is more pronounced in the apolar pCO than in the more polar pTHF and has therefore a greater contribution to the effective concentration and to the change of the effective concentration by varying the temperature. The presence of phase segregation in the polymer rationalizes the differences in steepness of the slopes of the Cotton effect versus temperature of **4c,d**.

3.3.4 Infrared spectroscopy

The mesophase to isotropic transition observed in compounds **4a,c-g** appears to be connected to the loss of the intermolecular hydrogen bonds and corresponding disappearance of the BTA aggregates in the solid state, while for compound p(CL)-bisBTA (**4b**) no such transition was observed at all. To investigate this in more detail, we performed IR measurements on polymers **4a-g**, since this is a sensitive technique to investigate hydrogen bonding in the solid state.[9, 16]

Table 3.3. Summary of the IR spectroscopy data of compounds **1** and **4a-g**. Determined at 20 °C in the solid state.

Compound	ν (N-H) [cm^{-1}]	ν (amide I) [cm^{-1}]	ν (amide II) [cm^{-1}]
1	3226	1637	1563
4a	3236	1637	1563
4b	3330	1645	1535
4c	3240	1642	1562
4d	3241	1640	1560
4e	3245	1641	1559
4f	3245	1641	1559
4g	3243	1641	1558

At room temperature, the solid state IR spectrum of **4a** shows vibrations at positions typical for amides involved in threefold helical hydrogen bonds (ν(NH) 3236 cm^{-1}, ν(amide I) 1637 cm^{-1} and ν(amide II) 1563 cm^{-1}).[9, 16] Variable temperature IR reveals shifting of the characteristic vibrations starting at 100 °C up to 200 °C (see Figure 3.4). This allows us to

attribute the phase transition around 200 °C to the loss of the threefold helical hydrogen bonds. In contrast, the vibrations typical for amides involved in threefold hydrogen bonded arrangement were absent in case of pCL-bisBTA (**4b**) at room temperature. In fact, polymer **4b** showed a very broad N-H stretching vibration signal with a maximum peak height at 3330 cm^{-1}. Also, the distance between the amide I and amide II vibrations signals is relatively large (1645 cm^{-1} - 1535 cm^{-1}). Moreover, the amide I vibration signal is split up. The most likely reason is that the broad structure of the vibrational mode is caused by the superposition of many sharper bands of a variety of species, indicative for the presence of randomly dispersed BTAs.[29] The IR spectrum of pTHF-bisBTA (**4c**) in the solid state at room temperature does show vibrations at positions typical for amides involved in the threefold hydrogen bonded arrangement. Variable temperature IR showed a gradual shifting of the characteristic vibrations starting at 95 °C to 120 °C and allows us to attribute the phase transition around 120 °C to the loss of threefold helical hydrogen bonds (Figure 3.4). At room temperature, polymers **4d**-**g** show also vibrations around the typical positions for amides involved in threefold hydrogen bonding. Variable temperature IR revealed a gradual shifting of the characteristic vibrations starting from room temperature up to the clearing temperature and allows us to attribute the transitions (T_{m2}) observed in DSC to the loss of threefold helical hydrogen bonds. The position of the NH-stretch and amide II vibration versus temperature is plotted in Figures 3.4. A shift in wavenumber with increasing temperature, which becomes more intense at the clearing temperature, is observed for all four polymers. Compound **4d** has the most abrupt shift very close to the clearing temperature around 190 °C. In contrast, **4g** has a more gradual shift towards the clearing temperature at 130 °C. The characteristic vibrations for amides involved in threefold hydrogen bonding disappear with increasing temperature. Moreover, this occurs at a lower temperature for polymers consisting of more polar ethoxy side groups.
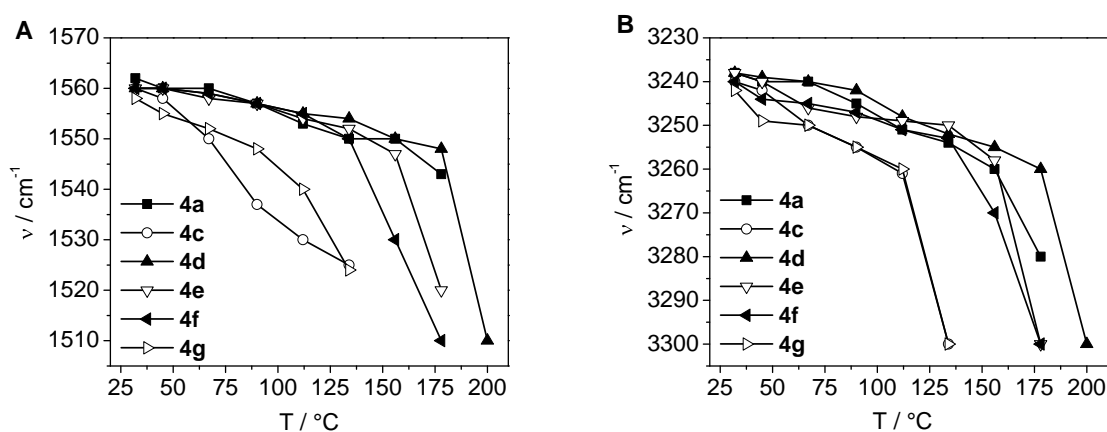
Figure 3.4. Infrared spectroscopy of **4a,c-g**. A) Position of the amide II vibration versus temperature. B) Position of the NH-stretch vibration versus temperature.

A significant difference is observed in the role of BTAs as physical cross-linker when coupled to pCL or the other polymers and copolymers. PEB-bisBTA (**4a**) has a clearing temperature close to the clearing temperature of *(R)*-**1** (236 °C).[9] This suggests that the aggregation of BTAs in **4a** is barely influenced by the presence of the polymer and therefore has the ability to form phase segregated nanorods. This phase transition is observed at a much lower temperature for pTHF-bisBTA and is totally absent in pCL-bisBTA. The pCL polymer backbone of **4b** consists of many ester bonds and particularly the carbonyls are strong hydrogen bonding accepting groups. The carbonyls compete with intermolecular hydrogen bonding, which results in less or in the absence of intermolecular hydrogen bonding of BTAs. Polymers **4d**-**g** showed a similar trend in which increasing the ether group content results in a decrease of the stability of BTA aggregates. This resulted in lower clearing temperatures caused by the loss of helical intermolecular hydrogen bonding, as evidenced by IR and CD spectroscopy.

3.4 Conclusions

The polarity of the environment is a determining factor in the hydrogen bonded directed self-assembly of BTAs in dilute solution and on their ability to act as physical cross-linkers in polymeric systems. Apolar solvents like heptane or MCH stabilize intermolecular hydrogen bonding of BTAs, resulting in the formation of stable helical aggregates even in very dilute conditions. Addition of small amounts of polar MTBE to solutions of BTAs in MCH decreased the stability of the system. This increase of polarity stimulates the presence of BTAs in the monomeric form, which results in a decrease of the CD effect. The elongation temperature (T_e) decreases with increasing polarity because more polar solvent mixtures are more capable of stabilizing the monomers. Also the enthalpy gain upon elongation decreases with increasing polarity indicating that less hydrogen bonds are formed in BTA aggregates. BTAs became molecularly dissolved after the addition of 7.5 volume % MTBE in MCH at 20 °C.

The polarity of the solvent evidently plays an important role in the stabilization of BTA aggregates in dilute solutions. Since aggregation in dilute conditions is an indication for the formation of phase segregated nanorods in the solid state, we translated the effect of polarity in dilute solution to the solid state. Functionalization of the highly apolar pEB with BTAs resulted in a phase segregated polymer. Unfortunately, functionalizing pCL with BTA motifs did not lead to any significant changes. DSC and IR suggest the absence of BTA phase segregated nanorods in pCL. Since pCL is a highly polar polymer we assume that the oxygen atoms in the ester groups compete with intermolecular hydrogen bonding and therefore destabilize BTA aggregates. Anticipating on this hypothesis we synthesized via ROMP four different amine telechelics comprising a predetermined amount of oxygen atoms in the polymer backbone. We found a direct relationship between the polarity of the polymer

backbone and the ability of the BTA to form phase segregated nanorods. We observed a decrease of the solid to isotropic phase transitions temperature with increasing polarity. This phase transition is related to the loss of intermolecular hydrogen bonds as confirmed with IR and CD spectroscopy. We can conclude that polarity effects play a key role in the formation and stabilization of BTA aggregates in dilute solution and in the solid state. On one hand, it clearly shows the limitations in choice of the environment in which BTAs can be applied as orderings motif in supramolecular materials. On the other hand, control over the self-assembly can be obtained, by introducing subtle changes in the polarity of the environment. Since hydrogen bond strength in general, highly depends on the environment, the outcome of this systematic study can be broadly applied in the design and development of novel hydrogen bonded supramolecular polymers.

3.5 Experimental

Materials

3,5-Bis-(3S)-(3,7-dimethyl-octylaminocarbonyl)-benzoic acid **(2a)**, 3,5-bis-octylaminocarbonyl-benzoic acid **(2b)**, N,N'(1,20-eicos-10-endiyl)-bis-(isoindole-1,3-dione) **(7)**, bis(3-aminopropyl)-poly(tetrahydrofuran) (DSC: T_m = 23 °C, ΔH = 70.69 J/g, M_n = 2800 g/mol, *PDI* = 1.33) **(3c)** and bisamino-poly(ε-caprolactone) (DSC: T_m = 43 °C, ΔH = 62 J/g, GPC: M_n = 5821 g/mol, *PDI* = 1.27) **(3b)** and poly(ethylene/butylene)-bisBTA (M_n = 3500 g/mol, *PDI* = 1.08) **(4a)** were synthesized according to literature procedures.[11, 20, 27, 30] All reagents were purchased from Aldrich or Acros Organics and used as received unless otherwise specified. All solvents were purchased from Biosolve. Dichloromethane and toluene were freshly distilled from sodium before use. THF and chloroform were dried over molecular sieves before use. All ring-opening metathesis polymerizations were performed using the second generation Grubbs-type initiator, which was purchased from Aldrich. Deuterated solvents were purchased from Cambridge Isotopes Laboratories. All reactions were run in flame-dried glassware under an argon atmosphere.

Instrumentation and Analysis

CD and UV spectra were recorded on a Jasco J-815 CD spectrometer equipped with a Jasco PTC-348 WI temperature controller. Experiments were conducted using spectroscopic grade methylcyclohexane or methyl *t*-butyl ether as the solvent. Cells with an optical path length of 1 cm were applied (for ~10^{-5} M solutions). The molar ellipticity is calculated as: $\Delta\varepsilon$ = CD-effect/(32980xcxl) where c is the concentration in mol/L and l = the optical path length in cm. Films of **4a,c-g** were prepared by making solutions of **4a,c-g** in chloroform (50 mg/mL) and spin-coating a volume of 0.5 mL on 0.40 cm^2 quartz slides at 800 rpm for two minutes. The film thickness was determined with a Tencor P-10 surface profiler. Variable temperature CD measurements on the spin-coated films were performed by mounting the Linkam THMS 600

heating device into the CD apparatus, which allowed heating up to 250 °C. ^{1}H-NMR and ^{13}C-NMR spectra were recorded on a Varian Gemini 400 MHz NMR (400 MHz for ^{1}H-NMR and 100 MHz for ^{13}C-NMR). Proton chemical shifts are reported in ppm downfield from tetramethylsilane (TMS). Carbon chemical shifts are reported downfield from TMS using the resonance of the deuterated solvent as the internal standard. IR spectra were recorded on a Perkin Elmer 1600 FT-IR. Temperature variable IR spectra were recorded on an Excalibur FTS 3000 MX FT-IR from Biorad. GC/MS measurements for performed on a GC-MS QP5000 by Shimadzu equipped with a Phenomenex Zebron ZB-35 column. POM measurements were performed using a Jenaval polarisation microscope equipped with a Linkam THMS 600 heating device. The thermal transitions were determined with DSC using a Perkin-Elmer DSC–7 or a TA Q2000 under a nitrogen atmosphere with heating and cooling rates of 40 K/min. The thermal transitions and the corresponding enthalpy changes were derived from the third heating run. GPC measurements were performed on a Resi Pore column with chloroform as the eluent (flow = 1 mL/min) and employing a PDA (λ = 254 nm) as the detector. The molecular weights were determined using the polystyrene calibration method.

Synthesis

pCL-bisBTA (**4b**). A solution of *N*-(3-dimethylaminopropyl)-*N'*-ethylcarbodiimide hydrochloride (EDC) (0.42 mmol, 105 mg) in 2 mL dry CHCl$_3$ was added to an ice cooled stirred solution of **2b** (0.3 mmol, 127 mg), 4-dimethylaminopyridine (DMAP) (0.42 mmol, 51 mg) and **3b** (0.14 mmol, 300 mg) in dry CHCl$_3$ (25 mL). The reaction mixture was allowed to warm to room temperature and stirred overnight. Then the mixture was diluted with CHCl$_3$ (50 mL) and washed successively with HCl (1M, 50 mL), NaHCO$_3$ (10%, 20 mL) and NaCl$_{aq}$ (saturated, 20 mL). CHCl$_3$ was removed *in vacuo*. The product was precipitated first in cold heptane and then in methanol, and obtained as a white solid. Yield = 170 mg, 50%. ^{1}H-NMR (400 MHz, CDCl$_3$, δ): 8.39 (s, 6H, Ar-H), 6.61 (t, 2H, NH), 6.51 (t, 4H, NH), 4.23 (t, 4H, OCH$_2$C$\underline{H}_2$OC=O), 4.06 (t, 2H, CH$_2$OC=O), 3.69 (t, 4H, OC$\underline{H}_2$CH$_2$OC=O) 3.47 (t, 12H, CONHC$\underline{H}_2$), 2.31 (t, 2H, OC=OCH$_2$), 1.8-0.85 (alkyl). ^{13}C-NMR (100 MHz, CDCl$_3$, δ): 173.8 (C=O), 165.9 (ArC=O), 135.3 (ArC), 127.9 (ArC), 64.4 (CH$_2$OC=O), 40.6 (CH$_2$NH), 34.0, 31.6, 29.1, 28.4, 26.9, 25.7, 24.8, 22.5, 14.3. IR: ν (cm^{-1}): 3333 (N-H stretch), 1664 (amide I), 1541 (amide II). GPC: M_n = 12.4 kg/mol, M_w = 14.2 kg/mol, *PDI* = 1.15. DSC (40 K/min): T_m = 43 °C, ΔH = 63 J/g.

pTHF-bisBTA (**4c**). A solution of EDC (0.54 mmol, 105 mg) in 15 mL dry CHCl$_3$ was added to an ice cooled stirred solution of **2a** (0.4 mmol, 173 mg), DMAP (0.54 mmol, 66 mg) and **3c** (0.18 mmol, 528 mg) in dry CHCl$_3$ (25 mL) The reaction mixture was allowed to warm to room temperature and stirred overnight. Then the mixture was diluted with CHCl$_3$ (50 mL) and washed successively with HCl (1M, 50 mL), NaHCO$_3$ (10%, 20 mL) and NaCl$_{aq}$

(saturated, 20 mL). The product was concentrated and precipitated in cold ether and obtained as a white solid. Yield = 223 mg, 64%. ^{1}H-NMR (400 MHz, CDCl$_3$, δ): 8.32 (s, 6H, Ar-H), 7.40 (s, 2H, NH), 6.81 (s, 4H, NH), 3.57 (t, 8H, C$\underline{H}_2$NH), 3.41 (t, 83H, OC$\underline{H}_2$CH$_2$) 3.24 (t, 4H, NHC$\underline{H}_2$(CH$_2$)$_2$O), 2.56 (m, 83H, OCH$_2$C$\underline{H}_2$), 1.88 (m, 4H, OCH$_2$C$\underline{H}_2$CH$_2$NH), 1.70-1.27 (42H, alkyl), 0.87 (t, 12H, CH$_3$). ^{13}C-NMR (100 MHz, CDCl$_3$, δ): 165.8 135.4, 128.0, 70.6, 40.1, 31.6, 29.3, 26.4, 22.5, 14.0. IR: ν (cm^{-1}): 3241 (N-H stretch), 1640 (amide I), 1557 (amide II). GPC: M_n = 4135 g/mol, M_w = 7055 g/mol, PDI = 1.7. DSC (40 K/min): T_m = 122 °C, ΔH = 1.9 J/g.

5-Ethoxycyclooctene (**6**). Cyclooctadiene (10.0 g, 92.5 mmol) was dissolved in 250 mL ethanol and added dropwise to a suspension of Hg(OAc)$_2$ (29.5 g, 92.5 mmol) in 250 mL ethanol and stirred for 1 hour at room temperature. Subsequently, 200 mL of NaOH (2 M) was added to the solution followed by the dropwise addition of a solution of NaBH$_4$ (3.78 g, 100 mmol) in 200 mL NaOH (2 M) and stirred for 1 hour at room temperature. Ethanol was removed *in vacuo* followed by the addition of NaCl (25 gram). The aqueous solution was washed two times with 250 mL diethylether. The organic layers were collected and washed two times with 300 mL NaCl$_{aq}$ (saturated) and dried over MgSO$_4$. Diethylether was removed *in vacuo* and the product was purified by column chromatography (Silica gel 40-63μm, 60Å CHCl$_3$/MeOH, 95/5, R_f = 0.4). Yield = 6.0 g, 55%. ^{1}H-NMR (400 MHz, CDCl$_3$, δ): 5.75-5.55 (m, 2H, -C$\underline{H}$=C$\underline{H}$-), 3.5-3.4 (m, 2H, -O-C$\underline{H}_2$CH$_3$), 3.38-3.35 (m, 1H, (CH$_2$)$_2$-C$\underline{H}$-O-), 2.39-1.3 (m, 10H, alkyl), 1.26-1.1 (m, 3H, -O-CH$_2$C$\underline{H}_3$), ^{13}C-NMR (100 MHz, CDCl$_3$, δ): 130.8 ($\underline{C}$=C), 129.5 (C=$\underline{C}$), 80.3 ((CH$_2$)$\underline{C}$H), 63.5 (O$\underline{C}$H$_2$CH$_3$), 34.4, 33.6, 29.7, 26.3, 25.8, 24.0, 22.7, 15.6. GC/MS: calculated for C$_{10}$H$_{18}$O (*m/z*) 154.25; found 154.

General procedure for the ring-opening metathesis polymerization of cyclic olefins in the presence of a chain transfer agent. The reactions were carried out in "dry" and oxygen poor toluene (oxygen was reduced by purging with argon) under an argon atmosphere. The monomers, or mixtures of monomers, were dissolved together with the chain transfer agent in toluene. The reaction mixtures were stirred and heated to 55 °C. Subsequently, the Grubbs 2nd generation catalyst was added. After 18 hours the reaction mixtures were cooled down to room temperature. The reaction mixtures were concentrated *in vacuo* and the polymers were precipitated from toluene in cold methanol. White/yellowish powdery or waxy solids were obtained by filtration or decantation in a typical yield of about 90%. All polymers were synthesized using similar amounts and ratios of monomer, chain transfer agent and catalyst at the same molar concentration.

p(CO) bis-phthalimide (**8d**). Cyclooctene (1.41 g, 12.8 mmol) was dissolved together with *N,N'(1,20-eicos-10-endiyl)-bis-(isoindole-1,3-dione)* (0.37 g, 0.641 mmol) in 5 mL toluene. Subsequently, a solution of Grubbs' 2nd generation initiator (2.17 mg, 0.00256 mmol) was added. The reaction mixture was stirred for 18 hours at 55 °C. The reaction mixture was

concentrated and precipitated from toluene in methanol. The polymer was obtained by filtration as a white powder. Yield = 95%. ^{1}H-NMR (400 MHz, CDCl$_3$, δ): 7.82 (m, 4H, Ar-H), 7.72 (m, 4H, Ar-H), 5.39 (m, 2H, C$\underline{H}$CH$_2$), 3.73 (t, 4H, (CO)$_2$NCH$_2$)), 1.97 (m, 4H, CHC$\underline{H}_2$), 1.64-1.15 (alkyl). M_n = 2812 g/mol (^{1}H-NMR).

p(CO-co-25%ECO) bis-phthalimide (**8e**). Yield = 94%. ^{1}H-NMR (400 MHz, CDCl$_3$, δ): 7.89 (m, 4H, Ar-H), 7.81 (m, 4H, Ar-H), 5.40 (m, 2H, C$\underline{H}$CH$_2$), 3.75 (t, 4H, (CO)$_2$NCH$_2$)) 3.50-3.40 (m, 2H, -O-C$\underline{H}_2$CH$_3$), 3.38-3.35 (m, 1H, (CH$_2$)$_2$-C$\underline{H}$-O-), 2.45-0.88 (alkyl). M_n = 2652 g/mol (^{1}H-NMR).

p(CO-co-50%ECO) bis-phthalimide (**8f**). Yield = 90%. ^{1}H-NMR (400 MHz, CDCl$_3$, δ): 7.87 (m, 4H, Ar-H), 7.75 (m, 4H, Ar-H), 5.40 (m, 2H, C$\underline{H}$CH$_2$), 3.73 (t, 4H, (CO)$_2$NCH$_2$)) 3.50-3.40 (m, 2H, -O-C$\underline{H}_2$CH$_3$), 3.38-3.35 (m, 1H, (CH$_2$)$_2$-C$\underline{H}$-O-), 2.45-0.88 (alkyl). M_n = 2600 g/mol (^{1}H-NMR).

p(ECO) bis-phthalimide (**8g**). Yield = 85%. ^{1}H-NMR (400 MHz, CDCl$_3$, δ): 7.84 (m, 4H, Ar-H), 7.72 (m, 4H, Ar-H), 5.40 (m, 2H, C$\underline{H}$CH$_2$), 3.65 (t, 4H, (CO)$_2$NCH$_2$)) 3.58-3.40 (m, 2H, -O-C$\underline{H}_2$CH$_3$), 3.38-3.35 (m, 1H, (CH$_2$)$_2$-C$\underline{H}$-O-), 2.45-0.88 (alkyl). M_n = 2348 g/mol (^{1}H-NMR).

General procedure for synthesis of amine end-functionalized polymers. The following procedure was used for all phthalimide end-capped polymers using the same reaction conditions. *p(CO) bis-amine* (**3d**). Hydrazine monohydrate and p(CO) bis-phthalimide (**8d**) (1.3 g, 0.46 mmol) were dissolved in 20 mL THF and heated at 90 °C for 18 hours. The reaction mixture was allowed to cool down to room temperature. THF and the excess of hydrazine were removed *in vacuo*. Then 50 mL of chloroform was added to the mixture. The mixture was washed three times with 75 mL NaOH (1M) and two times with 75 mL NaCl$_{aq}$ (sat.). The organic layer was dried over MgSO$_4$ and the solvent was removed *in vacuo*. Yield = 95%. ^{1}H-NMR (400 MHz, CDCl$_3$, δ): 5.39 (m, 2H, C$\underline{H}$CH$_2$), 2.65 (t, 2H, -C$\underline{H}_2$NH$_2$) 1.97 (m, 4H, CHC$\underline{H}_2$), 1.64-1.15 (alkyl). M_n = 2518 g/mol (^{1}H-NMR).

p(CO-co-25%ECO) bis-amine (**3e**). Yield = 93%. ^{1}H-NMR (400 MHz, CDCl$_3$, δ): 5.40 (m, 2H, C$\underline{H}$CH$_2$), 3.5-3.4 (m, 2H, -O-C$\underline{H}_2$CH$_3$), 3.38-3.35 (m, 1H, (CH$_2$)$_2$-C$\underline{H}$-O-), 2.65 (t, 2H, -C$\underline{H}_2$NH$_2$), 2.40-0.88 (alkyl). M_n = 2358 g/mol (^{1}H-NMR).

p(CO-co-50%ECO) bis-amine (**3f**). Yield = 90%. ^{1}H-NMR (400 MHz, CDCl$_3$, δ): 5.40 (m, 2H, C$\underline{H}$CH$_2$), 3.5-3.4 (m, 2H, -O-C$\underline{H}_2$CH$_3$), 3.38-3.35 (m, 1H, (CH$_2$)$_2$-C$\underline{H}$-O-), 2.62 (t, 2H, -C$\underline{H}_2$NH$_2$), 2.40-0.88 (alkyl). M_n = 2308 g/mol (^{1}H-NMR).

p(ECO) bis-amine (**3g**). Yield = 80%. ^{1}H-NMR (400 MHz, CDCl$_3$, δ): 5.40 (m, 2H, C$\underline{H}$CH$_2$), 3.5-3.4 (m, 2H, -O-C$\underline{H}_2$CH$_3$), 3.38-3.35 (m, 1H, (CH$_2$)$_2$-C$\underline{H}$-O-), 2.60 (t, 2H, -C$\underline{H}_2$NH$_2$), 2.39-0.88 (alkyl). M_n = 2056 g/mol (^{1}H-NMR).

General procedure for benzene-1,3,5-tricarboxamide end-capped polymers. The following procedure was used for polymers **4d**-**4f** using the same reaction conditions.

p(CO)-bisBTA (**4d**). Polymer **3d** (0.75 g, 0.35 mmol), 3,5-bis-(3*S*)-(3,7-dimethyl-octylaminocarbonyl)-benzoic acid (**2a**) (0.28 g, 0.78 mmol), *N,N′*-dicyclohexylcarbodiimide (DCC) (0.23 g, 1.5 mmol) and 4-dimethylaminopyridine *para*-toluenesulfonate (DPTS) (0.169 g, 1.5 mmol) were dissolved in 25 mL $CHCl_3$ and stirred for 18 hours at room temperature. The reaction mixture was concentrated to 3 mL and precipitated in methanol twice. Yield = 85%. ^{1}H-NMR (400 MHz, $CDCl_3$, δ): 8.34 (s, 6H, Ar-H), 6.43 (t, 6H, NH), 5.38-5.30 (m, 2H, C*H*CH_2), 3.47 (m, 12H, CONHC$\underline{H}_2$), 1.97 (m, 4H, CHC$\underline{H}_2$), 1.64-1.15 (alkyl), 0.88 (t, 12H, CH_3). ^{13}C-NMR (100 MHz, $CDCl_3$, δ): 165.8 (C=O), 135.5 (ArC), 130.3 (ArC), 129.8 (C=C), 128.0 (C=C), 40.5 (NH-CH_2), 32.6, 31.8, 29.6, 28.9, 27.1, 22.4, 14.0. IR: ν (cm^{-1}) 3241 (N-H stretch), 1640 (amide I), 1560 (amide II). GPC: M_n = 5.5 kg/mol, M_w = 6.9 kg/mol, *PDI* = 1.25.

p(CO-co-25%ECO)-bisBTA (**4e**). Yield = 75%. ^{1}H-NMR (400 MHz, $CDCl_3$, δ): 8.4 (s, 6H, Ar-H), 6.53 (t, 6H, NH), 5.38-5.30 (m, 2H, C*H*CH_2), 3.5-3.4 (m, 2H, -O-C$\underline{H}_2$CH$_3$), 3.47 (m, 12H, CONHC$\underline{H}_2$), 3.38-3.35 (m, 1H, (CH_2)$_2$-C*H*-O-), 1.97 (m, 4H, CHC$\underline{H}_2$), 1.64-1.15 (alkyl), 0.88 (t, 12H, CH_3). ^{13}C-NMR (100 MHz, $CDCl_3$, δ): 165.8 (C=O), 135.4 (ArC), 130.7 (ArC), 129.7 (C=C), 127.9 (C=C), 64.1 (CH-O-CH_2CH_3), 39.2 (NH-CH_2), 38.5, 36.6, 34.1, 30.7, 32.7, 29.5, 28.6, 28.0, 27.2, 25.4, 22.7, 19.9, 14.8. IR: ν (cm^{-1}) 3245 (N-H stretch), 1641 (amide I), 1559 (amide II). GPC: M_n = 6.5 kg/mol, M_w = 10.2 kg/mol, *PDI* = 1.55.

p(CO-co-50%ECO)-bisBTA (**4f**). Yield = 70%. ^{1}H-NMR (400 MHz, $CDCl_3$, δ): 8.36 (s, 6H, Ar-H), 6.65 (t, 6H, NH), 5.38-5.30 (m, 2H, C*H*CH_2), 3.5-3.4 (m, 2H, -O-C$\underline{H}_2$CH$_3$), 3.47 (m, 12H, CONHC$\underline{H}_2$), 3.38-3.35 (m, 1H, (CH_2)$_2$-C*H*-O-), 1.97 (m, 4H, CHC$\underline{H}_2$), 1.64-1.15 (alkyl), 0.88 (t, 12H, CH_3). ^{13}C-NMR (100 MHz, $CDCl_3$, δ): 165.6 (C=O), 135.3 (ArC), 130.3 (ArC), 129.7 (C=C), 127.9 (C=C), 64.1 (CH-O-CH_2CH_3), 40.4 (NH-CH_2), 38.5, 36.2, 34.1, 30.7, 29.5, 28.6, 27.9, 27.2, 25.4, 22.8, 19.9, 14.8. IR: ν (cm^{-1}) 3245 (N-H stretch), 1641 (amide I), 1559 (amide II). GPC: M_n = 8.0 kg/mol, M_w = 15.0 kg/mol, *PDI* = 1.87.

p(ECO)-bisBTA (**4g**). A solution of EDC (0.62 mmol, 119 mg) in 15 mL dry $CHCl_3$ was added to an ice cooled stirred solution of compound 20 (0.62 mmol, 271 mg), DMAP (0.62 mmol, 76 mg) and polymer **3g** (0.28 mmol, 1 gram) in dry $CHCl_3$ (25 mL). The reaction mixture was allowed to warm to room temperature and stirred overnight. Then the mixture was diluted with $CHCl_3$ (50 mL) and washed successively with HCl (1 M, 50 mL), $NaHCO_3$ (10%, 20 mL) and $NaCl_{aq}$ (saturated, 20 mL). $CHCl_3$ was removed *in vacuo*. The product dissolved in 2mL chloroform and subsequently precipitated in cold ether and obtained as a white/yellowish solid. Yield = 80%. ^{1}H-NMR (400 MHz, $CDCl_3$, δ): 8.42 (s, 6H, Ar-H), 6.7 (t, 6H, NH), 5.38-5.30 (m, 2H, C*H*CH_2), 3.5-3.4 (m, 2H, -O-C$\underline{H}_2$CH$_3$), 3.47 (m, 12H, CONHC$\underline{H}_2$), 3.38-3.34 (m, 1H, (CH_2)$_2$-C*H*-O-), 1.97 (m, 4H, CHC$\underline{H}_2$), 1.64-1.15 (alkyl), 0.88 (t, 12H, CH_3). ^{13}C-NMR (100 MHz, $CDCl_3$, δ): 165.6 (C=O), 135.3 (ArC), 130.3 (ArC), 129.7 (C=C), 127.9 (C=C), 64.1 (CH-O-CH_2CH_3), 40.4 (NH-CH_2), 38.5, 36.2, 34.1, 30.7, 29.5, 28.6, 27.9, 27.2, 25.4, 22.8, 19.9, 14.8. IR: ν (cm^{-1}) 3243 (N-H stretch), 1641 (amide I), 1558 (amide II). GPC: M_n = 6.7 kg/mol, M_w = 8.9 kg/mol, *PDI* = 1.32.

3.6 References and notes

[1]   Y. Yasuda, E. Iishi, H. Inada, Y. Shirota, *Chem. Lett.* **1996**, 575.

[2]   K. Hanabusa, A. Kawamaki, M. Kimura, H. Shirai, *Chem. Lett.* **1997**, 191.

[3]   A. Sakamoto, D. Ogata, T. Shikata, K. Hanabusa, *Macromolecules* **2005**, *38*, 8983.

[4]   T. Shikata, D. Ogata, K. Hanabusa, *J. Phys. Chem. B* **2004**, *108*, 508.

[5]   M. de Loos, J. H. van Esch, R. M. Kellogg, B. L. Feringa, *Tetrahedron* **2007**, *63*, 7285.

[6]   M. Blomenhofer, S. Ganzleben, D. Hanft, H.-W. Schmidt, M. Kristiansen, P. Smith, K. Stoll, D. Maeder, K. Hoffmann, *Macromolecules* **2005**, *38*, 3688.

[7]   N. Mohmeyer, N. Behrendt, X. Zhang, P. Smith, V. Altstädt, G. M. Sessler, H.-W. Schmidt, *Polymer* **2007**, *48*, 1612.

[8]   M. P. Lightfoot, F. S. Mair, R. G. Pritchard, J. E. Warren, *Chem. Commun.* **1999**, 1945.

[9]   L. Brunsveld, A. P. H. J. Schenning, M. A. C. Broeren, H. M. Janssen, J. A. J. M. Vekemans, E. W. Meijer, *Chem. Lett.* **2000**, 292.

[10]   M. M. J. Smulders, A. P. H. J. Schenning, E. W. Meijer, *J. Am. Chem. Soc.* **2008**, *130*, 606.

[11]   J. Roosma, T. Mes, P. Leclère, A. R. A. Palmans, E. W. Meijer, *J. Am. Chem. Soc.* **2008**, *130*, 1120.

[12]   K. J. C. van Bommel, C. van der Pol, I. Muizebelt, A. Friggeri, A. Heeres, A. Meetsma, B. L. Feringa, J. H. van Esch, *Angew. Chem., Int. Ed.* **2004**, *43*, 1663.

[13]   E. Obert, M. Bellot, L. Bouteiller, F. Andrioletti, C. Lehen-Ferrenbach, F. Boue, *J. Am. Chem. Soc.* **2007**, *129*, 15601.

[14]   M. Merschky, M. Wyszogrodzka, R. Haag, C. Schmuck, *Chem. Eur. J.* **2010**, *16*, 14242.

[15]   I. Yoshikawa, J. Sawayama, K. Araki, *Angew. Chem., Int. Ed.* **2008**, *47*, 1038.

[16]   P. J. M. Stals, J. F. Haveman, R. Martín-Rapún, C. F. C. Fitié, A. R. A. Palmans, E. W. Meijer, *J. Mater. Chem.* **2009**, *19*, 124.

[17]   T. F. A. de Greef, M. M. L. Nieuwenhuizen, P. J. M. Stals, C. F. C. Fitié, A. R. A. Palmans, R. P. Sijbesma, E. W. Meijer, *Chem. Commun.* **2008**, 4306.

[18]   P. J. M. Stals, M. M. J. Smulders, R. Martín-Rapún, A. R. A. Palmans, E. W. Meijer, *Chem. Eur. J.* **2009**, *15*, 2071.

[19]   P. Jonkheijm, P. van der Schoot, A. P. H. J. Schenning, E. W. Meijer, *Science* **2006**, *313*, 80.

[20]   R. M. Versteegen, R. P. Sijbesma, E. W. Meijer, *Macromolecules* **2005**, *38*, 3176.

[21]   R. M. Versteegen, R. Kleppinger, R. P. Sijbesma, E. W. Meijer, *Macromolecules* **2006**, *39*, 772.

[22]   R. A. Koevoets, R. M. Versteegen, H. Kooijman, A. L. Spek, R. P. Sijbesma, E. W. Meijer, *J. Am. Chem. Soc.* **2005**, *127*, 2999.

[23]   E. Wisse, A. J. H. Spiering, E. N. M. van Leeuwen, R. A. E. Renken, P. Y. W. Dankers, L. A. Brouwer, M. J. A. van Luyn, M. C. Harmsen, N. A. J. M. Sommerdijk, E. W. Meijer, *Biomacromolecules* **2006**, *7*, 3385.

[24]   R. H. Grubbs, *Handbook of Metathesis*, Wiley VCH, **2004**.

[25]   ROMP of cyclic olefins in the presence of a BTA functionalized chain transfer agent did result in less control over the molecular weight and PDI.

[26]   M. A. Hillmyer, R. H. Grubbs, *Macromolecules* **1995**, *28*, 8662.

[27]   O. A. Scherman, G. B. W. L. Ligthart, H. Ohkawa, R. P. Sijbesma, E. W. Meijer, *Proc. Natl. Acad. Sci. USA* **2006**, *103*, 11850.

[28]   J. S. Hrkach, K. Matyjaszewski, *J. Polym. Sci. Part A: Polym. Chem.* **1995**, *33*, 285.

[29]   G. C. Pimentel, A. L. McClellan, *The Hydrogen Bond*, W.H. Freeman and Company, San Francisco and London, **1960**.

[30]   D. J. M. van Beek, A. J. H. Spiering, G. W. M. Peters, K. te Nijenhuis, R. P. Sijbesma, *Macromolecules* **2007**, *40*, 8464.

4

Chiral hydrogelators from benzene-1,3,5-tricarboxamides

Abstract. A new class of hydrogelators based on the benzene-1,3,5-tricarboxamide (BTA) motif is presented. BTAs equipped with two aliphatic side chains act as end-cappers for bifunctional polyethylene glycols (pEGs). These amphiphilic polymers self assemble in water and form long elongated aggregates or stacks. These stacks of BTAs bundle as a result of the hydrophobic effect of the aliphatic side chains of the BTA motif. The long pEG connecting two BTAs allows cross-linking of BTA bundles, which results in the formation of a network. At higher concentration, strong and stable hydrogels are obtained. The supramolecular structure of the gel is investigated with infrared spectroscopy, circular dichroism (CD) spectroscopy, ultraviolet spectroscopy and cryogenic transmission electron microscopy. By adjusting the length of the aliphatic spacer that connects the BTA motif to pEG from 8 to 10 and 12 carbon atoms, we are able to tune the properties of the hydrogel. The significant influence of the aliphatic spacer length on the stability of BTA aggregates is detected by CD spectroscopy and by differences in the critical gelation concentration. The stability differences result from the hydrophobic effect exerted by the apolar spacer. Finally, we explored the mechanical properties of the gel using oscillating shear measurements and found that BTA end-capped pEG forms strong gels with interesting visco-elastic properties.

4.1 Introduction

The development of molecules that can form hydrogels –also called hydrogelators– has evolved enormously the past decades.[1] The use of hydrogelators is particularly interesting in the field of biomedical and biotechnological applications due to their structural similarities with natural tissue.[1-6] They offer mechanical support in biologically relevant media such as tissue scaffolds,[7, 8] encapsulation media or drug delivery agents for regenerative medicine.[2, 9-11] The performance of hydrogels critically depends on a large number of parameters including mechanical properties, pore size, water content, micro- and macroscopic structure, shape persistency, control over functional group incorporation/release and much more.[12] Large amounts of water up to 99% are immobilized in a continuous three-dimensional (3D) network resulting in a solid-like appearance of the gel. The 3D network can be formed by cross-linking or entangling of molecules. The resulting gel is called a "chemical gel" if cross-linking is based on covalent bonds and a "supramolecular gel" if cross-linking is obtained by self-assembly due to non-covalent bond formation. Cross-linking in chemical gels is often strengthened by physical interactions, such as seen in hydrogels based on polyvinyl alcohol.[13] Supramolecular gels, except the ionomers, are mainly based on low molecular weight (LMW) molecules.[14-18] The self-assembling properties are obtained by non-covalent interactions, such as hydrogen bonding, π-π interactions and hydrophobic interactions. The use of non-covalent interactions has led to fully thermo reversible,[19] pH-[20, 21] or enzymatic-triggered[22] systems, which makes them excellent candidates for biological related applications. Supramolecular gels are typically mechanically weak, compared to chemical gels, and their use is restricted to applications needing low or moderate mechanical strength.

The design of LMW gelators is based on the following general criteria: LMW gelators must contain unidirectional intermolecular interactions, controlled solubility/crystallization properties and the possibility to form a 3D network through physical cross-linking.[23, 24] True understanding of molecular gels is not achieved yet and a correlation between (supra)molecular structure and gel morphology or mechanical properties is rarely reported.[25-29] According to van Esch,[24] two problems are responsible for this: the limited knowledge of the energetic landscape of gel formation and the lack of knowledge of the supramolecular structure within the gel fibers. Characterization of the supramolecular packing of a gelator is often derived from crystal structures in the solid state, which does not necessarily mean that this packing is preserved in the gel state.

Triggered by the challenges in relating molecular structure to gel morphology and properties, we here introduce a new hydrogel system based on the benzene-1,3,5-tricarboxamide (BTA). The self-assembly of BTAs has been studied in great detail in our group and is the core of this thesis.[30-33] BTAs cooperatively self-assemble into columnar aggregates in apolar solvents and in the solid state. A threefold, helical arrangement of the

intermolecular hydrogen bonds between consecutive discs stabilizes the columnar packing, and a preferred helical sense is induced upon introducing one or more stereogenic centra in the alkyl side chains. BTAs have previously been applied as LMW gelators in a variety of organic solvents[29, 34-37] but rarely in water.[38]

In this study we investigate a new hydrogelator based on apolar BTAs end-capped to a bifunctional polyethylene glycol (pEG) backbone (Scheme 4.1). It has been shown before that attaching relatively small associating end-groups to a telechelic pEG can result in the formation of a physically cross-linked network in water. Under the right conditions, the associating groups aggregate and form flowerlike micellar structures at low concentration. At sufficiently high concentration, a transient network is formed by bridging of neighboring micelles. A variety of associating groups has been employed, such as hydrocarbon[39, 40] or fluorocarbon[41] alkyl side chains, apolar polymers[42] and hydrogen bonding motifs.[43-45] We here make use of the directional hydrogen bonding of the BTAs, so that long elongated aggregates are formed. Network formation results from entanglements and bridging of the separate aggregates by the pEG backbone. Our extensive knowledge on BTAs in combination with their potential to probe the self-assembly process *in situ*, will allow us to unravel the hierarchical self-assembly process that takes place upon formation of BTA based supramolecular hydrogels.

Scheme 4.1 Overview of BTA functionalized pEG **1-2**.
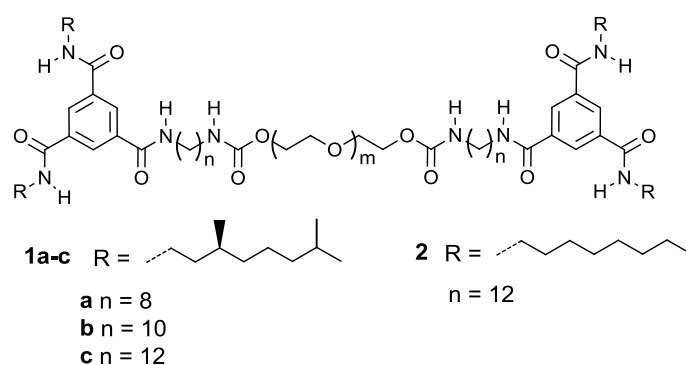
4.2 Design, synthesis and characterization

We demonstrated in Chapter 3 that the self-assembly of BTAs depends on the polarity of the environment. The tendency to form stable aggregates decreases significantly upon increasing the polarity of the medium, both in the solid state and in dilute solutions. Therefore, in the design of hydrogelators, we have to introduce an aliphatic spacer between the pEG and the BTA. We expect that pEG end-capped with BTAs will lack the ability to form fibrillar structures in the bulk or many organic solvents. In contrast, in water the

additional hydrophobic effect will aid the formation of stable BTA aggregates due to this hydrophobic shielding (Figure 4.1). This spacer must have a sufficient length to prevent backfolding of the pEG backbone.[46] The spacer length between the polymer backbone and the BTAs is varied (8, 10 and 12 carbon atoms) to determine the effect of hydrophobicity on the stabilization of aggregated BTAs. We selected pEG with a relatively large molecular weight of 20 kg/mol to increase compatibility of the apolar BTAs in water. The BTAs are equipped with two (*S*)-3,7-dimethyloctyl side chains to ensure bundling of the individual stacks and with that to increase the stability of the hydrogel formed. Furthermore, the chiral side chains offer the possibility to follow the self-assembly with circular dichroism (CD) spectroscopy.
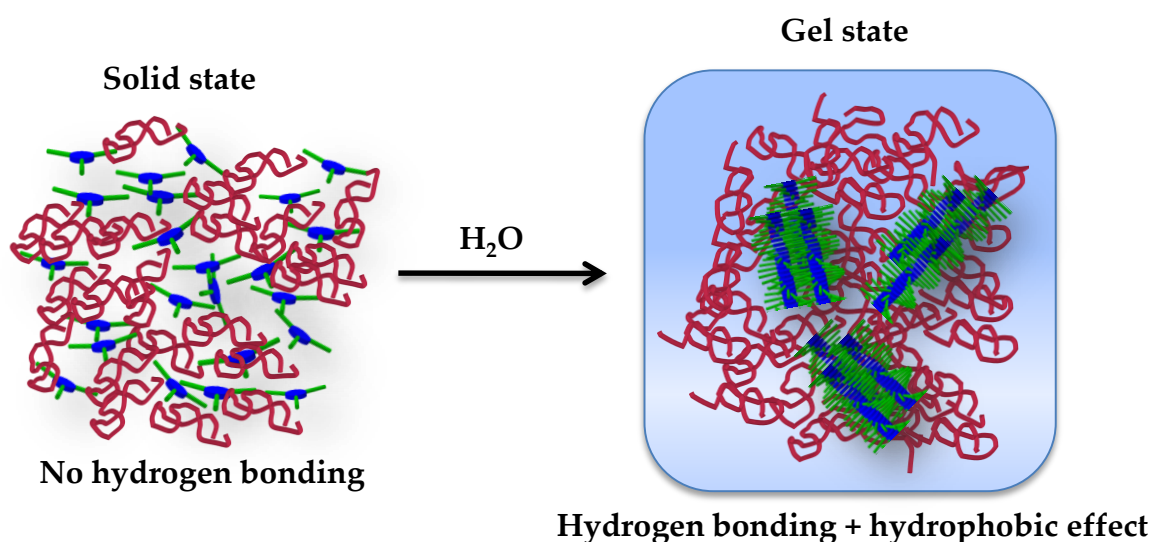
Figure 4.1 BTAs are molecularly dissolved in the solid state. After the addition of water, the hydrophobic effect may result in the formation of stable phase segregated nanorods, which subsequently bundle due to the hydrophobic side chains.

Compounds **1**-**2** were synthesized in a straightforward fashion using a similar strategy as discussed for the BTA telechelic polymers discussed in Chapter 3 (Scheme 4.2). PEG (M_w = 20 kg/mol) bearing hydroxyl end-groups was reacted with carbonyldiimidazole (CDI) yielding the activated carbamate difunctional pEG (**3**). Subsequently, **3** was added to a solution containing an eightfold excess of the appropriate diaminoalkane in chloroform yielding amino end-functionalized pEG **4a**-**c**. Finally, the hydrogelators were obtained via a PyBOP coupling of the BTA precursors (chiral and achiral) with the amine end-functionalized pEG. All polymers were purified by dialysis in methanol followed by precipitation from diethylether and obtained in an average yield of 55% and in high purity as evidenced by NMR and GPC. As an example, the ^{1}H-NMR spectrum of **1c** is given in Figure 4.2.

Scheme 4.2 Synthesis of BTA end-capped polyethylene glycols **1-2**.
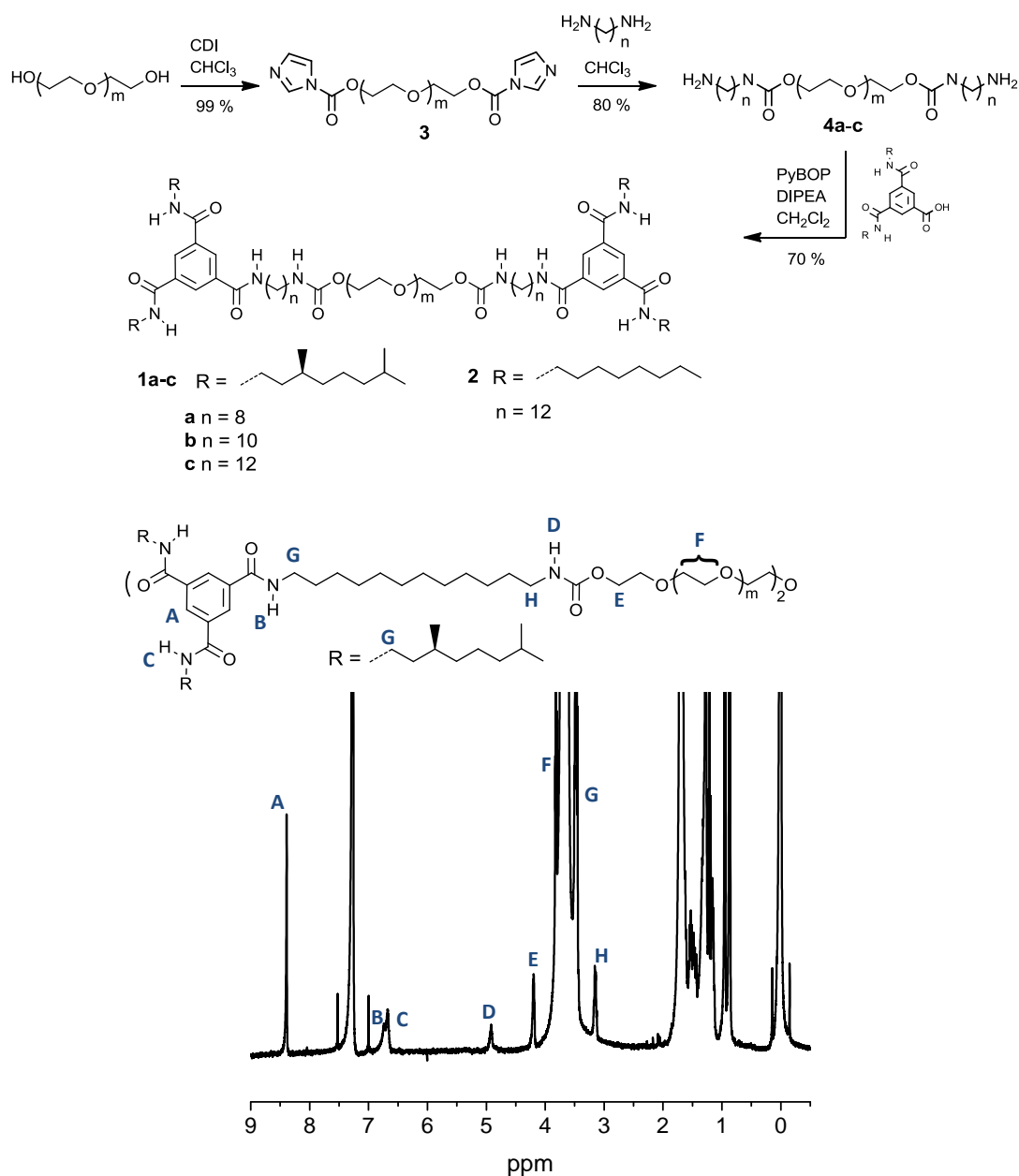
Figure 4.2 ^{1}H-NMR of polymer **1c** in CDCl$_3$ at 20 °C.

According to GPC, polymers **1-2** possess a molecular weight of around 17 kg/mol with a *PDI* of around 1.4 (based on polystyrene standards). Due to repeated precipitations during purification and the underestimation of the molecular weight of pEG using polystyrene standards, the observed molecular weights are lower than expected. Infrared spectroscopy (IR) measured on **1-2** in the solid state revealed the NH stretch, amide I and II vibrations at ~3348, ~1654 and ~1538 cm^{-1}, respectively, typical for molecularly dissolved BTAs lacking the presence of intermolecular hydrogen bonds (Table 4.1). Differential scanning calorimetric (DSC) measurements showed only one phase transition at 57 °C, which was attributed to

melting of the pEG backbone. Polarized optical microscopy showed that polymers **1-2** possess an isotropic phase above this melting point. Based on the phase behavior and IR spectroscopy, we conclude that BTAs are not aggregated in the bulk.

Table 4.1 Summary of the ^{1}H-NMR, GPC and DSC and IR data of compounds **1-2**.

Compound	M_n[a]	M_n[b]	PDI[b]	T_g[c]	T_m[c]	ΔH[c]	ν(N-H)	ν(amide I)	ν(amide II)
	[kg/mol]	[kg/mol]	[-]	[°C]	[°C]	[J/g]	[cm^{-1}]	[cm^{-1}]	[cm^{-1}]
1a	21.3	18.6	1.43	-60	57	136	3348	1654	1538
1b	21.4	16.1	1.52	-60	56	136	3348	1654	1538
1c	21.4	17.5	1.38	-61	57	144	3350	1653	1538
2	21.3	18.2	1.34	-62	57	141	3351	1554	1538

[a] Theoretical molecular weight. [b] Determined by GPC in chloroform. [c] Derived from the third heating run (40 K min^{-1}).

4.3 Self-assembly in dilute solution

Compounds **1-2** are designed to code for elongated columnar assemblies via intermolecular hydrogen bonding. In addition, the hydrophobic effect in water induces the nanorods to bundle.[47, 48] To verify if this two-stage self-assembly process is operative, we investigated the morphology of **1c** in water (1 mg/mL, c_{BTA} = 4.6 x 10^{-5} M) in more detail with cryo-TEM. At this low concentration we expect that the two BTAs end-capped to one pEG backbone are present in the same nanorod and can interchange between nanorods when bundles are formed. Gratifyingly, compound **1c** forms long elongated fibers with a width of ~80 nm (Figure 4.3). These fibers consist of bundles of nanorods, which are clearly visible in Figure 4.3C. The individual nanorods have an average diameter of ~3 nm.[49] The formation of bundles is proposed to be the result of the hydrophobic effect by the aliphatic side chains of the BTA.[50] Due to the strong directionality of the hydrogen bonds very long elongated structures are formed.
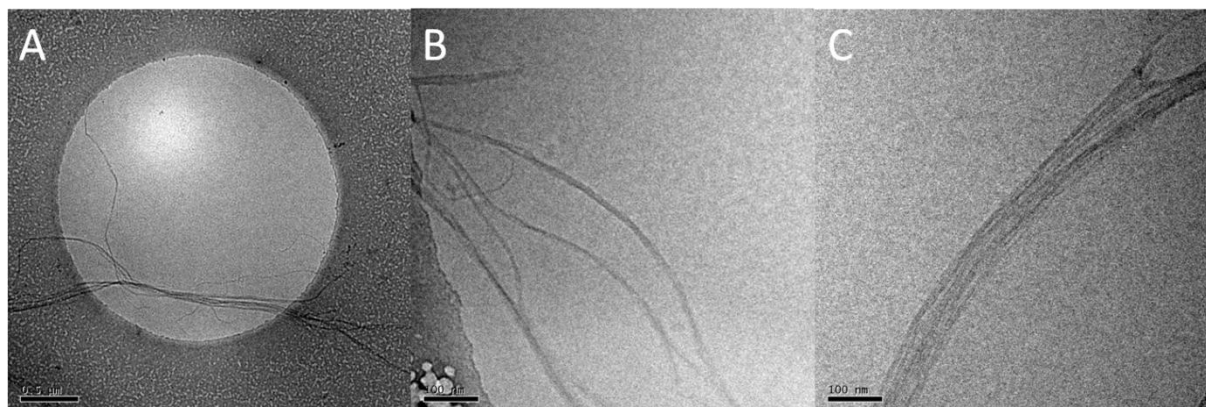
Figure 4.3 Cryo-TEM of **1c** (c$_{BTA}$ = 4.6 x 10^{-5} M in water). A) Fiber structure of **1c**. Fibrils are bundled into micrometer long fibers and have a width of 80 nm (scale bar 0.5 μm). B, C) magnification of **1c** (scale bar 100 nm).

To obtain more insight into the origin and the structure of the observed fibrillar objects in cryo-TEM of **1c**, we decided to study the self-assembly of **1-2** with CD and ultraviolet (UV) spectroscopy. Helical BTA aggregates in alkane solvents are characterized by a λ$_{max}$ of 192 nm in UV spectroscopy and a Cotton effect at 223 nm with $|\Delta\varepsilon|$ = 43 L mol^{-1} cm^{-1} at room temperature.[31, 51] To verify the presence of helical aggregates and the influence of bundling on the supramolecular structure, we performed CD and UV spectroscopy measurements on solutions containing chiral **1c** and the achiral variant **2** at around a similar concentration as used in cryo-TEM (c$_{BTA}$ = 5.1 x 10^{-5} M in water at 20 °C). Polymer **1c** showed a Cotton effect of -60 mdeg ($\Delta\varepsilon$ = -36 L/mol cm), while the achiral compound **2**, in which both helical senses are present in equal amounts, was CD silent (Figure 4.4A). The size and shape of the Cotton effect of **1c** suggest that BTAs form helical aggregates in water, which possess a similar packing as the C_3-symmetrical BTAs in dilute solutions of apolar solvents. The UV absorption spectra of **1c** and **2** are almost similar in shape and size. The UV spectrum is dominated by pEG absorption and could therefore not be used to investigate self-assembly (Figure 4.4B).
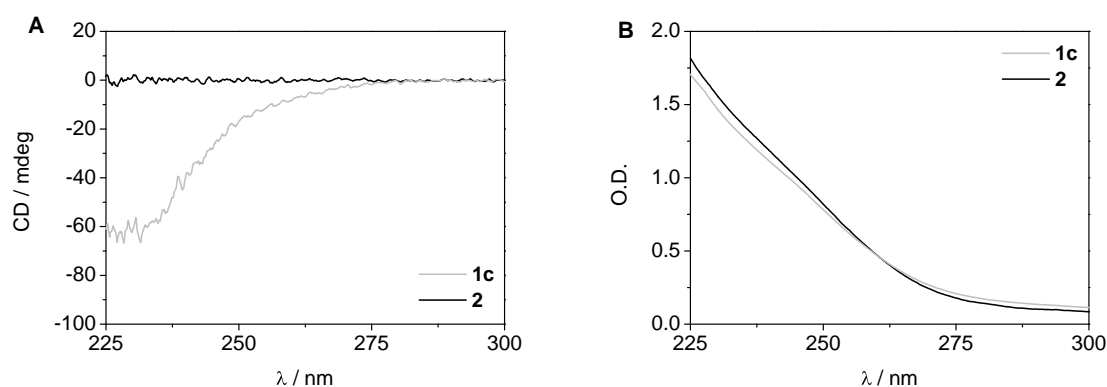
Figure 4.4 CD (A) and UV (B) of **1** and **2** (c$_{BTA}$ = 5.1 x 10^{-5} M in water, l = 1.0 cm, T = 20 °C).

Next, we investigated the influence of the length of the aliphatic spacer between the pEG backbone and the BTA motif on the aggregation of BTAs. The BTA concentration was 9.6 x 10^{-5} M for **1a,b** and 6.6 x 10^{-5} M for **1c** (Figure 4.5A). The poor solubility of **1c** did not allow measurements at the higher concentrations used for **1a,b**. The Cotton effect, expressed as the concentration independent molar ellipticity ($\Delta\varepsilon$), at 223 nm for **1a**-**c** was -16, -24 and -36 L mol^{-1} cm^{-1}, respectively. The $\Delta\varepsilon$ increases significantly with an increase of the spacer length. Since the molecular structures of **1a**-**c** are identical except for the spacer length, the impact of this spacer on the packing is unexpectedly large. Since the value of $\Delta\varepsilon$ correlates with the degree of aggregation of BTAs,[31] a possible explanation for the reduction in $\Delta\varepsilon$ upon decreasing the spacer length is a decrease in the degree of aggregation.
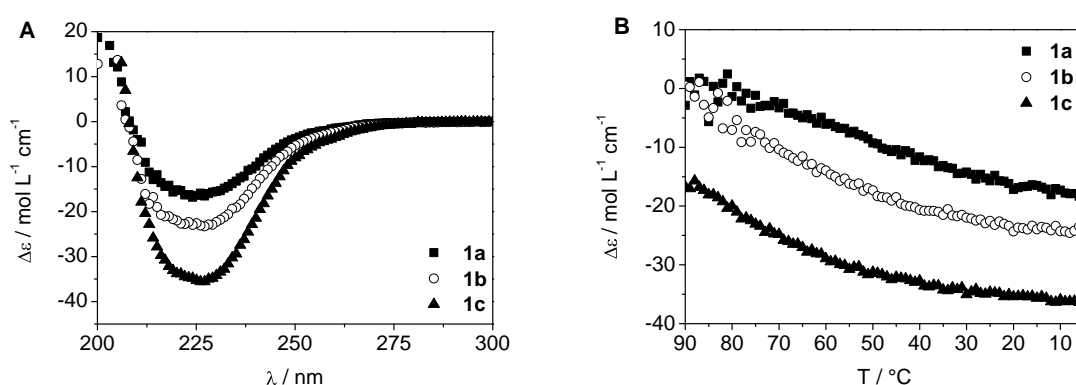
Figure 4.5 A) Molar ellipticity $\Delta\varepsilon$ of **1a**-**c** (c_{BTA} for **1a** = 9.6 x 10^{-5} M, **1b** = 9.6 x 10^{-5} M and **1c** = 6.6 x 10^{-5} M in water, l = 1.0 cm, T = 20 °C). B) Molar ellipticity $\Delta\varepsilon$ of **1a**-**c** as a function of temperature (c_{BTA} for **1a** = 9.6 x 10^{-5} M, **1b** = 9.6 x 10^{-5} M and **1c** = 6.6 x 10^{-5} M in water, l = 1.0 cm, λ = 223 nm).

To further investigate the effect of the spacer length, we performed temperature-dependent CD spectroscopy and UV measurements on the same solutions of **1a**-**c** (Figure 4.5B). From the UV experiments we could infer that **1a** and **1b** became turbid at 68 and 74 °C, respectively. The solution of **1c** did not become turbid within the applied temperature range. Probing the Cotton effect at 223 nm showed a gradual increase upon cooling the solutions from 90 °C to 5 °C (cooling rate = 1 K min^{-1}). The Cotton effect of **1a** and **1b** appeared around 80 and 90 °C, respectively. The precise temperature of aggregation could not be determined because of the turbidity and the resulting saturation of the detector. Compound **1c**, possessing the 12 carbon spacer, still showed a significant Cotton effect at 90 °C. The temperature at which aggregation starts is the highest in polymer **1c** in which the BTA is connected via the largest spacer. This shows that the increase of the spacer length results in the formation of aggregates with a higher thermal stability.

Top view
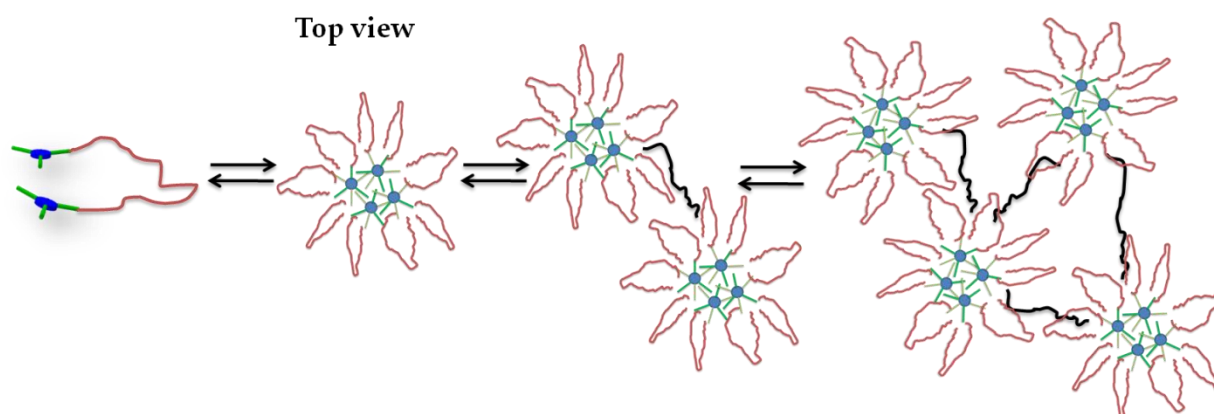
Figure 4.6 Schematic drawing of the formation of flowerlike micelles and bridging that eventually can lead to phase segregation / demixing from water. At a higher temperature, the associating groups (BTAs) become more dynamic and form bridges (black) between bundles of BTA aggregates. At a certain degree of bridging, the network is not longer dissolved and precipitates.

PEG with a molecular weight of 20 kg/mol has a lower critical solution temperature (LCST) in water of ~103 °C (determined between 0.3 and 10 weight %).[52] As a result, the turbidity of the solutions of **1a,b** at elevated temperature presumably originates from the LCST. The temperature is reduced, compared to the LCST of pure pEG, because of the presence of hydrophobic BTA end-groups. In general, association of hydrophobically end-capped pEG results in the formation of flowerlike micelles.[53] At elevated temperature, the associating end-groups can exchange between micelles and form bridges. Bridging eventually results in phase segregation (demixing from water), which leads to precipitation of the polymer (turbidity). Although the turbidity has probably a different physical origin than the LCST of pure pEG, it can still be called the LCST.[53]

We propose that BTA end-capped pEG forms long elongated micelles that consist of bundles of BTA nanorods (Figure 4.6). Interchange of BTAs between micelles can also lead to the formation of bridges, which eventually may result in precipitation. It is also known that bridging more easily occurs at elevated temperature due to an increase of dynamics of the associating end-groups. This explains why solutions of **1a**-**c** become turbid at temperatures close to their temperature of aggregation. Furthermore, it has been observed that the size of the hydrophobic associating group has a large influence on the dynamics due to the hydrophobic effect.[40, 54-56] Annable *et al.* showed that the lifetime of the hydrophobic group in one micelle exponentially increased with the length of the hydrophobic groups.[56] The spacer length in **1a**-**c** affects the lifetime as well, which explains the difference in temperature at which the individual solutions become turbid.

An increase in the stability of BTA aggregates is expected to impact the dynamics of the system. This prompted us to perform a Sergeants and Soldiers experiment.[30] In dilute conditions in apolar solvents, the transfer of chirality from chiral BTAs to achiral BTAs occurs within 40 seconds when adding one solution to the other.[57] The short time-scale needed to fully bias one helicity demonstrates that assembly and disassembly (via polymerization-depolymerization) of BTAs is a highly dynamic process in apolar organic solvents. In contrast, mixing an aqueous solution of **1c** with an aqueous solution of achiral **2** (c_{BTA} = 5.1 x 10^{-5} M, T = 20 °C) in a 50/50 ratio resulted in a 50% reduction of the value of $\Delta\varepsilon$. This suggests that the transfer of chirality does not occur under these conditions. However, when the solution was prepared by the addition of water to a solid mixture of **1c** and **2** — prepared by evaporating chloroform from this mixture to ensure ideal mixing in the solid state— the $\Delta\varepsilon$ is twice as large as the $\Delta\varepsilon$ of only **1c**. Hence, provided that the sample is made in the correct way, amplification through ideal mixing can occur. The absence of transfer of chirality in solution obtained by mixing both solutions compared to the presence of chirality transfer when preparing a solution from the solid state, clearly shows that the ability of BTAs to move between aggregates via depolymerization-polymerization is significantly lower compared to BTAs in apolar solutions. This is the result of the barrier that BTAs have to overcome when they interchange between bundles of nanorods due to the hydrophobic effect.

4.4 BTA-based hydrogels and their supramolecular structure

4.4.1 Gelation properties

To investigate the capacity of compounds **1**-**2** to form hydrogels, we prepared solutions in water that contained around 10 wt % of solid polymer in water. At room temperature, compounds **1**-**2** did not dissolve. The samples were heated at 70 °C resulting in the formation of clear, viscous solutions. Upon cooling, compounds **1**-**2** form transparent, elastic gels. Subsequently, we determined the critical gelation concentration (cgc) for each compound (Table 4.2). Gels were first prepared by dissolving 110 mg of the appropriate compound in 1 mL of water in vials of identical size. The samples were heated to 70 °C, subsequently cooled to room temperature and after 30 minutes subjected to tube inversion tests. The cgc was derived after the step-wise addition of water (50 mg) with a subsequent heating and cooling step. The tube inversion test was performed after 30 minutes of resting at room temperature (Table 4.2). The lowest cgc was obtained for **1c** (3.3 mM). This is in line with the aggregation behavior in dilute conditions as observed with CD spectroscopy measurements, in which **1c** formed the most stable BTA aggregates due to the longer spacer. Compound **2** is also connected to pEG by a dodecyl spacer, but shows a slightly higher cgc of 3.8 mM, which is presumably related to the presence of two octyl side chains that contain two methyl groups less compared to the side chains of **1a**-**c**, decreasing its hydrophobicity slightly.

Table 4.2 Critical gelation concentration of compounds **1-2**.

Compound	Spacer length	cgc	cgc	cgc
	$(-CH_2-)_n$	[wt %]	[wt_{BTA} %]	[mM]
1a	8	11	0.73	5.2
1b	10	9.5	0.62	4.4
1c	12	7	0.45	3.3
2	12	8	0.52	3.8

4.4.2 Determination of the supramolecular structure

Insight into the supramolecular structure of the gel was gathered by performing CD and UV spectroscopy measurements on **1a**-**c**. Gels of **1a**-**c** were prepared containing 10 - 11 weight % of solid material. CD spectroscopy was performed in 0.2 mm cuvets at room temperature.[58] Each sample was heated to 70 °C and cooled to 20 °C (rate = 20 K min⁻¹) before each measurement and was checked for linear dichroism effects, which were absent in all cases. The samples were measured till 212.5 nm due to saturation of the detector that started at 225 nm.
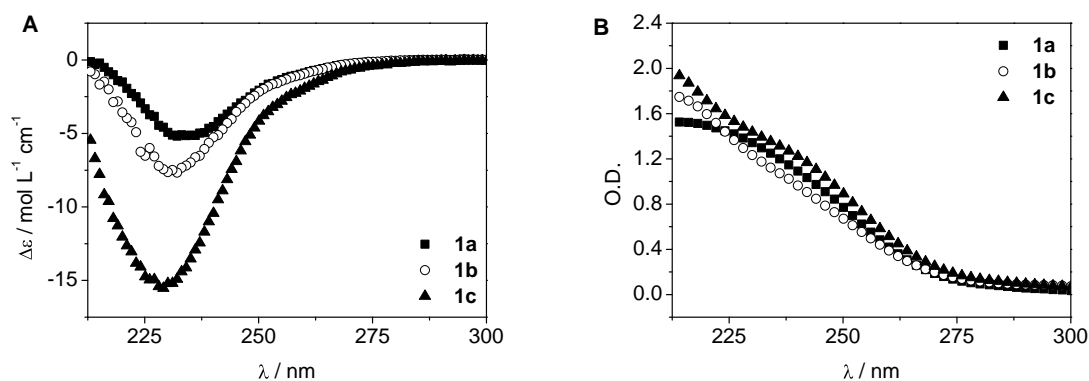
Figure 4.7 CD expressed in as $\Delta\varepsilon$ (A) and UV (B) of **1a**-**c** (c_{BTA} = 9.4 x 10⁻³ M in water, l = 0.2 mm, T = 20 °C).

The CD spectra of polymers **1a**-**c** show large differences in $\Delta\varepsilon$ (Figure 4.7A) although according to UV, all samples contained about the same amount of material (Figure 4.7B). In all cases, the shape of the Cotton effects differs from those of the diluted solutions of **1a**-**c**. The λ_{max} of the Cotton effect decreases from 233 nm to 232 nm and 228 nm in **1a**-**c**, respectively. The difference in the shape might be a result of a different packing of BTAs in the gel compared to those of BTAs in more dilute conditions. The values of $\Delta\varepsilon$ determined at λ_{max} for **1a**-**c** are -5, -7.5 and -16 L mol⁻¹ cm⁻¹, respectively. These values are significantly lower in the gel state compared to those for **1a**-**c** in dilute solutions.

The $\Delta\varepsilon$ increases significantly with an increase of the spacer length. This relation was also observed in the CD measurements performed in dilute conditions. The value of $\Delta\varepsilon$ represents the equilibrium between BTAs in the aggregated state and in the monomeric state and suggests that BTAs in the gel state are in a more disordered state. However, a true comparison of $\Delta\varepsilon$ for **1a-c** between dilute conditions and in the gel state cannot be made because of the difference in the shape of the Cotton effect, which shows that the supramolecular structure and self-assembly of BTAs is influenced by the concentration. The difference in the supramolecular structure might be related to a kinetic effect, since the higher degree of cross-linking can result in a lower mobility of the BTAs. All measurements were immediately conducted after a heating and cooling step using a relatively high rate of 20 K min^{-1}. This could lead to self-assembly that is not under thermodynamic control, and can therefore induce a kinetically trapped state.

Interestingly, the solubility of **1c** was not a problem in the gel state, which is in contrast to the poor solubility of **1c** in more dilute conditions. We rationalize this observation by assuming that BTAs have more chance to form aggregates with neighboring BTAs at higher concentration, resulting in a much faster formation of stable polar and apolar domains in water. This also strongly suggests that at high concentration more BTAs are kinetically trapped, while in dilute condition this is less likely due to the lower number of junction points.

IR spectroscopy of freeze-dried xerogels of **1-2** is useful to investigate the arrangement of amides in the gel state.[50] BTA amides involved in threefold helical hydrogen bonding show characteristic vibrations (ν(N-H) 3240 cm^{-1}, ν(amide I) 1642 cm^{-1} and ν(amide II) 1562 cm^{-1}).[30, 32] Freeze-dried xerogels of **1-2** were prepared and subjected to IR spectroscopy measurements. Unfortunately, we were not able to observe these characteristic vibrations in **1-2**. However, compound **1c** showed broad vibrations with two maxima (ν(N-H) = 3345 and 3260 cm^{-1}, ν(amide I) = 1653 and 1640 cm^{-1} and ν(amide II) = 1562 cm^{-1}). The second set of wavenumbers is closer to the characteristic values for hydrogen bonding in the gel, but presumably the time between isolating the sample and measuring was too long and sufficient for the hydrogen bonds to break or reorganize.

4.4.3 Mechanical properties

For a more quantitative study on the visco-elastic properties of the gel, we performed shear controlled oscillatory rheological measurements. We selected **1c** because it has the lowest cgc and it is expected to give the best mechanical properties. The measurements were performed on a gel that contains 10 wt % of solid material in water. We performed strain-sweep measurements as a function of temperature (Figure 4.7). The strain-sweep measurements were all performed within the linear frequency-dependent regime.
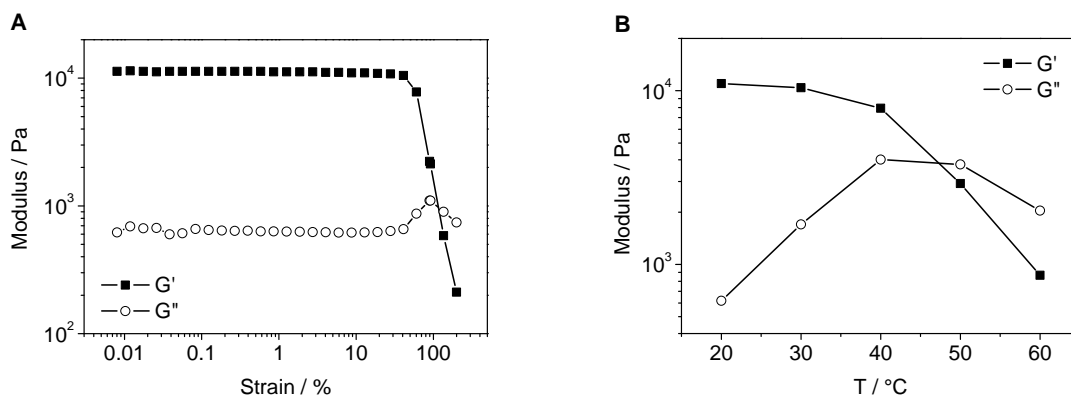
Figure 4.8 A) Strain-dependent measurements of G′ and G″ of **1c** (at 20 °C, 2 rad/s). B) Temperature-dependent G′ and G″ of **1c** (at 10% strain, 2 rad/s).

It is clear that **1c** forms a strong visco-elastic network at 20 °C, which is characterized by a storage modulus (G′) of 10^4 Pa and loss modulus (G″) of 600 Pa (Figure 4.8A). G′ is larger than G″, which is indicative for a solid-like visco-elastic network. The behavior at high strain is characterized by the high value (100%) at which the linear behavior ends. Regarding the supramolecular nature of the system this is remarkable, but not unprecedented for non-covalent hydrogels.[59] The increase in the loss modulus before decreasing is a sign of a structural relaxation process and has also been observed in other systems *e.g.* bentonite suspensions.[60] The temperature dependence of the gel **1c** was investigated by determining the values of G′ and G″ in the linear strain and frequency regime (2 rad/s). Figure 4.8B, clearly shows that the storage modulus drops with increasing temperature, until around 50 °C where it drops below the loss modulus. From this point the hydrogel is a liquid-like visco-elastic network and this temperature is assigned to the loss of the 3D network. Also the loss modulus (G′) increases with increasing temperature and this suggest that the system becomes richer in the viscous component while the solid component becomes smaller.

4.5 Discussion and conclusions

This chapter introduces a novel system that can form interesting hydrogels and is based on pEG end-capped with the BTA motif and includes preliminary results on the characterization of the supramolecular structure. The behavior discussed for BTAs end-capped to pEG is very reminiscent to that of telechelic hydrophobically modified pEG, which are industrially applied as thickeners in water-based coatings. While traditional studies on the molecular structure of hydrophically modified pEGs are mainly performed by NMR- and fluorescence spectroscopy and scattering techniques, the BTA motifs allows the use of CD spectroscopy to obtain insights into the molecular structure. A preliminary model for the hierarchical self-assembly of BTA end-capped pEG is proposed in Figure 4.9.

Solution state **Gel state** **Solid state**
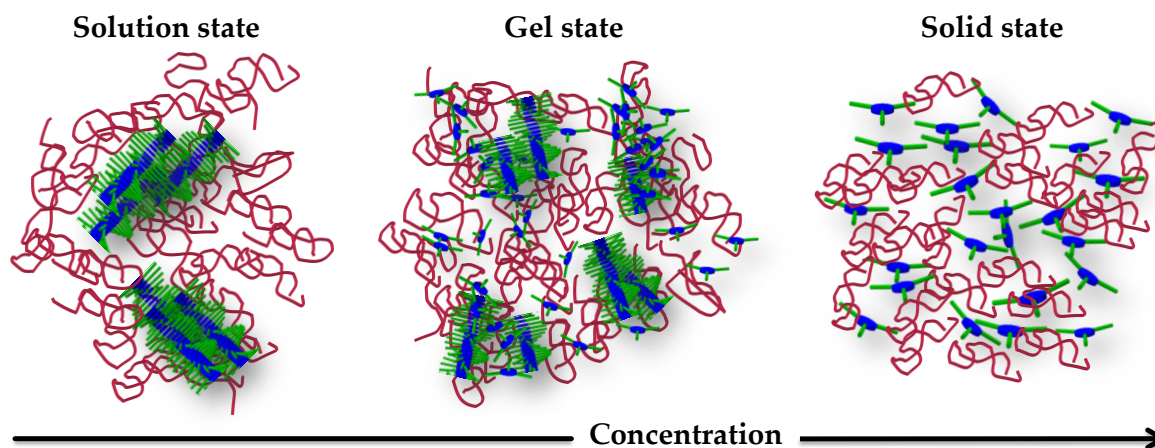
Concentration

Figure 4.9 Proposed (supra)molecular structure of BTA end-capped pEG at different concentrations.

First, BTA end-capped pEG in dilute solutions (10^{-5} M), clearly showed the presence of bundled nanorods as revealed by cryo-TEM. CD measurements at this concentration convincingly showed the presence of helical structures within the nanorods. Interestingly, significant differences were observed upon increasing the aliphatic spacer length, or in other words increasing the hydrophobicity. The Cotton effect increased with increasing spacer length due to an increase of the hydrophobic effect. The contribution of the spacer to the stability was also demonstrated by temperature-dependent CD spectroscopy in which the temperature of aggregation increased with increasing spacer length. The solutions showed a LCST close to the temperature of aggregation. This might be explained by the possible exchange of the BTAs between bundles of BTA nanorods, which leads to the formation of bridges. Bridging eventually results in phase segregation (demixing from water) that leads to precipitation of the polymer. Bridging occurred more easily at elevated temperature, close to the temperature of aggregation, due to an increase of the dynamics. The dynamics of the system are influenced by the spacer length, and this presumably explains the difference in temperature at which the solutions became turbid. Sergeants and Soldiers experiments revealed that the dynamics of aggregated BTAs at room temperature are very slow, which makes these systems highly suitable for encapsulation of functional guests molecules in a supramolecular fashion.

At higher concentration (~10^{-3} M), all compounds formed stable transparent gels. The cgc was determined by tube inversion tests and is around 7 - 11 wt %. Polymers with the longest aliphatic spacer formed gels at the lowest concentration. This clearly demonstrated the significant contribution of the spacer length on the stability of BTA aggregates and can be explained by the difference in the hydrophobic effect on the apolar spacer. Dynamic oscillating shear measurements showed the presence of a strong visco-elastic network at room temperature, which transformed in a more liquid-like visco-elastic network at elevated

temperature. The enhancement of the rheological properties was significantly larger compared to that of telechelic hydrophobically modified pEG based on aliphatic side-chains[40] and in the same order as found for UPy-urea end-capped pEG.[45]

CD spectroscopy was used to investigate the supramolecular structure of the gel. Cotton effects were observed, with a different shape compared to those of BTAs in dilute solutions. This strongly indicates that BTA are self-assembled in a different arrangement in the gel. The size of the Cotton effect seems to be related to the spacer length in a similar fashion as observed in more dilute conditions. The smaller Cotton effect of BTAs in the gel suggests that more BTAs are in a monomeric or disordered state. However, a true comparison of $\Delta\varepsilon$ for BTA end-capped pEG between dilute conditions and in the gel state cannot be made because of the difference in the shape of the Cotton effect. All measurements were immediately performed after a heating and cooling step using a relatively high rate of 20 K min^{-1}. This could lead to self-assembly, which is not under thermodynamic control, and can therefore induce a kinetically-trapped state. Temperature-dependent and time-resolved measurements have to be performed to obtain insights into the formation and supramolecular structure of BTAs in the gel. Also scattering techniques, such as dynamic light scattering and X-ray scattering can provide valuable information about the structure. BTAs do not form phase segregated nanorods in the solid state, due to the high polar nature of pEG and the lack of the hydrophobic effect due to the absence of water.

This study presents preliminary results of the self-assembly and gel formation of BTA end-capped pEG. Full characterization of a larger library of BTA end-capped polymers has to be performed to provide detailed information on the formation and behavior of hydrophobically end-capped pEG gelating systems. It is clearly demonstrated that the chiral nature of the BTA reveals insights into the dynamics and the supramolecular structure of the gel and offers a unique opportunity to unravel in detail the structure of hydrophobically modified pEG gelating systems. BTA hydrogels are also highly suitable to visualize controlled release and encapsulation of guest molecules and are therefore attractive candidates to be used in biotechnological applications.

4.6 Experimental

Materials

All reagents were purchased from Aldrich or Acros Organics and used as received unless otherwise specified. All solvents were of AR quality and were purchased from Biosolve. Chloroform was dried over molecular sieves and dichloromethane was dried over an aluminium oxide column. CD and UV measurements were conducted in demineralized water. Deuterated solvents were purchased from Cambridge Isotopes Laboratories. All reactions were run in flame-dried glassware under an argon atmosphere. 3,5-Bis-(3S)-(3,7-

dimethyl-octylaminocarbonyl) benzoic acid and 3,5-bis-octylaminocarbonylbenzoic acid were synthesized according to literature procedures.[61]

Instrumentation and Analysis

CD and UV spectra were recorded on a Jasco J-815 CD spectrometer equipped with a Jasco PTC-348 WI temperature controller. Cells with an optical path length of 1.0 cm (for ~10^{-5} M solutions) or 0.2 mm (for ~10^{-3} M gels) were applied. The molar ellipticity is calculated as: $\Delta\varepsilon$ = Cotton-effect/(32980xcxl) where c is the concentration in mol/L and l = the optical path length in cm. ^{1}H-NMR and ^{13}C-NMR spectra were recorded on a Varian Gemini 400 MHz NMR (400 MHz for ^{1}H-NMR and 100 MHz for ^{13}C-NMR). Proton chemical shifts are reported in ppm downfield from tetramethylsilane (TMS). Carbon chemical shifts are reported downfield from TMS using the resonance of the deuterated solvent as the internal standard. IR spectra were recorded on a Perkin Elmer 1600 FT-IR. GPC measurements were performed on a Resi Pore column with Chloroform (at room temperature) as the eluent (flow = 1 mL/min) and employing a RI and PDA (λ = 254 nm) as the detector. The molecular weights were determined using the polystyrene calibration method. DSC measurements were performed on a TA Q2000 (third heating run, 40 K min^{-1}).

Cryo-TEM

The sample vitrification procedure was carried out using an automated vitrification robot (FEI Vitrobot™ Mark III). CryoTEM grids, R2/2 Quantifoil Jena grids, were purchased from Quantifoil Micro Tools GmbH. Prior to the vitrification procedure (3 µL aliquots, blotting time varied from 8 s to 12 s, -4 mm blotting offset, 100 % relative humidity) the grids were surface plasma treated using a Cressington 208 carbon coater operating at 5 mA for 40 s. The cryoTEM experiments were performed on a FEI Technai 20, type Sphera (www.cryotem.nl). The Technai 20 is equipped with a LaB6 filament operating at 200 kV and the images were recorded using a 1k x 1k Gatan CCD camera.

Rheometry

Shear controlled dynamic oscillatory rheology experiments were performed on an Anton Paar RheoplusV32 rheometer. Measurements were performed in a plate-plate geometry with a gap of 0.3 mm and a diameter of 25 mm. Motor and plate-plate distance calibrations were performed before the experiment. All strain-dependent measurements were performed in the linear frequency regime along with the frequency-dependent measurements that were performed in the linear strain regime for each individual sample. Experiments above room temperature were performed after the sample was equilibrated at the higher temperature. Stability checks were performed by short measurements at constant strain and frequency until a stable value was obtained.

Synthesis

CDI activated pEG (**3**). Bishydroxy functionalized pEG (20 kg/mol) (2.5 mmol, 50 g) was dried at 100 °C for 3 hours *in vacuo* and subsequently dissolved in 190 mL of chloroform. Carbonyl diimidazole (4 mmol, 656 mg) in 10 mL chloroform was added to the solution. The reaction mixture was stirred for 24 hours at room temperature. After full conversion, the reaction mixture was concentrated to 50 mL by the removal of chloroform *in vacuo*. Diethyl ether (400 mL) was added to the mixture that resulted in precipitation of the product. The product was obtained as a white solid after filtration and an additional washing step with diethyl ether. Yield = 46 g, 95%. ^{1}H-NMR (400 MHz, CDCl$_3$, δ): 8.15 (s, 2H, Ar-H), 7.68 (s, 4H, Ar-H) 4.50 (t, 4H, CH$_2$OC=O), 3.7-3.4 (b, 900H, O-(CH$_2$)$_2$-O).

General procedure for the synthesis of bisamino alkane functional pEG. The following procedure was used for all bisaminoalkane functional pEGs (**4a**-**c**) using the same reaction conditions as described for compound **4a**.

Bisamino octane functionalized pEG (**4a**). Compound **3** (0.5 mmol, 10 g) was dried *in vacuo* at 60 °C for three hours and subsequently dissolved in 75 mL of chloroform. The solution was added dropwise to a solution of 1,8-diaminooctane (8 mmol, 1.15 g) in 25 mL of chloroform. The reaction mixture was stirred for 24 hours at room temperature. After full conversion, the reaction mixture was concentrated to 50 mL by the removal of chloroform *in vacuo*. Diethyl ether (350 mL) was added to the mixture that resulted in precipitation of the product. The product was obtained by filtration and subsequently redissolved in 50 mL of chloroform and precipitated from diethyl ether. Precipitation in diethyl ether was repeated till full removal of the excess of 1,8-diaminooctane was achieved. Yield = 8.1 g, 80%. ^{1}H-NMR (400 MHz, CDCl$_3$, δ): 4.85 (s, 2H, NHC=O), 4.21 (t, 4H, CH$_2$O-C=O), 3.7 (b, 900H, O-(CH$_2$)$_2$-O), 3.15 (q, 4H, CH$_2$NHC=O), 2.65 (t, 4H, CH$_2$NH$_2$), 1.9-1.2 (mm, 16H, aliphatic).

Bisamino decane functionalized pEG (**4b**). Yield = 8 g, 78%. ^{1}H-NMR (400 MHz, CDCl$_3$, δ): 4.83 (s, 2H, NHC=O), 4.22 (t, 4H, CH$_2$O-C=O), 3.7 (b, 900H, O-(CH$_2$)$_2$-O), 3.16 (q, 4H, CH$_2$NHC=O), 2.65 (t, 4H, CH$_2$NH$_2$), 1.9-1.2 (mm, 20H, aliphatic).

Bisamino dodecane functionalized pEG (**4c**). Yield = 7.5 g, 73%. ^{1}H-NMR (400 MHz, CDCl$_3$, δ): 4.87 (s, 2H, NHC=O), 4.21 (t, 4H, CH$_2$O-C=O), 3.7 (b, 900H, O-(CH$_2$)$_2$-O), 3.18 (q, 4H, CH$_2$NHC=O), 2.64 (t, 4H, CH$_2$NH$_2$), 1.9-1.2 (mm, 24H, aliphatic).

General procedure for the synthesis of bisBTA alkane functional pEG. The following procedure was used for all bisBTA alkane functional pEGs (**1-2**) using the same reaction conditions as described for compound **1a**. For the synthesis of **2** we have used 3,5-bis-octylaminocarbonylbenzoic acid instead 3,5-bis-(3*S*)-(3,7-dimethyl-octylaminocarbonyl) benzoic acid that was used for the synthesis of **1a**-**c**.

BisBTA octane functionalized pEG (**1a**). Compound **4a** (0.05 mmol, 1 g), 3,5-bis-(3*S*)-(3,7-dimethyl-octylaminocarbonyl)-benzoic acid (0.12 mmol, 59 mg) were dissolved in 10 mL dry dichloromethane. Benzotriazol-1-yl-oxytripyrrolidinophosphonium hexafluorophosphate (PyBOP) (126 mg, 0.24 mmol) and *N,N*-diisopropylethylamine (DIPEA) (31 mg, 0.24 mmol) were added to the solution. The solution was stirred for 24 hours at room temperature. Dichloromethane was removed *in vacuo*. Subsequently, 50 mL of chloroform was added. The precipitates were removed by filtration. Chloroform was removed *in vacuo* and the product was dissolved in 10 mL of methanol and subsequently purified by dialysis. Yield = 0.72 g, 70%. ^{1}H-NMR (400 MHz, CDCl$_3$, δ): 8.41 (s, 6H, Ar), 6.9-6.6 (t, 6H, NH(C=O)), 4.85 (s, 2H, NH(C=O)O), 4.21 (t, 4H, C$\underline{H}_2$O-C=O), 3.7 (b, 900H, O-(C$\underline{H}_2$)$_2$-O), 3.48 (t, 12H, C$\underline{H}_2$NH(C=O)), 3.15 (q, 4H, C$\underline{H}_2$NH(C=O)O), 1.9-0.9 (mm, 58H, aliphatic). ^{13}C-NMR (100 MHz, CDCl$_3$, δ): 165.7, 135.3, 128.1, 69.7, 69.2, 67.7, 63.7, 63.2, 61.3, 60.9, 39.2, 38.4, 37.1, 36.7, 30.8, 29.2, 24.6, 22.7, 22.6, 19.5. GPC (chloroform, polystyrene standards): M_n = 18.6 kg/mol, *PDI* = 1.43. DSC (40 °C/min, third heating run): T_g = -60 °C, T_m = 57 °C with Δ*H* 136 J/g.

BisBTA decane functionalized pEG (**1b**) Yield = 0.65 g, 63%. ^{1}H-NMR (400 MHz, CDCl$_3$, δ): 8.40 (s, 6H, Ar), 6.9-6.6 (t, 6H, NH(C=O)), 4.95 (s, 2H, NH(C=O)O), 4.20 (t, 4H, C$\underline{H}_2$O-C=O), 3.7 (b, 900H, O-(C$\underline{H}_2$)$_2$-O), 3.50 (t, 12H, C$\underline{H}_2$NH(C=O)), 3.14 (q, 4H, C$\underline{H}_2$NH(C=O)O), 1.7-0.9 (mm, 66H, aliphatic). ^{13}C-NMR (100 MHz, CDCl$_3$, δ): 165.7, 135.4, 128.2, 67.7, 63.7, 39.2, 28.5, 37.1, 36.7, 30.8, 27.9, 24.6, 22.7, 22.6, 19.5. GPC (chloroform, polystyrene standards): M_n = 16.1 kg/mol, *PDI* = 1.52. DSC (40 °C/min, third heating run): T_g = -60 °C, T_m = 56 °C with Δ*H* 136 J/g.

BisBTA dodecane functionalized pEG (**1c**) Yield = 0.25 g, 75%. ^{1}H-NMR (400 MHz, CDCl$_3$, δ): 8.40 (s, 6H, Ar), 6.9-6.6 (t, 6H, NH(C=O)), 4.84 (s, 2H, NH(C=O)O), 4.26 (t, 4H, C$\underline{H}_2$O-C=O), 3.7 (b, 900H, O-(C$\underline{H}_2$)$_2$-O), 3.48 (t, 12H, C$\underline{H}_2$NH(C=O)), 3.15 (q, 4H, C$\underline{H}_2$NH(C=O)O), 1.9-0.9 (mm, 74H, aliphatic). ^{13}C-NMR (100 MHz, CDCl$_3$, δ): 165.7, 135.2, 128.1, 69.8, 69.1, 67.6, 63.7, 63.2, 61.2, 60.8, 39.2, 38.4, 37.1, 36.7, 30.8, 29.2, 27.0, 26.9, 24.6, 22.7, 22.6, 19.3. GPC (chloroform, polystyrene standards): M_n = 17.5 kg/mol, *PDI* = 1.38. DSC (40 °C/min, third heating run): T_g = -61 °C, T_m = 57 °C with Δ*H* 144 J/g.

BisBTA decane functionalized pEG (**2**) Yield = 0.30 g, 85%. ^{1}H-NMR (400 MHz, CDCl$_3$, δ): 8.42 (s, 6H, Ar), 6.82 (t, 6H, NH(C=O)), 4.85 (t, 2H, NH(C=O)O), 4.21 (t, 4H, C$\underline{H}_2$O-C=O), 3.7 (b, 900H, O-(C$\underline{H}_2$)$_2$-O), 3.48 (t, 12H, C$\underline{H}_2$NH(C=O)), 3.10 (q, 4H, C$\underline{H}_2$NH(C=O)O), 1.6-0.9 (mm, 58H, aliphatic). ^{13}C-NMR (100 MHz, CDCl$_3$, δ): 165.8, 135.2, 128.2, 70.5, 63.7, 41.0, 40.3, 31.7, 29.9, 29.4, 29.3, 29.2, 27.0, 26.9, 26.7, 22.6, 14.1. GPC (chloroform, polystyrene standards): M_n = 18.2 kg/mol, *PDI* = 1.34. DSC (40 °C/min, third heating run): T_g = -62 °C, T_m = 57 °C with Δ*H* 141 J/g.

4.7 References and notes

[1]   B. V. Slaughter, S. S. Khurshid, O. Z. Fisher, A. Khademhosseini, N. A. Peppas, *Adv. Mater.* **2009**, *21*, 3307.

[2]   H. Dai, Q. Chen, H. Qin, Y. Guan, D. Shen, Y. Hua, Y. Tang, J. Xu, *Macromolecules* **2006**, *39*, 6584.

[3]   N. A. Peppas, J. Z. Hilt, A. Khademhosseini, R. Langer, *Adv. Mater.* **2006**, *18*, 1345.

[4]   T. R. Hoare, D. S. Kohane, *Polymer* **2008**, *49*, 1993.

[5]   I. Tokarev, S. Minko, *Adv. Mater.* **2010**, *22*, 3446.

[6]   C. Wang, R. R. Varshney, D.-A. Wang, *Adv. Drug Deliver. Rev.* **2010**, *62*, 699.

[7]   P. N. Desai, Q. Yuan, H. Yang, *Biomacromolecules* **2010**, *11*, 666.

[8]   K. Y. Lee, D. J. Mooney, *Chem. Rev.* **2001**, *101*, 1869.

[9]   H.-J. Yoon, W.-D. Jang, *J. .Mater. Chem.* **2010**, *20*, 211.

[10]   V. Kozlovskaya, S. A. Sukhishvili, *Macromolecules* **2006**, *39*, 6191.

[11]   Y. Xu, K. Sato, K. Mawatari, T. Konno, K. Jang, K. Ishihara, T. Kitamori, *Adv. Mater.* **2010**, *22*, 3017.

[12]   P. Calvert, *Adv. Mater.* **2009**, *21*, 743.

[13]   E. Carretti, S. Grassi, M. Cossalter, I. Natali, G. Caminati, R. G. Weiss, P. Baglioni, L. Dei, *Langmuir* **2009**, *25*, 8656.

[14]   J. W. Steed, *Chem. Commun.* **2010**, *47*, 1379.

[15]   M. George, R. G. Weiss, *Acc. Chem. Res.* **2006**, *39*, 489.

[16]   P. Dastidar, *Chem. Soc. Rev.* **2008**, *37*, 2699.

[17]   L. A. Estroff, A. D. Hamilton, *Chem. Rev.* **2004**, *104*, 1201.

[18]   P. Terech, R. G. Weiss, *Chem. Rev.* **1997**, *97*, 3133.

[19]   F. Rodriguez-Llansola, B. Escuder, J. F. Miravet, *J. Am. Chem. Soc.* **2009**, *131*, 11478.

[20]   V. Jayawarna, M. Ali, T. A. Jowitt, A. F. Miller, A. Saiani, J. E. Gough, R. V. Ulijn, *Adv. Mater.* **2006**, *18*, 611.

[21]   E. F. Banwell, E. S. Abelardo, D. J. Adams, M. A. Birchall, A. Corrigan, A. M. Donald, M. Kirkland, L. C. Serpell, M. F. Butler, D. N. Woolfson, *Nat. Mater.* **2009**, *8*, 596.

[22]   R. J. Williams, A. M. Smith, R. Collins, N. Hodson, A. K. Das, R. V. Ulijn, *Nat. Nano.* **2009**, *4*, 19.

[23]   P. Terech, *Langmuir* **2009**, *25*, 8370.

[24]   J. H. van Esch, *Langmuir* **2009**, *25*, 8392.

[25]   J. Chen, J. W. Kampf, A. J. McNeil, *Langmuir* **2010**, *26*, 13076.

[26]   F. Allix, P. Curcio, Q. N. Pham, G. Pickaert, B. Jamart-Grégoire, *Langmuir* **2010**, *26*, 16818.

[27]   A. R. Hirst, I. A. Coates, T. R. Boucheteau, J. F. Miravet, B. Escuder, V. Castelletto, I. W. Hamley, D. K. Smith, *J. Am. Chem. Soc.* **2008**, *130*, 9113.

[28]   L. Chen, S. Revel, K. Morris, L. C. Serpell, D. J. Adams, *Langmuir* **2010**, *26*, 13466.

[29]   M. de Loos, J. H. van Esch, R. M. Kellogg, B. L. Feringa, *Tetrahedron* **2007**, *63*, 7285.

[30]   L. Brunsveld, A. P. H. J. Schenning, M. A. C. Broeren, H. M. Janssen, J. A. J. M. Vekemans, E. W. Meijer, *Chem. Lett.* **2000**, 292.

[31]   M. M. J. Smulders, A. P. H. J. Schenning, E. W. Meijer, *J. Am. Chem. Soc.* **2008**, *130*, 606.

[32]   P. J. M. Stals, J. F. Haveman, R. Martín-Rapún, C. F. C. Fitié, A. R. A. Palmans, E. W. Meijer, *J. Mater. Chem.* **2009**, *19*, 124.

[33]   M. M. J. Smulders, T. Buffeteau, D. Cavagnat, M. Wolffs, A. P. H. J. Schenning, E. W. Meijer, *Chirality* **2008**, *20*, 1016.

[34]   K. Hanabusa, C. Koto, M. Kimura, H. Shirai, A. Kakehi, *Chem. Lett.* **1997**, 429.

[35]   T. Shikata, D. Ogata, K. Hanabusa, *J. Phys. Chem. B* **2004**, *108*, 508.

[36]   T. Shikata, Y. Kuruma, A. Sakamoto, K. Hanabusa, *J. Phys. Chem. B* **2008**, *112*, 16393.

[37]   Y. Yasuda, E. Iishi, H. Inada, Y. Shirota, *Chem. Lett.* **1996**, 575.

[38]   S. Lee, J.-S. Lee, C. H. Lee, Y.-S. Jung, J.-M. Kim, *Langmuir* **2011**, *27*, 1560.

[39]   K. C. Tam, R. D. Jenkins, M. A. Winnik, D. R. Bassett, *Macromolecules* **1998**, *31*, 4149.

[40]   S. X. Ma, S. L. Cooper, *Macromolecules* **2001**, *34*, 3294.

[41]   J.-F. Berret, D. Calvet, A. Collet, M. Viguier, *Curr. Opin. Colloid In.* **2003**, *8*, 296.

[42]   T. Vermonden, N. A. M. Besseling, M. J. van Steenbergen, W. E. Hennink, *Langmuir* **2006**, *22*, 10180.

[43]   F. van de Manakker, L. M. J. Kroon-Batenburg, T. Vermonden, C. F. van Nostrum, W. E. Hennink, *Soft Matter* **2010**, *6*, 187.

[44]   F. Zeng-guo, Z. Sanping, *Polymer* **2003**, *44*, 5177.

[45]   P.Y.W. Dankers, T.M. Hermans, T.W. Baughman, Y. Kamikawa, R.E. Kieltyka, M.M.C. Bastings, N.A.J.M. Sommerdijk, A. Larsen. A.W. Bosman, M.J.A van Luyn, E.R. Popa, G. Fytas, E.W. Meijer. **2011** in prep.

[46]   T. F. A. Greef, M. M. L. Nieuwenhuizen, P. J. M. Stals, C. F. C. Fitié, A. R. A. Palmans, R. P. Sijbesma, E. W. Meijer, *Chem. Commun.* **2008**, 4306.

[47]   E. Obert, M. Bellot, L. Bouteiller, F. Andrioletti, C. Lehen-Ferrenbach, F. Boue, *J. Am. Chem. Soc.* **2007**, *129*, 15601.

[48]   N. Chebotareva, P. H. H. Bomans, P. M. Frederik, N. A. J. M. Sommerdijk, R. P. Sijbesma, *Chem. Commun.* **2005**, 4967.

[49]   The nanorod width is determined with the graphic analysis software ImageJ.

[50]   J. Boekhoven, P. van Rijn, A. M. Brizard, M. C. A. Stuart, J. H. van Esch, *Chem. Commun.* **2010**, *46*, 3490.

[51]   P. J. M. Stals, M. M. J. Smulders, R. Martín-Rapún, A. R. A. Palmans, E. W. Meijer, *Chem. Eur. J.* **2009**, *15*, 2071.

[52]   S. Saeki, N. Kuwahara, M. Nakata, M. Kaneko, *Polymer* **1976**, *17*, 685.

[53]   J. Francois, E. Beaudoin, O. Borisov, *Langmuir* **2003**, *19*, 10011.

[54]   L. A. Hough, H. D. Ou-Yang, *Phys. Rev. E* **2006**, *73*, 031802.

[55]   M. A. Winnik, A. Yekta, *Curr. Opin. Colloid In.* **1997**, *2*, 424.

[56]   T. Annable, R. Buscall, R. Ettelaie, D. Whittlestone, *J. Rheol.* **1993**, *37*, 695.

[57]   M.M.J. Smulders, PhD Thesis, Chapter 2, **2009**.

[58]   Sample preparation of 1a-c was not straightforward and all samples suffered from small air bubbles.

[59]   R. G. Weiss, P. Terech, *Molecular Gels. Materials with Self-Assembled Fibrillar Networks*, Springer, Dordrecht, **2006**.

[60]   H. Barnes, *A Handbook of Elementary Rheology*, University of Wales, Aberystwyth, **2000**.

[61]   J. R. Roosma, T. Mes, P. E. L. G. Leclere, A. R. A. Palmans, E. W. Meijer, *J. Am. Chem. Soc.* **2008**, *130*, 1120.

5

Supramolecular cross-linking via orthogonal self-assembly

Abstract. Low molecular weight polymers end-functionalized with supramolecular motifs exhibit macroscopic material properties similar to those of large macromolecules as a result of the presence of phase segregated nanorods formed by aggregated supramolecular motifs. This leads to strong, multiple physical cross-linking points in two or three dimensions that can result in thermoplastic elastomeric properties. Supramolecular motifs end-capped to a bifunctional telechelic polymer can phase segregate in the same or in another nanorod. Only in the latter case, a cross-link is formed that strengthens the polymer network. This chapter introduces a supramolecular polymer system, which consists of a mixture of benzene-1,3,5-tricarboxamides (BTAs) and ureidopyrimidinones (UPys) end-capped to monofunctional polymers. Both supramolecular motifs self-assemble in an orthogonal fashion into two separate types of phase segregated nanorods without forming cross-links. As a result, the macroscopic properties are poor. We added an α, ω-telechelic polymer containing both the BTA and UPy motif (compatibilizer) to this system. The addition of only a small amount (15 mol%) of this compatibilizer to the mixture of the monofunctional polymers transforms a viscous sticky liquid into a solid material with elastomeric properties.

5.1 Introduction

Supramolecular polymers are an exciting class of polymers because of their reversible and dynamic character. Their reversible character is a consequence of the non-covalent nature of interactions applied such as hydrogen bonding, π-π interactions, dipole interactions, metal-ligand complexation, hydrophobic or solvophobic interactions. Particularly interesting are low molecular weight polymer chains end-capped[1-8] or grafted in the side-chain[9-13] with multiple hydrogen bonding motifs. Tunable thermal and material properties result from the controlled assembly and disassembly of these hydrogen bonds,[1, 14-22] which gives rise to unique material properties with applications envisioned in biomaterials,[23-25] self-healing materials,[26-30] and hydrogels.[31-34] In suitable conditions, these supramolecular polymers display macroscopic material properties comparable to high molecular weight macromolecules. A significant increase in potential applications is found in systems that make use of different types of non-covalent interactions, or different supramolecular motifs that self-assemble in an orthogonal fashion[35-41] Orthogonal self-assembly is the independent formation of two different supramolecular structures, each with their own characteristics that co-exist within a single system.[42] Applying different stimuli on these materials can give rise to versatile material properties arising from the same compound.[43-45]

The group of Weck investigated side-[11, 12, 46] and end-functionalized[39-41, 47] supramolecular polymers bearing orthogonal binding sites in great detail. Particularly elegant is the combination of different recognition motifs based on hydrogen bonding, in which complementary pairs based on the Hamilton receptor - cyanuric acid and diamidonaphtyridine - ureidoguanosine form tricoblockpolymers in an orthogonal fashion.[40] Studies on these polymers were carried out in solution, with the aim to increase the level of functionality in supramolecular polymers. It is anticipated, however, that also in the solid state these well-defined polymers with multiple recognition units can impart novel properties.

We here investigate the ability of benzene-1,3,5-tricarboxamide (BTA) and 2-ureido-4[1*H*]-pyrimidinone (UPy) functionalized materials to self-assemble in an orthogonal fashion in solution and also in the solid state. BTAs cooperatively self-assemble into columnar aggregates in apolar solvents via a nucleation-elongation mechanism.[48] A threefold, helical arrangement of the intermolecular hydrogen bonds between consecutive discs stabilizes the columnar packing, and a preferred helical sense is induced upon introducing one or more stereogenic centra in the alkyl side chain.[48, 49] In contrast, the UPy motif dimerizes via strong, quadruple hydrogen bonds (K_{dim} = 6 x 10^7 M^{-1} in chloroform) in an isodesmic fashion.[50, 51] Based on the significant differences in the hydrogen bonding arrays and the mechanistic differences in the self-assembly process of both motifs, an orthogonal self-assembly process of both units is expected.

Previously, it has been shown that thermoplastic elastomeric properties can be obtained, when the quadruple hydrogen bonding UPy unit, in combination with additional lateral interactions, is attached to low molecular weight bifunctional telechelic polymers.[1, 7, 52] We also showed the presence of one dimensional columnar structures in various telechelics functionalized with the BTA motif.[5, 53] In both cases, the material properties arose from the presence of cross-linked phase segregated nanorods consisting of BTAs or UPys. Supramolecular motifs that possess the ability to form phase segregated nanorods, attached to bifunctional telechelics can phase segregate into the same (homo) or into another (hetero) nanorod. In the latter case, a hetero (functional) cross-link is formed. These heterofunctional cross-links contribute significantly to the network strength and are responsible for the elastomeric properties. Here, we present a supramolecular polymeric system that consists of a mixture of low molecular weight polymers monofunctionalized with either a BTA or a UPy motif that forms separate phase segregated nanorods. To this mixture we added a hetero bifunctional α-BTA ω-UPy polymer as a supramolecular compatibilizer to induce cross-linking of the phase segregated nanorods. Our approach is illustrated in Scheme 5.1.

Scheme 5.1 The addition of a supramolecular compatibilizer generates material properties in a supramolecular polymer blend.
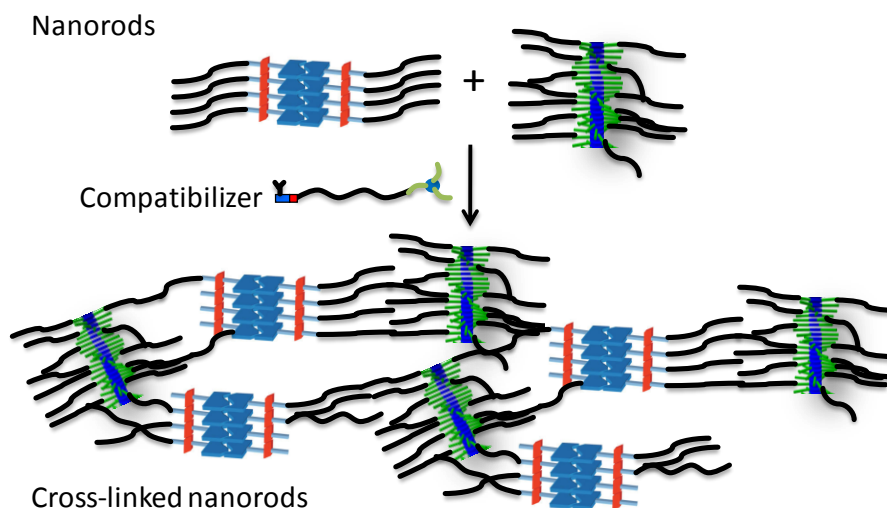
5.2 Synthesis

We synthesized two compounds (**1**-**2**) containing both the BTA and UPy motif, and four compounds (**3**-**6**) containing only one supramolecular motif (BTA or UPy) (Scheme 5.2). Compound **1** consists of a BTA connected to a UPy via a short spacer and is used as a model compound to study the self-assembly properties in the solid state and in dilute solution. Compound **2** consists of a BTA connected to a UPy via a long poly(ethylene-*co*-butylene)

(pEB) spacer making it suitable to act as a compatibilizer. The apolar and amorphous pEB does not interfere with hydrogen bonding interactions[53] and shows excellent solubility properties in apolar solvents. Compounds **3** and **4** are based on the compatibilizer (**2**) but contain only one supramolecular motif. Compound **3** and **4** are used as reference compounds to investigate the self-assembly of both motifs individually. Compound **5** and **6** are used to demonstrate the principle of the supramolecular compatibilizer on a macroscopic scale.

Scheme 5.2 Molecular structure of mono- and α, ω-bifunctionalized supramolecular compounds **1-6**.
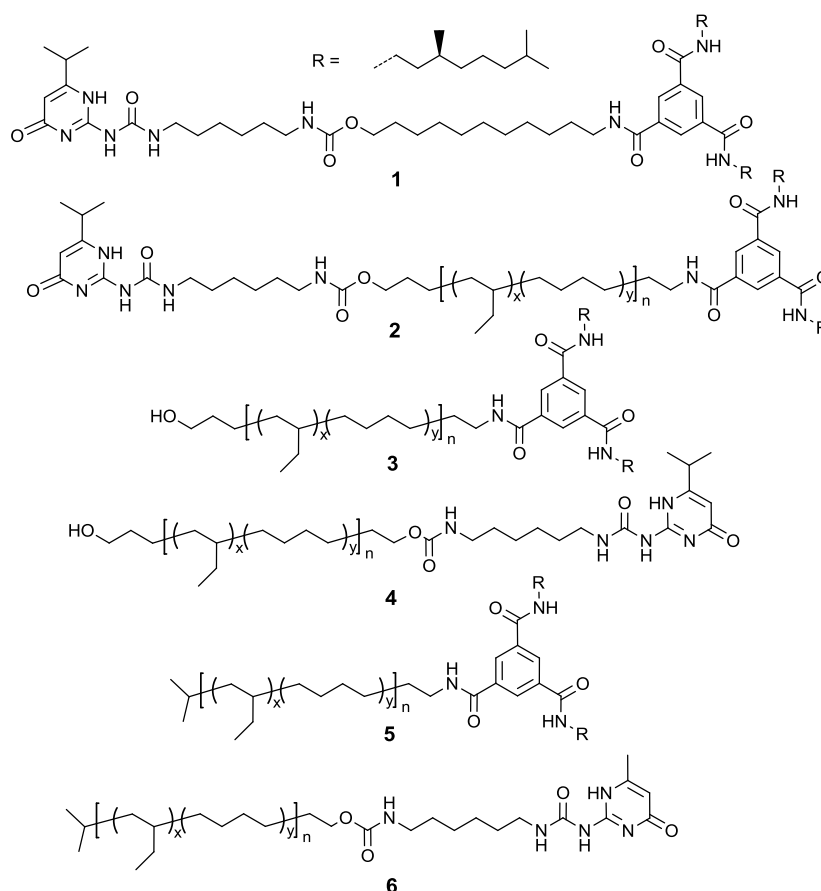
Table 5.1 Summary of NMR, GPC and DSC data of compounds **1-6**.

Compound	Ratio BTA/UPy	Yield [%]	M_n[a] [kg/mol]	M_n[b] [kg/mol]	PDI[b] [-]	T_g[c] [°C]	T_{m1}[c] [°C]	ΔH_1[c] [J/g]	T_{m2}[c] [°C]	ΔH_2[c] [J/g]
1	50/50	80	1.1	n.a.	n.a.	-	40	2.53	85	3.75
2	50/50	60	6.2	12.7	1.03	-60	-	-	140	0.7
3	100/0	95	6.0	12.0	1.03	-60	-	-	170	1.89
4	0/100	90	5.8	11.6	1.03	-60	-	-	-	-
5	100/0	95	4.0	7.6	1.03	-60	-	-	192	4.09
6	0/100	95	3.9	7.9	1.03	-61	39	2.93	-	-
5/6	50/50	n.a.	n.a.	n.a.	n.a.	-60	38	0.18	153	1.02
2/5/6	50/50	n.a.	n.a.	n.a.	n.a.	-62	37	0.29	147	1.01

n.a. = not applicable. [a] Determined by ^{1}H-NMR. [b] Determined by GPC in chloroform. [c] Derived from the second heating run (40 K min^{-1}).

Model compound **1** consists of a BTA connected via a short undecanyl spacer to an isopropyl substituted UPy (Scheme 5.3). The isopropyl UPy was chosen to ensure the solubility of **1** in apolar solvents. Compound **1** was obtained via the coupling of a hydroxyl functionalized BTA (**7**) with an isocyanate functionalized UPy (**8**) in the presence of dibutyltin dilaurate (DBTDL) as a catalyst.

Scheme 5.3 Synthesis of model compound **1**.
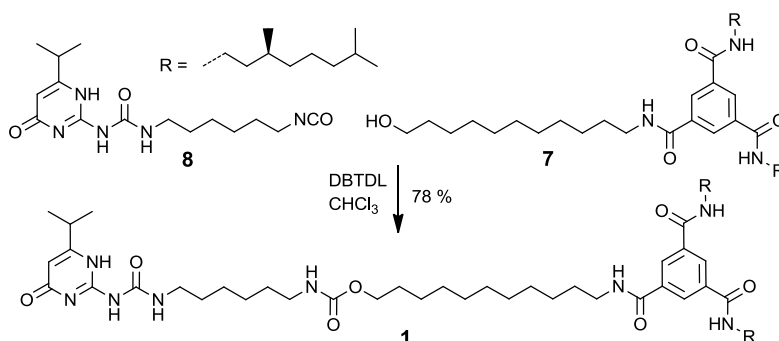
The synthesis of **9** was performed by Vincent Scalfani from the Department of Chemistry, Colorado State University in the United States of America. The hetero-telechelic pEB backbone **9** required for the synthesis of compound **2** was procured via the anionic polymerization of 1,3-butadiene, employing a silyl protected hydroxyl-propyllithium

derivative as the initiator (Scheme 5.4). The polymerization was terminated with an excess of ethyleneoxide and quenched with aqueous methanol to generate a hydroxyl group. According to ^{1}H-NMR, the polymer backbone consisted of perfect α-siloxy ω-hydroxy functional groups. Gel permeation chromatography (GPC) analysis of **9** showed a M_n of 11.4 kg/mol and a *PDI* of 1.03, with respect to polystyrene standards. The 1,2 content was 57% resulting in ethylene/butylene ratio of 43/57. Subsequently, the hydroxyl group was converted into an amine by a Mitsunobu reaction with phthalimide followed by hydrolysis using hydrazine, to afford polymer **11**. The BTA precursor (**15**) was coupled to the amine **11** using PyBOP as the coupling agent. Then, the double bonds present in polymer **12** were saturated by a homogeneous hydrogenation reaction with *para*-toluene sulfonyl hydrazide (*p*TSH) in the presence of a base. Coincidentally, the silyl protecting group was cleaved during the hydrogenation yielding polymer **3**, which contains a free hydroxyl group. BTA-pEB-UPy **2** was finally obtained after the addition of the isocyanate functionalized UPy motif in the presence of DBTDL.

Scheme 5.4 Synthesis of compound **2** and **3**.

The UPy mono-functional reference compound (**4**) was synthesized starting from compound **9** by adding the isocyanate UPy (**8**) (Scheme 5.5). The double bonds present in polymer **13** were saturated by a homogeneous hydrogenation reaction with *p*TSH in the presence of a base. The silyl protecting group was cleaved during the hydrogenation yielding polymer **4**.

Scheme 5.5 Synthesis of compound **4**.
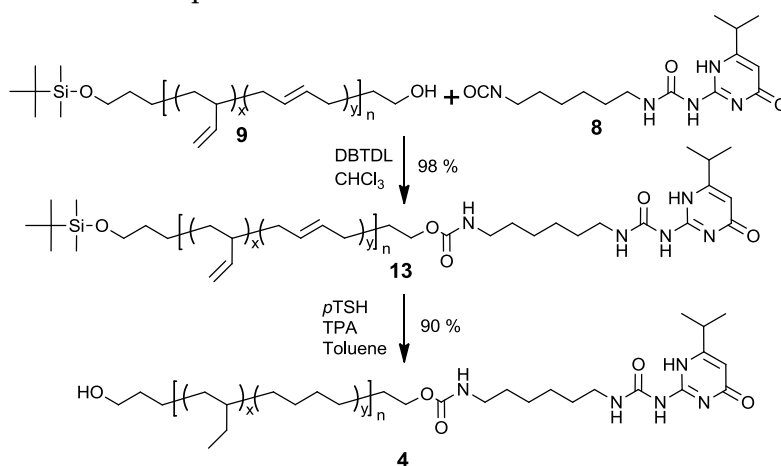
Compound **5** was synthesized starting from the commercially available mono hydroxyl functionalized pEB produced by Kraton®. This pEB has a molecular weight of ~3500 g/mol and the ratio of ethylene/butylene is 45/55. The hydroxyl group was converted into an amine by a Mitsunobu reaction with phthalimide followed by hydrolysis using hydrazine, to afford polymer **14**. The BTA precursor (**15**) was coupled to the amine **11** using PyBOP as the coupling agent.

Scheme 5.6 Synthesis of compound **5**.
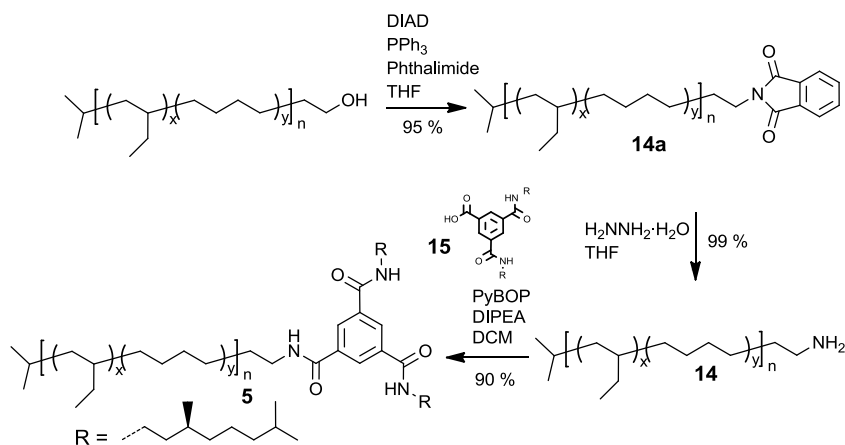
Compound **6** was obtained via the coupling of a commercially available mono hydroxyl functionalized pEB with an isocyanate functionalized methyl substituted UPy (**16**) in the presence of DBTDL as a catalyst (Scheme 5.7).

Scheme 5.7 Synthesis of compound **6**.
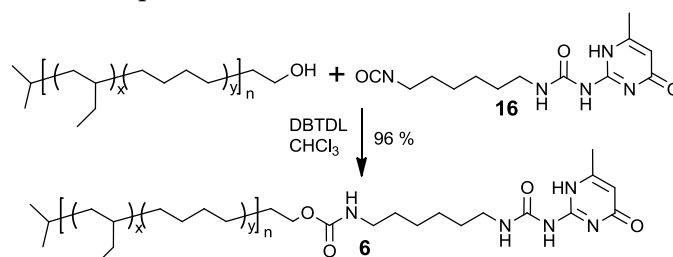
GPC analysis of polymers **2**-**6** showed narrow polydispersities and molecular weights between 7.6 and 12.7 kg/mol (Table 5.1). The proposed structure of compound **1** and polymers **2**-**6** was consistent with the results obtained from NMR.

5.3 Phase behavior and infrared spectroscopy

The thermal properties of compounds **1**-**6** were fully characterized with differential scanning calorimetry (DSC) and the origin of the thermal transitions were assigned with the help of polarized optical spectroscopy (POM) and infrared spectroscopy (IR). The data are summarized in Table 5.1. The DSC trace of compound **1** showed a phase transition at 40 °C (ΔH = 2.53 J/g) and at 85 °C (ΔH = 3.76 J/g). With the help of POM, we could assign a crystalline state below 40 °C, a liquid crystalline state between 40 °C and 85 °C, and an isotropic state above 85 °C. Polymer **2** showed a T_g at -60 °C, resulting from the pEB part, and a small transition around 140 °C (ΔH = 0.7 J/g). The mobile, birefringent texture present from 50 °C up to around 135 °C was typical for a nematic phase and at 135 °C the sample became isotropic. The thermal behavior of BTA-functionalized polymers **3** and **5** was very similar. For both polymers, a T_g was found at -60 °C. An additional, small transition was found at around 170 °C (ΔH = 0.92 J/g) and 192 °C (ΔH = 4.09 J/g) for polymer **3** and **5,** respectively. In both cases, POM revealed a mobile, birefringent texture typical for a nematic phase starting from room temperature up to the clearing temperature at around 170 °C and 190 °C, for **3** and **5** respectively. In contrast, the DSC trace of UPy-functionalized polymer **4** only showed a T_g at -60 °C. Polymer **6** showed a T_g at around -61 °C, and a small transition around 37 °C (ΔH = 2.93 J/g). Between room temperature and the clearing temperature of 45 °C, an unidentified, birefringent texture was observed.

The phase transitions observed in compounds **1**-**6** appear to be connected to the loss of the intermolecular hydrogen bonds and the corresponding disappearance of the BTA and/or UPy-urethane nanorods in the solid state. To investigate this in more detail, we performed

variable temperature IR measurements on compounds **1**-**6**, since this is a sensitive technique to investigate hydrogen bonding in the solid state.[49, 54] The IR spectra of compound **1** showed significant changes in the v = 3400-3150 cm^{-1} and 1750-1500 cm^{-1} region upon increasing the temperature (Figure 5.1).
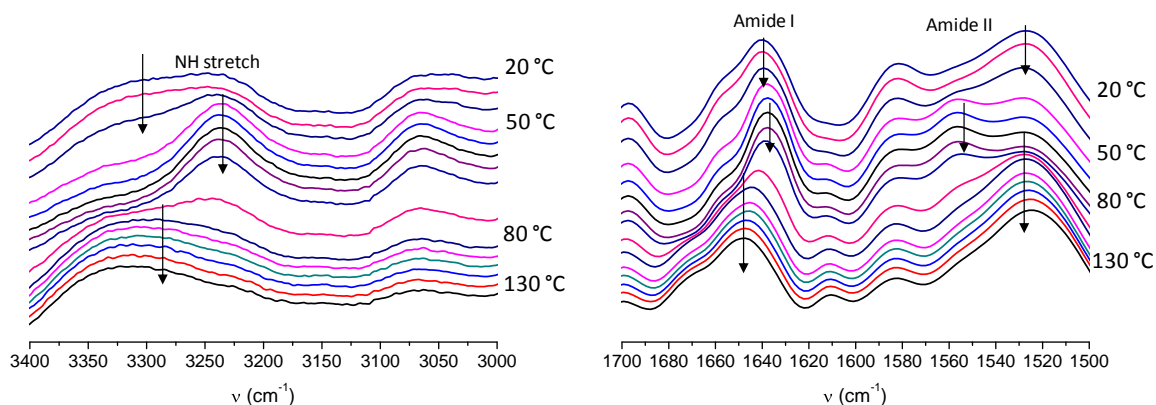
Figure 5.1 IR spectra of **1** at different temperatures.

Although the vibrational signals from the BTA and UPy-urethane motif slightly overlap, the temperatures at which the signals started shifting coincide with the temperatures at which the phase transitions were observed in DSC for compound **1**. From the DSC transition temperatures and the changes in IR, we attribute the first phase transition at 45 °C to the loss of lateral hydrogen bonds between the UPy-urethane groups. Interestingly, this transition coincides with the occurrence of vibrations typical for BTAs involved in threefold intermolecular hydrogen bonding, visible from 45 °C to 85 °C (v(N-H) 3240 cm^{-1}, v(amide I) 1640 cm^{-1} and v(amide II) 1555 cm^{-1}). Above 85 °C, the BTA hydrogen bonds are lost resulting in the isotropic phase as observed with DSC and POM. The concurrence of the loss of hydrogen bonding between the UPy-urethane groups and formation of threefold intermolecular hydrogen bonding between BTAs in combination with the relatively low clearing temperature (85 °C) suggests that the thermal behavior of **1** at room temperature, is dominated by crystallization of the UPy-urethane part and therefore destabilizes the BTA aggregates. In polymers **2** and **3** the thermal transition at 140 °C and 170 °C, respectively, are attributed to the loss of the threefold intermolecular hydrogen bonding of BTA motifs (Figure 5.2A). Around 50 °C, a small shift at v = 1700 cm^{-1} to v = 1695 cm^{-1} was observed in polymer **2** (Figure 5.2B). The comparison with polymer **4** shows that this vibration arises from the isocytosine part of the UPy and is presumably connected to the loss of UPy-urethane hydrogen bonding.[55]
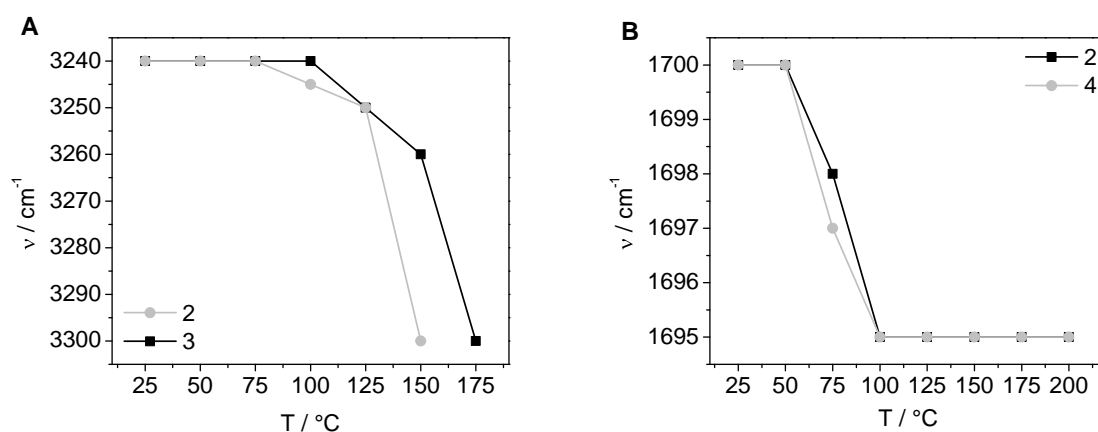
Figure 5.2 A) IR spectra of **2** and **3**. The position of the NH stretch vibration is plotted versus temperature. B) IR spectra of **2** and **4**. The position of the UPy isocytosine C=O vibration is plotted versus temperature.

5.4 Self-assembly in dilute solution

While the mechanistic aspects of the self-assembly behavior of BTAs and of UPys has been studied in great detail in our group, their self-assembly in a mixed system containing both BTAs and UPys is unexplored. The self-assembly of **1** was studied with temperature-dependent circular dichroism (CD) and ultraviolet (UV) spectroscopy. The helical BTA aggregates formed in alkane solvents are characterized by a λ_{max} of 192 nm in UV spectroscopy and a Cotton effect at 223 nm with $|\Delta\varepsilon|$ = 43 L/mol cm.[48, 54] In contrast, the dimerization of the UPy group can be probed by UV spectroscopy since the 4[1*H*] pyrimidinone tautomer (dimerized UPy) has a λ_{max} of 260 nm, while the 6[1*H*] pyrimidinone tautomer (monomeric UPy) has a λ_{max} of 285 nm.[56] We selected methylcyclohexane (MCH) as the solvent of choice because of its capability to stabilize hydrogen bonds. A solution of **1** (c = 1.5 x 10^{-5} M) was heated to 80 °C and cooled to 10 °C at a rate of 1 K min^{-1}. The CD signal at 223 nm and UV signals at 211 nm, which is close to λ_{max} for BTAs in a molecularly dissolved state, and 285 nm, the λ_{max} for UPy in the monomeric tautomeric form, were probed as a function of temperature (Figure 5.3A,B).
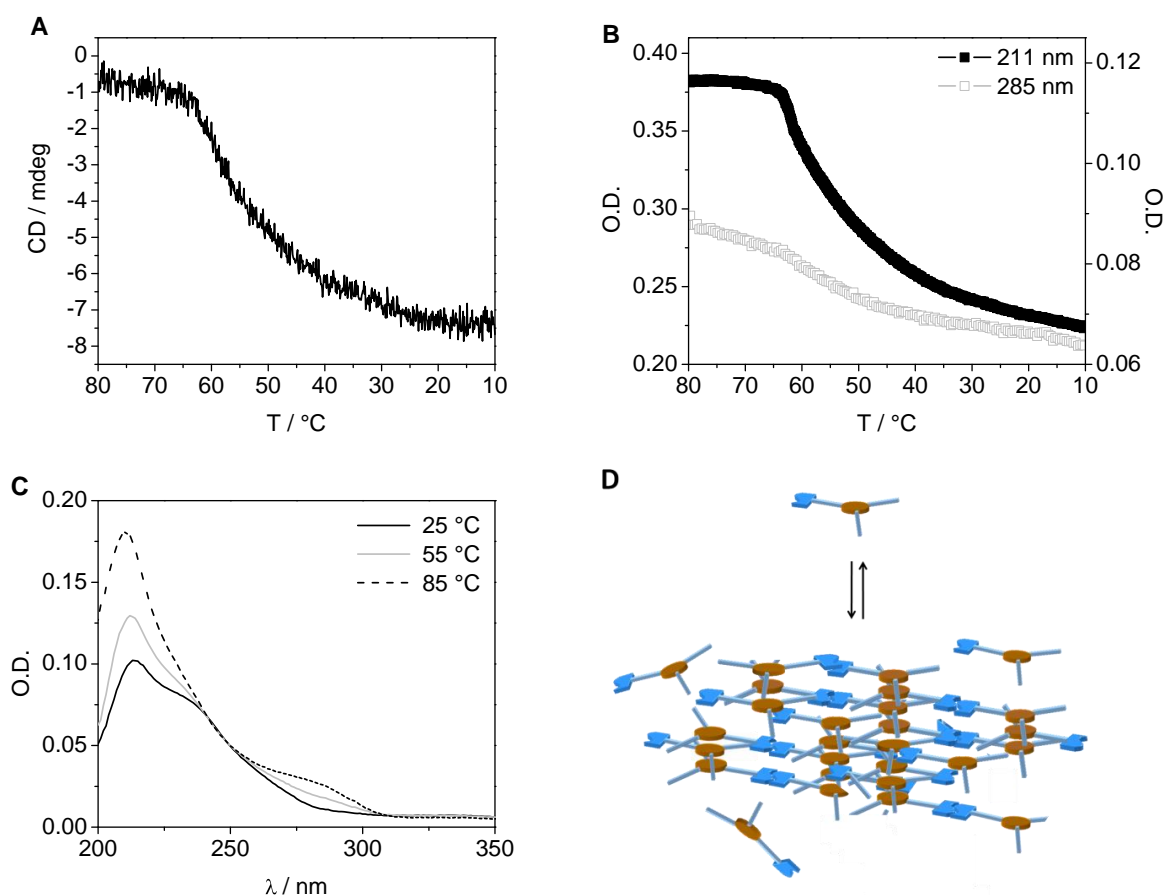
Figure 5.3 A) CD cooling curve of **1** at 223 nm (c = 1.5 x 10⁻⁵ M in MCH, l = 1.0 cm.) B) UV cooling curves of **1** at 211 (black line) and 285 nm (grey line) (c = 1.5 x 10⁻⁵ M in MCH, l = 1.0 cm). C) UV spectra of **1** at different temperatures (c = 1.5 x 10⁻⁵ M in MCH, l = 1.0 cm). D) Schematic representation of the self-assembly of **1**. UPy dimerization and BTA aggregation occurs at the same moment, which results in the formation of a network.

The sudden appearance of a Cotton effect upon cooling the solution from 80 °C, at which **1** is molecularly dissolved, to 10 °C is typical for a nucleation-elongation type self-assembly process, in which an unfavorable nucleation phase is separated by a favorable elongation phase by the temperature of elongation T_e.[48] Surprisingly, the molar ellipticity ($\Delta\varepsilon$ = -16 L/mol cm), which reflects the degree of aggregation of BTAs, is around 3 times lower than we previously found for unbound BTAs.[48] Presumably, the formation of BTA aggregates is hindered by the presence of the UPy-urethane group. In addition, the T_e of 65 °C is significant higher than expected at this concentration. This is probably the result of the poor solubility of compound **1**. Temperature-dependent UV measurements also showed a sudden decrease in optical density, coinciding at 65 °C for both wavelengths (Figure 5.3B,C). The results show convincingly that the self-assembly of BTAs and of UPys coexists in solution. Remarkably, the self-assembly of both motifs start at the same temperature, which suggests

that they are connected. The relatively short and rigid linker separating both motifs may be responsible for this phenomenon (Figure 5.3D).
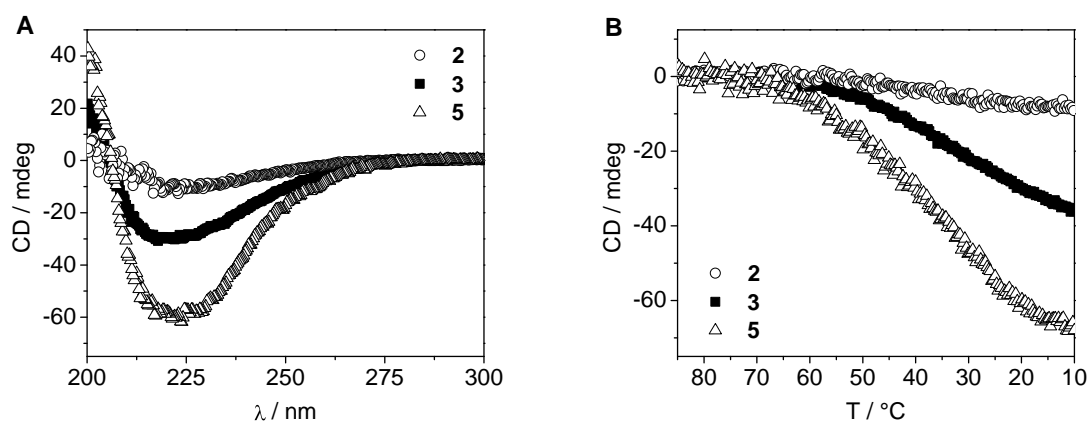

Figure 5.4 A) CD spectra of **2**, **3** and **5** (c = 5 x 10^{-4} M in MCH, T = 20 °C, l = 1.0 mm). B) CD cooling curve of **2**, **3** and **5** (λ = 223 nm, c = 5 x 10^{-4} M in MCH, l = 1.0 mm).

In BTA-pEB-Upy (**2**) both supramolecular motifs are separated by a flexible polymer (Scheme 5.1). CD spectroscopy was performed on solutions of **2** and reference polymers **3** and **5** at c = 5 x 10^{-4} M in MCH. At room temperature, polymers **2**, **3** and **5** showed Cotton effects similar in shape but different in size. The Cotton effect of **2**, **3** and **5** at 223 nm is -10, -28 and -58 mdeg, respectively (Figure 5.4A). Temperature-dependent CD measurements showed the appearance of a Cotton effect upon cooling the solutions from 85 °C, at which the BTAs in **2**, **3** and **5** are molecularly dissolved, to 10 °C (Figure 5.4B). The T_e for polymers **2**, **3** and **5** are 55, 65 and 75 °C, respectively. The appearance of the Cotton effect at the T_e is a more gradual process for **2**, **3** and **5** compared to that of **1** or unbound BTAs (Chapter 3).

Interestingly, the Cotton effect and the T_e of BTA-pEB-UPy **2** are lower than that of HO-pEB-BTA **3**. PEB-BTA (**5**), which consists of one BTA connected to a pEB with a molecular weight of 3.8 kg/mol, displayed the largest Cotton effect and the highest T_e. It has been observed previously that the association constants of supramolecular motifs decrease when they are connected to a polymer backbone, presumably as a result of the steric crowding that the polymer imposes.[57, 58] The molecular weight of the pEB part in **3** and in **5** is 5.5 kg/mol and 3.8 kg/mol, respectively. Therefore, it is assumed that steric crowding is more pronounced in **3** than in **5**, resulting in a smaller degree of aggregation with a smaller corresponding Cotton effect. This rationalizes the difference of the aggregation behavior of **3** and **5**. The aggregation of BTAs in compound **2** is less strong as seen in **3** but the polymer backbone has the same length. Since UPy groups possess a strong dimerization constant in chloroform (K_{dim} = 6 x 10^7 M^{-1}), it is likely that in the less polar MCH, UPy groups of **2** are dimerized at this concentration. In fact, the presence of UPy dimers in a solution of **2** was verified by UV spectroscopy measurements (Figure 5.5A). The absorption of the 6[1*H*]

pyrimidinone tautomer (monomeric UPy) at 285 nm was only visible at 80 °C in a 1.25×10^{-6} M solution in MCH, confirming the presence of UPy dimers in a solution with a concentration of 5×10^{-4} M in MCH. As a result, the dimerization of the UPy groups lead to an increase of the virtual molecular weight of the pEB backbone, which results in a lower degree of BTA aggregation in **2**.
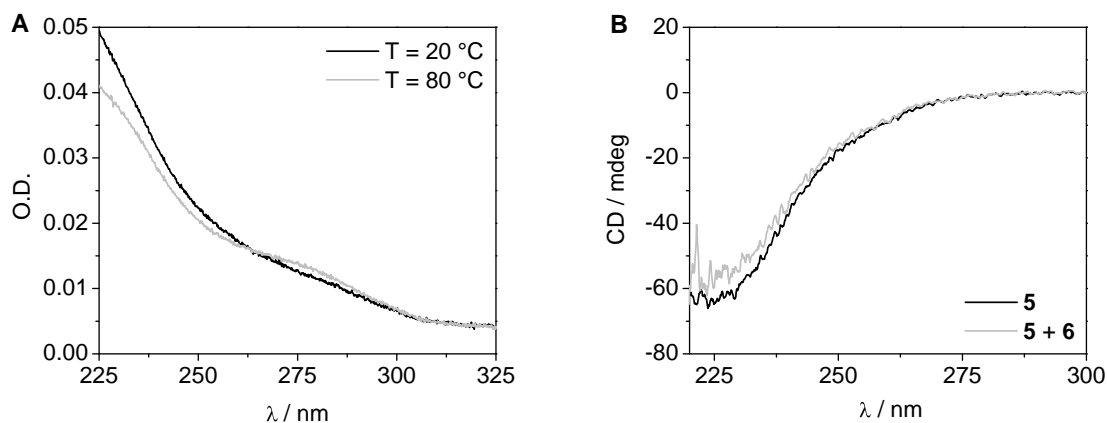
Figure 5.5 A) UV spectroscopy measurements of compound **2** at 20 and 80 °C in MCH (c = 1.25×10^{-6} M, l = 1.0 cm). B) CD spectroscopy of compound **5** in MCH (c = 5×10^{-4} M, l = 1.0 mm) and compound **5** in MCH in the presence of **6** (c = 5×10^{-4} M, l = 1.0 mm) at 20 °C.

Finally, we investigated the propensity of the UPy group to influence BTA aggregation. We performed CD measurements on the BTA-pEB (**5**) (c = 5×10^{-4} M) in the presence and absence of UPy-pEB (**6**) in MCH (c = 5×10^{-4} M) (Figure 5.5B). The Cotton effect of compound **5** mixed with **6** was almost equal in size compared to the Cotton effect of compound **5**. This convincingly shows that the UPy group itself does not significantly interfere with BTA aggregation.

5.5 Self-assembly in the solid state

In order to investigate the ability of BTAs and UPys to self-assemble in an orthogonal fashion and the ability to form separate phase segregated nanorods in the solid state, we studied the self-assembly of spin-coated films of compounds **2**, **3** and **5** with CD spectroscopy. Films of **2**, **3** and **5** with a thickness of 340 nm, 340 nm and 260 nm, respectively, were obtained by spin-coating from a CHCl₃ solution (c$_{BTA}$ = 4×10^{-3} M) on quartz plates. CD spectra were recorded at room temperature and are shown in Figure 5.6A. The CD effect was independent of the orientation of the quartz plate with respect with the beam, excluding linear dichroism effects.
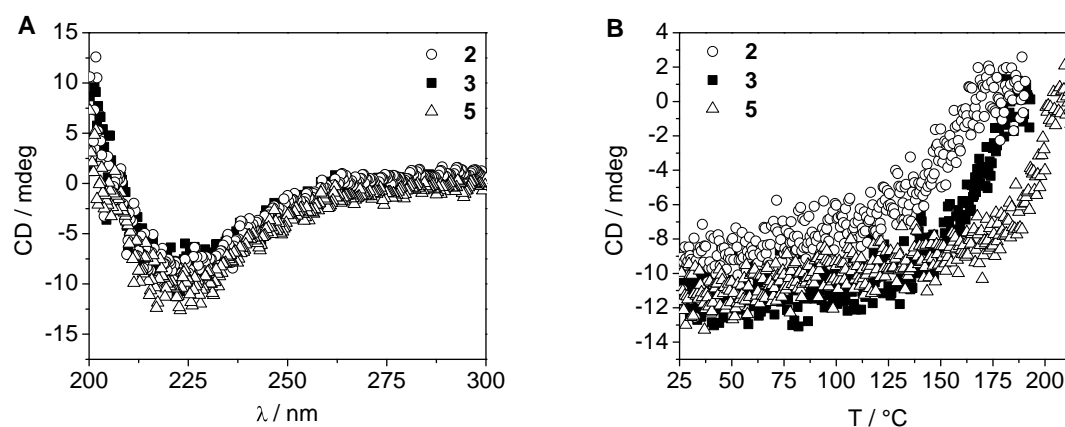
Figure 5.6 A) CD spectra of **2**, **3** and **5** (film thickness = 340, 340 and 260 nm, respectively, T = 20 °C). B) CD cooling curve of **2**, **3** and **5** (λ = 223 nm, film thickness = 340, 340 and 260 nm, respectively).

A clear Cotton effect was observed for all polymers. In contrast to the solutions, the Cotton effects for the films of polymers **2**, **3** and **5** are almost equal in size (Cotton effect = -10 mdeg). This suggests that at 20 °C the degree of aggregation is the same for all polymers. We then measured temperature-dependent CD spectra of these films by increasing the temperature from 25 °C to 200 °C at a rate of 5 K min^{-1}. The CD effect was monitored at λ_{max} = 223 nm and plotted versus temperature (Figure 5.6B). All three polymers showed a decrease of the CD effect upon heating and a disappearance of the CD effect of **2**, **3** and **5** above 160, 180 and 200 °C, respectively. The hydrogen bonded helical arrangement of BTAs in compound **2** disappeared at the lowest temperature, which is in correspondence to the behavior in dilute conditions. This indicates that also in the solid state the virtual molecular weight of the polymer backbone influences the association constant, but the effect is less pronounced than in solution. While BTA aggregation in **2** is less stable compared to that of **3** and **5**, it is evident that the presence of the UPy motif does not significantly hinder BTA aggregation. The curves of the temperature-dependent CD measurements of **2**, **3** and **5** in the solid state appeared to be significantly steeper than those of **2**, **3** and **5** in dilute conditions. This phenomenon was also observed for the BTA end-capped polymers in Chapter 2, in which the CD cooling curves in the solid state are much steeper than those in dilute conditions. This was attributed to additional phase segregation between the BTAs and the soft polymer in the solid state, which resulted in a more cooperative self-assembly process.

5.6 Phase segregation, nanorod formation and cross-linking

CD spectroscopy measurements suggest the orthogonal self-assembly of BTAs and UPys in the solid state in polymer **2**. The observed Cotton effect is indicative for the presence of aggregated BTAs that form 1D nanorods in the solid state. In contrast, UPy dimers can only

form nanorods if an additional lateral hydrogen bonding motif is operating close to the UPy motif. Kautz and coworkers showed that the introduction of a urethane or urea group close to the UPy indeed results in the formation of long, elongated nanorods.[7] Also the nature of the substituent at the 6-position of the isocytosine group is of high importance for nanorod formation.[59] We selected the isopropyl UPy (**1**, **2** and **4**) and a methyl UPy (**6**), in which the latter shows an enhanced formation of nanorods.
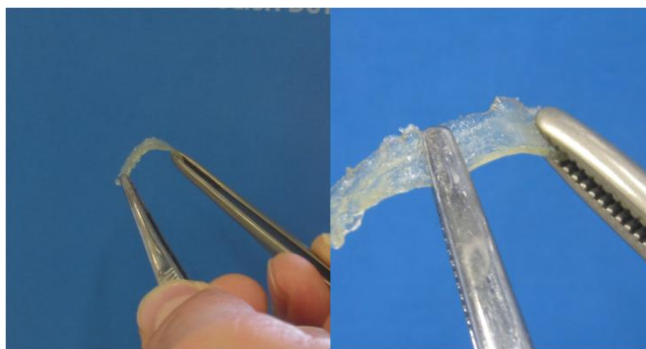
Figure 5.7 Physical appearance of a blend of **2/5/6** in a ratio of 15/42.5/42.5 mol% in which **2** functions as a physical cross-linker.

We investigated the ability of **2** to cross-link a mixture of **5** and **6**, in which both BTA-based and UPy-based nanorods are present but they are not connected (Scheme 5.1). Compound **5** and **6** are both viscous sticky liquids. DSC traces of pure **5** and **6** showed the presence of a phase transition at 192 °C and 39 °C, respectively, resulting from the melting of phase segregated nanorods by the loss of intermolecular hydrogen bonding. We prepared a ternary blend of **2/5/6** in a ratio of 15/42.5/42.5 mol% by preparing a solution in dichloromethane, and slowly evaporating the solvent by exposure to air. Subsequently, the polymer blend was annealed at 35 °C *in vacuo* for 2 hours. DSC measurements on the polymer blend consisting of **2/5/6** showed two phase transitions, at 38 °C (0.286 J/g) and at 147 °C (1.012 J/g). These phase transitions indicate that both types of nanorods are present although the enthalpy changes are small compared to the enthalpy changes observed for pure **5** and **6** separately (Table 5.1). This can be attributed, at least partly, to a reduction in the relative amount of each supramolecular motif in the polymer blend. In addition, it is likely that less and smaller aggregates are formed in the polymer blend. In fact, DSC measurement of a blend consisting of **5** and **6** showed two phase transitions at 38 °C (0.18 J/g) and at 152 °C (1.016 J/g). The similar phase behavior of **5** and **6** in the presence or absence of **2** shows that the compatibilizer does not influence the formation of nanorods on a molecular scale. However, after the addition of the compatibilizer (**2**), visual inspection of the polymer blend reveals its elastomeric properties (Figure 5.7).

To quantify the increase in elasticity, dynamic oscillatory rheological measurements on the binary blend of **5/6** (50/50 mol%) and the ternary blend of **2/5/6** (15/42.5/42.5 mol%) were performed. The measurements were conducted with a 10% strain, which was well within the linear viscoelastic regime (Figure 5.8).
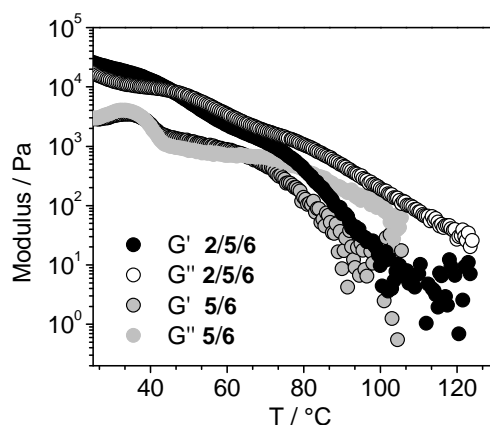
Figure 5.8 Temperature dependence of the storage (G′) and loss (G″) moduli in blends of **5/6** and **2/5/6** (heating at 1 K min^{-1}, 1 rad s^{-1} and 10% strain).

The temperature ramp test on **5/6** revealed a phase transition ending at 43 °C, which is consistent with the transition observed in DSC at 38 °C and attributed to the loss of lateral hydrogen bonds between the UPy-urethane groups, as observed in IR analysis. Continued heating showed a decrease in modulus and crossover of the moduli at 65 °C with the loss modulus (G″) higher than the storage modulus (G′), indicating the material becomes more liquid-like and exhibits substantial viscous flow. The ternary blend of **2/5/6** has an order of magnitude higher modulus, consistent with the elastomeric physical properties observed in the material. A subtle transition around 39 °C, attributed to the loss of lateral UPy-urethane hydrogen bonds, was again observed in the dynamic temperature ramp test of **2/5/6**, which is also consistent with the transition observed in DSC and IR. The moduli, of **2/5/6** above 39 °C, are still an order of magnitude higher than those of **5/6**, which can presumably be related to the presence of dimerized UPys. Dimerization of UPys leads to species that possess two BTA end-groups which have the ability to cross-link BTA nanorods. Continued heating of **2/5/6** results in viscous flow similar to the **5/6** blend.
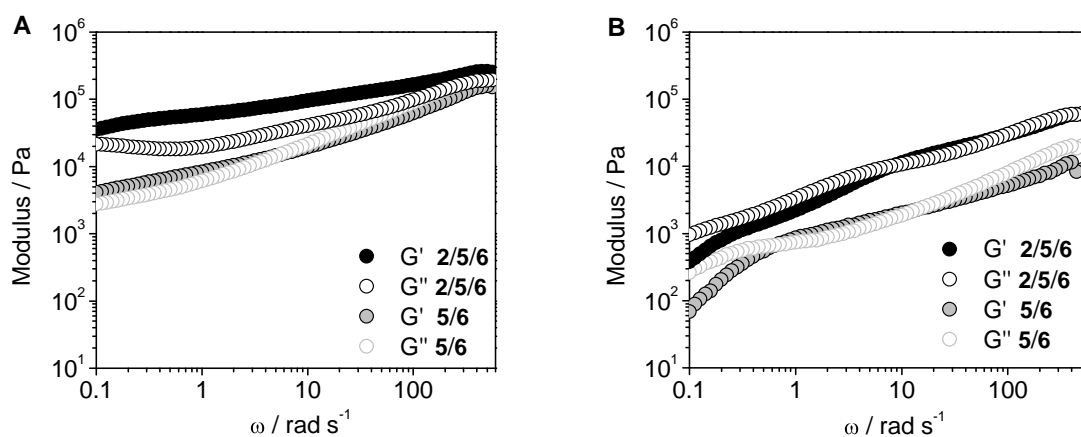
Figure 5.9 Frequency dependence of dynamic modulus of blends **5/6** and **2/5/6** at 25 °C (A) and 60 °C (B) (10% strain).

The frequency dependence of the dynamic modulus of blends of **5/6** and **2/5/6** at 25 and 60 °C is shown in Figure 5.9. The **5/6** blend displayed a frequency response similar to what is expected for concentrated polymer liquids, that is a steady decrease in modulus until approaching terminal flow where the loss modulus crosses over and above the storage modulus. In contrast, sample **2/5/6** with the compatibilizer exhibits elastomeric properties at 25 °C, where there is a region of near plateau in the storage modulus coupled with an elastic recovery of the loss modulus at low frequencies. The loss modulus also tracks below the storage modulus, which is expected for rubber-like materials.[60] Upon heating sample **2/5/6** to 60 °C, the elastic response was no longer present in the frequency dependence, instead the material behaved similarly to sample **5/6** where there is a steady decrease in modulus approaching terminal flow. The absence of elastomeric properties above the phase transition at 39 °C was attributed to the loss of lateral hydrogen bonds between the UPy-urethane groups, and is consistent with behavior expected for the disappearance of physical cross-links in the system. These measurements confirm the ability of the compatibilizer to physically cross-link BTA and UPy nanorods. In addition, the temperature dependence of the melt modulus allows these low molecular weight supramolecular polymers to be easily processed in the melt as the viscosity is substantially decreased upon heating. This is particularly important in the physically cross-linked **2/5/6** blend as the material exhibits excellent solid elastomeric properties and little viscous flow at room temperature.

5.7 Conclusions

We successfully synthesized four monofunctional polymers of different molecular weight, containing either a BTA or an UPy motif. We also synthesized two α, ω-functionalized compounds bearing a BTA and an UPy motif, in two different approaches. In the first approach, a model compound, in which the BTA and UPy motif were connected via an

undecanyl spacer, was obtained by a straightforward coupling of an isocyanate functional UPy to a hydroxyl functional BTA. The second approach involved the anionic polymerization of 1,3-butadiene, employing a silyl-protected hydroxyl-propyllithium derivative as the initiator, yielding a perfectly defined α, ω-functional polymer that was subsequently functionalized with BTA and UPy motifs. This small library of supramolecular polymers was used to investigate the ability of the BTA and UPy motif to self-assemble in an orthogonal fashion. Self-assembly was investigated with a variety of spectroscopic and thermal analytical techniques.

The model compound bearing a BTA and UPy motif connected via a short undecanyl spacer showed that self-assembly of both supramolecular motifs occurred in dilute solutions of apolar solvents and in the solid state. However, the self-assembly of both motifs start at the same temperature suggesting that they are connected. Also in the solid state, we observed that the thermal behavior at room temperature is dominated by crystallization of the UPy-urethane part, which hinders BTA aggregation. The relatively short and rigid linker separating both motifs may be responsible for this phenomenon. The α, ω- functional polymer consisting of a much longer pEB spacer did show orthogonal self-assembly of the UPy and BTA motif in dilute solution and in the solid state. We also observed that the tendency of BTAs to self-assemble in solution is strongly influenced by the length of the polymer backbone. Steric crowding of the BTA core is more pronounced when it is attached to a longer pEB backbone resulting in a lower degree of aggregation.

BTAs and UPys endcapped to monofunctional pEB in a polymer blend, self-assemble into separate, phase segregated nanorods. The presence of these nanorods did not lead to an enhancement of the material properties. To this polymer blend we added the α, ω-functionalized telechelic containing both supramolecular motifs, which is capable of cross-linking the two separate phase segregated nanorods. The addition of a small amount of cross-linker (15 mol%) led to a polymer exhibiting elastomeric properties as evidenced by dynamic oscillating shear measurements. These preliminary results show that a significant enhancement of the material properties can be obtained by cross-linking a relatively small part of the nanorods in a supramolecular fashion. Further research in this area can lead to a new class of polymeric materials in which orthogonally operating supramolecular motifs are used to introduce specific bonds or cross-links in polymer blends. This concept could lead to the creation of complex polymer morphologies, such as seen in traditional block copolymers, but now combined with the attractive features of supramolecular chemistry.

5.8 Experimental

Materials

Hydroxyundecyl-3,5-bis((3*S*)-3,7-dimethyloctylcarbamoyl)benzoate (**7**) and 3,5-bis((3*S*)-3,7-dimethyloctylcarbamoyl)benzoic acid (**15**) were synthesized according to literature procedures.[5, 61] 6-(((6-Isopropyl-4-oxo-1,4-dihydro-2-pyrimidinyl)amino)carbonyl_amino) hexylcarbamate (**8**) and 6-(((6-methyl-4-oxo-1,4-dihydro-2-pyrimidinyl)amino)carbonyl_amino) hexylcarbamate (**16**) were kindly provided by SyMO-Chem BV. Kraton mono hydroxy (Kraton-OH) was purchased from Kraton Polymer Research (L-1203, M_w = 3500 g/mol, *PDI* = 1.03). All other reagents were purchased from Aldrich or Acros Organics and used as received unless otherwise specified. All solvents were purchased from Biosolve. Deuterated solvents were purchased from Cambridge Isotopes Laboratories. All reactions were run in flame-dried glassware under an argon atmosphere.

Instrumentation and Analysis

CD and UV spectra were recorded on a Jasco J-815 CD spectrometer equipped with a Jasco PTC-348 WI temperature controller. Experiments were conducted using spectroscopic grade methylcyclohexane as the solvent. Cells with an optical path length of 0.1 cm or 1.0 cm were applied (for ~10^{-4} M or ~10^{-6} M solutions). The molar ellipticity is calculated as: $\Delta\varepsilon$ = CD-effect/(32980xcxl) where c is the concentration in mol/L and l = the optical path length in cm. Films of **2**, **3** and **5** were prepared by making solutions of **2**, **3** and **5** in chloroform (50 mg/mL) and spin-coating a volume of 0.5 mL on 0.40 cm² quartz slides at 800 rpm for two minutes. The film thickness was determined by introducing scratches on the polymer surfaces, followed by measuring the difference in height using AFM (by Asylum Research, tapping mode). The ternary blend of **5/6/2** in a mol ratio of 42.5/42.5/15 was prepared by making a solution of **5** (100 mg) + **6** (100 mg) + **2** (50 mg) in dichloromethane (2 mL). The solvent was slowly evaporated by exposure to air. Subsequently, the polymer blend was annealed at 35 °C *in vacuo* for 2 hours. Variable temperature CD measurements on the spin-coated films were performed by mounting the Linkam THMS 600 heating device into the CD apparatus, which allowed heating up to 250 °C. ¹H-NMR and ¹³C-NMR spectra were recorded on a Varian Gemini 400 MHz NMR (400 MHz for ¹H-NMR and 100 MHz for ¹³C-NMR). Proton chemical shifts are reported in ppm downfield from tetramethylsilane (TMS). Carbon chemical shifts are reported downfield from TMS using the resonance of the deuterated solvent as the internal standard. IR spectra were recorded on a Perkin Elmer 1600 FT-IR. Variable temperature IR spectra were recorded on an Excalibur FTS 3000 MX FT-IR from Biorad. POM measurements were performed using a Jenaval polarisation microscope equipped with a Linkam THMS 600 heating device, with crossed polarisers. The thermal transitions were determined with DSC using a TA Q2000 under a nitrogen atmosphere with

heating and cooling rates of 40 K min^{-1} (second heating run). GPC measurements were performed on a Resi Pore column with chloroform as the eluent (flow = 1 mL/min) and employing a PDA (λ = 254 nm) as the detector. The molecular weights were determined using a polystyrene calibration method.

Rheometry

Dynamic Mechanical Spectroscopy. Rheological melt experiments were run on a TA Instruments Advanced Rheometric Expansion System (ARES) rheometer. Samples were roughly formed as discs (**5/6** blend has a sticky viscous consistency, while **2/5/6** is rubbery and can be molded by hand) and put between two parallel plates (8 mm). The gap was adjusted to ensure even distribution of the sample. Typical gaps were 0.3–0.5 mm. Dynamic temperature ramp tests were performed while heating and cooling at 1 K min^{-1} at angular frequency of 1 rad s^{-1} and a strain of 10% (well within the linear viscoelastic regime, determined by dynamic strain sweep experiments for each polymer). Dynamic frequency sweep experiments were performed at a strain of 10 % at 25 °C and 60 °C.

Synthesis

11-((3,5-Bis((((3S)-3-methyloctyl)amino)carbonyl)benzoyl)amino)undecyl 6-(((((6-isopropyl-4-oxo-1,4-dihydro-2-pyrimidinyl)amino)carbonyl)amino) hexylcarbamate (**1**) Hydroxyundecyl-3,5-bis((3S)-3,7-dimethyloctylcarbamoyl)benzoate (**7**) (0.614 mmol, 0.381 gram) was dissolved in 15 mL CHCl$_3$. *N*-(6-Isocyanatohexyl)-*N'*-(6-isopropyl-4-oxo-1,4-dihydro-2-pyrimidinyl)urea (**8**) (0.676 mmol, 0.222 gram) was added to the reaction mixture. One drop of dibutyl tin dilaurate (DBTDL) was added as catalyst and the mixture was stirred for 12 hours at 90 °C. Silicagel (2.0 g) was added and after 3 hours the mixture was diluted with 50 mL CHCl$_3$ and the silicagel was removed by filtration. After evaporation of the solvent *in vacuo* the product was obtained as a white solid. Compound **1** was purified by precipitation in cold ether. Yield = 0.352 g, 78%. ^{1}H-NMR (400 MHz, CDCl$_3$, δ): 13.30 (s, 1H, NH, UPy), 11.91 (s, 1H, NH, UPy), 10.13 (s, 1H, NH, UPy), 8.36 (s, 3H, ArH), 6.67 (m, 3H, NH, BTA), 5.86 (C=CH, s, 1H), 4.85 (s, 1H, NH(C=O)O), 4.05 (t, 2H, NHOCO-C$\underline{H}_2$), 3.46 (t, 6H, NHC$\underline{H}_2$ BTA,), 3.24 (t, 2H, C$\underline{H}_2$OCONH), 3.18 (t, 2H, C$\underline{H}_2$-NH-CO-NH), 2.57 (m, 1H, (CH$_3$)$_2$C$\underline{H}$, UPy), 1.66-1.19 (68H, alkyl) ^{13}C-NMR (100 MHz, CDCl$_3$, δ): δ 165.7, 156.7, 154.8, 135.3, 128.0, 103.8, 65.9, 40.4, 39.7, 39.3, 38.6, 37.1, 36.6, 31.6, 30.7, 29.7, 29.4, 26.9, 26.1, 25.8, 24.6, 22.7, 20.4, 19.4, 15.2. MALDI-ToF, m/z = 979.54 (M+H$^+$), 1001.52 (M+Na$^+$).

α-3-t-Butyldimethylsiloxy-1-propyl-ω-hydroxy-polybutadiene (TBDMS-PB-OH) (**9**) 3-*t*-Butyldimethylsiloxy-1-propyllithium (9.37 mL, 0.5 M) was added to a cooled reactor (10 °C) containing 650 mL of cyclohexane and 1.88 mL THF (5:1 eq THF–Li ion). Purified 1,3-butadiene monomer (15.3 g, 18 h) was then added slowly over a period of 30 min to the

reactor at a slight initial positive pressure of argon (1 psi). During the monomer addition, the temperature of the reactor was allowed to slowly warm to room temperature. Upon complete monomer addition, the reactor temperature was raised to 30 °C. A large excess of ethylene oxide (9.5 g, 1 h) was added to the reactor as an end-capping agent (Note: if the newly formed alkoxide chain-ends are not quenched within about an hour, significant deprotection of the TBDMS initiator will occur). After purging the reactor of excess ethylene oxide, the terminal alkoxide was quenched with wet methanol (20 mL, 200:1 MeOH-H_2O). The protected initiator polymer solution was reduced in volume by half *in vacuo*, washed (2x) with 100 mL deionized water, and precipitated from cold (-20 °C) 4/1 MeOH/EtOH (2.5 L). The product was dissolved in benzene and freeze-dried *in vacuo* (25 °C, 48 hours). A sticky, clear, viscous liquid was recovered. Yield: 14.9 g, 97%. GPC (polystyrene standards): M_n = 11.4 kg/mol, *PDI* = 1.03. ^{1}H-NMR (400 MHz, CDCl$_3$, δ): 5.2-5.9 (b, -CH$_2$-C$\underline{H}$=C$\underline{H}$-CH$_2$- and CH$_2$=C$\underline{H}$-CH-), 4.7-5.1 (b, C$\underline{H}_2$=CH-), 3.5-3.7 (m, 2H, -Si-O-C$\underline{H}_2$- and t, 2H, -C$\underline{H}_2$-OH), 1.7-2.3 (b, -C$\underline{H}_2$-CH=CH-C$\underline{H}_2$- and CH$_2$=CH-C$\underline{H}$-), 1.0-1.7 (b, CH$_2$=CH-C(R)H-C$\underline{H}_2$-), 0.8-0.9 (s, 9H (C$\underline{H}_3$)$_3$-Si(CH$_3$)$_2$-O-), 0 (s, 6H, (CH$_3$)$_3$-Si(C$\underline{H}_3$)$_2$-O-). M_n (calcd. from ^{1}H-NMR integrations) = 5403 g mol^{-1}. 1,2 Content = 57%.

α-3-t-Butyldimethylsiloxy-1-propyl-ω-phthalimide-polybutadiene (TBDMS-PB-Phthalimide) (**10**) TBDMS-PB-OH (**9**) (0.5 g, 0.093 mmol) was dissolved in 5 mL THF. Then, triphenylphosphine (36 mg, 0.14 mmol) and phthalimide (20 mg, 0.14 mmol) were added. The solution was cooled with an ice bath. Diisopropyl azodicarboxylate (DIAD) (28 mg, 0.14 mmol) was dissolved in 2 mL THF and added dropwise to the cooled solution. The mixture was stirred for 48 hours. The resulting clear yellow solution was concentrated and precipitated twice in methanol. The product was obtained as a viscous, sticky oil. Yield = 0.45 g, 95%. ^{1}H-NMR (400 MHz, CDCl$_3$, δ): 7.87 (m, 2H, Ar-H), 7.72 (m, 2H, Ar-H), 5.2-5.9 (b, -CH$_2$-C$\underline{H}$=C$\underline{H}$-CH$_2$- and CH$_2$=C$\underline{H}$-CH-), 4.7-5.1 (b, C$\underline{H}_2$=CH-), 3.71 (t, 2H, CH$_2$-C$\underline{H}_2$-N), 3.6 (m, 2H, -Si-O-C$\underline{H}_2$), 1.7-2.3 (b, -C$\underline{H}_2$-CH=CH-C*H$_2$*- and CH$_2$=CH-C$\underline{H}$-), 1.0-1.7 (b, CH$_2$=CH-C(R)H-C$\underline{H}_2$-), 0.8–0.9 (s, 9H, (C$\underline{H}_3$)$_3$-Si(CH$_3$)$_2$-O-), 0 (s, 6H, (CH$_3$)$_3$-Si(C$\underline{H}_3$)$_2$-O-).

α-3-t-Butyldimethylsiloxy-1-propyl-ω-amino-polybutadiene (**11**) (TBDMS-PB-NH$_2$). TBDMS-PB-phthalimide (**10**) (0.45 g, 0.08 mmol) was dissolved in 20 mL THF. After the addition of hydrazine monohydrate (100 mg, 2 mmol), the solution was stirred under reflux for 48 hours. THF was removed *in vacuo*. Subsequently, 50 mL of chloroform was added. The organic phase was washed with NaOH (2 x 50 mL) and with brine (50 mL), respectively. After removal of chloroform *in vacuo* TBDMS–PB–NH$_2$ was obtained as a sticky oil. Yield = 0.42 g, 99%. ^{1}H-NMR (400 MHz, CDCl$_3$, δ): 5.2-5.9 (b, -CH$_2$-C$\underline{H}$=C$\underline{H}$-CH$_2$- and CH$_2$=C$\underline{H}$-CH-), 4.7-5.1 (b, C$\underline{H}_2$=CH-), 3.6 (m, 2H, -Si-O-C$\underline{H}_2$), 2.65 (t, 2H, CH$_2$-C$\underline{H}_2$-NH$_2$), 1.7–2.3 (b, -C$\underline{H}_2$-CH=CH-

C$\underline{H}_2$- and CH$_2$=CH-C$\underline{H}$-), 1.0-1.7 (b, CH$_2$=CH-C(R)H-C$\underline{H}_2$-), 0.8-0.9 (s, 9H, (C$\underline{H}_3$)$_3$-Si(CH$_3$)$_2$-O-), 0 (s, 6H, (CH$_3$)$_3$-Si(C$\underline{H}_3$)$_2$-O-).

α-3-t-Butyldimethylsiloxy-1-propyl-ω-BTA-polybutadiene (**12**) (TBDMS-PB-BTA). TBDMS-PB-NH$_2$ (0.41 g, 0.076 mmol) and 3,5-bis((3S)-3,7-dimethyloctylcarbamoyl)benzoic acid (**15**) (40 mg, 0.084 mmol) were dissolved in 10 mL dry dichloromethane. Benzotriazol-1-yl-oxytripyrrolidinophosphonium hexafluorophosphate (PyBOP) (63 mg, 0.12 mmol) and *N,N*-diisopropylethylamine (DIPEA) (15.5 mg, 0.12 mmol) were added to the solution. The solution was stirred for 12 hours at room temperature. Dichloromethane was removed *in vacuo*. Subsequently, 50 mL of chloroform was added. The originating precipitates were removed by filtration. The solution was concentrated *in vacuo* and precipitated in methanol (three times). The product was obtained as a sticky oil. Yield = 0.37 g, 95%. ^{1}H-NMR (400 MHz, CDCl$_3$, δ): 8.4 (s, 3H, Ar-H), 6.4 (t, 3H, NHC=O), 5.2-5.9 (b, -CH$_2$-C$\underline{H}$=C$\underline{H}$-CH$_2$- and CH$_2$=C$\underline{H}$-CH-), 4.7-5.1 (b, C$\underline{H}_2$=CH-), 3.6 (m, -Si-O-C$\underline{H}_2$), 3.48 (t, 6H, C$\underline{H}_2$-NHC=O), 1.7-2.3 (b, -C$\underline{H}_2$-CH=CH-C$\underline{H}_2$- and CH$_2$=CH-C$\underline{H}$-), 1.0-1.7 (b, CH$_2$=CH-C(R)H-C$\underline{H}_2$-), 0.8-0.9 (s, 9H, (C$\underline{H}_3$)$_3$-Si(CH$_3$)$_2$-O-), 0 (s, (CH$_3$)$_3$-Si(C$\underline{H}_3$)$_2$-O-).

α-Hydroxy-1-propyl-ω-BTA-polyethylenebutylene (**3**) (BTA-PEB-OH). TBDMS-PB-BTA (**12**) (650 mg, 0.12 mmol) was dissolved in 30 mL of toluene. *p*-Toluenesulfonyl hydrazide (*p*TSH) (5.28 g, 28 mmol) and tripropylamine (TPA) (2.03 g, 14 mmol) were added to the solution. The solution was stirred for 18 hours at reflux temperature. The solution was concentrated *in vacuo* and subsequently precipitated in methanol (three times). The product was obtained as a sticky oil. Yield = 580 mg, 90%. GPC (Polystyrene standards): M_n = 12.0 kg/mol, M_w = 12.3 kg/mol, *PDI* = 1.03. ^{1}H-NMR (400 MHz, CDCl$_3$, δ): 8.4 (s, 3H, Ar-H), 6.4 (t, 3H, NHC=O), 3.68 (t, C$\underline{H}_2$OH), 3.48 (t, 6H, C$\underline{H}_2$-NHC=O), 1.7-0.8 (alkyl).

α-UPy-1-propyl_UT-ω-BTA-polyethylenebutylene (**2**) (BTA-PEB-UPy). BTA-PEB-OH (**3**) (0.5 g, 0.083 mmol) was dissolved in 15 mL chloroform. *N*-(6-Isocyanatohexyl)-*N*'-(6-isopropyl-4-oxo-1,4-dihydro-2-pyrimidinyl)urea (**8**) (30 mg, 0.092 mmol) was added to the reaction mixture. One drop of DBTDL was added as a catalyst and stirred for 12 hours at 90 °C. Silicagel (2.0 g) was added and after 3 hours the mixture was diluted with 50 mL chloroform. Subsequently, the silicagel was removed by filtration. After evaporation of the solvent *in vacuo* the product was obtained as a yellowish solid. Compound **2** was purified by precipitation in methanol. Yield = 0.42 g, 82%. GPC (Polystyrene standards): M_n = 12.7 kg/mol, M_w = 13.0 kg/mol, *PDI* = 1.03. ^{1}H-NMR (400Mhz, CDCl$_3$, δ): 13.30 (s, 1H, NH, UPy), 11.91 (s, 1H, NH, UPy), 10.13 (s, 1H, NH, UPy), 8.36 (s, 3H, ArH), 6.67 (m, 3H, NH, BTA), 5.86 (s, 1H, C=CH), 4.85 (s, 1H, NH(C=O)O), 4.05 (t, 2H, NHOCO-C$\underline{H}_2$), 3.46 (t, 6H, NHC$\underline{H}_2$, BTA), 3.24 (t, 2H, C$\underline{H}_2$OCONH), 3.18 (t, 2H, C$\underline{H}_2$-NH-CO-NH), 2.57 (m, 1H, (C$\underline{H}_3$)$_2$CH, UPy), 1.66-

1.19 (alkyl). ^{13}C-NMR (100 MHz, CDCl$_3$, δ): 173.5, 165.5, 157.6, 156.7, 154.8, 135.2, 127.9, 103.8, 64.9, 40.7, 39.7, 39.2, 39.1, 39.0, 38.9, 38.5, 38.4, 37.9, 37.1, 36.8, 36.6, 36.1, 36.0, 34.3, 33.6, 33.5, 33.4, 33.2, 32.9, 31.6, 30.7, 30.6, 30.2, 29.7, 29.3, 29.1, 27.9, 26.7, 26.6, 26.4, 26.1, 24.6, 22.7, 22.5, 20.4, 19.5, 10.8, 10.6, 10.4, 10.2.

α-3-t-Butyldimethylsiloxy-1-propyl-ω-UT_UPy-polybutadiene (TBDMS-PB-UPy) (**13**). TBDMS-PB-OH (**9**) (0.5 g, 0.093 mmol) was dissolved in 15 mL chloroform. *N*-(6-Isocyanatohexyl)-*N'*-(6-isopropyl-4-oxo-1,4-dihydro-2-pyrimidinyl)urea (**8**) (33 mg, 0.102 mmol) was added to the reaction mixture. One drop of DBTDL was added as a catalyst and stirred for 18 hours at 90 °C. Silicagel was added and after 5 hours the mixture was diluted with 50 mL chloroform. Subsequently, the silicagel was removed by filtration. The solution was concentrated *in vacuo* and subsequently precipitated in methanol (twice). The product was obtained as a sticky oil. Yield = 0.48 g, 98%. ^{1}H-NMR (400Mhz, CDCl$_3$, δ): 13.30 (s, 1H, NH, UPy), 11.91 (s, 1H, NH, UPy), 10.13 (s, 1H, NH, UPy), 5.86 (s, 1H, C=CH), 5.2-5.8 (b, -CH$_2$-C<u>H</u>=C<u>H</u>-CH$_2$- and C<u>H</u>$_2$=CH-CH-), 4.7-5.1 (b, C<u>H</u>$_2$=CH-), 4.05 (t, 2H, NHOCO-C<u>H</u>$_2$,), 3.6 (m, 2H, -Si-O-C<u>H</u>$_2$), 3.24 (t, 2H, C<u>H</u>$_2$OCONH), 3.18 (t, 2H, C<u>H</u>$_2$-NH-CO-NH), 2.57 (m, 1H, (CH$_3$)$_2$C<u>H</u>, UPy), 1.7-2.3 (b, -C<u>H</u>$_2$-CH=CH-C<u>H</u>$_2$- and CH$_2$=CH-C<u>H</u>-), 1.0-1.7 (b, CH$_2$=CH-C(R)H-C<u>H</u>$_2$-), 0.8-0.9 (s, (C<u>H</u>$_3$)$_3$-Si(CH$_3$)$_2$-O-), 0 (s, (CH$_3$)$_3$-Si(C<u>H</u>$_3$)$_2$-O-).

α-Hydroxy-1-propyl-ω-UT_UPy-polyethylenebutylene (UPy-PEB-OH) (**4**). TBDMS-PB-UPy (**13**) (0.48 g, 0.091 mmol) was dissolved in 25 mL of toluene. *p*TSH (3.9 g, 21 mmol) and TPA (1.5 g, 10.5 mmol) were added to the solution. The solution was stirred for 18 hours at reflux temperature. The solution was concentrated *in vacuo* and subsequently precipitated in methanol (three times). The product was obtained as a sticky oil. Yield = 425 mg, 90%. GPC (Polystyrene standards): M_n = 11.6 kg/mol, M_w = 12.0 kg/mol, *PDI* = 1.03. ^{1}H-NMR (400Mhz, CDCl$_3$, δ): 13.30 (s, 1H, NH, UPy), 11.91 (s, 1H, NH, UPy), 10.13 (s, 1H, NH, UPy), 5.86 (s, 1H, C=CH), 4.85 (s, 1H, NH(C=O)O), 4.05 (t, 2H, NHOCO-C<u>H</u>$_2$), 3.68 (t, 2H, C<u>H</u>$_2$OH), 3.24 (t, 2H, C<u>H</u>$_2$OCONH) 3.18 (t, 2H, C<u>H</u>$_2$-NH-CO-NH), 2.57 (m, 1H, (CH$_3$)$_2$C<u>H</u>, UPy), 1.7-0.8 (alkyl).

Kraton-NH$_2$ (**14**). Kraton-OH (0.5 g, 0.14 mmol) was was dissolved in 10 mL THF. Then triphenylphosphine (39.6 mg, 0.154 mmol) and phthalimide (22 mg, 0.154 mmol) were added. The solution was cooled with an ice bath. DIAD (30.8 mg, 0.154 mmol) was dissolved in 2 mL THF and added drop wise to the cooled solution. The mixture was stirred for 48 hours. The resulting clear yellow solution was concentrated and precipitated twice in methanol. The product was obtained as a viscous, sticky oil in a 95% yield. ^{1}H-NMR (400 MHz, CDCl$_3$, δ): 7.87 (m, 2H, Ar-H), 7.72 (m, 2H, Ar-H), 3.71 (t, 2H, CH$_2$-C<u>H</u>$_2$-N), 1.7-0.8 (alkyl). Kraton-phthalimide (**14a**) was dissolved in 20 mL THF. After the addition of hydrazine monohydrate (150 mg, 3 mmol), the solution was stirred under reflux for 48 hours.

THF was removed *in vacuo*. Subsequently 50 mL of chloroform was added. The organic phase was washed with NaOH (2 x 50 mL) and with brine (50 mL), respectively. After removal of chloroform *in vacuo* Kraton-NH$_2$ was obtained as a sticky oil. Yield = 0.49 g, 99%. ^{1}H-NMR (400 MHz, CDCl$_3$, δ): 2.65 (t, 2H, -C$\underline{H}_2$-NH$_2$) 1.7-0.8 (alkyl).

Kraton-BTA (5). Kraton-NH$_2$ (**14**) (0.46 g, 0.13 mmol) and 3,5-bis((3S)-3,7-dimethyloctylcarbamoyl)benzoic acid (**15**) (69 mg, 0.145 mmol) were dissolved in 10 mL dry dichloromethane. PyBOP (101.4 mg, 0.195 mmol) and DIPEA (25.3 mg, 0.195 mmol) were added to the solution. The solution was stirred for 12 hours at room temperature. Dichloromethane was removed *in vacuo*. Subsequently, 50 mL of chloroform was added. The originating precipitates were removed by filtration. The solution was concentrated *in vacuo* and precipitated in methanol (three times). The product was obtained as a sticky oil. Yield = 0.48 g, 95%. GPC (Polystyrene standards): M_n = 7.6 kg/mol, M_w = 7.8 kg/mol, *PDI* = 1.03. ^{1}H-NMR (400 MHz, CDCl$_3$, δ): 8.38 (s, 3H, Ar-H), 6.49 (t, 3H, NHC=O), 3.50 (t, 6H, C$\underline{H}_2$-NHC=O), 1.7-0.8 (alkyl). ^{13}C-NMR (100 MHz, CDCl$_3$, δ): 165.4, 136.8, 127.7, 40.2, 39.2, 38.8, 38.4, 37.9, 36.8, 36.1, 34.4, 33.5, 33.2, 31.8, 30.7, 30.3, 29.7, 29.5, 29.3, 27.0, 26.8, 26.6, 26.5, 26.3, 26.2, 26.1, 25.8, 25.0, 22.7, 14.2, 10.9, 10.6, 10.7.

Kraton-UPy (6). Kraton-OH (2.0 g, 0.57 mmol) was dissolved in 50 mL chloroform. *N*-(6-Isocyanatohexyl)-*N'*-(6-methyl-4-oxo-1,4-dihydro-2-pyrimidinyl)urea (**16**) (183 mg, 0.629 mmol) was added to the reaction mixture. One drop of DBTDL was added as a catalyst and stirred for 18 hours at 90 °C. Silicagel (2.0 g) was added and after 5 hours the mixture was diluted with 150 mL chloroform. Subsequently, the silicagel was removed by filtration. The solution was concentrated *in vacuo* and subsequently precipitated in methanol (three times). The product was obtained as a sticky oil. Yield = 2.0 g, 96%. GPC (Polystyrene standards): M_n = 7.9 kg/mol, M_w = 8.1 kg/mol, *PDI* = 1.03. ^{1}H-NMR (400 MHz, CDCl$_3$, δ): 13.30 (s, 1H, NH, UPy), 11.91 (s, 1H, NH, UPy), 10.13 (s, 1H, NH, UPy), 5.86 (s, 1H, C=CH), 4.85 (s, 1H, NH(C=O)O), 4.05 (t, 2H, NHOCO-C$\underline{H}_2$), 3.68 (t, 2H, C$\underline{H}_2$OH), 3.24 (t, 2H, C$\underline{H}_2$OCONH), 3.18 (t, 2H, C$\underline{H}_2$-NH-CO-NH), 2.2 (s, 3H, C$\underline{H}_3$, UPy), 1.7-0.8 (alkyl). ^{13}C-NMR (100 MHz, CDCl$_3$, δ): 168.2, 158.2, 157.3, 156.8, 130.6, 38.9, 38.4, 37.9, 36.7, 36.1, 34.4, 33.4, 33.2, 30.7, 30.2, 29.7, 29.5, 26.8, 26.8, 26.4, 26.1, 26.0, 25.9, 19.2, 11.4, 10.9, 10.7, 10.6.

5.9 References

[1] B. J. B. Folmer, R. P. Sijbesma, R. M. Versteegen, J. A. J. van der Rijt, E. W. Meijer, *Adv. Mater.* **2000**, *12*, 874.

[2] J. D. Fox, S. J. Rowan, *Macromolecules* **2009**, *42*, 6823.

[3] R. M. Versteegen, R. P. Sijbesma, E. W. Meijer, *Macromolecules* **2005**, *38*, 3176.

[4] L. Brunsveld, B. J. Folmer, E. W. Meijer, R. P. Sijbesma, *Chem. Rev.* **2001**, *101*, 4071.

[5] J. R. Roosma, T. Mes, P. E. L. G. Leclere, A. R. A. Palmans, E. W. Meijer, *J. Am. Chem. Soc.* **2008**, *130*, 1120.

[6]   N. E. Botterhuis, K. Sivasubramanian, D. Veldman, S. C. J. Meskers, R. P. Sijbesma, *Chem. Commun.* **2008**, 3915

[7]   H. Kautz, D. J. M. van Beek, R. P. Sijbesma, E. W. Meijer, *Macromolecules* **2006**, *39*, 4265.

[8]   L. Bouteiller, O. Colombani, F. Lortie, P. Terech, *J. Am. Chem. Soc.* **2005**, *127*, 8893.

[9]   R. J. Thibault, P. J. Hotchkiss, M. Gray, V. M. Rotello, *J. Am. Chem. Soc.* **2003**, *125*, 11249.

[10]   G. Cooke, V. M. Rotello, *Chem. Soc. Rev.* **2002**, *31*, 275.

[11]   J. M. Pollino, M. Weck, *Chem. Soc. Rev.* **2005**, *34*, 193.

[12]   K. P. Nair, V. Breedveld, M. Weck, *Macromolecules* **2008**, *41*, 3429.

[13]   C. R. South, C. Burd, M. Weck, *Acc. Chem. Res.* **2007**, *40*, 63.

[14]   A. Ciferri, *Supramolecular Polymers*, New York, **2000**.

[15]   A. W. Bosman, L. Brunsveld, B. J. B. Folmer, R. P. Sijbesma, E. W. Meijer, *Macromol. Symp.* **2003**, *201*, 143.

[16]   A. Ciferri, *Macromol. Rapid Comm.* **2002**, *23*, 511.

[17]   C. Hilger, R. Stadler, *Macromolecules* **1990**, *23*, 2095.

[18]   O. Colombani, C. Barioz, L. Bouteiller, C. Chaneac, L. Fomperie, F. Lortie, H. Montes, *Macromolecules* **2005**, *38*, 1752.

[19]   T. Park, S. C. Zimmerman, *J. Am. Chem. Soc.* **2006**, *128*, 13986.

[20]   W. H. Binder, S. Bernstorff, C. Kluger, L. Petraru, M. J. Kunz, *Adv. Mater.* **2005**, *17*, 2824.

[21]   W. H. Binder, R. Zirbs, *Adv. Polym. Sci.* **2007**, *207*, 1.

[22]   B. D. Mather, M. B. Baker, F. L. Beyer, M. A. G. Berg, M. D. Green, T. E. Long, *Macromolecules* **2007**, *40*, 6834.

[23]   P. Y. W. Dankers, M. C. Harmsen, L. A. Brouwer, M. J. A. van Luyn, E. W. Meijer, *Nat. Mater.* **2005**, *4*, 568.

[24]   E. Wisse, R. A. E. Renken, J. R. Roosma, A. R. A. Palmans, E. W. Meijer, *Biomacromolecules* **2007**, *8*, 2739.

[25]   P. Y. W. Dankers, J. M. Boomker, A. Huizinga-van der Vlag, E. Wisse, W. P. J. Appel, F. M. M. Smedts, M. C. Harmsen, A. W. Bosman, W. Meijer, M. J. A. van Luyn, *Biomaterials* **2011**, *32*, 723.

[26]   J.-L. Wietor, A. Dimopoulos, L. E. Govaert, R. A. T. M. van Benthem, G. de With, R. P. Sijbesma, *Macromolecules* **2009**, *42*, 6640.

[27]   S. D. Bergman, F. Wudl, *J. Mater. Chem.* **2008**, *18*, 41.

[28]   A. W. Bosman, R. P. Sijbesma, E. W. Meijer, *Mater. Today* **2004**, *7*, 34.

[29]   S. Burattini, B. W. Greenland, D. H. Merino, W. Weng, J. Seppala, H. M. Colquhoun, W. Hayes, M. E. Mackay, I. W. Hamley, S. J. Rowan, *J. Am. Chem. Soc.* **2010**, *132*, 12051.

[30]   P. Cordier, F. Tournilhac, C. Soulié-Ziakovic, L. Leibler, *Nature* **2008**, *451*, 977.

[31]   A R. Hirst, B. Escuder, J F. Miravet, D K. Smith, *Angew. Chem., Int. Ed.* **2008**, *47*, 8002.

[32]   J. D. Hartgerink, E. Beniash, S. I. Stupp, *Science* **2001**, *294*, 1684.

[33]   S. Kyle, A. Aggeli, E. Ingham, M. J. McPherson, *Biomaterials* **2010**, *31*, 9395.

[34]   F. van de Manakker, L. M. J. Kroon-Batenburg, T. Vermonden, C. F. van Nostrum, W. E. Hennink, *Soft Matter* **2010**, *6*, 187.

[35]   C. F. C. Fitié, I. Tomatsu, D. Byelov, W. H. de Jeu, R. P. Sijbesma, *Chem. Mater.* **2008**, *20*, 2394.

[36]   H. Hofmeier, R. Hoogenboom, M. E. L. Wouters, U. S. Schubert, *J. Am. Chem. Soc.* **2005**, *127*, 2913.

[37]   H. Hofmeier, A. El-ghayoury, A. P. H. J. Schenning, U. S. Schubert, *Chem. Commun.* **2004**, *3*, 318.

[38]   S. K. Yang, M. Weck, *Soft Matter* **2009**, *5*, 582.

[39]   A. V. Ambade, S. K. Yang, M. Weck, *Angew. Chem., Int. Ed.* **2009**, *48*, 2894.

[40]   S. K. Yang, A. V. Ambade, M. Weck, *J. Am. Chem. Soc.* **2010**, *132*, 1637.

[41]   A. V. Ambade, C. Burd, M. N. Higley, K. P. Nair, M. Weck, *Chem. Eur. J.* **2009**, *15*, 11904.

[42]   A. Heeres, C. Van der Pol, M. Stuart, A. Friggeri, B. L. Feringa, J. Van Esch, *J. Am. Chem. Soc.* **2003**, *125*, 14252.

[43]   S. Dong, Y. Luo, X. Yan, B. Zheng, X. Ding, Y. Yu, Z. Ma, Q. Zhao, F. Huang, *Angew. Chem., Int. Ed.* **2011**, *50*, 1905.

[44]   G. Groger, V. Stepanenko, F. Würthner, C. Schmuck, *Chem. Commun.* **2009**, 698.

[45]   G. Groger, W. Meyer-Zaika, C. Bottcher, F. Grohn, C. Ruthard, C. Schmuck, *J. Am. Chem. Soc.* **2011**, *133*, 8961.

[46]   M. Weck, *Polym. Int.* **2007**, *56*, 453.

[47]   S. K. Yang, A. V. Ambade, M. Weck, *Chem. Eur. J.* **2009**, *27*, 6605.

[48]   M. M. J. Smulders, A. P. H. J. Schenning, E. W. Meijer, *J. Am. Chem. Soc.* **2008**, *130*, 606.

[49]   L. Brunsveld, A. P. H. J. Schenning, M. A. C. Broeren, H. M. Janssen, J. A. J. M. Vekemans, E. W. Meijer, *Chem. Lett.* **2000**, 292.

[50]   M. M. L. Nieuwenhuizen, T. F. A. de Greef, R. L. J. van der Bruggen, J. M. J. Paulusse, W. P. J. Appel, M. M. J. Smulders, R. P. Sijbesma, E. W. Meijer, *Chem. Eur. J.* **2010** *16*, 1601.

[51]   R. P. Sijbesma, F. H. Beijer, L. Brunsveld, B. J. B. Folmer, J. H. K. K. Hirschberg, R. F. M. Lange, J. K. L. Lowe, E. W. Meijer, *Science* **1997**, *278*, 1601.

[52]   N. E. Botterhuis, D. J. M. van Beek, G. M. L. van Gemert, A. W. Bosman, R. P. Sijbesma, *J. Polym. Sci. Part A: Polym. Chem.* **2008**, *46*, 3877.

[53]   T. Mes, M. M. J. Smulders, A. R. A. Palmans, E. W. Meijer, *Macromolecules* **2010**, *43*, 1981.

[54]   P. J. M. Stals, M. M. J. Smulders, R. Martín-Rapún, A. R. A. Palmans, E. W. Meijer, *Chem. Eur. J.* **2009**, *15*, 2071.

[55]   E. Wisse, A. J. H. Spiering, P. Y. W. Dankers, B. Mezari, P. C. M. M. Magusin, E. W. Meijer, *J. Polym. Sci. Part A: Polym. Chem.* **2011**, *49*, 1764.

[56]   T. F. A. Greef, M. M. L. Nieuwenhuizen, P. J. M. Stals, C. F. C. Fitié, A. R. A. Palmans, R. P. Sijbesma, E. W. Meijer, *Chem. Commun.* **2008**, 4306.

[57]   F. Ilhan, M. Gray, V. M. Rotello, *Macromolecules* **2001**, *34*, 2597.

[58]   S. Chen, A. Bertrand, X. Chang, P. Alcouffe, C. Ladviàre, J.-F. Gérard, F. Lortie, J. Bernard, *Macromolecules* **2010**, *43*, 5981.

[59]   W. P. J. Appel, G. Portale, E. Wisse, P. Y. W. Dankers, E. W. Meijer, *Macromolecules* **2011**, DOI: 10.1021/ma201303s.

[60]   H. Barnes, *A Handbook of Elementary Rheology*, University of Wales, Aberystwyth, **2000**.

[61]   T. Terashima, T. Mes, T. F. A. De Greef, M. A. J. Gillissen, P. Besenius, A. R. A. Palmans, E. W. Meijer, *J. Am. Chem. Soc.* **2011**, *133*, 4742.

6

Single-chain polymeric nanoparticles by stepwise folding

Abstract.

Single-chain polymeric nanoparticles comprising an internal helical architecture are obtained as a result of the self-assembly of pendent benzene-1,3,5-tricarboxamides (BTAs) as side chains of polymethacrylate backbones. Our recognition unit of choice, the BTA motif, self-assembles into helical stacks stabilized by threefold intermolecular hydrogen bonding. Self-assembly of BTAs can be followed with ultraviolet and circular dichroism spectroscopy and allowed us to study the formation and structure of the nanoparticles obtained. We have been able to control the folding into an ordered chiral single-chain polymeric nanoparticle by photo-irradiation and the aid of heating and cooling steps. The high stability and chiral conformation of the folded particles make them excellent candidates for compartmentalized systems that express specific functions such as sensing or catalysis. In this sense, single-chain polymeric nanoparticles partially mimic the properties of biomacromolecules, but can be made using the large number of monomers and polymerization techniques available.

6.1 Introduction

In an effort to mimic the folding of natural polymers, [1-3] foldamers —*i.e.* oligomers that adopt well-defined secondary structures— have been studied in great detail.[4, 5] Also dendrimers have been developed that adopt folded conformations in solution.[6-9] In all of these systems, the conformational synchronization that occurs over extended distances amplifies small energy differences leading to highly stable, folded macromolecules.[10] The benefits of introducing synchronized conformational motions into macromolecules have been clearly demonstrated by Parquette and coworkers. They showed high enantioselectivity in a catalytic hydrogenation reaction, which resulted from chiral information at the periphery of dendrimers relayed to an achiral catalyst complex in the core.[11]

Well-defined nanosized objects formed by the folding of a single-chain polymer offer many possibilities. These polymers are functionalized in the side chains with recognition units and can, after folding into a well-defined object, express specific functions such as sensing or catalysis. In that way, they partially mimic the properties of biomacromolecules, but can be made using the large number of monomers and polymerization techniques available. Initially, these single-chain polymeric nanoparticles have been obtained by covalent intramolecular cross-linking.[12-20] Using this approach, a variety of nanometer-sized macromolecules in the range of 5-20 nm became available that showed great potential in drug delivery systems,[21] (multistep) catalytic conversions[22-25] and nanotechnology.[14-19] Non-covalent interactions such as hydrogen bonds, $\pi-\pi$ interactions and hydrophobic interactions also generate these particles, but now with the ability to respond to external stimuli. This approach has been successfully introduced by our[26-28] and other[29, 30] groups using hydrogen bonding motifs, with the ureidopyrimidinone group (UPy) as a well-known example.[31-34] The characterization of UPy-functionalized nanoparticles has been restricted to size exclusion chromatography (SEC) and atomic force microscopy (AFM). Both techniques showed a significant collapse of the polymer chains, but no evidence for true folding was observed.

In this chapter, we show that single-chain polymeric nanoparticles (SCPNs) comprising an internal helical architecture can be obtained by non-covalent interactions and that the folding process can be followed by circular dichroism (CD) spectroscopy. Our recognition unit of choice is the chiral benzene-1,3,5-tricarboxamide (BTA) motif. BTAs self-assemble into helical stacks stabilized by threefold intermolecular hydrogen bonding.[35-39] The BTAs self-assemble in a cooperative fashion and follow a nucleation-elongation growth mechanism. The transition from the molecularly dissolved state to the aggregated state, indicated by the temperature of elongation T_e, is abrupt and highly concentration dependent.[37] We anticipated that the cooperative self-assembly of pendent BTAs as side chains would supply us with detailed information on the folding behavior and that the inner structure of the

polymeric nanoparticles would be revealed by CD spectroscopy. The schematic design of the system is given in Scheme 6.1. In order to follow the folding process, we introduced a photochemical switch to turn on the secondary interactions. We have chosen to use the photolabile *o*-nitrobenzyl protecting group. This protecting group is used to avoid solubility issues and allows controlled BTA self-assembly.[40, 41]

Scheme 6.1 Schematic representation of a random coil polymer that folds into an ordered chiral single-chain polymeric nanoparticle.
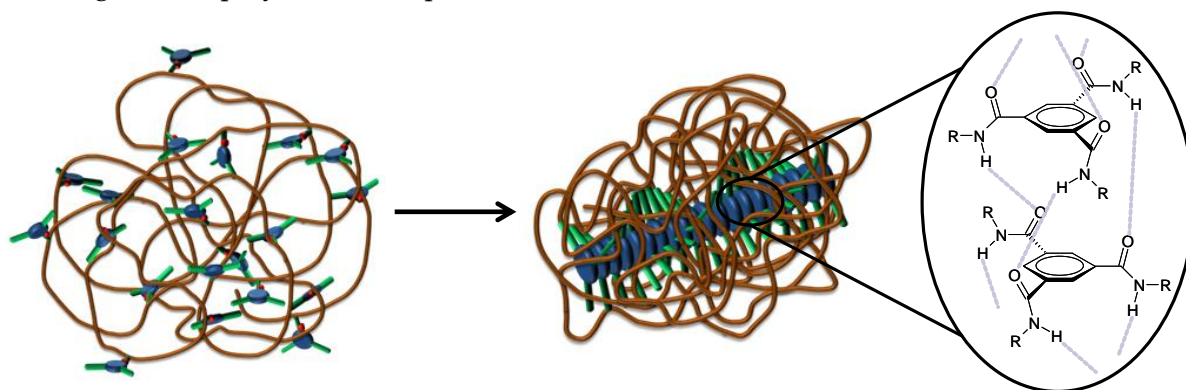
6.2 Synthetic strategies towards side-functionalized polymers

6.2.1 General considerations

Two general strategies can be used to obtain BTA based side-functionalized polymers. The monomer containing the BTA motif can directly be (co)polymerized or the BTA motif can be attached to the backbone after polymerization by post-functionalization. Direct copolymerization has the advantage that the predetermined degree of functionality immediately is obtained without performing further reactions. This is only achieved when all monomers have a similar reactivity and do not interfere chemically or physically with active species during polymerization. Post-functionalization of polymers has the main advantage that the degree of functionalization can be chosen afterwards. For example, post-functionalization of polymers from a similar batch with different amounts of functionality or different functionalities enables a systematic study on the influence of the introduced functionality on the polymer. In this chapter, we evaluate both methods to obtain BTA side-functionalized polymers.

We have selected controlled radical polymerization (CRP) as the polymerization technique of choice.[42-46] Two criteria have to be met for a polymerization to be controlled: (*i*) termination reactions must be suppressed, rendering all chains to be active at the same time and in the ideal case indefinitely, and (*ii*) initiation should be much faster than propagation, giving all polymer chains an equal chance of growth. In a CRP, the molecular weight will increase linearly with conversion. By manipulating the monomer/initiator ratio, control over

the polymer molecular weight is obtained. Since each chain has an equal chance of growth and will ideally not terminate, all chains are of similar length resulting in a narrow molecular weight distribution.

We selected two different CRP methods for the synthesis of the polymer backbones: (*i*) activators regenerated by electron transfer - atom transfer radical polymerization (ARGET ATRP)[44, 48] and (*ii*) reversible addition-fragmentation chain transfer (RAFT) polymerization.[43, 50, 51] ARGET ATRP and RAFT polymerization have been applied in the polymerization of various monomers, ranging from styrenes, (meth)acrylates and (meth)acrylamides.[47] Methacrylates are the most commonly used monomers due to their stability, reactivity and synthetic accessibility. The methacrylate functionality is easily introduced by esterification of alcohols with the commercially available methacryloyl chloride. Therefore we have chosen to synthesize polymethacrylate polymer backbones. Direct (co)polymerization is performed with methacrylate functionalized BTAs in combination with butylmethacrylate (BMA) or isobornylmethacrylate (IMA). In the post-functionalization approach we copolymerized alkyne functional methacrylates with IMA. The alkyne allows "click" chemistry by doing copper(I) catalyzed cycloaddition reactions with azide functional BTAs.

6.2.2 ARGET ATRP

ATRP is frequently based on copper(I) in combination with various multidentate nitrogen ligands.[44, 48] We applied tris[(2-pyridyl)methyl]amine since it provides solubility for the copper catalyst and it tunes the catalytic activity of the system.[48] As initiator species, ethyl 2-bromo-2-methylpropanoate and benzyl bromoisobutyrate were used. In ATRP the active species are generated through a reversible redox process catalyzed by the copper/ligand complex (Scheme 6.2). The metal complex undergoes a one electron oxidation whereby bromine (X) is abstracted from dormant species (P_n-X). This process is controlled with a rate constant of activation k_{act} and deactivation k_{deact}. Polymer chains grow by addition of the intermediate radicals to monomers (k_P) and can terminate through radical coupling and side reactions (k_t). As the rate of propagation is linearly dependent on radical concentration and the rate of termination quadratically, termination can be suppressed by diminishing the radical concentration by shifting k_{act}/k_{deact} to the dormant (P_n-X) side of the reaction. Furthermore, if initiation of dormant species is fast in comparison to propagation, each individual chain will have an equal chance of growth, resulting in well-defined polymers. The proposed mechanism is quite generally accepted, although new insights into the oxidation state of Cu have opened a debate concerning the mechanisms of ATRP.[49]

Scheme 6.2 Proposed mechanism of ARGET-ATRP.
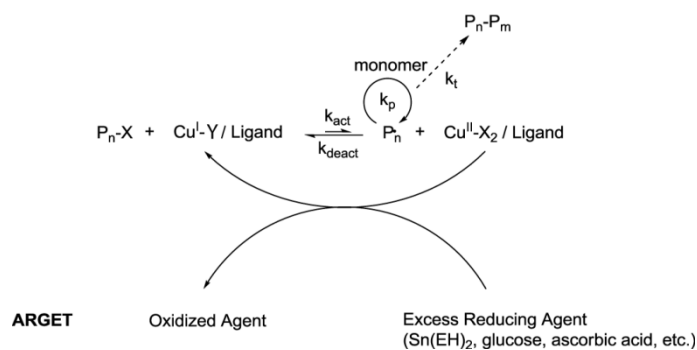
In ARGET ATRP an excess of reducing agent with respect to the ATRP catalyst is used to continuously reduce deactivated catalyst back to the active species (Cu^I-Y / Ligand). ARGET ATRP reduces the sensitivity of the polymerization to oxygen and radical inhibitors, resulting in polymers with narrow molecular weight distributions.

6.2.3 RAFT

RAFT polymerization is a convenient and versatile controlled polymerization technique.[43, 50, 51] The RAFT polymerization process uses conventional radical initiators and a chain transfer agent and avoids the use of a metal catalyst. We have chosen for azobisisobutyronitrile (AIBN) as the radical source and 4-cyano-4-((phenylcarbonothioyl)thio)pentanoic acid as the chain-transfer agent because of its ability to mediate methacrylate polymerizations.[52, 53]

Scheme 6.3 Proposed mechanism of RAFT.
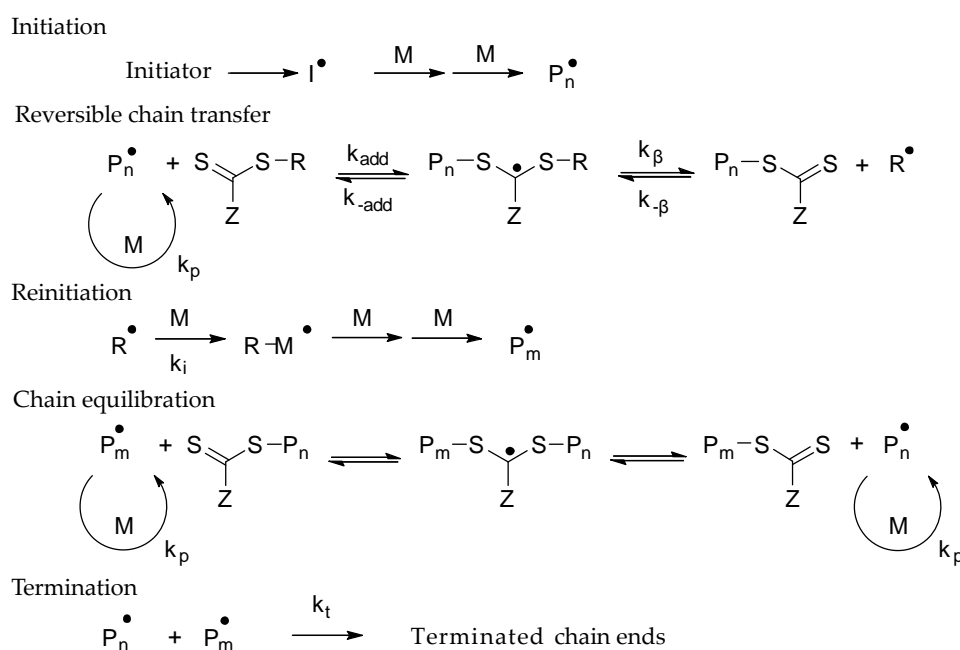
In a RAFT polymerization, initiation and radical-radical termination occur as in a conventional radical polymerization process (Scheme 6.3). The polymer chains grow through monomer addition to the propagating radicals. Addition of the propagating radical ($P_n\cdot$) to the chain transfer agent (RSC(Z)=S) results in an intermediate radical. Fragmentation of this intermediate radical results in a polymeric chain transfer agent ($P_nSC(Z)=S$) and a new radical ($R\cdot$). This radical can form a new propagating radical ($P_m\cdot$) by the addition of a monomer. Rapid equilibrium between the active propagating radicals ($P_n\cdot$ and $P_m\cdot$) and the dormant polymeric chain transfer agent provides equal probability for all chains to grow and results in well defined polymers. The average molecular weight (M_n) of each polymer chain is determined by the amount of chain transfer with respect to monomer. Termination reactions are suppressed by lowering the overall radical concentration.

6.2.4 Copper (I) catalyzed azide-alkyne cycloadditions

Post-functionalization of a polymer chain is a viable alternative for the preparation of polymeric materials. The development of these materials often requires the use of highly selective and efficient modification reactions. An efficient class of reactions termed "click" reactions has recently successfully been applied for post-functionalization of polymers.[54, 55] General characteristics of "click" reactions are high fidelity, high yields, mild reaction conditions, tolerance to a variety of functional groups and minimal synthetic work-up. A well known "click" type reaction is the azide-alkyne Huisgen cycloaddition. The reaction is a 1,3-dipolar cycloaddition between an azide and an alkyne to give a 1,2,3-triazole ring. The copper(I) catalyzed variant results in the selective formation of 1,4-regioisomers of 1,2,3-triazoles and was first reported by Meldal *et al.*[56] Though 1,2,3-triazoles are formed, the copper(I)-catalyzed azide-alkyne cycloaddition (CuAAC) is formally not a 1,3-dipolar cycloaddition. As shown by Sharpless *et al.* the copper(I) catalyzed cycloaddition proceeds via a non-concerted mechanism (Scheme 6.4).[57, 58]

Scheme 6.4 Proposed mechanism of copper(I)-catalyzed azide-alkyne cycloaddition.[57, 58]
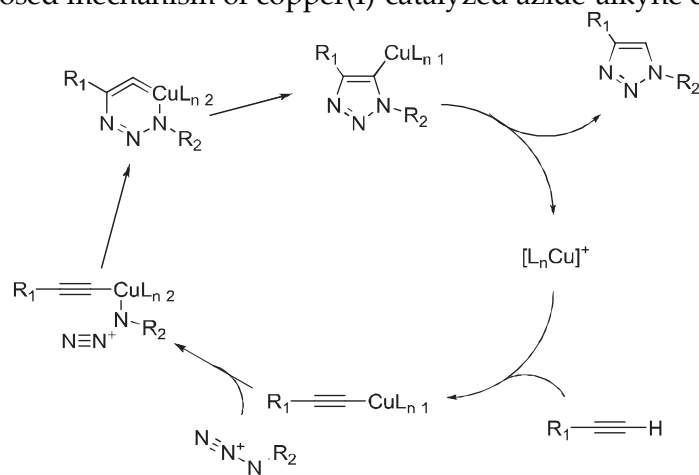
6.3 Synthesis

6.3.1 Syntheses of asymmetric BTAs for single-chain polymeric nanoparticles

This paragraph describes the synthetic procedures, which are applied for the preparation of BTAs, to be used in direct copolymerizations and in the post-functionalization approach. An overview of the BTAs is given in Scheme 6.5.

Scheme 6.5 Overview of the BTA precursors used for the synthesis of side-functionalized polymers.
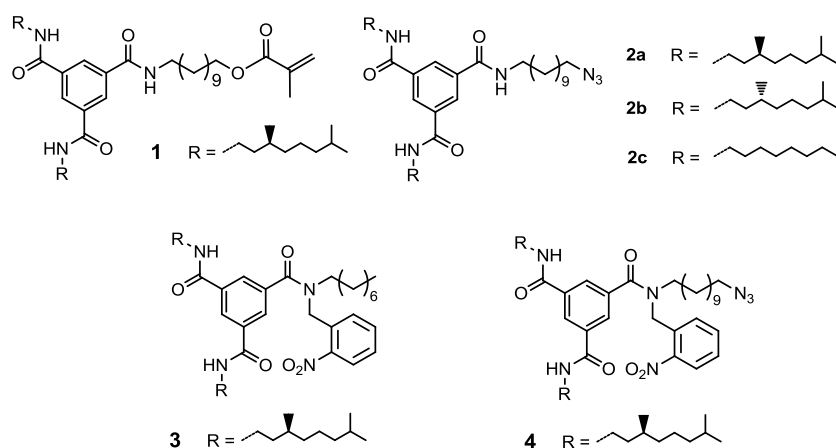
Compound **1** is a BTA with a methacrylate functionality. This BTA can be used in the direct copolymerization applying ARGET ATRP or RAFT polymerization. Compounds **2a-c** consist of BTAs with an azide functionality for post-functionalization. We have synthesized two chiral BTAs bearing enantiomerically pure side chains and an achiral BTA. BTA **3** is model compound in which one of the three amides is substituted with *o*-nitrobenzyl group. This UV labile protecting group can be cleaved with light (λ = 354 nm). Photo-deprotection is used to switch on the secondary interactions. Compound **4** has the same photolabile protecting group as **3**, but also bears an azide functionality that allows post-functionalization.

Compound **1** was synthesized in a statistical approach (Scheme 6.6). The chiral amine (**7**) was procured starting from (*S*)-citronellol by hydrogenation of the double bond followed by conversion of the hydroxy group to an amine by doing a Mitsunobu reaction. 11-Aminoundecanol (**9**) was prepared by performing a Gabriel synthesis on the commercially available 11-bromoundecanol. Two equivalents of **7** and one equivalent of **9** were added to trimesyl chloride yielding **10a**. Compound **1** was obtained by the addition of methacryloyl chloride to **10a**. The low overall yield was mainly a result of the statistical formation of the asymmetrical hydroxy functional BTA (**10a**).

Scheme 6.6 Synthesis of methacrylate functionalized BTA **1**.

The azide functional BTAs (**2a**-**c**) were synthesized starting from the corresponding hydroxy functional BTAs. The *S*-enantiomer (**10a**) was already available since it is used in the synthesis of **1**. The *R*-enantiomer (**10b**) and achiral **10c** were synthesized in a similar fashion as **10a** (Scheme 6.7).

Scheme 6.7 Synthesis of hydroxy functionalized BTAs. A) **10b**, B) **10c**.

(R)-dihydrocitronellylamine (**13**) was synthesized starting from *R*-citronellylbromide by converting it into the corresponding phthalimide. Subsequently, a catalytic hydrogenation was performed followed by the hydrolysis of the phthalimide using hydrazine monohydrate yielding the free amine **13**. Two equivalents of **13** and one equivalent of **9** were added to trimesyl chloride yielding **10a**. The achiral derivative **10c** was synthesized by the addition of two equivalents of *n*-octylamine and one equivalent of **9** to trimesyl chloride.

The hydroxy functionalized BTAs **10a**-**c** were converted into tosylates (**14a**-**c**) using using *p*-toluenesulfonyl chloride in the presence of trimethyl ammonium chloride and triethylamine.[59] Subsequently, sodium azide was added yielding the azide functionalized BTAs **2a**-**c** (Scheme 6.8).

Scheme 6.8 Synthesis of azide functionalized BTAs **2a**-**c**.
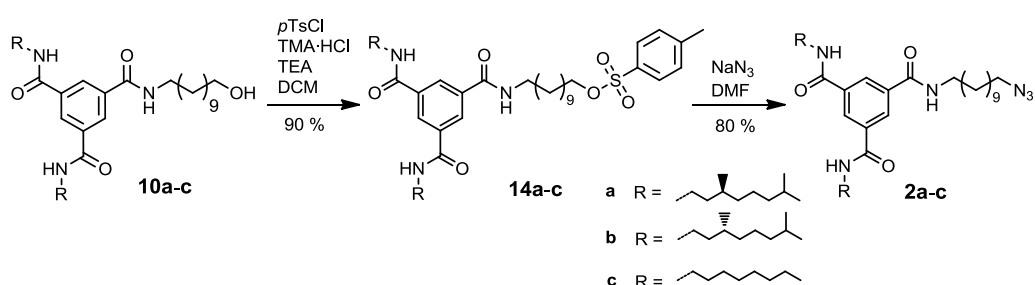
Model compound **3** was acquired starting from a reductive amination of *n*-octylamine and *o*-nitrobenzaldehyde. The secondary amine (**16**) was coupled to the acid chloride functional BTA precursor (**18**), which was synthesized from the carboxylic acid functional BTA precursor **17** (Scheme 6.9).

Scheme 6.9 Synthesis of photolabile protected model compound **3**.
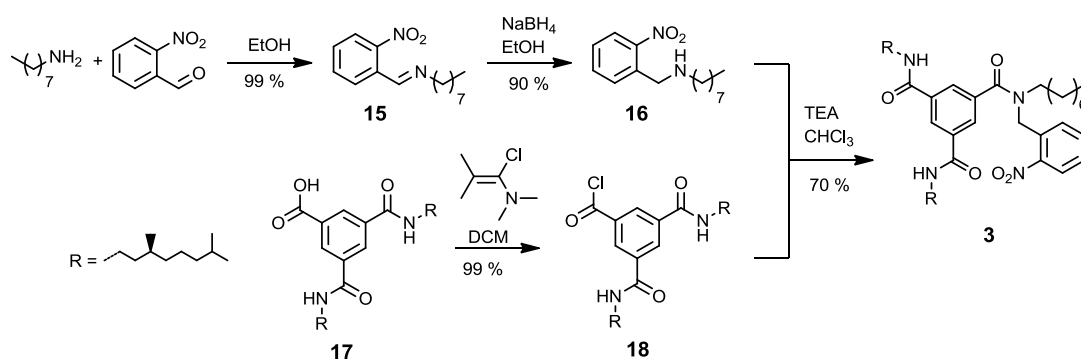
The enantiomerically pure, azide functional photolabile protected BTA unit was synthesized in five steps. The photolabile *o*-nitrobenzyl group was introduced by doing a reductive amination of *n*-aminoundecanol (**9**) with *o*-nitrobenzaldehyde. Subsequently, this

secondary amine (**20**) was coupled to the acid chloride functional BTA precursor (**18**). The hydroxy group was converted into a tosyl group, using *p*-toluenesulfonyl chloride. Finally, the tosylate was converted into an azide using sodium azide yielding compound **4** (Scheme 6.10).

Scheme 6.10 Synthesis of photolabile protected azide functionalized BTA **4**.
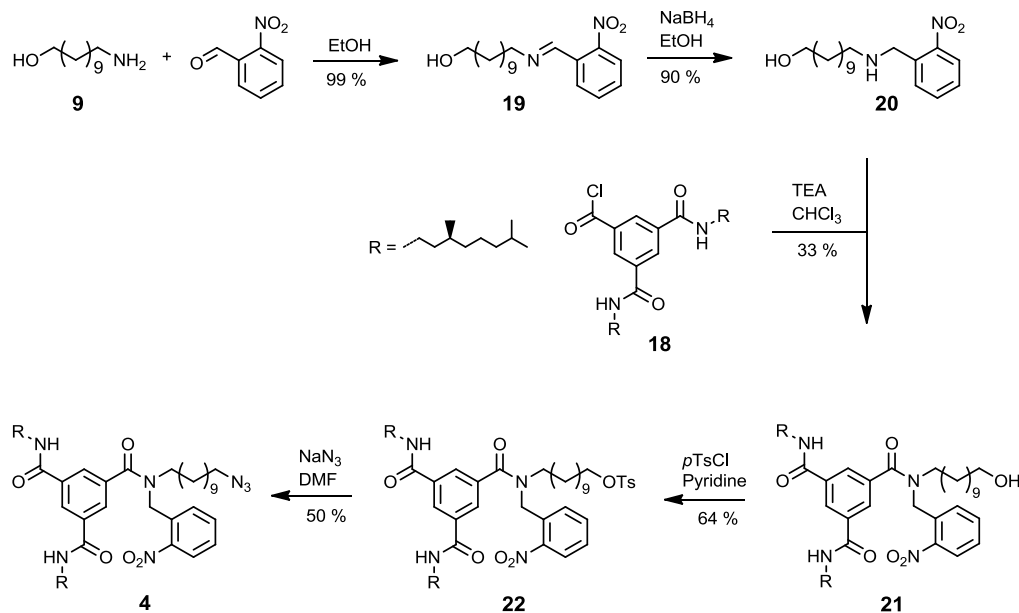
6.3.2 Syntheses of BTA side-functionalized polymers

As described in paragraph 6.2, we synthesized BTA side-functionalized polymers in a direct copolymerization and in a post-functionalization approach. An overview of the BTA functionalized polymers is given in Scheme 6.11. Polymers **23**-**25** were synthesized by a direct copolymerization by performing either ARGET ATRP or RAFT polymerization on a methacrylate functional BTA (**1**) and butylmethacrylate (BMA) or isobornylmethacrylate (IMA). We used racemic IMA and it did not show a detectable optical rotation. Furthermore, pIMA equipped with achiral BTAs (**27c**) (*vide infra*) did not show a Cotton effect suggesting that the chirality of IMA has no influence on the internal helical architecture of the nanoparticles. Polymers **26**-**32** were synthesized by post functionalization of an alkyne side-functionalized polymer backbone with various azide functional BTAs. The polymer backbones were synthesized by performing ARGET ATRP (**26**) or RAFT (**27**-**32**) (co)polymerization of silyl protected alkyne methacrylate monomers and IMA.

Scheme 6.11 Overview of the BTA side-functionalized polymers **23**-**32**.
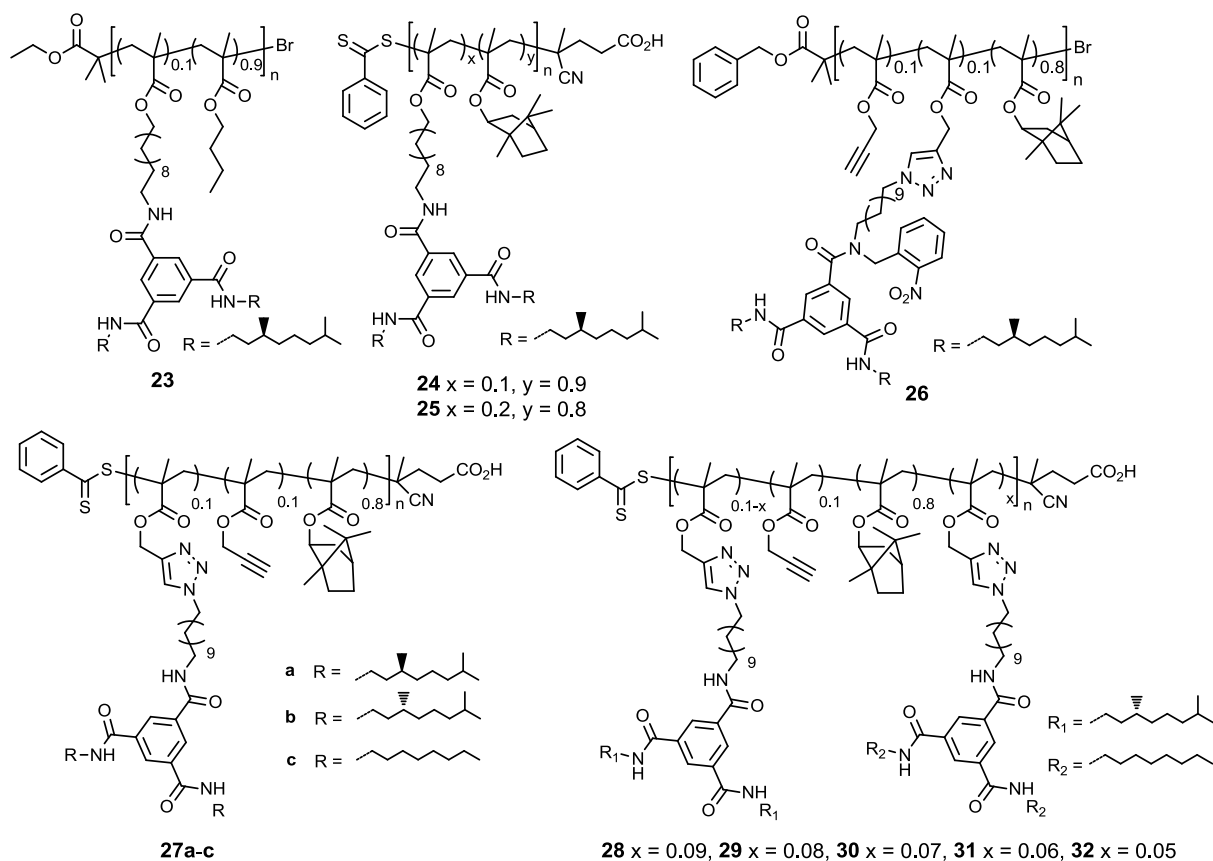
Table 6.1 Summary of the functionalization, NMR and GPC data of polymers **23**-**32**, **34**, **36**.

Polymer	Functionality	Degree of functionalization	DP	M_n^a [kg/mol]	M_n^b [kg/mol]	PDI^b [-]
23	S-BTA	0.1	70	-	14.4[c]	1.91[c]
24	S-BTA	0.1	180	43.5	21.4[c]	1.60[c]
25	S-BTA	0.2	180	51.6	16.6[c]	1.47[c]
26	Protected S-BTA	0.1	180	47.0	26.0[c]	1.65[c]
27a	S-BTA	0.088	250	65.0	27.0	1.52
27b	R-BTA	0.084	250	64.3	28.5	1.55
27c	A-BTA	0.089	250	63.2	28.4	1.62
28	R-BTA/A-BTA	0.008/0.07	250	63.3	25.0	1.60
29	R-BTA/A-BTA	0.021/0.076	250	66.2	28.0	1.53
30	R-BTA/A-BTA	0.025/0.058	250	64.1	27.1	1.55
31	R-BTA/A-BTA	0.033/0.05	250	64.1	22.3	1.61
32	R-BTA/A-BTA	0.043/0.043	250	64.9	27.2	1.58
34	Propargyl	0.25	180	32.0	22.0	1.63
36	Propargyl	0.27	250	50.0	28.0	1.49

[a] Determined by ^{1}H-NMR. [b] Determined by GPC in THF at 20 °C. [c] Determined by GPC in ODCB at 80 °C.

Scheme 6.12 Synthesis of polymer **23**.
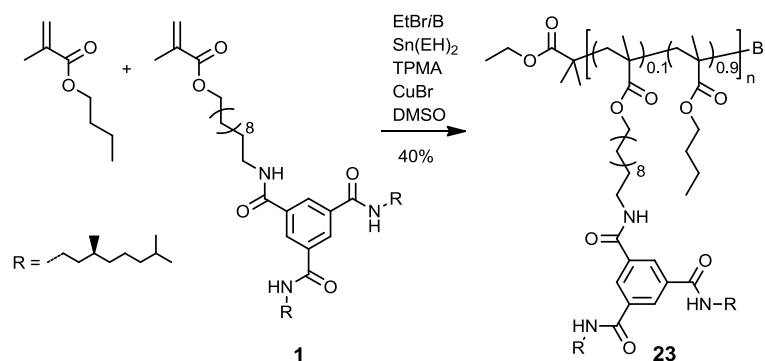
Polymer **23** was synthesized using ARGET ATRP in DMSO (Scheme 6.12). Although DMSO was selected to prevent inter- and intramolecular hydrogen bonding of BTAs during polymerization, the polymer precipitated during the polymerization reaction. As a result, we stopped the polymerization at 40 % conversion. Polymer **23** was purified by precipitation in methanol, yielding a white solid. GPC analysis of polymer **23** in o-dichlorobenzene (ODCB) (80 °C, polystyrene standards) showed a polymer with M_n = 14400 g/mol and a PDI = 1.91. The average degree of polymerization (DP) is 70. ¹H-NMR analysis in 1,1,2,2-tetrachloroethane (TCE-d^2, 90 °C) of **23** revealed a polymer with 10% BTA incorporation (Figure 6.1). The good agreement of the feed ratio and the observed ratio of BTA-methacrylate / BMA suggests that **23** is a random copolymer.
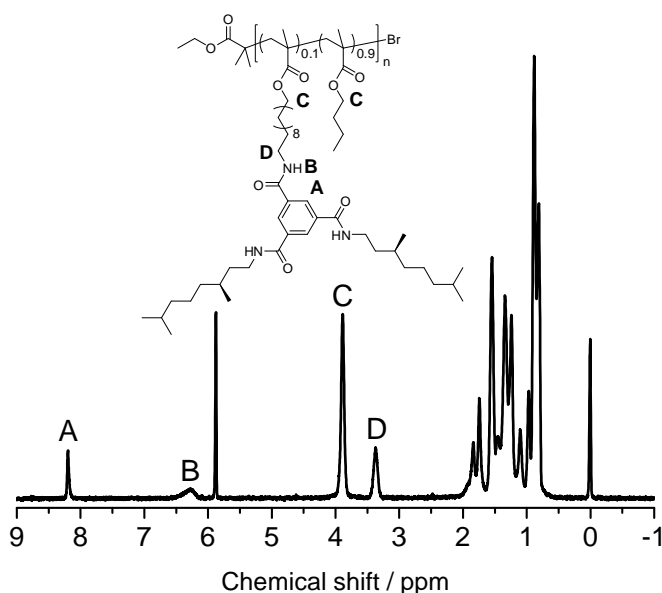
Figure 6.1 ¹H-NMR of polymer **23** in TCE-d^2 at 90 °C.

To increase the solubility, further polymerizations were conducted with IMA. Copolymerization of IMA and **1** is performed by a RAFT polymerization in dioxane, yielding copolymers **24** and **25** (Scheme 6.13). Dioxane was selected as a solvent because it is a good

solvent for polymethacrylates and BTAs are molecularly dissolved. Copolymers **24** and **25** were purified by precipitation in methanol.

Scheme 6.13 Synthesis of polymers **24** and **25**.

The BTA content of **24** and **25** was determined with ^{1}H-NMR (TCE-d_2, 90 °C). Polymers **24** and **25** contain 10 mol% and 20 mol% BTA, respectively, which is in agreement with the feed ratio. The polymerizations reached a conversion of 80% after 52 hours. Based on the conversion and chain transfer agent/monomer ratio the theoretical molecular weights for **24** and **25** are 43500 g/mol and 51600 g/mol, respectively. GPC analysis (ODCB, 80 °C) of **24** showed a M_n of 21400 g/mol and PDI = 1.60 and a M_n of 16600 g/mol and PDI = 1.47 for polymer **25**. The molecular weights, which are determined with GPC are somewhat underestimated due to the use of polystyrene standards.

Scheme 6.14 Synthesis of polymer **26**.

IMA and silyl protected propargyl methacrylate were copolymerized using ARGET ATRP yielding polymer **33** (Scheme 6.14). A silyl protection was used to prevent interference of the alkyne functionalities with the polymerization, as they are known to interact with a copper catalyst.[60] The use of benzyl bromoisobutyrate as the initiator allowed the determination of the molecular weight by ^{1}H-NMR, since the benzylic and aromatic signals have a distinct position in the NMR spectrum. Polymer **33** was purified by precipitation from methanol. The silyl protecting group was removed using TBAF and acetic acid in THF. Polymer **34** was purified by precipitation from methanol. Polymer **34** contained 25 mol% alkyne functionalities, which is close to the feed ratio (20 mol%). GPC analysis of **34** showed a M_n of 22000 g/mol and a *PDI* = 1.63. The *DP* was 180 (Table 6.1). The final polymer **26** was prepared by a copper(I) catalyzed click reaction using the azide functional BTA **4**. ^{1}H-NMR of **26** showed a BTA content of 10%. The *DP* of polymer **26** is 180 and it contains 18 BTAs per chain. According to NMR, **26** has a M_n of 47000 g/mol. GPC analysis revealed a M_n = 26000 g/mol and a *PDI* of 1.65.

Scheme 6.15 Synthesis of polymers **27a-c**.
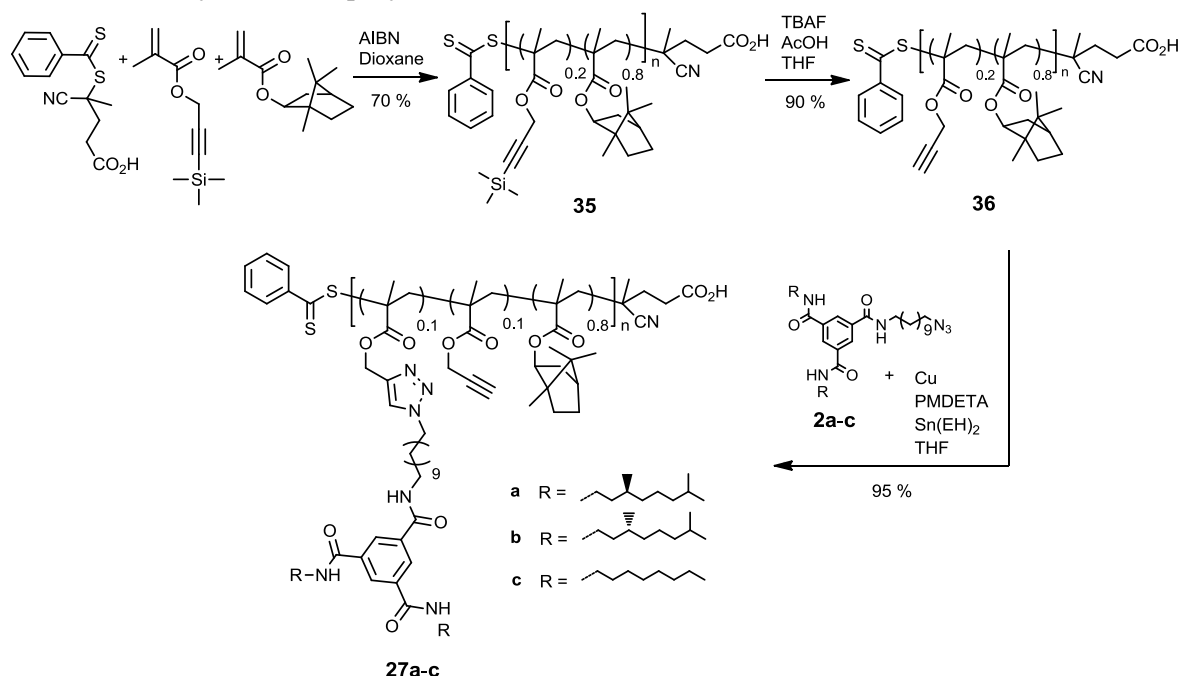
Polymers **27a-c** were synthesized by RAFT polymerization followed by post-functionalization (Scheme 6.15). A mixture of silylprotected propargyl methacrylate and IMA in a 1:4 ratio was polymerized using AIBN as the radical source and 4-cyano-4-((phenylcarbonothioyl)thio)pentanoic acid as the chain transfer agent. The silyl protecting group was removed using TBAF and acetic acid in THF. Polymer **36** was purified by precipitation from methanol. Polymer **36** contains 27 mol% alkyne functionalities which is slightly more than the feed ratio (20 mol%). GPC analysis of **36** showed a M_n of 28000 g/mol

and a *PDI* = 1.49. The *DP* is 250 (Table 6.1). Polymers **27a-c** were prepared by a copper(I) catalyzed click reaction using the azide functional BTAs **2a-c**. Half of the available alkyne groups were coupled to the BTA azides (**2a-c**), resulting in an average BTA content of ~9%. As an example, the ^{1}H-NMR spectrum of **27c** is given in Figure 6.2.

Figure 6.2 ^{1}H-NMR of polymer **27c** in CDCl$_3$ at 20 °C.

Scheme 6.16 Synthesis of polymers **28**-**32**.

28 x = 0.09, **29** x = 0.08, **30** x = 0.07, **31** x = 0.06, **32** x = 0.05

Finally, polymers **28**-**32** were synthesized by post-functionalization of polymer **36** (Scheme 6.16), using copper(I) catalyzed click reactions to couple azide functional BTAs. Mixtures of chiral (**2b**) and achiral (**2c**) BTAs in different ratios were used to obtain polymers **28**-**32**. Half of the available alkyne groups were functionalized with BTAs resulting in an average BTA content of ~9%. ^{1}H-NMR and GPC were used to determine the degree of functionalization and the molecular weight (Table 6.1).

6.4 Folding of BTA side-functionalized polymers

6.4.1 Self-assembly of BTAs by photodeprotection

The cooperative self-assembly of BTAs attached to the polymer backbone is expected to fold the polymer backbone into a polymeric nanoparticle. The folding behavior and the inner structure of the polymeric nanoparticles will be investigated by CD spectroscopy. In order to follow this folding process, we introduce a photochemical switch to turn on the secondary interactions. To confirm the feasibility of our approach to "cage" the BTA motifs by one UV labile *o*-nitrobenzyl group, we have synthesized a model compound (**3**). Compound **3** exists of a single BTA in which one amide is substituted with the *o*-nitrobenzyl group. Upon irradiation, the *o*-nitrobenzyl group is cleaved affording **37** (Scheme 6.17). It is expected that compound **3** cannot self-assemble and that **37** can self-assemble into helical aggregates under the right conditions.

Scheme 6.17 Design of a "caged" BTA. Upon irradiation of **3** the *o*-nitrobenzyl group is cleaved to afford **37**, allowing self-assembly under selected conditions.
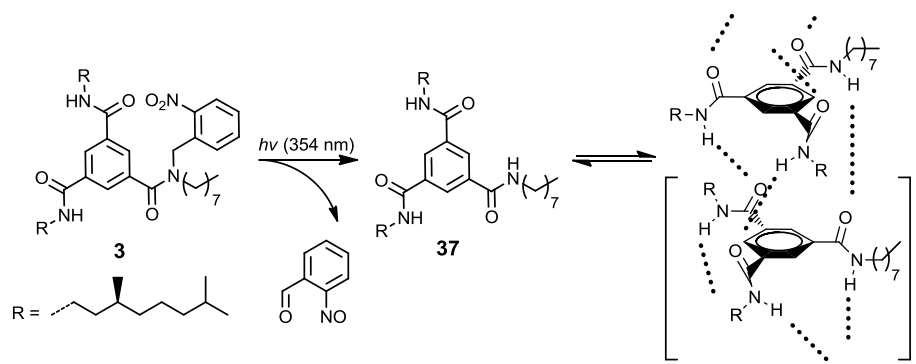
Irradiation of **3** in methanol-d^4 with UV light (λ = 354 nm, T = 20 °C, c = 5 mg mL^{-1}) in a photoreactor resulted in full conversion of **3** into **37** within two hours of irradiation as determined by ^{1}H-NMR (Figure 6.3). The conversion was calculated based on the disappearance of the benzylic protons at 5.07 ppm (x = 1 - (integral t_x / integral t_0) * 100%). Irradiation did not result in degradation of the BTA motif.
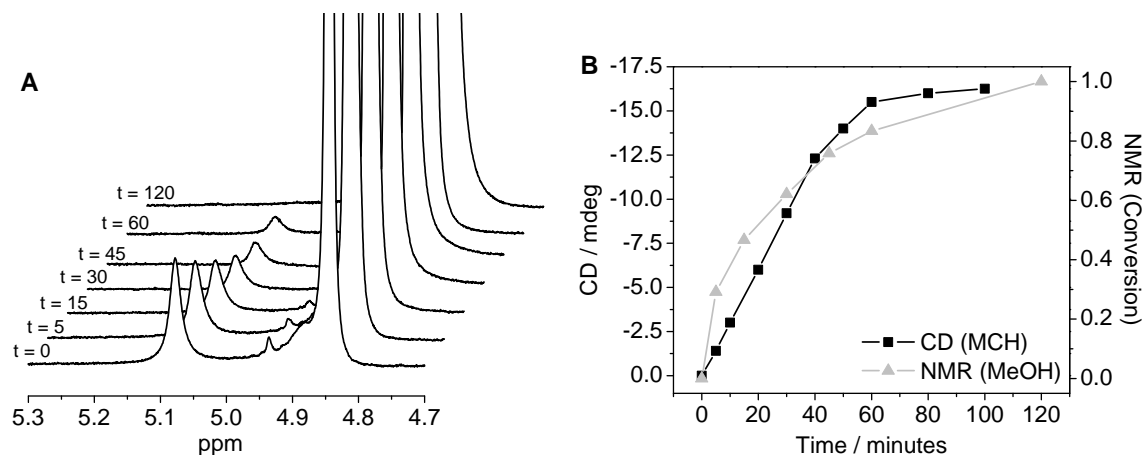
Figure 6.3 A) NMR spectra of **3** versus photoirradiation time B) The conversion of **3** into **37** by ^{1}H-NMR in methanol-d^4 and the development of the Cotton effect in the conversion of **3** into **37** as measured at 225 nm as a function of irradiation time (T = 20 °C, c = 1.2 x 10^{-5} M in MCH).

Both **3** and **37** are molecularly dissolved in methanol-d^4, preventing the formation of helical supramolecular polymers.[61] Next, we deprotected **3** in methylcyclohexane (MCH), a solvent in which **3** is molecular dissolved and **37** self-assembles into supramolecular polymers with preferred *M* helicity.[36, 37] Indeed, CD spectroscopy of **3** in MCH (c = 1.2 x 10^{-5} M) showed no Cotton effect. A Cotton effect arose upon irradiating the solution, which showed saturation after about 60 minutes of irradiation (Figure 6.3B). The magnitude (16 mdeg at λ = 223 nm), sign and shape of the CD spectrum is similar to those found in other chiral BTAs dissolved in MCH at similar concentration and temperature.[62] This indicates that the *o*-nitrosobenzaldehyde, which is released during the process,[40] does not interfere with the self-assembly process and that supramolecular polymers with a preferred helicity are formed upon deprotection. A remarkable difference is observed in the shape of the plot of the conversion in methanol-d^4 and the Cotton effect in MCH upon deprotection of **3**. This is presumably a result of the different nature of the solvents or amplification effects in the CD measurements.

6.4.2 Self-assembly and folding of BTA side-functionalized polymers

Scheme 6.18 Upon irradiation of **26**, the *o*-nitrobenzyl group is cleaved to afford **38**, allowing self-assembly under selected conditions.
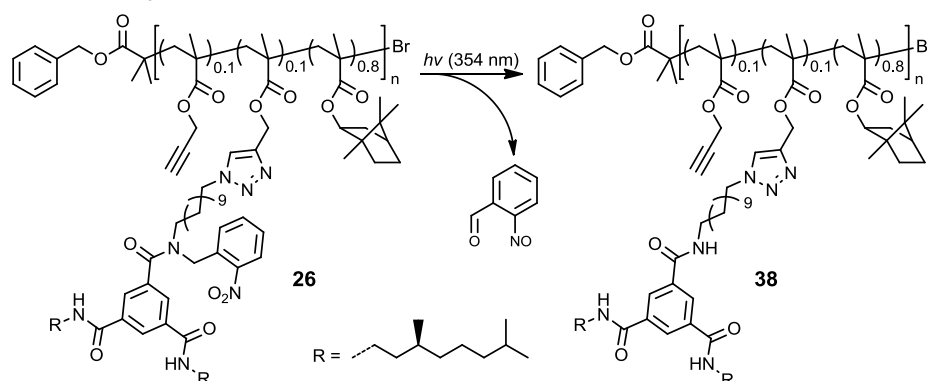
Next, the feasibility to fully deprotect polymer **26** to polymer **38** (Scheme 6.18) was evaluated. Irradiation of polymer **26** (c = 3 mg mL^{-1} in TCE-*d*^{2}) with UV light (λ = 354 nm) resulted in full photolytic cleavage of the *o*-nitrobenzyl group within 20 minutes as evidenced by the disappearance of the benzylic signal in ^{1}H-NMR (Figure 6.4A). The necessary photoirradiation time to obtain full conversion was significantly shorter compared to that of model compound **3** for unknown reasons.
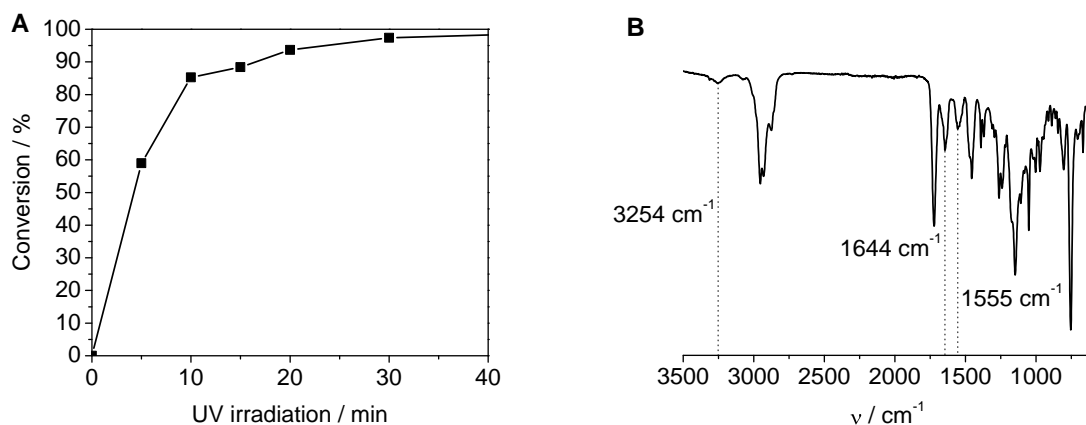
Figure 6.4 A) The conversion of **26** into **38** by ^{1}H-NMR in TCE-*d*^{2}. B) Infrared spectroscopy data of **38** (T = 20 °C).

After removal of the solvent, the infrared spectrum of polymer **38** in the solid state showed vibrations at positions typical for threefold helical intermolecular hydrogen bonding in BTAs. The NH stretching vibration occurred at 3254 cm^{-1} while the amide I and amide II vibrations occurred at 1644 cm^{-1} and 1555 cm^{-1}, respectively (Figure 6.4B), indicating that threefold helical intermolecular hydrogen bonding between BTA molecules can be formed in the polymer in the solid state after full deprotection.[36, 38, 39]

In dilute solutions, the nature of the solvent is of high importance to induce self-assembly of the BTA motifs in polymer **38**.[63] While the helical self-assembly of model BTA **37** was demonstrated in MCH, polymer **26** and **38** were found to be insoluble in this solvent. To reconcile the solvent preferences of the polymethacrylate backbone and BTA self-assembly, we decided to apply solvent mixtures. We selected a mixture of 1,2-dichloroethane (DCE) and MCH for the deprotection reaction of **26**. Importantly, the CD spectra were measured after heating the sample to 80 °C and slow cooling to room temperature. A pronounced negative Cotton effect in the deprotected polymer **38** was observed in a mixture of DCE/MCH 65/35 vol% (c_{BTA} = 7.5 x 10^{-5} M, T = 20 °C). The Cotton effect has a maximum at λ = 225 nm, which is typical of helical hydrogen bonded BTA aggregates (Figure 6.5A).[64]

A systematic investigation of the effect of solvent composition on the absolute CD intensity resulted in the data summarized in Figure 6.4B. We used the concentration independent anisotropy value (g_{value}) of the Cotton effect at λ = 225 nm. Interestingly, in pure DCE polymer **38** already showed a negative Cotton effect which increased upon increasing the MCH concentration. A maximum value of the Cotton effect was found in a 70/30 DCE/MCH mixture. Increasing the amount of MCH, results in a decrease of the CD intensity. Hence, the solvent has to balance the backbone solubility, of both the protected and deprotected polymer, and the self-assembly capability of the chiral BTA unit.[63]
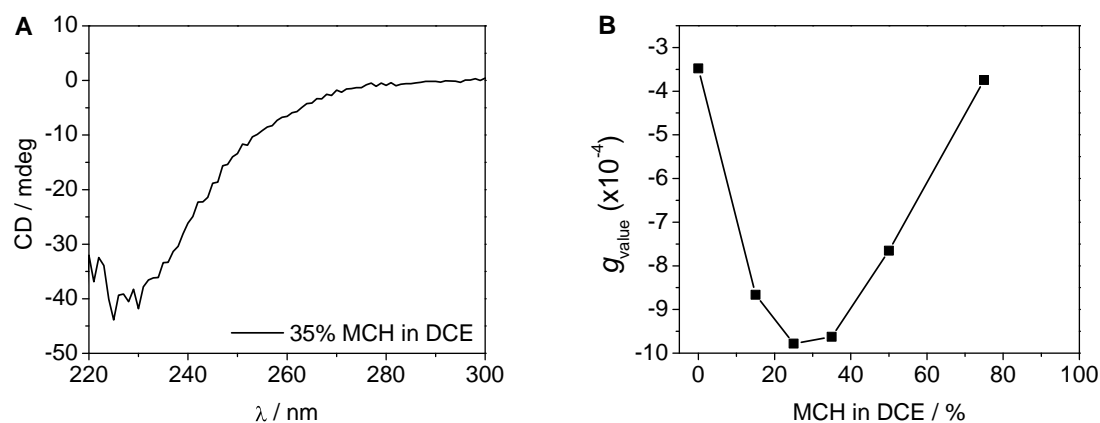
Figure 6.5 A) CD spectrum of polymer **38** (200 µg/mL) measured in a mixture of DCE/MCH 65/35 vol% (c_{BTA} = 7.5 x 10^{-5} M, T = 20 °C, l = 0.5 cm). B) Dependence of the g_{value} of **2** on the solvent composition (c_{BTA} = 7.5 x 10^{-5} M, λ = 225 nm, T = 20 °C).

Having established an optimal solvent mixture, the deprotection reaction of **26** (c_{BTA} = 7.5 x 10^{-5} M, DCE/MCH 70/30 vol%) was followed as a function of time using UV spectroscopy (Figure 6.6). During deprotection of **26** two new absorption bands become visible at λ = 280 nm and λ = 324 nm (Figure 6.6A). These absorption bands are attributed to the *o*-nitrosobenzaldehyde byproduct formed upon deprotection. The change in intensity of the absorption band (λ = 324 nm) is plotted as a function of photoirradiation time (Figure 6.6B).

After 10 minutes of irradiation, the deprotection reaction is complete, evidenced by saturation of the UV absorption signal. The significant increase in reaction rate, compared to the photodeprotection reaction of model compound **3** is not studied, but solvent and concentration effects can play an important role.
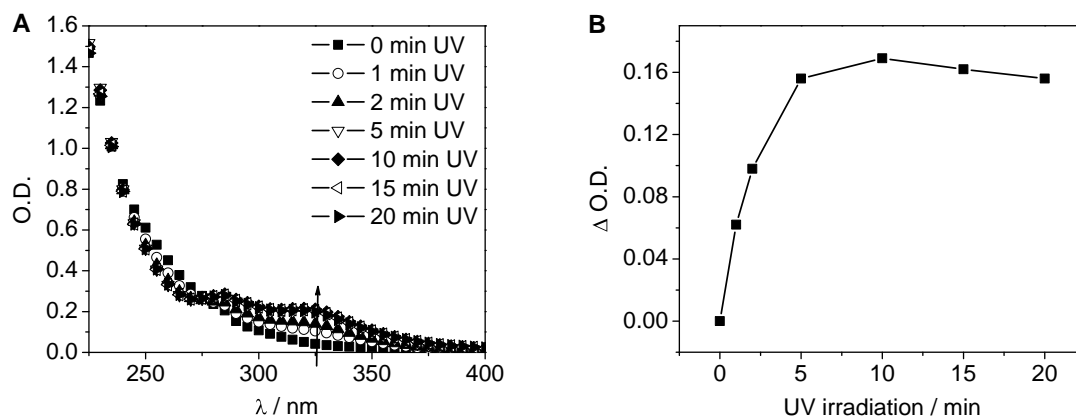
Figure 6.6 A) UV spectra of **26** upon the irradiation. B) UV absorption of **26** at $\lambda = 324$ nm as a function of irradiation time ($c_{BTA} = 7.5 \times 10^{-5}$ M, DCE/MCH 70/30 vol%, l = 0.5 cm).

Surprisingly, CD analysis of the sample that was deprotected at room temperature for 20 min showed a very small Cotton effect of -2 mdeg at $\lambda = 225$ nm (Figure 6.7A, black line). This Cotton effect is significantly lower than the maximum value of -40 mdeg ($g_{value} = -9.8 \times 10^{-4}$) found for polymer **38** in the same solvent mixture but after heating and cooling (Figure 6.5B). Gratifyingly, heating the solution to 80 °C followed by cooling to 20 °C at a rate of 5 K min^{-1}, resulted in a pronounced CD effect of -37 mdeg at $\lambda = 225$ nm (Figure 6.7A, grey line).
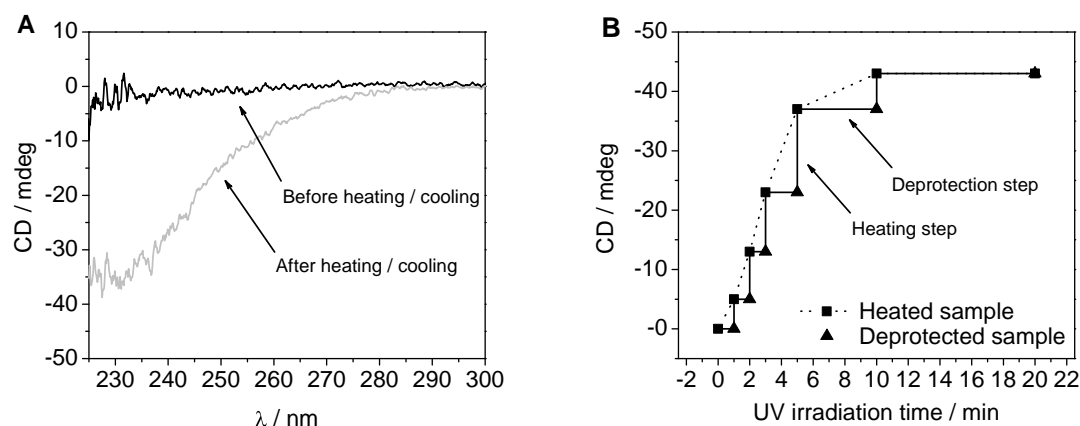
**Figure 6.7** A) Fully deprotected polymer **38** before and after heating to 80 °C and cooling to 20 °C ($c_{BTA} = 7.5 \times 10^{-5}$ M, DCE/MCH 70/30 vol%, T = 20 °C, 20 minutes UV irradiation). B) Evolution of the Cotton effect of **26** as a function of photoirradiation time with intermittent heating to 80 °C and cooling to 20 °C ($c_{BTA} = 7.5 \times 10^{-5}$ M, DCE/MCH 70/30 vol%, $\lambda = 225$ nm, T = 20 °C).

This interesting behavior was evaluated in further detail by performing CD measurements on a solution of **26** (c_{BTA} = 7.5 x 10^{-5} M, DCE/MCH 70/30 vol%) after irradiating the solution for short time intervals. CD spectra were measured immediately after UV irradiation and also after heating to 80 °C and cooling to 20 °C (Figure 6.7B). For each individual deprotection step, it was observed that the Cotton effects before and after irradiation were of similar size. Heating to 80 °C resulted in complete disappearance of the Cotton effect. However, upon cooling, the Cotton effect increased proportionally to the amount of deprotected BTAs.

Folding is achieved by controlled cooling of solutions of the polymers in order to arrive at the thermodynamically stable state. When polymers are made by deprotection of BTAs by irradiation at room temperature, the system resides in a kinetically trapped or collapsed state. The more thermodynamically favorable folded state is achieved by an additional heating/cooling step. At high temperatures, BTAs are not aggregated, the polymer is unfolded, and at the same time the polymer backbone is flexible. Slowly reducing the temperature induces BTA aggregation because there is sufficient mobility within the polymer to adopt an optimal conformation for self-assembly to occur.

6.4.3 Elucidation of inter- or intramolecular self-assembly by variable temperature CD spectroscopy

BTAs side-functionalized to polymers could self-assemble in an inter- or intramolecular fashion. Only intramolecular self-assembly leads to the formation of single-chain polymeric nanoparticles. To experimentally prove our concept of the single-chain polymeric nanoparticle by stepwise folding, it is important to exclude intermolecular self-assembly. Therefore, we compared the self-assembly of BTAs present in polymer **26** with the self-assembly of the "free" unbound BTAs (**39**) that have been studied before.[36, 37] BTA **39** self-assembles in a cooperative fashion and follows the nucleation-elongation growth mechanism.[65] The transition from the molecularly dissolved state to the aggregated state is visualized with CD spectroscopy by a drastic increase in CD intensity (MCH, c_{BTA} = 1 - 5x10^{-5} M, l = 1 cm). The temperature, at which this increase is observed, depends on the concentration and is called the elongation temperature (T_e). The CD intensity and T_e decrease with decreasing concentration (Figure 6.8A). In contrast, polymer **38** showed a concentration independent onset of optical activity (Figure 6.8C), and the increase of the CD intensity was a more gradual process. Normalizing the curves in Figures 6.8C for concentration, by plotting the g_{value} as a function of temperature (Figure 6.8D) reveals that all cooling curves can be superimposed indeed. Because the onset of aggregation for polymer **38** is independent of the concentration, the *local* concentration presumably determines the self-assembly process. This strongly suggests that BTAs attached to the polymer backbone self-assemble in an intramolecular fashion.
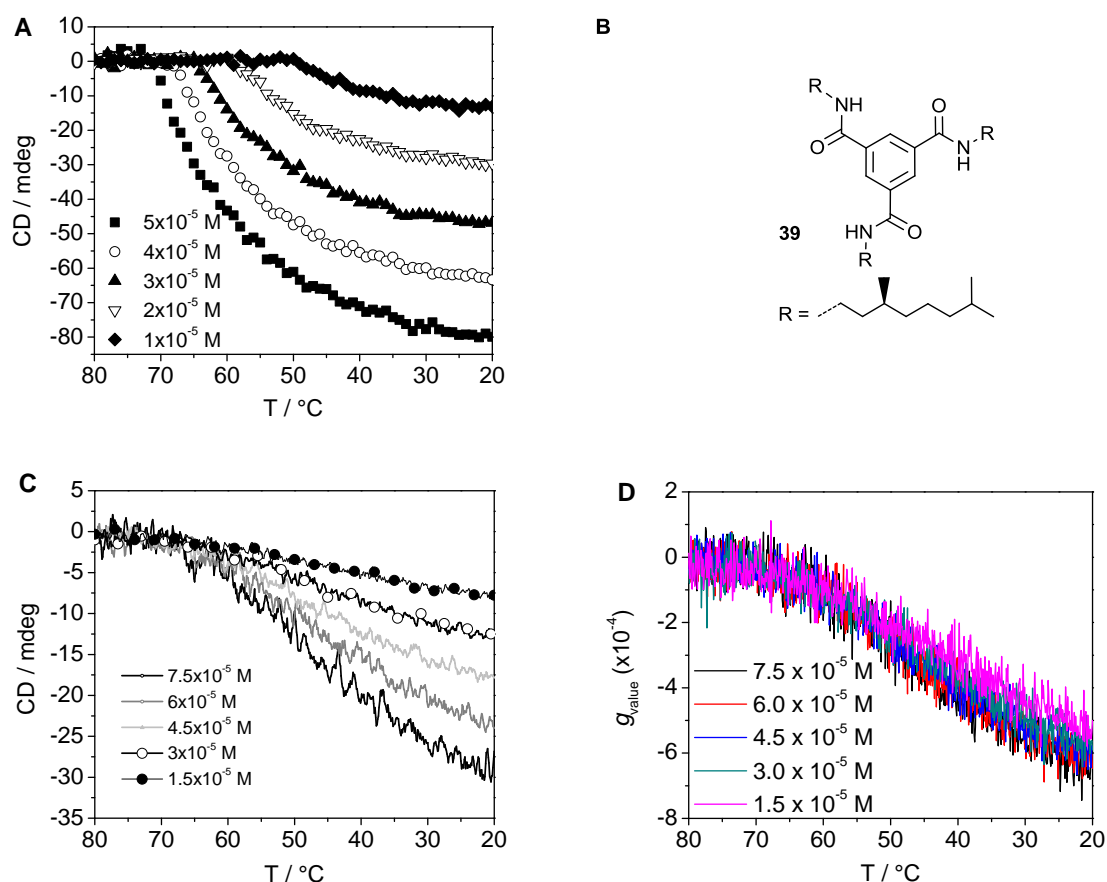
Figure 6.8 A) CD spectra of **39** versus temperature at different concentrations (MCH, λ = 225 nm, l = 1 cm. B) Chemical structure of the unbound chiral BTA **39**. C) CD spectra of **38** versus temperature at different concentrations (DCE/MCH 70/30 vol%, λ = 225 nm, l = 0.5 cm). D) CD spectra of **38** versus temperature at different concentrations (DCE/MCH 70/30 vol%, λ = 225 nm, l = 0.5 cm). The Cotton effect is corrected for concentration and expressed as the anisotropy factor (g_{value}).

Next we studied the onset of aggregation by changing the BTA incorporation. The degree of functionalization of BTAs was controlled by varying the irradiation time during the photodeprotection reaction. Polymer **26** was irradiated with light for 2 and 5 minutes, generating a half and fully deprotected polymer, respectively. In addition, we used polymer **24** and **25**, which possess a BTA content of 10 and 20 mol%. The absolute concentration of **24** was doubled, which results in equal amounts of BTAs in both solutions. Polymers **24**-**26** were subjected to variable temperature CD measurements (Figure 6.9).
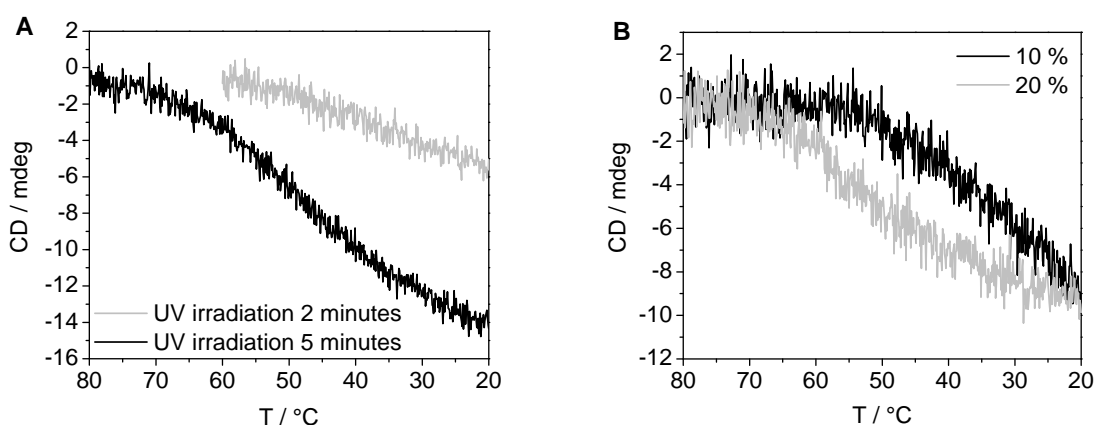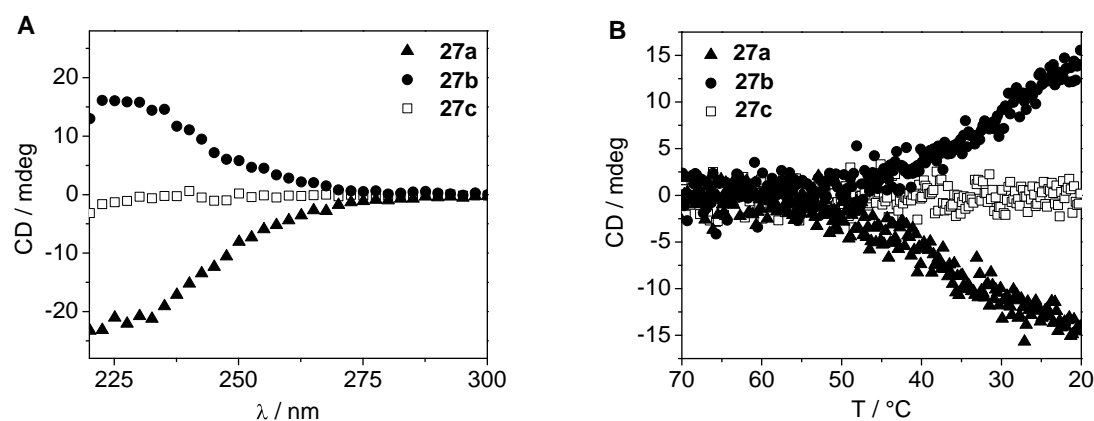
Figure 6.9 A) CD spectra of **26** versus temperature after 2 and 5 minutes of irradiation (c_{BTA} = 3.25 x 10^{-5} M, DCE/MCH 70/30 vol%, λ = 225 nm, l = 0.5 cm) B) CD cooling curves of **24** and **25** (c_{BTA} = 2.5 x 10^{-5} M, DCE, λ = 230 nm, l = 0.5 cm)

CD cooling curves of **26** after 2 and 5 minutes of irradiation showed and onset of aggregation temperature of 60 °C and 75 °C, respectively. The Cotton effect at 20 °C after 2 minutes was -6 mdeg and -14 mdeg after 5 minutes. CD cooling curves of polymer **24** and **25** containing 10 mol% BTA or 20 mol% BTA (corresponding to 17 and 35 BTA molecules per chain, respectively) when keeping the absolute BTA content constant showed that the onset of aggregation of the latter was increased by approximately 20 °C. Since the onset strongly depends on the *local* BTA concentration and not on the overall concentration, the aggregation process is predominantly a single-chain folding process.

6.4.4 Elucidation of inter- or intra-molecular self-assembly by transfer of chirality

To further verify that folding is predominantly intramolecular chain folding process, we investigated the possibility of BTA side-functionalized polymers to interact intermolecularly. Unbound BTAs form highly dynamic supramolecular polymers in dilute solution. The addition of a small amount of chiral BTAs in a solution of achiral BTAs instantly directs the helicity to one handedness (Sergeants and Soldiers effect).[36] We here mix chiral BTA side-functionalized polymers (**27a,b**) with achiral (**27c**) ones. Transfer of chirality would be indicative for intermolecular interactions during the folding of BTA side-functionalized polymers. Before mixing experiments were performed, the self-assembly of all three polymers separately was studied with CD spectroscopy. Polymers **27a-c** were dissolved in DCE (c_{BTA} = 10^{-4} M) and measured at 20 °C (Figure 6.10A). Subsequently, cooling experiments were performed on the same solutions (Figure 6.10B).

143

Figure 6.10 A) CD spectra of **27a-c** (c_{BTA} = 10^{-4} M, in DCE, l = 0.5 cm). B) CD spectra of **27a-c** versus temperature (c_{BTA} = 10^{-4} M in DCE, λ = 225 nm, l = 0.5 cm).

The Cotton effects of polymers **27a** and **27b** were almost similar in height and opposite in sign. Achiral polymer **27c** was CD silent. Cooling experiments for **27a** and **27b** showed a temperature of 55 °C for **27a** and 50 °C for **27b**, at which aggregation starts. The slightly higher degree of functionalization of polymer **27a** is the likely explanation for this small temperature difference.
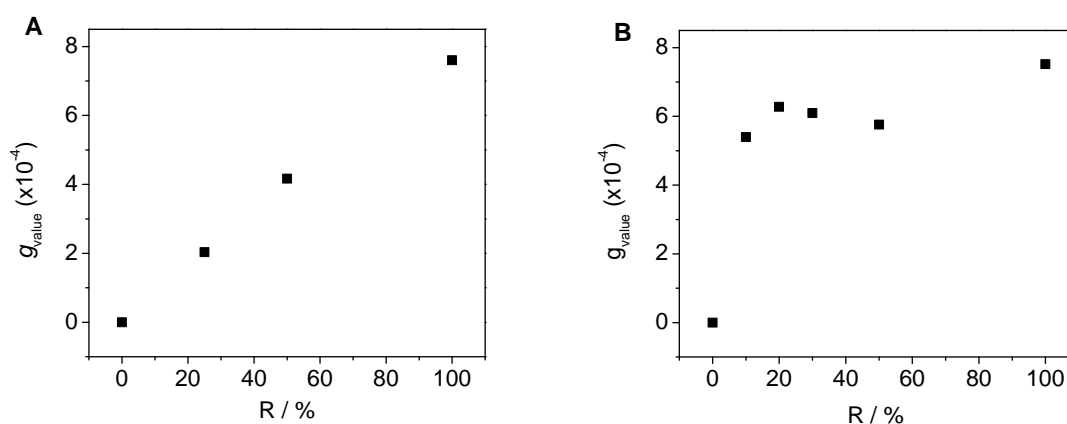
Figure 6.11 A) The g_{value} as a function of the *R*-enantiomer content in mixtures of **27b** and **27c** (λ = 225 nm, c_{BTA} = 10^{-4} M in DCE). B) The g_{value} as a function of the *R*-enantiomer content in polymers **28-32** (λ = 225 nm, c_{BTA} = 10^{-4} M in DCE, T = -10 °C).

Next, chiral BTA NPs with achiral BTA NPs were mixed, to see whether chirality transfer is present. Four solutions were prepared containing 0, 25, 50, and 100% chiral polymer **27b** with respect to achiral polymer **27c**. The total concentration of polymer was kept content (c_{BTA} = 10^{-4} M in DCE). All solutions were heated to 70 °C in which the BTAs are molecularly dissolved and cooled to 20 °C before measuring. The addition of chiral BTA side-functionalized

polymers to achiral BTA side-functionalized polymers led to a linear increase of CD absorption (Figure 6.11A). This is in contrast with the unbound BTA, in which the presence of <10 % chiral sergeant is sufficient to obtain a fully homochiral system.[36] The absence of chirality transfer in the BTA polymer system is indicative for the absence of intermolecular self-assembly.

In order to confirm the capability of BTAs to transfer chirality in a less dynamic polymeric system, we also performed CD measurements on polymers containing both chiral and achiral BTAs. Polymers **28**-**32** are functionalized with almost the same amount of BTAs only the ratio of chiral/achiral BTAs is changed (Table 6.1). Measurements were performed at -10 °C, at which the Cotton effect was saturated.[66] A non-linear increase of the Cotton effect (expressed as the g_{value}) is visible (Figure 6.11B). The non-linear increase confirms that chirality is transferred within the polymeric nanoparticle.

6.4.5 Stability of BTA side-functionalized polymers

Finally, we investigated the influence of additives on the stability of the folded structures. We prepared a solution of **38** (c_{BTA} = 8.5 x 10^{-5} M, DCE/MCH 70/30 vol%) and added various amounts of hexafluoroisopropanol (HFIP) (Figure 6.12A).
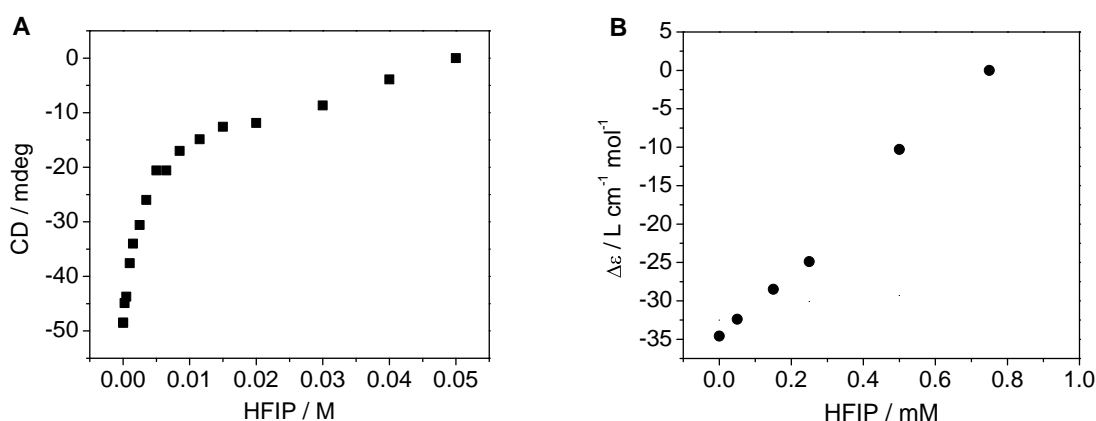
Figure 6.12 A) Cotton effect of **38** versus HFIP concentration (c_{BTA} = 8.5 x 10^{-5} M in DCE/MCH 70/30 vol%, λ = 225 nm, T = 20 °C, l = 0.5 cm). B) Molar ellipticity of **39** versus HFIP concentration (c = 5 x 10^{-5} M in MCH, λ = 223 nm, T = 20 °C, l = 1 cm).

The Cotton effect gradually disappeared upon the addition of HFIP and it was completely absent after the addition of 1000 equivalents. In contrast, the addition of 15 equivalents of HFIP was sufficient to fully disrupt aggregation of unbound BTAs (**39**) (Figure 6.12B). We anticipated that the addition of base to a solution of **38** in the presence of 1000 eq of HFIP would restore folding. The base is able to bind to the acid and is therefore no longer capable of interfering with intramolcular hydrogen bonding. The folding of polymer **38** was

reversible as the Cotton effect was almost completely recovered after the addition of >1000 equivalents of quinuclidine (Figure 6.13).[67]
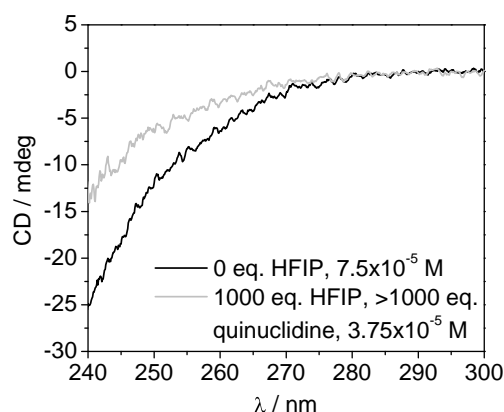
Figure 6.13 The Cotton effect of a solution of **38** before (black line, c_{BTA} = 7.5 x 10^{-5} M) and after (grey line, c_{BTA} = 3.75 x 10^{-5} M) the addition of 1000 equivalents of HFIP and quinuclidine (70/30 DCE/MCH vol%, T = 20 °C, l = 0.5 cm).

6.5 Conclusions

We have successfully synthesized BTA side-functionalized polymers using two different approaches and two different polymerization techniques. ARGET ATRP and RAFT polymerization were used to copolymerize methacrylate functional BTAs with methacrylate comonomers leading directly to BTA side-functionalized polymers. The copolymerization of silyl protected propargyl methacrylates with methacrylate comonomers led to the formation of alkyne side-functionalized polymers, which allowed post-functionalization with azide functional BTAs. The use of silyl protected propargyl methacrylate led to a slightly higher degree of functionalization compared to the feed ratio, suggesting enrichment of functionality at one end of the polymer. Copper(I) catalyzed cycloaddition reactions were successfully employed to functionalize polymers with azide functional BTAs. Furthermore, the available propargyl groups after BTA functionalization could be used for post functionalization with different motifs. We also introduced a photochemical switch that allows controlled aggregation of BTAs upon photoirradiation.

Single-chain polymeric nanoparticles are successfully formed by stepwise folding of BTA side-functionalized polymers. By careful selection of the solvent, we were able to balance the solubility of the main chain with the hydrogen bonding required for folding of BTA side-functionalized polymers. Folding was achieved by controlled cooling of solutions of the polymers in order to arrive at the thermodynamically stable state. When folded polymers were made by deprotection of BTAs by photoirradiation at room temperature, the system resides in a kinetically trapped or collapsed state; a unimolecular glass or "molten globule"

state. The more thermodynamically favorable folded state was achieved by an additional heating/cooling step. Temperature plays a decisive role. At high temperatures, BTAs are not aggregated, the polymer is unfolded, and at the same time the polymer backbone is flexible. Slowly reducing the temperature induces BTA aggregation because there is sufficient mobility within the polymer to adopt an optimal conformation for self-assembly to occur.

We anticipate that the self-assembly occurs within a single-chain, since the onset of self-assembly is determined by the local concentration of pendent BTAs on the chain and is independent of the overall concentration of the polymer. Moreover, Sergeants and Soldiers experiments between polymers did not show transfer of chirality, which is indicative for the absence of interaction between polymeric particles. BTA side-functionalized polymers consisting of chiral and achiral BTAs showed transfer of chirality. The absence of chirality transfer between polymeric nanoparticles confirms that self-assembly occurs within a single-chain. Unfolding experiments with the hydrogen bond breaking solvent HFIP showed a significant increase in stability of the BTA helix in the single-chain polymeric nanoparticle, compared to the same helix of unbound or "free" BTAs. The observed aggregation behavior in the SCPNs we describe here, partly mimics the folding of proteins, and has also been described in synthetic systems such as foldamers and DNA origami structures.[4, 68, 69] The latter also requires small temperature jumps to arrive at a fully self-assembled state. The high stability and chiral conformation of the folded particles make them excellent candidates for compartmentalized catalytic systems and sensing devices.[70] Further development of nanoparticles bearing a compartmentalized chiral inner structure could lead to asymmetric catalytically active systems, which can function in exotic media.

6.6 Experimental

Materials

All reagents were purchased from Aldrich or Acros Organics and used as received unless otherwise specified. All solvents were of AR quality and were purchased from Biosolve. Chloroform was dried over molecular sieves before use. CD and UV measurements were conducted in spectrophotometric grade methylcyclohexane and 1,2-dichloroethane from Aldrich. Deuterated solvents were purchased from Cambridge Isotopes Laboratories. All reactions were run in flame-dried glassware under an argon atmosphere. Compound **17** was synthesized according to literature.[39]

Instrumentation and Analysis

CD and UV spectra were recorded on a Jasco J-815 CD spectrometer equipped with a Jasco PTC-348 WI temperature controller. Cells with an optical path length of 1 or 0.5 cm were applied (for ~10^{-5} M solutions). The anisotropy factor (g_{value}) is calculated as: g_{value} = CD/(UVx32980) and the molar ellipticity is calculated as: $\Delta\varepsilon$ = Cotton-effect/(32980xcxl)

where c is the concentration in mol/L and l = the optical path length in cm. ^{1}H-NMR and ^{13}C-NMR spectra were recorded on a Varian Gemini 400 MHz NMR (400 MHz for ^{1}H-NMR and 100 MHz for ^{13}C-NMR). Proton chemical shifts are reported in ppm downfield from tetramethylsilane (TMS). Carbon chemical shifts are reported downfield from TMS using the resonance of the deuterated solvent as the internal standard. IR spectra were recorded on a Perkin Elmer 1600 FT-IR. Matrix assisted laser desorption/ionization mass spectra were obtained on a PerSeptive Biosystems Voyager DE-PRO spectrometer using α-cyano-4-hydroxycinnamic acid (CHCA) or 2-[(2E)-3-(4-*tert*-butylphenyl)-2-methylprop-2-enylidene]malononitrile (DCTB) as matrices. Photo irradiation experiments were performed in a Luzchem LZC-4V UV reactor equipped with 8 x 8 Watt light bulbs (354 nm). The photo irradiation reactions were performed in a quartz cuvet or NMR tube at 25 °C. GPC measurements were performed on a Resi Pore column with THF (at room temperature) or ODCB (at 80 °C) as the eluent (flow = 1 mL/min) and employing a PDA (λ = 254 nm) as the detector. The molecular weights were determined using the polystyrene calibration method.

Synthesis

(3S)-3,7-Dimethyloctanol (**5**) (3*S*)-3,7-Dimethyl-6-octen-1-ol [(*S*)-citronellol] (326.22 mmol, 50.89 g) was charged in a 250 mL flask and dissolved in ethyl acetate (150 mL). Palladium on coal (1.25 g) was added to the solution and the resulting mixture was flushed with argon for 10 minutes. The mixture was exposed to an H_2 atmosphere in a Parr reactor and the progress of the reaction was followed by the H_2 pressure drop. Upon completion, the reaction mixture was filtered over a double paper filter and the solvent was removed *in vacuo*. The resulting colorless liquid was used without further purification. Yield = 41.97 g, 83%. ^{1}H-NMR (400 MHz, CDCl$_3$, δ): 3.69 (m, 2H, -C$\underline{H}_2$OH), 1.6-0.8 (mm, 19H, aliphatic).

(3S)-2-(3,7-Dimethyloctyl)isoindoline-1,3-dione (**6**) Compound **5** (269 mmol, 41.97 g), phthalimide (529 mmol, 77.89 g) and triphenylphosphine (529 mmol, 138.87 g) were charged in a 1 L flask and were partially dissolved in diethyl ether (500 mL). Diisopropyl azodicarboxylate (DIAD) (470 mmol, 75.1 g) was dissolved in diethyl ether (150 mL) and the resulting solution was slowly added to the solution. After addition, a yellow suspension became visible. The mixture was stirred for 24 hours at room temperature. The resulting suspension was filtered by Büchner filtration. The residue was washed with diethyl ether (3x 100 mL) and the combined ether fractions were concentrated *in vacuo*. The resulting oil was used without further purification. Yield = 41 g, 99%. ^{1}H-NMR (400 MHz, CDCl$_3$, δ): 8.0-7.3 (m, 4H, aromatic), 3.7 (t, J = 7 Hz, 2H, -CH$_2$N-), 1.6-0.8 (mm, 19H, aliphatic).

(3S)-3,7-Dimethyloctanamine (**7**) Compound **6** (269 mmol, 77.5 g) was dissolved in THF (500 mL) and hydrazine monohydrate (1.345 mol, 80 mL) was added to the mixture. The resulting

solution was heated at reflux temperature. The formation of a salt was observed in the yellow/orange solution. The extent of the reaction was monitored by ^{1}H-NMR in CDCl$_3$ and by GC-MS. After completion, the solvent and the excess hydrazine were evaporated *in vacuo*. CHCl$_3$ (700 mL) was added to the solid residu and the organic phase was washed with NaOH (3 x 600 mL) and brine (1 x 600 mL). The organic phase was dried over MgSO$_4$ and the solvent was removed *in vacuo*. The crude mixture was purified by vacuum distillation at p = 0.14 mbar and T = 45 °C and afforded a colorless liquid. Yield = 27.2 g, 64%. ^{1}H-NMR (400 MHz, CDCl$_3$, δ): 2.71 (m, 2H, NH$_2$C$\underline{H}_2$-), 1.8-0.8 (mm, 19H, aliphatic).

2-(Hydroxyundecyl)isoindoline-1,3-dione (**8**) 11-Bromoundecanol (39.2 mmol, 9.85 g) was charged in a 500 mL flask and dissolved in DMF (200 mL). Potassium phthalimide (51.3 mmol, 9.51 g) was added to the mixture. The resulting mixture was stirred under an argon atmosphere at 70 °C. Full conversion was confirmed by TLC (3% MeOH in CHCl$_3$). The mixture was cooled to room temperature and the precipitate was washed with ethyl acetate (500 mL). The filtrate was washed with H$_2$O (3 x 150 mL) and saturated KCl (2 x 75 mL). The organic layer was dried with MgSO$_4$ and the solvent was evaporated *in vacuo* to yield a solid. Yield = 6.38 g, 51%. ^{1}H-NMR (400 MHz, CDCl$_3$, δ): 7.84 (d-d, 2H, J = 3.2 Hz, aromatic), 7.71 (d-d, 2H, J = 3.2 Hz, aromatic), 3.67 (t, 2H, J = 7.2 Hz, CH$_2$N), 3.63 (t, 2H, J = 5.6 Hz, C$\underline{H}_2$OH), 1.67 (t, 2H, 7.2 Hz), 1.56 (t, 2H, 5.6 Hz) 1.4-1.2 (m, 14H).

11-Aminoundecanol (**9**) Compound **8** (39,2 mmol 12,45 g) was charged in a 250 mL flask and dissolved in dry THF (200 mL). Hydrazine monohydrate (0.61 mol, 19.02 mL) was added to the mixture. The resulting solution was heated at reflux temperature for 18 hours. An off-white solid precipitated. The solvent and the excess of hydrazine were removed *in vacuo*. CHCl$_3$ (400 mL) and 0.5 M NaOH (400 mL) were added to the residue and the organic layer was separated and washed with 1M NaOH (1 x 100 mL), H$_2$O (1 x 100 mL) and brine (1 x 100 mL). The organic layer was dried over MgSO$_4$ and the solvent was removed *in vacuo*. This afforded a white solid. Yield = 6.58 g, 90%. T_m lit. = 72 °C, found = 69-74 °C. ^{1}H-NMR (400 MHz, CDCl$_3$, δ): 3.6 (t, J = 6.6 Hz, 2H, C$\underline{H}_2$OH), 2.6 (t, J = 7 Hz, 2H, -C$\underline{H}_2$NH$_2$), 1.6-1.0 (m-m, 18H, aliphatic protons).

(3R)-2-(3,7-Dimethyloct-6-enyl)isoindoline-1,3-dione (**11**) (*R*)-Citronellyl bromide (45.5 mmol, 10.0 g) and potassium phthalimide (50.0 mmol, 9.3 g) were brought into a 250 mL flask and dissolved in DMF (100 mL). The mixture was stirred for 24 hours at 50 °C. After 2 hours, a yellow precipitate was observed. After 24 hours the extend of the reaction was monitored by TLC and I$_2$ staining. The starting material was no longer present. DMF was evaporated *in vacuo* and chloroform (200 mL) was added to the solid product. The suspension was heated and the KBr salt was removed with filtration. The filtrate was further diluted with an

additional 200 mL chloroform and the organic layer was washed with 1M NaOH (150 mL) and brine (150 mL). The chloroform was evaporated *in vacuo* to give a yellow oil. The product was used without further purification. Yield: 12.18 gram, 94%. ^{1}H-NMR (400 MHz, CDCl$_3$, δ): 7.8 (m, 2H, aromatic), δ 7.7 (m, 2H, aromatic), δ 5.1 (t, 1H, C=CH-C), 3.7 (t, 2H, -CH$_2$N-), δ 1.8-1 (mm, 18H, aliphatic).

(3R)-2-(3,7-Dimethyloctyl)isoindoline-1,3-dione (**12**) Compound **11** (42.69 mmol, 12.18 g) was dissolved in ethyl acetate (55 mL). Palladium on coal (10%) was added to the solution and the resulting mixture was flushed with Argon for 20 minutes. The mixture was exposed to an H$_2$ atmosphere in a Parr reactor. The progress of the reaction was followed by the H$_2$ pressure drop. Upon completion (48 hours), the resulting mixture was further diluted with an additional 200 mL ethyl acetate and filtered over a double paper filter. The ethyl acetate was evaporated *in vacuo*. The resulting colorless oil was used without further purification. Yield: 11.5 g, 94%. ^{1}H-NMR (400 MHz, CDCl$_3$, δ): 7.8 (m, 2H, aromatic), δ 7.7 (m, 2H, aromatic), 3.7 (t, 2H, -CH$_2$N-), δ 1.7-0.8 (mm, 21H, aliphatic).

(3R)-3,7-Dimethyloctanamine (**13**) Compound **12** (40.0 mmol, 11.5 g) was dissolved in THF (115 mL) and hydrazine (200 mmol, 10 mL). The resulting mixture was heated at reflux conditions (110 °C). The formation of a salt was observed in the yellow/green solution after several hours. After 48 hours, the solvent and the excess of hydrazine were evaporated *in vacuo*. CHCl$_3$ (300 mL) was added to the solid residue and the non soluble salt was filtered of by gravity filtration. The residue was washed with CHCl$_3$ (50 mL). The organic layer was washed with 1M NaOH (2 x 150 mL) and brine (1 x 150 mL). Because of the high purity revealed by ^{1}H-NMR, the product was used without further purification. Yield: 5.7 gram, 91%. ^{1}H-NMR (400 MHz, CDCl$_3$, δ): 2.7 (m, 2H, NH$_2$-C$\underline{H}_2$), δ 1.7-0.8 (mm, 21H, aliphatic).

General procedure for the synthesis of hydroxy functional BTAs. The following procedure was used for all hydroxy functional BTAs (**10a-c**) using the same reaction conditions as described for compound **10a**.

N^1,N^3-Bis((S)-3,7-dimethyloctyl)-N^5-(11-hydroxyundecyl)benzene-1,3,5-tricarboxamide (**10a**). In a 250 mL flask compound **7** (24.83 mmol, 3.89 g), compound **9** (12.41 mmol, 2.33 g) and triethylamine (67.69 mmol, 6.85 g) were charged, and dissolved in dry CHCl$_3$ (150 mL) and cooled with an ice bath. Benzene-1,3,5-tricarbonyl trichloride (10.10 mmol, 2.68 g) was dissolved in chloroform (25 mL) and added dropwise to the cooled amine / chloroform solution. After 24 hours, the chloroform and the excess of triethylamine were removed *in vacuo.* The residue was dissolved in chloroform (200 mL) and washed with 1M HCl (2 x 150 mL) and brine (1 x 150 mL). The chloroform was evaporated *in vacuo* and the product was subsequently purified by column chromatography (40% ethyl acetate, 60% chloroform) and

obtained as a sticky white solid. Yield = 1.8 g, 27%. T_i = 178-181°C. ^{1}H-NMR (400 MHz, CDCl$_3$, δ): 8.35 (s, 2H, aromatic), 8.33 (s, 1H, aromatic), 6.53 (b, 3H, NH), 3.63 (m, 2H, OCH$_2$-) 3.48 (m, 6H, -NHC$\underline{H}_2$-), 1.8-0.8 (m-m, 64H, aliphatic). ^{13}C-NMR (100 MHz, CDCl$_3$, δ): 166.0, 165.9, 135.2, 128.1, 65.8, 62.8, 40.3, 39.2, 38.5, 37.1, 36.6, 32.7, 30.7, 29.4, 29.3, 29.2, 29.1, 29.0, 27.9, 26.9, 25.6, 24.6, 22.7, 22.6, 19.4, 15.2. MALDI-ToF-MS (m/z) calc for C$_{40}$H$_{71}$N$_3$O$_4$ 657.54, found 658.40 (M+H)$^+$ 680.39 (M+Na)$^+$ 641.23 (M-H$_2$O+H)$^+$.

N^1,N^3-Bis((R)-3,7-dimethyloctyl)-N^5-(11-hydroxyundecyl)benzene-1,3,5-tricarboxamide (**10b**). Yield = 0.81 g, 28%. ^{1}H-NMR (400 MHz, CDCl$_3$, δ): 8.38 (s, 2H, aromatic), 8.37 (s, 1H, aromatic), 6.59 (b, 3H, NH), 3.63 (m, 2H, C$\underline{H}_2$OH) 3.46 (m, 6H, -NHC$\underline{H}_2$-), 1.8-0.8 (mm, 64H, aliphatic).

N^1-(11-Hydroxyundecyl)-N^3,N^5-dioctylbenzene-1,3,5-tricarboxamide (**10c**). Yield = 2.0 g, 29%. ^{1}H-NMR (400 MHz, CDCl$_3$, δ): 8.39 (s, 3H, aromatic), 6.53 (b, 3H, NH), 3.63 (m, 2H, C$\underline{H}_2$OH) 3.48 (m, 6H, -NHC$\underline{H}_2$-), 1.8-0.8 (mm, 56H, aliphatic).

11-(3,5-Bis(((S)-3,7-dimethyloctyl)carbamoyl)benzamido)undecyl methacrylate (**1**). Compound **10a**. (2.55 mmol, 1.68 g) and triethylamine (2.55 mmol, 258 mg) were dissolved in dry CH$_2$Cl$_2$ (20mL) in a 100 mL flask. The solution was cooled with an ice bath under an argon atmosphere. Methacryloyl chloride (2.55 mmol, 267 mg) was dissolved in dry CH$_2$Cl$_2$ (20 mL) and this solution was added dropwise to the reaction flask. After stirring overnight, the crude mixture was washed with 1M NaOH (2 x 40 mL), 1M HCl (2 x 40 mL), H$_2$O (2 x 40 mL) and brine (40mL). The product was purified by column chromatography (50% ethyl acetate, 50% CHCl$_3$) and afforded a sticky white solid. Yield: 1.01 g, 55%. T_i = 193-196°C. ^{1}H-NMR (400 MHz, CDCl$_3$, δ): 8.34 (s, 3H, aromatic), 6.5 (3H, NH), 6.09 (s, 1H, CC$\underline{H}$H), 5.54 (s, 1H, -CCH$\underline{H}$), 4.13 (t, J = 7.1 Hz, 2H, -OCH$_2$), 3.46 (m, 6H, -NHC$\underline{H}_2$), 1.94 (s, 2H, -CCH$_3$), 1.8-0.8 (mm, 64H, aliphatic). ^{13}C-NMR (100 MHz, CDCl$_3$, δ): 167.6, 165.6, 136.5, 135.3, 127.9, 125.1, 64.8, 40.4, 39.2, 38.5, 37.1, 36.6, 30.7, 29.5, 29.4, 29.3, 29.2, 28.6, 28.0, 27.0, 25.0, 24.6, 22.7, 22.6, 19.5, 18.3. FT-IR (cm^{-1}): 3236, 3072, 2953, 2925, 2855, 1721, 1653, 1557, 1461, 1295, 1160. MALDI-ToF-MS (m/z) calc for C$_{44}$H$_{75}$N$_3$O$_5$ 725.57, found 726.65 (M+H)$^+$ 748.64 (M+Na)$^+$ 764.90 (M+K)$^+$.

General procedure for the synthesis of tosyl functional BTAs. The following procedure was used for all tosyl functional BTAs (**14a-c**) using the same reaction conditions as described for compound **14a**.

11-(3,5-Bis(((S)-3,7-dimethyloctyl)carbamoyl)benzamido)undecyl 4-methylbenzenesulfonate (**14a**). Compound **10a** (4.03 mmol, 2.65 g), trimethylammonium chloride (0.6 mmol, 58 mg) and triethylamine (8.05 mmol, 0.81 g) were charged in a 50 mL flask and dissolved in dry DCM (10 mL). The resulting mixture was cooled by an ice-water-salt bath. 4-Toluenesulfonyl chloride (4.23 mmol, 0,82 g) was dissolved in DCM (10 mL) and added dropwise to the

solution. The extent of the reaction was checked with TLC (40% ethyl acetate, 60% CHCl$_3$) and ^{1}H-NMR in CDCl$_3$. After six hours, the solvent was evaporated *in vacuo* and the residue was dissolved in CHCl$_3$ (350 mL). The organic layer was washed with 1M HCl (2 x 150 mL) and brine (2 x 150 mL). The solvent was removed *in vacuo* resulting in the target material as a white sticky solid. The crude product was used without further purification. Yield = 3.09 g, 94%. ^{1}H-NMR (400 MHz, CDCl$_3$, δ): 8.35 (s, 2H, aromatic), 8.33 (s, 1H, aromatic), 7.80 (d, 2H, aromatic), 7.38 (d, 2H, aromatic), 6.70 (m, 3H, NH), 4.01 (t, 2H, Ts-C$\underline{H}_2$-), 3.41 (m, 6H, -NC$\underline{H}_2$-), 2.42 (s, 3H, C$\underline{H}_3$-aromatic) 1.8-0.8 (mm, 64H, aliphatic).

11-(3,5-Bis(((R)-3,7-dimethyloctyl)carbamoyl)benzamido)undecyl 4-methylbenzenesulfonate (**14b**). Yield = 0.78 g, 59%. ^{1}H-NMR (400 MHz, CDCl$_3$, δ): 8.35 (s, 2H, aromatic), 8.33 (s, 1H, aromatic), 7.80 (d, 2H, aromatic), 7.38 (d, 2H, aromatic), 6.69 (m, 3H, NH), 4.01 (t, 2H, Ts-C$\underline{H}_2$) 3.40 (m, 6H, -NC$\underline{H}_2$-), 2.42 (s, 3H, C$\underline{H}_3$-aromatic) 1.8-0.8 (mm, 64H, aliphatic).

11-(3,5-Bis(octylcarbamoyl)benzamido)undecyl 4-methylbenzenesulfonate (**14c**). Yield = 1.45 g, 94%. ^{1}H-NMR (400 MHz, CDCl$_3$, δ): 8.38 (s, 3H, aromatic), 7.80 (d, 2H, aromatic), 7.39 (d, 2H, aromatic), 6.70 (m, 3H, NH), 4.0 (t, 2H, Ts-C$\underline{H}_2$), 3.41 (m, 6H, -NC$\underline{H}_2$-), 2.42 (s, 3H, C$\underline{H}_3$-aromatic) 1.8-0.8 (mm, 56H, aliphatic).

General procedure for the synthesis of azide functional BTAs. The following procedure was used for all azide functional BTAs (**2a-c**) using the same reaction conditions as described for compound **2a**.

N^1-(11-Azidoundecyl)-N^3,N^5-bis((S)-3,7-dimethyloctyl)benzene-1,3,5-tricarboxamide (**2a**). Compound **14a** (3.8 mmol, 3.09 g) and NaN$_3$ (22.8 mmol, 1.48 g) were charged in a 100 mL flask and DMF (30 mL) was added resulting in a yellow solution. This mixture was stirred overnight at room temperature. The solution was poured in ice water (170 mL) and the aqueous layer was extracted with CHCl$_3$ (4 x 100 mL). The combined CHCl$_3$ layers were washed with 1M NaOH (4 x 100 mL) and brine (2 x 150 mL). The organic layer was dried over MgSO$_4$ and the solvent was removed *in vacuo*. The crude product was purified with column chromatography (20% ethyl acetate, 80% CHCl$_3$). Yield = 2.11 g, 82%. ^{1}H-NMR (400 MHz, CDCl$_3$, δ): 8.35 (s, 2H, aromatic), 8.33 (s, 1H, aromatic), 6.70 (m, 3H, NH), 3.45 (m, 6H, -NC$\underline{H}_2$-), 3.18 (t, 2H, C$\underline{H}_2$-N$_3$) 1.76-0.80 (mm, 64H, aliphatic). MALDI-ToF-MS (m/z) calc for C$_{40}$H$_{70}$N$_6$O$_3$ 683.02, found 655.53 (M-N$_2$+H)$^+$ and 705.47 (M+Na)$^+$.

N^1-(11-Azidoundecyl)-N^3,N^5-bis((R)-3,7-dimethyloctyl)benzene-1,3,5-tricarboxamide (**2b**). Yield = 0.58 g, 78%. ^{1}H-NMR (400 MHz, CDCl$_3$, δ): 8.35 (s, 3H, aromatic), 6.70 (m, 3H, NH), 3.45 (m, 6H, -NC$\underline{H}_2$-), 3.21 (t, 2H, C$\underline{H}_2$-N$_3$) 1.80-0.80 (mm, 64H, aliphatic). MALDI-ToF-MS (m/z) calc for C$_{40}$H$_{70}$N$_6$O$_3$ 683.02 found 655.54 (M-N$_2$+H)$^+$ and 705.32 (M+Na)$^+$.

N^1-(11-Azidoundecyl)-N^3,N^5-dioctylbenzene-1,3,5-tricarboxamide (**2c**). Yield = 0.65 g, 50%. ^{1}H-NMR (400 MHz, CDCl$_3$, δ): 8.38 (s, 3H, aromatic), 7.01 (m, 3H, NH), 3.39 (m, 6H, -NC$\underline{H}_2$-),

3.21 (t, 2H, C$\underline{H}_2$-N$_3$) 1.90-0.80 (mm, 56H, aliphatic). MALDI-ToF-MS (m/z) calc for C$_{36}$H$_{62}$N$_6$O$_3$ 626.92 found 599.45 (M-N$_2$+H)$^+$ and 649.41 (M+Na)$^+$.

2-Nitrobenzyloctylimine (**15**). 2-Nitrobenzaldehyde (6.6 mmol, 1.0 g) was added to a solution of *n*-octylamine (6.6 mmol, 0.86 g) in ethanol (30 mL). The mixture was heated for 12 hours at reflux temperature. The mixture was cooled to room temperature and subsequently used for the next reaction without purification. ^{1}H-NMR (400 MHz, CDCl$_3$, δ): 8.63 (s, 1H, CHC$\underline{H}$=N), 7.92 (d, 1H, Ar), 7.58 (q, 2H, Ar), 7.41 (t, 1H, Ar), 3.60 (t, 2H, CH$_2$N=C), 1.55-1.05 (alkyl).

2-Nitrobenzyloctylamine (**16**). NaBH$_4$ (26.4 mmol, 1 g) was added to a solution of **15** (6.6 mmol, 1.73 g) in ethanol (30 mL) and stirred for 18 hours at room temperature. HCl (20 mL, 1M) was added to the solution followed by removal of ethanol *in vacuo*. Subsequently, chloroform (30 mL) was added to the water mixture. Then, the organic layer was washed successively with HCl (30 mL, 1M), two times with NaOH (30 mL, 1M) and two times with NaCl$_{aq}$ (saturated, 50 mL). Yield: 1.57 g, 90%. ^{1}H-NMR (400 MHz, CDCl$_3$, δ): 7.95 (d, 1H, Ar), 7.60 (q, 2H, Ar), 7.42 (t, 1H, Ar), 4.05 (s, 2H, HNC$\underline{H}_2$Ar), 2.62 (t, 2H, CH$_2$C$\underline{H}_2$NH), 1.55-1.05 (alkyl).

3,5-Bis-(3S)-(3,7-dimethyl-octylaminocarbonyl)-benzoic acid chloride (**18**). 3,5-Bis-(3*S*)-(3,7-dimethyl-octylaminocarbonyl)-benzoic acid (**17**) (0.52 mmol, 250 mg) was dissolved in dry chloroform (20 mL) under argon atmosphere. After addition of 1-chloro-*N*,*N*,-2-trimethyl-1-propenylamine (0.76 mmol, 103 mg). After 5 hours, the resulting clear solution was concentrated *in vacuo*. The residue was dried thoroughly using high vacuum to assure removal of the excess of 1-chloro-*N*,*N*,2-trimethyl-1-propenylamine. Full conversion was confirmed with infrared spectroscopy, no further characterization was performed. The resulting product was directly used in further synthesis.

N^1,N^3-Bis((S)-3,7-dimethyloctyl)-N^5-(2-nitrobenzyl)-N^5-octylbenzene-1,3,5-tricarboxamide (**3**). Compound **18** (0.52 mmol, 250 mg) was dissolved in dry chloroform (20 mL) and cooled to 4 °C. To this solution, a mixture of 2-nitrobenzyloctylamine (0.58 mmol, 153 mg) (**16**) and triethylamine (2 mmol, 202 mg) in dry chloroform (20 mL) was slowly added via a dropping funnel. The reaction mixture was allowed to warm up to room temperature and was stirred for 18 hours. Choroform and the excess of triethylamine were removed *in vacuo*, subsequently chloroform (100 mL) was added. The solution was washed two times with HCl (50 mL, 1M) and two times with NaCl$_{aq}$ (50 mL, saturated). Chloroform was removed *in vacuo*. The product was purified with column chromatography (40/60 ethylacetate/chloroform). Yield = 240 mg, 90%. ^{1}H-NMR (400 MHz, TCE-*d$_2$*, T = 100 °C, δ): 8.20 (s, 1H, Ar), 8.05 (d, 1H, Ar), 7.95 (s, 2H, Ar), 7.68 (t, 1H, Ar), 7.50 (m, 2H, Ar), 6.12 (t, 2H,

NH), 4.98 (s, 2H, ArC$\underline{H}_2$N), 3.48 (t, 4H, C$\underline{H}_2$NHC=O), 3.38 (t, 2H, C$\underline{H}_2$N(CH$_2$Ar)C=O), 1.65-1.05 (alkyl). ^{13}C-NMR (100 MHz, CDCl$_3$, δ): 171.9, 165.7, 137.0, 136.7, 135.2, 133.9, 129.5, 129.1, 127.4, 126.5, 40.6, 39.9, 38.3, 37.8, 34.0, 32.1, 31.2, 29.3, 26.7, 26.0, 24.1, 24.0, 20.9. MALDI-ToF-MS (m/z) calc for C$_{44}$H$_{70}$N$_4$O$_5$ 734.53 found 735.60 (M+H)$^+$ 757.57 (M+Na)$^+$.

2-Nitrobenzylideneaminoundecanol (**19**). Compound **9** (13.72 mmol, 2.51 g) was dissolved in ethanol (60 mL). 2-Nitrobenzaldehyde (14.41 mmol, 2.20 g) was added to the solution. The resulting solution was heated overnight at reflux conditions. The progress of the reaction was checked with ^{1}H-NMR in CDCl$_3$. The mixture was cooled to room temperature and used without further purification. ^{1}H-NMR (400 MHz, CDCl$_3$, δ): 8.68 (s, 1H), 8.02 (t, J = 7.9 Hz, 2H, aromatic), 7.67 (t, J = 7.5 Hz, 1H, aromatic), 7.56 (t, J = 7.9 Hz, 1H, aromatic), 3.68 (t, 2H, CH$_2$N), 3.63 (t, J = 6.6 Hz, 2H, C$\underline{H}_2$OH), 1.8-1.2 (mm, 18H, aliphatic).

2-Nitrobenzylaminoundecanol (**20**). NaBH$_4$ (68.6 mmol, 2.57 g) was added to the crude reaction mixture of compound **19**. The mixture was stirred overnight at room temperature. The extent of the reaction was monitored with ^{1}H-NMR in CDCl$_3$. Upon completion, the excess NaBH$_4$ was neutralized using H$_2$O and 1M HCl. Ethanol was evaporated *in vacuo* and CHCl$_3$ (100 mL) was added to the remaining mixture. The organic layer was separated and the foamy aqueous phase was extracted with CHCl$_3$. The combined organic layers where washed with 1M NaOH (2 x 100 mL) and brine (100 mL), dried over MgSO$_4$ and concentrated *in vacuo*, yielding the product as a yellow oil. Yield = 4.5 gram, 90%. ^{1}H-NMR (400 MHz, CDCl$_3$, δ): 7.94 (d, J = 8.8 Hz, 1H, aromatic), 7.60 (d+t, 2H, aromatic), 7.40 (t, J = 7.8 Hz, 1H, aromatic), 4.03 (s, 2H, benzylic CH$_2$), 3.63 (t, J = 6.5 Hz, C$\underline{H}_2$OH), 2.62 (t, J = 7.5 Hz, C$\underline{H}_2$NH), 1.6-1.2 (mm, 18H, aliphatic).

N^1,N^3-Bis((3S)-3,7-dimethyloctyl)-N^5-(hydroxyundecyl)-N^5-(2-nitrobenzyl)benzene-1,3,5-tricarboxamide (**21**). Compound **18** (2.64 mmol, 0.85 g) was dissolved in CHCl$_3$ (75 mL) and charged in a 50 mL flask. K$_2$CO$_3$ (4.42 mmol, 0.61 g) was added to the solution and the resulting mixture was cooled with an ice bath. Compound **18** (2.21 mmol, 1.08 g) was dissolved in CHCl$_3$ (15 mL) and added drop wise to **20**. The resulting mixture was stirred overnight at room temperature. CHCl$_3$ (70 mL) was added to the crude reaction mixture and the organic phase was washed with 1M HCl (3 x 100 mL), 1M NaOH (1 x 100 mL) and brine (1 x 100 mL). The organic layer was dried over MgSO$_4$ and concentrated *in vacuo*. The crude product was purified by column chromatography (ethyl acetate) giving the product as an orange oil. Yield = 0.57 g, 33%. ^{1}H-NMR (400 MHz, TCE-d^2, 90 °C, δ): 8.12 (s, 1H, aromatic), 7.93 (d, J = 8.5 Hz, 1H, aromatic), 7.85 (s, 2H, aromatic), 7.62 (t, J = 8.0 Hz, 1H, aromatic), 7.47 (d, J = 7.9 Hz, 1H, aromatic), 8.42 (t, J = 7.9 Hz, 1H, aromatic), 6.11 (b, 2H, NH), 4.92 (s, 2H, benzylic CH$_2$), 3.55 (t, J = 5.8 Hz, 2H, -C$\underline{H}_2$OH), 3.40 (m, 2H, -C$\underline{H}_2$NH-), 3.27 (b, 1H, -CH$_2$N-),

1.7-0.8 (mm, 56H, aliphatic). ^{13}C-NMR (100 MHz, TCE-d^2, 25 °C, δ): 172.0, 166.7, 138.0, 136.7, 135.3, 133.8, 129.9, 129.1, 127.8, 126.5, 64.3, 40.6, 39.9, 38.5, 37.9, 34.0, 32.1, 30.6, 29.3, 27.0, 26.0, 24.1, 24.0, 20.9. FT-IR: (cm^{-1}) 3315, 1074, 2925, 2855, 1681, 1597, 1528, 1466, 1339, 1289, 1192, 1055, 912, 857, 788, 727. MALDI-ToF-MS (m/z) calc for $C_{47}H_{76}N_4O_6$ 792.58 found 793.46 (M+H)$^+$ 815.46 (M+Na)$^+$.

11-(3,5-Bis(((S)-3,7-dimethyloctyl)carbamoyl)-N-(2-nitrobenzyl)benzamido)undecyl   4-methyl benzenesulfonate (**22**). 4-Toluenesulfonyl chloride (0.440 mmol, 84 mg) was dissolved in pyridine (1 mL). The resulting solution was cooled with and ice-water-salt bath. Compound **21** (0.378 mmol, 300 mg) was dissolved in pyridine (1.8 mL) and added slowly to the cooled solution with and addition funnel. The progress of the reaction was checked with TLC (20% ethyl acetate in chloroform). Upon completion (48 hours), the reaction mixture was poured in ice water (20 mL). CHCl$_3$ (20 mL) was added to dissolve the sticky precipitate. The phases were separated and the organic phase was washed with 1M HCl (7 x 20 mL, checked for pyridine with CuSO$_4$). The organic phase was washed with H$_2$O (2 x 20 mL) and dried over MgSO$_4$. The solvent was removed *in vacuo* resulting in the target material. The crude product was used without further purification. Yield = 230 mg, 64%. ^{1}H-NMR (400 MHz, CDCl$_3$, δ): 8.2 (s, 1H, aromatic), 8.00 (d, *J* = 8 Hz, aromatic), 7.92 (s, 2H, aromatic), 7.70 (t, *J* = 7.4 Hz, aromatic), 7.54 (d, *J* = 7.7 Hz, 1H, aromatic) 7.50 (t, *J* = 7.8 Hz), 6.13 (b, 2H, NH), 5.01 (s, 2H, benzylic), 4.01 (t, *J* = 6.7 Hz, 2H, Ts-CH$_2$-), 3.49 (m, 4H, -NHC$\underline{H}_2$-), 3.35 (m, 2H, -NCH$_2$-), 1.8-0.8 (mm, 56H, aliphatic).

N^1-(11-Azidoundecyl)-N^3,N^5-bis((R)-3,7-dimethyloctyl)-N^1-(2-nitrobenzyl)benzene-1,3,5-tricarboxamide (**4**). Compound **22** (0.243 mmol, 230 mg) was dissolved in DMF (1.5 mL) and charged in a 10 mL flask. Sodium azide (1.43 mmol, 160 mg) was added and the resulting mixture was stirred at 70 °C. The extent of the reaction was checked with TLC (20% ethyl acetate in CHCl$_3$). Upon completion, the reaction mixture was poured in ice water (50 mL). The aqueous layer was extracted with CHCl$_3$ (4 x 25 mL). The combined CHCl$_3$ layers were washed with 1M NaOH (5 x 50 mL) and H$_2$O (1 x 50 mL). The organic layer was dried over MgSO$_4$ and the solvent was removed *in vacuo*. The crude product was purified with column chromatography (20% ethyl acetate in chloroform). R_f = 0.25. Impurities R_f = 0 and 0.03. Yield = 97 mg, 50%. ^{1}H-NMR (400 MHz, CDCl$_3$, δ): 8.2 (s, 1H, aromatic), 8.00 (d, *J* = 8 Hz, aromatic), 7.92 (s, 2H, aromatic), 7.70 (t, *J* = 7.4 Hz, aromatic), 7.54 (d, *J* = 7.7 Hz, 1H, aromatic) 7.50 (t, *J* = 7.8 Hz), 6.13 (b, 2H, NH), 5.01 (s, 2H, benzylic), 3.49 (m, 4H, -NHC$\underline{H}_2$-), 3.35 (m, 2H, -NCH$_2$-), 3.25 (t, *J* = 7.1 Hz, 2H, N$_3$CH$_2$-), 1.8-0.8 (mm, 56H, aliphatic). MALDI-ToF-MS (m/z) calc for $C_{47}H_{75}N_7O_5$ 817.58 found 790.63 (M-N$_2$+H)$^+$ 840.57 (M+Na)$^+$.

Poly[(butylmethacrylate)-co-(11-(3,5-bis((3S)-3,7-dimethyloctylcarbamoyl)benzamido) undecyl methacrylate)] (**23**). Compound **1** (0.314 mmol, 228.22 mg), butyl methacrylate (2.83 mmol, 402.24 mg), ethyl 2-bromo-2-methylpropanoate (0.0157 mmol, 3.062 mg), tin(II) 2-ethylhexanoate (0.157 mmol, 63.6 mg) and DMSO (3 mL) were charged in a Schlenk tube. The Schlenk tube was capped and subjected to five consecutive freeze-pump-thaw cycles. CuBr (0.0157 mmol, 2.25 mg) and compound **14** (0.0181 mmol, 5.27 mg) were charged in a second Schlenk tube. The Schlenk tube was capped and evacuated and back filled with argon. Under argon counter flow, the monomer solution was transferred to the Schlenk tube containing CuBr using a syringe. The reaction mixture turned green. The Schlenk tube was capped and heated at 50 °C. The reaction was quenched by exposure to air and the solvent was removed *in vacuo*. The polymer was redissolved in THF and precipitated in MeOH. Yield = 70 mg, 11%. ^{1}H-NMR (400 MHz, CDCl$_3$, δ): 8.2 (s, 3H, aromatic), 6.5-6.1 (b, 3H, NH), 4-3.7 (s, 20H - OCH$_2$-), 3.4 (s, -NH-C$\underline{H}_2$-), 2.0-0.6 (m, 169H, aliphatic). GPC (ODCB, polystyrene standards): M_n = 14400, M_w = 27662, *PDI* = 1.92. $\overline{DP}$ $_{H-NMR}$ = 70. FT-IR: 3243, 3073, 2957, 2929, 1726, 1640, 1556, 1465, 1381, 1365, 1297, 1261, 1240, 1145, 1064, 1020, 965, 946, 905, 860, 802, 747, 691.

Poly[(isobornylmethacrylate)-co-(11-(3,5-bis((3S)-3,7-dimethyloctylcarbamoyl)benzamido) undecyl methacrylate)] (**24**). 4-Cyano-4-((phenylcarbonothioyl)thio)pentanoic acid (3.5 µmol, 0.96 mg), AIBN (0.69 µmol, 0.11 mg), compound **1** (0.069 mmol, 50 mg), isobornyl methacrylate (0.62 mmol, 137 mg) and 0.8 mL dioxane were charged in a Schlenk tube. The Schlenk tube was capped and subjected to four consecutive freeze-pump-thaw cycles. The Schlenk tube was heated at 80 °C for 52 hours. The conversion was checked by ^{1}H-NMR analysis in CDCl$_3$. The reaction was quenched by the addition of CHCl$_3$ and exposure to air. The crude product was purified by precipitation in methanol yielding a white solid. The solids were collected by filtration and dried in a vacuum oven at 50 °C to constant weight. Yield = 125 mg, 67%. ^{1}H-NMR (400 MHz, TCE-d^2, T = 90 °C, d1 = 10 s, δ): 8.27 (b, 48H, aromatic), 6.30 (b, 48H, NH), 4.6-4.3 (b, 144H, -OCH-), 3.93 (b, 32H, -OCH$_2$-), 3.44 (b, 96H, C$\underline{H}_2$NH), 2.2-0.6 (m, 3200H, aliphatic). ^{13}C-NMR (100 MHz, TCE-d^2, T = 25 °C, δ): 138.2, 132.3, 83.5, 81.0, 80.7, 80.3, 52.1, 50.2, 48.2, 44.1, 42.7, 42.0, 40.7, 40.1, 37.6, 34.2, 33.1, 31.5, 30.8, 29.2, 27.1, 26.1, 26.1, 23.8, 23.0, 16.8; GPC (ODCB, 80 °C): M_n = 21400 g/mol, *PDI* = 1.60. $\overline{DP}$ $_{H-NMR}$ = 180. FT-IR (cm^{-1}): 3240, 2954, 2934, 2878, 1721, 1644, 1556, 1470, 1454, 1390, 1369, 1310, 1294, 1262, 1240, 1214, 1149, 1107, 1081, 1051, 1002, 985, 972, 944, 911, 888, 861, 844, 804, 754. DSC (40 °C/min, third heating run): T_g = 103 °C, T_m = 148 °C with ΔH 1.9 J/g.

Poly[(isobornylmethacrylate)-co-(11-(3,5-bis((3S)-3,7-dimethyloctylcarbamoyl)benzamido) undecyl methacrylate)] (**25**) 4-Cyano-4-((phenylcarbonothioyl)thio)pentanoic acid (2.6 µmol, 0.73 mg), AIBN (0.51 µmol, 0.09 mg), compound **1** (0.103 mmol, 75 mg), isobornyl methacrylate (0.41

mmol, 92 mg) and 0.8 ml dioxane were charged in a Schlenk tube. The Schlenk tube was capped and subjected to four consecutive freeze-pump-thaw cycles. The Schlenk tube was heated at 80 °C for 52 hours. The conversion was checked by ^{1}H-NMR analysis in CDCl$_3$. The reaction was quenched by the addition of CHCl$_3$ and exposure to air. The crude product was purified by precipitation in methanol yielding a white solid. The solids were collected by filtration and dried *in vacuo* at 50 °C. Yield = 125 mg, 67%. ^{1}H-NMR (400 MHz, TCE-d^2, T = 90 °C, d1 = 10 s, δ): 8.27 (b, 96H, aromatic), 6.30 (b, 96H, NH), 4.6-4.3 (b, 128H, -OCH-), 3.93 (b, 64H, -OCH$_2$-), 3.44 (b, 192H, C$\underline{H}_2$NH), 2.2-0.6 (m, 3840H, aliphatic). ^{13}C-NMR (100 MHz, TCE-d^2, T = 25 °C, δ): 138.2, 132.3, 83.5, 81.0, 80.7, 80.3, 52.1, 50.2, 48.2, 44.1, 42.7, 42.0, 40.7, 40.1, 37.6, 34.2, 33.1, 31.5, 30.8, 29.2, 27.1, 26.1, 26.1, 23.8, 23.0, 16.8; GPC (ODCB, 80 °C): M_n = 16600 g/mol, *PDI* = 1.48. $\overline{DP}$ $_{H-NMR}$ = 180. FT-IR (cm^{-1}): 3240, 3074 2955, 2926, 1723, 1644, 1556, 1455, 1390, 1369, 1294, 1261, 1241, 1148, 1105, 1050, 1017, 972, 944, 911, 861, 844, 800, 753. DSC (40 °C/min, third heating run): T_g = 101 °C, T_m = 172 °C with ΔH 2.34 J/g.

Poly[(isobornyl methacrylate)-co-(trimethylsilylpropynyl methacrylate)] (**33**). Tris[(2-pyridyl)methyl]amine (13.6 x 10^{-3} mmol, 4.05 mg), benzyl bromoisobutyrate (6.8 x 10^{-3} mmol, 1.66 mg), isobornyl methacrylate (2.25 mmol, 500 mg) trimethylsilylpropynyl methacrylate (0.46 mmol, 90 mg), Sn(EH)$_2$ (0.136 mmol, 55 mg) and toluene (0.5 mL) were charged in a Schlenk tube. The Schlenk tube was capped and five consecutive freeze-pump-thaw cycles were conducted to remove oxygen from the reaction system. CuBr (6.8 x 10^{-3} mmol, 1.05 mg) was charged in a second Schlenk tube. The Schlenk tube was capped and evacuated and backfilled with argon five times. Under argon counter flow, the monomer solution was transferred with a syringe to the Schlenk tube containing CuBr. The Schlenk tube was capped and heated at 90 °C. The solution was stirred under an argon atmosphere for 20 hours. ^{1}H-NMR in CDCl$_3$ showed a conversion of 50%. The reaction was terminated by exposure to air. The crude product in toluene was purified by precipitation in methanol (twice) and the polymer was dried in a vacuum oven at 40 °C. Yield = 200 mg, 45%. ^{1}H-NMR (400 MHz, CDCl$_3$, δ): 7.35 (s, 5H, aromatic), 4.7-4.2 (m, 218H, -C(O)O-CH$_2$- and -C(O)O-CH-), 2.0-0.6 (m, 3348 aliphatic), 0.2 (s, 330H, -Si(CH$_3$)$_3$). GPC (THF, polystyrene standards) M_n = 22945 g/mol, M_w = 37960 g/mol, *PDI* = 1.66. $\overline{DP}$ $_{H-NMR}$ = 180. Ratio isobornyl methacrylate/trimethyl-silylpropynyl methacrylate: theoretical 80/20, found 75/25.

Poly[(isobornyl methacrylate)-co-(propargyl methacrylate)] (**34**). Compound **33** (3.55 x 10^{-3} mmol polymer, 0.13 mmol of Si(CH$_3$)$_3$ groups, 142 mg) was dissolved in THF (10 mL). Acetic acid (0.195 mmol, 0.011 mL) was added to the solution. The mixture was flushed with argon for 15 minutes and cooled with and ice-water-salt bath to -5 °C. Tetra *n*-butylammonium fluoride (TBAF) in THF solution (1M) (0.2 mmol, 0.2 mL) was added slowly. The resulting

mixture was stirred overnight at room temperature. ^{1}H-NMR in CDCl$_3$ confirmed the absence of the Si(CH$_3$)$_3$ protecting group. The solvent was removed *in vacuo*. The crude product was redissolved in CHCl$_3$, precipitated twice in MeOH and dried *in vacuo* at 40 °C. Yield = 150 mg, 95%. ^{1}H-NMR (400 MHz, CDCl$_3$, δ): 7.35 (s, 5H, aromatic), 4.7-4.2 (m, 218H, -O-CH$_2$- and -O-CH-), 2.45 (s, 37H, CC-H) 2.0-0.6 (m, 3348 aliphatic). GPC (THF, polystyrene standards) M_n = 21910 g/mol, M_w = 35708 g/mol, *PDI* = 1.63. $\overline{DP}$ $_{H-NMR}$ = 180.

Poly[(isobornylmethacrylate)-co-((1-(11-(3,5-bis((3S)-3,7-dimethyloctylcarbamoyl)-N-(2-nitrobenzyl)benzamido)undecyl)-1H-1,2,3-triazol-4-yl)methylmethacrylate)-co-(propargyl methacrylate)] (**26**). Compound **4** (0.028 mmol, 23.5 mg), compound **34** (7.6 x 10^{-4} mmol polymer, 0.028 mmol reactive groups, 28 mg) and CuI (0.0028 mmol, 0.58 mg) were charged in a Schlenk tube. The Schlenk tube was capped and subjected to three consecutive freeze-pump-thaw cycles. 1,8-Diazabicyclo[5.4.0]undec-7-ene (DBU) (0.56 mmol, 85 mg) and dry THF (2 mL) were added under argon counter flow. The Schlenk tube was capped and heated at 35 °C. After stirring for 18 hours, the solvent was removed *in vacuo*. The crude mixture was redissolved in CHCl$_3$ (15 mL) and washed with a 0.065 M EDTA solution (3 x 15 mL), 1M HCl (1 x 15 mL) and brine (1 x 15 mL). The organic layer was dried over MgSO$_4$ and the solvent was removed *in vacuo*. The crude polymer was dissolved in chloroform and precipitated in methanol (twice), to yield the pure polymer as a yellowish solid. Yield = 195 mg, 90%. ^{1}H-NMR (400 MHz, TCE-d^2, 90 °C, δ): 8.11 (b, 18H, aromatic), 7.92 (b, 18H, aromatic), 7.84 (b, 36H, aromatic), 7.7-7.3 (b, 72H, aromatic and -C=CH-N-), 6.4-6 (b, 36H, NH), 5.05 (b, 36H, -O-CH$_2$-C=C-), 4.91 (b, 36H, benzylic), 4.6-4.2 (b, 180H, -O-CH- and O-C$\underline{H}_2$-CC-H), 3.4 (b, 72H, -NH-C$\underline{H}_2$-), 3.27 (b, 36H, -CO-N-CH$_2$-), 2.0-0.6 (m, 4500H, aliphatic). GPC (CHCl$_3$, polystyrene standards) M_n = 26329 g/mol, M_w = 44911 g/mol, *PDI* = 1.65. $\overline{DP}$ $_{H-NMR}$ = 180. The average number of protected BTAs per chain is 20.

Poly[(isobornylmethacrylate)-co-(trimethylsilylpropynylmethacrylate)] (**35**). Isobornyl methacrylate (18 mmol, 4 g), trimethylsilylpropynyl methacrylate (5.5 mmol, 0.88 g), 4-cyano-4-(phenylcarbonothioylthio)pentanoic acid (0.0562 mmol, 15.4 mg), AIBN (0.00562 mmol, 0.92 mg) and dioxane (20 mL) were charged in a Schlenk tube. The mixture was stirred at 80 °C in an argon atmosphere for 3 days. ^{1}H-NMR showed a conversion of 70%. The reaction was terminated by exposure to air. The crude product was two times precipitated from chloroform in methanol and subsequently dried *in vacuo* at 40 °C. Yield = 2.8 g, 70%. ^{1}H-NMR (400 MHz, CDCl$_3$, δ): 4.7-4.2 (m, -C(O)O-CH$_2$- and -C(O)O-CH-), 2.0-0.6 (m, aliphatic), 0.2 (s, H, -Si(CH$_3$)$_3$). *PDI* = 1.47. $\overline{DP}$ $_{H-NMR}$ = 250.

Poly[(isobornylmethacrylate)-co-(propargylmethacrylate)] (**36**). Compound **35** (0.1 mmol polymer and 5 mmol of Si(CH$_3$)$_3$ groups, 5 gram) were dissolved in THF (20 mL). Acetic acid (30 mmol, 1.7 ml) was added to the solution. The mixture was flushed with argon for 15 minutes and cooled with an ice-water-salt bath to -5 °C. TBAF in THF solution (1M) (30 mmol, 30 mL) was added slowly. The resulting mixture was stirred overnight at room temperature. ^{1}H-NMR confirmed the absence of the Si(CH$_3$)$_3$ group. The solvent was removed *in vacuo* and the crude product was purified by precipitation two times from chloroform in methanol. The product was dried *in vacuo* at 40 °C. Yield = 2.52 g, 90%. ^{1}H-NMR (400 MHz, CDCl$_3$, δ): 4.7-4.2 (m, -C(O)O-CH$_2$- and -C(O)O-CH-), 2.42 (s, C≡C-H), 2.1-0.6 (m, aliphatic). GPC (THF, polystyrene standards) M_n = 19 kg/mol, M_w = 28 kg/mol, *PDI* = 1.49. $\overline{DP}$ $_{H\text{-}NMR}$ = 250.

General procedure for the synthesis BTA side-functionalized polymers by copper(I)-catalyzed azide-alkyne cycloaddition reactions. The following procedure was used for all BTA side-functionalized polymers that were synthesized using the copper(I)-catalyzed azide-alkyne cycloaddition reaction as described for compound **27a**.

Poly[(isobornylmethacrylate)-co-(S-BTA-methacrylate)] (**27a**). Compound **2a** (0.08 mmol, 54.6 mg), compound **36** (3.2x10^{-3} mmol polymer, 0.16 mmol alkyne groups, 160 mg), N,N,N',N',N-Pentamethyldiethylenetriamine (PMDETA) (1 drop), Sn(II)-2-ethylhexanoate (1 drop) and a copper wire twisted stirring bar were charged in a 25 mL flask. Dry THF (10 mL) was added and the colorless solution was stirred at 35 °C in an argon atmosphere. The solution turned green within one hour. After 48 hours the solvent was removed *in vacuo.* And the white/ yellowish residue was dissolved in 50 mL chloroform. The organic phase was washed with a 0.065M EDTA solution (3 x 25 mL) and 1M HCl (1 x 25 mL). Chloroform was removed *in vacuo.* The crude polymer was dissolved in chloroform and precipitated in methanol (twice), to yield the pure polymer as a white solid. Yield = 190 mg, 95%. ^{1}H-NMR (400 MHz, CDCl$_3$, δ): 8.38 (b, 3H, aromatic), 7.8 - 7.5 (b, 1H, aromatic triazole), 6.8 (b, 3H, NH), 5.1 (b, 3H, COO-C<u>H$_2$</u>-C=C), 4.7-4.0 (b, 2H, C<u>H$_2$</u>-triazole and 2H, COO-C<u>H$_2$</u> and 1H, COO-C<u>H</u>), 3.4 (b, 6H, NH-C<u>H$_2$</u>), 2.4-0.6 (b, C≡C-<u>H</u> and aliphatic). GPC (THF, polystyrene standards) M_n = 27 kg/mol, M_w = 41 kg/mol, *PDI* = 1.52.

Poly[(isobornylmethacrylate)-co-(R-BTA-methacrylate)] (**27b**). Yield = 187 mg, 93%. ^{1}H-NMR (400 MHz, CDCl$_3$, δ): 8.38 (b, 3H, aromatic), 7.8-7.5 (b, 1H, aromatic triazole), 6.8 (b, 3H, NH), 5.1 (b, 3H, COO-C<u>H$_2$</u>-C=C), 4.6-4.0 (b, 2H, C<u>H$_2$</u>-triazole and 2H, COO-C<u>H$_2$</u> and 1H, COO-C<u>H</u>), 3.4 (b, 6H, NH-C<u>H$_2$</u>), 2.4-0.6 (b, C≡C-<u>H</u> and aliphatic). GPC (THF, polystyrene standards) M_n = 29 kg/mol, M_w = 45 kg/mol, *PDI* = 1.52.

Poly[(isobornylmethacrylate)-co-(A-BTA-methacrylate)] (**27c**). Yield = 190 mg, 95%. ^{1}H-NMR (400 MHz, CDCl$_3$, δ): 8.38 (b, 3H, aromatic), 7.8-7.5 (b, 1H, aromatic triazole), 6.8 (b, 3H, NH), 5.1 (b, 3H, COO-CH$_2$-C=C), 4.6-4.0 (b, 2H, C<u>H$_2$</u>-triazole and 2H, COO-C<u>H$_2$</u> and 1H, COO-C<u>H</u>),

3.4 (b, 6H, NH-C$\underline{H}_2$), 2.4-0.6 (b, C≡C-$\underline{H}$ and aliphatic). GPC (THF, polystyrene standards) M_n = 28 kg/mol, M_w = 45 kg/mol, *PDI* = 1.57.

Poly[(isobornylmethacrylate)-co-(R-BTA/A-BTA-methacrylate)] (**28**). Yield = 180 mg, 92%. ^{1}H-NMR (400 MHz, CDCl$_3$, δ): 8.38 (b, 3H, aromatic), 7.8 - 7.5 (b, 1H, aromatic triazole), 7.01 (b, 3H, NH), 5.1 (b, 3H, COO-C$\underline{H}_2$-C=C), 4.7-4.0 (b, 2H, C$\underline{H}_2$-triazole and 2H, COO-C$\underline{H}_2$ and 1H, COO-C$\underline{H}$), 3.4 (b, 6H, NH-C$\underline{H}_2$), 2.4-0.6 (b, C≡C-$\underline{H}$ and aliphatic). GPC (THF, polystyrene standards) M_n = 25 kg/mol, M_w = 40 kg/mol, *PDI* = 1.6.

Poly[(isobornylmethacrylate)-co-(R-BTA/A-BTA-methacrylate)] (**29**). Yield = 187 mg, 93%. ^{1}H-NMR (400 MHz, CDCl$_3$, δ): 8.38 (b, 3H, aromatic), 7.8 - 7.6 (b, 1H, aromatic triazole), 7.0 (b, 3H, NH), 5.1 (b, 3H, COO-C$\underline{H}_2$-C=C), 4.7-4.0 (b, 2H, C$\underline{H}_2$-triazole and 2H, COO-C$\underline{H}_2$ and 1H, COO-C$\underline{H}$), 3.4 (b, 6H, NH-C$\underline{H}_2$), 2.4-0.6 (b, C≡C-$\underline{H}$ and aliphatic). GPC (THF, polystyrene standards) M_n = 28 kg/mol, M_w = 42.9 kg/mol, *PDI* = 1.53.

Poly[(isobornylmethacrylate)-co-(R-BTA/A-BTA-methacrylate)] (**30**). Yield = 190 mg, 95%. ^{1}H-NMR (400 MHz, CDCl$_3$, δ): 8.38 (b, 3H, aromatic), 7.8 - 7.5 (b, 1H, aromatic triazole), 6.9 (b, 3H, NH), 5.1 (b, 3H, COO-C$\underline{H}_2$-C=C), 4.7-4.0 (b, 2H, C$\underline{H}_2$-triazole and 2H, COO-C$\underline{H}_2$ and 1H, COO-C$\underline{H}$), 3.4 (b, 6H, NH-C$\underline{H}_2$), 2.4-0.6 (b, C≡C-$\underline{H}$ and aliphatic). GPC (THF, polystyrene standards) M_n = 26 kg/mol, M_w = 42 kg/mol, *PDI* = 1.55.

Poly[(isobornylmethacrylate)-co-(R-BTA/A-BTA-methacrylate)] (**31**). Yield = 180 mg, 90%. ^{1}H-NMR (400 MHz, CDCl$_3$, δ): 8.38 (b, 3H, aromatic), 7.8 - 7.5 (b, 1H, aromatic triazole), 6.9 (b, 3H, NH), 5.1 (b, 3H, COO-C$\underline{H}_2$-C=C), 4.7-4.0 (b, 2H, C$\underline{H}_2$-triazole and 2H, COO-C$\underline{H}_2$ and 1H, COO-C$\underline{H}$), 3.4 (b, 6H, NH-C$\underline{H}_2$), 2.4-0.6 (b, C≡C-$\underline{H}$ and aliphatic). GPC (THF, polystyrene standards) M_n = 22 kg/mol, M_w = 36 kg/mol, *PDI* = 1.61.

Poly[(isobornylmethacrylate)-co-(R-BTA/A-BTA-methacrylate)] (**32**). Yield = 195 mg, 97%. ^{1}H-NMR (400 MHz, CDCl$_3$, δ): 8.38 (b, 3H, aromatic), 7.8 - 7.5 (b, 1H, aromatic triazole), 6.9 (b, 3H, NH), 5.1 (b, 3H, COO-C$\underline{H}_2$-C=C), 4.7-4.0 (b, 2H, C$\underline{H}_2$-triazole and 2H, COO-C$\underline{H}_2$ and 1H, COO-C$\underline{H}$), 3.4 (b, 6H, NH-C$\underline{H}_2$), 2.4-0.6 (b, C≡C-$\underline{H}$ and aliphatic). GPC (THF, polystyrene standards) M_n = 27 kg/mol, M_w = 43 kg/mol, *PDI* = 1.58.

6.7 References and notes

[1]   C. B. Anfinsen, *Science* **1973**, *181*, 223.
[2]   E. Haber, C. B. Anfinsen, *J. Biol. Chem.* **1961**, *236*, 422.
[3]   A. E. Mirsky, L. Pauling, *Proc. Natl. Acad. Sci. USA* **1936**, *22*, 439.
[4]   D. J. Hill, M. J. Mio, R. B. Prince, T. S. Hughes, J. S. Moore, *Chem. Rev.* **2001**, *101*, 3893.
[5]   R. P. Cheng, S. H. Gellman, W. F. DeGrado, *Chem. Rev.* **2001**, *101*, 3219.
[6]   C. J. Gabriel, J. R. Parquette, *J. Am. Chem. Soc.* **2006**, *128*, 13708.
[7]   A. L. Hofacker, J. R. Parquette, *Angew. Chem., Int. Ed.* **2005**, *44*, 1053.
[8]   A. J. Preston, J. C. Gallucci, J. R. Parquette, *Org. Lett.* **2006**, *8*, 5885.
[9]   J. R. Parquette, *CR. Chim.* **2003**, *6*, 779.
[10]   J. W. Lockman, N. M. Paul, J. R. Parquette, *Prog. Polym. Sci.* **2005**, *30*, 423.
[11]   J. F. Yu, T. V. RajanBabu, J. R. Parquette, *J. Am. Chem. Soc.* **2008**, *130*, 7845.
[12]   D. Mecerreyes, V. Lee, C. J. Hawker, J. L. Hedrick, A. Wursch, W. Volksen, T. Magbitang, E. Huang, R. D. Miller, *Adv. Mater.* **2001**, *13*, 204.

[13] E. Harth, B. Van Horn, V. Y. Lee, D. S. Germack, C. P. Gonzales, R. D. Miller, C. J. Hawker, *J. Am. Chem. Soc.* **2002**, *124*, 8653.

[14] L. Cheng, G. L. Hou, J. J. Miao, D. Y. Chen, M. Jiang, L. Zhu, *Macromolecules* **2008**, *41*, 8159.

[15] T. A. Croce, S. K. Hamilton, M. L. Chen, H. Muchalski, E. Harth, *Macromolecules* **2007**, *40*, 6028.

[16] A. E. Cherian, F. C. Sun, S. S. Sheiko, G. W. Coates, *J. Am. Chem. Soc.* **2007**, *129*, 11350.

[17] J. B. Beck, K. L. Killops, T. Kang, K. Sivanandan, A. Bayles, M. E. Mackay, K. L. Wooley, C. J. Hawker, *Macromolecules* **2009**, *42*, 5629.

[18] A. W. Bosman, R. Vestberg, A. Heumann, J. M. J. Frechet, C. J. Hawker, *J. Am. Chem. Soc.* **2003**, *125*, 715.

[19] A. W. Bosman, A. Heumann, G. Klaerner, D. Benoit, J. M. J. Frechet, C. J. Hawker, *J. Am. Chem. Soc.* **2001**, *123*, 6461.

[20] T. Terashima, M. Kamigaito, K. Y. Baek, T. Ando, M. Sawamoto, *J. Am. Chem. Soc.* **2003**, *125*, 5288.

[21] P. A. Bertin, J. M. Gibbs, C. K. F. Shen, C. S. Thaxton, W. A. Russin, C. A. Mirkin, S. T. Nguyen, *J. Am. Chem. Soc.* **2006**, *128*, 4168.

[22] T. Terashima, M. Ouchi, T. Ando, M. Sawamoto, *J. Polym. Sci. Part A: Polym. Chem.* **2010**, *48*, 373.

[23] B. Helms, S. J. Guillaudeu, Y. Xie, M. McMurdo, C. J. Hawker, J. M. J. Frechet, *Angew. Chem., Int. Ed.* **2005**, *44*, 6384.

[24] Y. G. Chi, S. T. Scroggins, J. M. J. Frechet, *J. Am. Chem. Soc.* **2008**, *130*, 6322.

[25] Y. G. Chi, S. T. Scroggins, E. Boz, J. M. J. Frechet, *J. Am. Chem. Soc.* **2008**, *130*, 17287.

[26] E. J. Foster, E. B. Berda, E. W. Meijer, *J. Am. Chem. Soc.* **2009**, *131*, 6964.

[27] E. B. Berda, E. J. Foster, E. W. Meijer, *Macromolecules* **2010**, *43*, 1430.

[28] E. J. Foster, E. B. Berda, E. W. Meijer, *J. Polym. Sci. Part A: Polym. Chem.* **2011**, *49*, 118.

[29] R. Deans, F. Ilhan, V. M. Rotello, *Macromolecules* **1999**, *32*, 4956.

[30] M. Seo, B. J. Beck, J. M. J. Paulusse, C. J. Hawker, S. Y. Kim, *Macromolecules* **2008**, *41*, 6413.

[31] F. H. Beijer, R. P. Sijbesma, H. Kooijman, A. L. Spek, E. W. Meijer, *J. Am. Chem. Soc.* **1998**, *120*, 6761.

[32] R. P. Sijbesma, F. H. Beijer, L. Brunsveld, B. J. B. Folmer, J. H. K. K. Hirschberg, R. F. M. Lange, J. K. L. Lowe, E. W. Meijer, *Science* **1997**, *278*, 1601.

[33] B. J. B. Folmer, R. P. Sijbesma, R. M. Versteegen, J. A. J. van der Rijt, E. W. Meijer, *Adv. Mater.* **2000**, *12*, 874.

[34] H. Kautz, D. J. M. van Beek, R. P. Sijbesma, E. W. Meijer, *Macromolecules* **2006**, *39*, 4265.

[35] M. P. Lightfoot, F. S. Mair, R. G. Pritchard, J. E. Warren, *Chem. Commun.* **1999**, 1945.

[36] L. Brunsveld, A. P. H. J. Schenning, M. A. C. Broeren, H. M. Janssen, J. A. J. M. Vekemans, E. W. Meijer, *Chem. Lett.* **2000**, 292.

[37] M. M. J. Smulders, A. P. H. J. Schenning, E. W. Meijer, *J. Am. Chem. Soc.* **2008**, *130*, 606.

[38] P. J. M. Stals, J. F. Haveman, R. Martín-Rapún, C. F. C. Fitié, A. R. A. Palmans, E. W. Meijer, *J. Mater. Chem.* **2009**, *19*, 124.

[39] J. Roosma, T. Mes, P. Leclère, A. R. A. Palmans, E. W. Meijer, *J. Am. Chem. Soc.* **2008**, *130*, 1120.

[40] T. Muraoka, H. Cui, S. I. Stupp, *J. Am. Chem. Soc.* **2008**, *130*, 2946.

[41] T. Muraoka, C.-Y. Koh, H. Cui, S. I. Stupp, *Angew. Chem., Int. Ed.* **2009**, *48*, 5946.

[42] C. J. Hawker, A. W. Bosman, E. Harth, *Chem. Rev.* **2001**, *101*, 3661.

[43] J. Chiefari, Y. K. Chong, F. Ercole, J. Krstina, J. Jeffery, T. P. T. Le, R. T. A. Mayadunne, G. F. Meijs, C. L. Moad, G. Moad, E. Rizzardo, S. H. Thang, *Macromolecules*, **1998**, *31*, 5559.

[44] K. Matyjaszewski, J. Xia, *Chem. Rev.* **2001**, *101*, 2921.

[45] M. Kamigaito, T. Ando, M. Sawamoto, *Chem. Rev.* **2001**, *101*, 3689.

[46] N. V. Tsarevsky, K. Matyjaszewski, *Chem. Rev.* **2007**, *107*, 2270.

[47] C. Barner-Kowollik, S. Perrier, *Polym. Sci. Part A: Polym Chem.* **2008**, *46*, 5715.

[48] K. Matyjaszewski, N. V. Tsarevsky, *Nat. Chem.* **2009**, *1*, 276.

[49] P. De Paoli, A. A. Isse, N. Bortolamei, A. Gennaro, *Chem. Commun.* **2011**, *47*, 3580. A. A. Isse, A. Gennaro, C. Yeh Lin, J. L. Hodgson, M. L. Coote, T. Guliashvili, *J. Am. Chem. Soc.* **2011**, *133*, 6254.

[50] G. Moad, E. Rizzardo, S. H. Thang, *Aust. J. Chem.* **2006**, *59*.

[51] G. Moad, E. Rizzardo, S. H. Thang, *Acc. Chem. Res.* **2008**, *41*, 1133.

[52] V. r. Mellon, D. Rinaldi, E. Bourgeat-Lami, F. D'Agosto, *Macromolecules* **2005**, *38*, 1591.

[53] H. Matahwa, J. B. McLeary, R. D. Sanderson, *Polym. Sci. Part A: Polym. Chem.* **2006**, *44*, 427.

[54] J.-F. Lutz, *Angew. Chem., Int. Ed.* **2007**, *46*, 1018.

[55] W. H. Binder, R. Sachsenhofer, *Macromol. Rapid Commun.* **2007**, *28*, 15.

[56] C. W. Tornøe, C. Christensen, M. Meldal, *J. Org. Chem.* **2002**, *67*, 3057.

[57] V. V. Rostovtsev, L. G. Green, V. V. Fokin, K. B. Sharpless, *Angew. Chem., Int. Ed.* **2002**, *41*, 2596.

[58]   F. Himo, T. Lovell, R. Higraf, V. V. Rostovtsev, L. Noodleman, K. B. Sharpless, V. V. Fokin, *J. Am. Chem. Soc.* **2005**, *127*, 210.

[59]   Y. Yoshida, Y. Sakakura, N. Aso, S. Okada, Y. Tanabe, *Tetrahedron* **1999**, *55*, 2183.

[60]   J. A. Opsteen, J. C. M. van Hest, *Chem. Commun.* **2005**, 57.

[61]   P. J. M. Stals, M. M. J. Smulders, R. Martín-Rapún, A. R. A. Palmans, E. W. Meijer, *Chem. Eur. J.* **2009**, *15*, 2071.

[62]   The deprotection of the polymer is remarkably much faster than the model compound, for reasons that are still under investigation.

[63]   T. Mes, M. M. J. Smulders, A. R. A. Palmans, E. W. Meijer, *Macromolecules* **2010**, *43*, 1981.

[64]   All of the samples were sonicated for one hour at elevated temperature. Subsequently heated to 80 °C and cooled (20 K/min) to 20 °C before each measurement.

[65]   P. Jonkheijm, P. van der Schoot, A. P. H. J. Schenning, E. W. Meijer, *Science* **2006**, *313*, 80.

[66]   The g_{value} of **31** is not plotted because it is significantly lower due to a lower degree of functionalization.

[67]   After the addition of 1000 equivalents of HFIP the initial concentration of the solution was decreased to 3.75×10^{-5} M in 70/30 DCE/MCH vol%.

[68]   P. W. K. Rothemund, *Nature* **2006**, *440*, 297.

[69]   R. D. Barish, R. Schulman, P. W. K. Rothemund, E. Winfree, *Proc. Natl. Acad. Sci. USA* **2009**, *106*, 6054.

[70]   T. Terashima, T. Mes, T. F. A. de Greef, M. A. J. Gillissen, P. Besenius, A. R. A. Palmans, E. W. Meijer, *J. Am. Chem. Soc.* **2011**, *133*, 4742.

Hydrogen bonding induced order in supramolecular polymers

The self-assembly of small and relatively simple molecules has proven to be a powerful tool for the development of complex supramolecular nanostructures of defined size and shape. More recently, the understanding of supramolecular polymeric aggregates has become a research interest, with the aim to increase the knowledge of the non-covalent interactions in factors that govern self-assembly in these systems. This thesis addresses the development of supramolecular polymers, which are based on benzene-1,3,5-tricarboxamides (BTAs) and traditional polymers. BTAs comprising alkyl side chains form helical supramolecular polymers in dilute solution and in the solid state as a result of the threefold helical arrangement of the intermolecular hydrogen bonds. The self-assembly properties of BTAs combined with traditional polymers has led to the development of novel supramolecular materials. Because the chirality of monomeric BTAs is expressed at the supramolecular level, these systems allow the use of a wide range of spectroscopic techniques to study the self-assembly. As a result, valuable insights into the formation of the supramolecular structure of the resulting polymers were obtained, which are crucial to further develop the field of supramolecular polymers.

In Chapter 1, an overview is given of supramolecular systems that self-assemble by the formation of hydrogen bonds. Special attention is paid to hydrogen bond strength and to approaches to increase the binding strength. In addition, three classes of supramolecular assemblies, in which the formation is hydrogen bonding driven, are discussed based on literature examples. This short literature overview includes systems such as supramolecular polymeric networks, disc-shaped motifs with the ability to form long elongated supramolecular polymers and the final class describes supramolecular assemblies, which are limited in size and shape as a result of their design.

In Chapter 2, the self-assembly of BTAs into helical aggregates when end-capped to or copolymerized with low molecular weight poly(ethylene-*co*-butylene) is investigated in solution and in the solid state. Self-assembly is evaluated with a variety of spectroscopic techniques such as CD, UV and IR. The introduction of BTAs results in the formation of phase segregated nanorods. In some cases, this leads to drastic improvements of the material properties, as revealed by tensile testing and oscillating shear rheology measurements.

A systematic study on the role of polarity on the self-assembly of BTAs in solution and on their ability to phase segregate in the solid state is performed in Chapter 3. In dilute solution, the polarity is varied by mixing polar and apolar solvents. In the solid state, a wide range of backbone polarities is covered by end-capping of telechelics of varying polarity with the BTA motif. In both cases, an increase of polarity leads to a significant decrease of the stability of BTA aggregates, which in the solid state eventually results in the loss of nanorod formation.

This study gives a detailed understanding of the scope and limitations of BTA based polymers for various applications.

In Chapter 4, the use of BTA functionalized polymers as hydrogelators is explored. BTAs equipped with aliphatic side chains are end-capped to polyethylene glycol via a short apolar spacer. In water, long entangled nanorods were formed as a result of intermolecular hydrogen bonding stabilized by hydrophobic interactions. At higher concentrations, strong and transparent gels were obtained. The supramolecular structure and the material properties of the gel are determined with CD spectroscopy and with oscillating shear measurements.

A supramolecular polymer system that consists of a mixture of BTAs and UPys, end-capped to monofunctional polymers is introduced in Chapter 5. Both supramolecular motifs self-assemble in an orthogonal fashion in two separate types of phase segregated nanorods. After the addition of an α, ω-telechelic polymer containing both the BTA and UPy motif (compatibilizer) to this system, a cross-linked network is formed. This is observed by the transformation of a viscous sticky liquid into a solid material with elastomeric properties as evidenced by oscillating shear rheology measurements. The preliminary results presented in this study show the potential of orthogonal self-assembly based on hydrogen bonding motifs.

In the final Chapter, the ability of BTAs grafted to the side chain of polymethacrylate to form well-defined nanosized objects comprising an internal helical architecture is investigated. These polymeric structures form ordered chiral single-chain polymeric nanoparticles in a controlled fashion. Controlled folding is achieved by making use of photolabile deprotection chemistry and with the aid of heating and cooling steps. This process is quantitatively followed with CD spectroscopy. The high stability and chiral conformation of the folded particles make them excellent candidates for compartmentalized catalytic systems.

Waterstofbrug geïnduceerde orde in supramoleculaire polymeren

Het gebruik van zelf-assemblerende, relatief eenvoudige moleculen voor het creëren van complexe supramoleculaire structuren, is een bewezen krachtige methode. Door een beter begrip van de toegepaste omkeerbare interacties, is recentelijk ook de ontwikkeling van zelf-assemblerende polymeeraggregaten een onderzoeksdoel geworden. Dit proefschrift beschrijft de ontwikkeling van supramoleculaire polymeren gebaseerd op benzeen-1,3,5-tricarboxamide (BTA) eenheden, welke covalent gebonden zijn aan traditionele polymeren. BTAs gefunctionaliseerd met alkyl zij-ketens vormen een supramoleculair polymeer in oplossing en in de vaste fase als gevolg van de vorming van intermoleculaire waterstofbruggen. Het gebruik van zelf-assemblerende BTAs in combinatie met traditionele polymeren heeft geleid tot de ontwikkeling van nieuwe supramoleculaire materialen. Omdat de chiraliteit van een BTA monomeer tot expressie komt in het supramoleculaire niveau, zijn de vorming en de structuur van deze systemen in groot detail te bestuderen met verschillende spectroscopische technieken. Als gevolg hiervan zijn waardevolle inzichten verkregen die cruciaal zijn voor de verdere ontwikkeling van supramoleculaire polymeren.

In Hoofdstuk 1 is een overzicht gegeven van supramoleculaire systemen die zelf-assembleren als gevolg van waterstofbrugvorming. Hierbij is speciale aandacht besteed aan de sterkte van de waterstofbrug en aan strategieën om de bindingssterkte te verhogen. Aan de hand van literatuurvoorbeelden wordt een drietal klassen supramoleculaire systemen beschreven. Dit zijn supramoleculaire polymerennetwerken, discotische monomeren die de mogelijkheid bezitten om lange supramoleculaire polymeren te vormen, en tot slot supramoleculaire assemblages welke gelimiteerd zijn in grootte en vorm als gevolg van hun ontwerp.

Hoofdstuk 2 beschrijft de vorming van helische supramoleculaire polymeren uit BTAs welke eindstandig gebonden zijn aan, of gecopolymeriseerd met, laag moleculair gewicht poly(ethyleen-*co*-butyleen) (pEB) in oplossing en in de vaste fase. De zelf-assemblage is geëvalueerd met een verscheidenheid aan technieken zoals circulair dichroisme (CD), ultraviolet en infrarood spectroscopie. De introductie van BTAs aan pEB resulteert in de vorming van fasescheiding tussen de BTAs en de polymere matrix. In sommige gevallen leidt dat tot een drastische verbetering van de materiaaleigenschappen. De materiaaleigenschappen zijn vervolgens gekwantificeerd met trekproeven en dynamische oscillerende afschuif rheologiemetingen.

Een systematische studie van de rol van polariteit in de zelf-assemblage van BTAs in oplossing en in de vaste toestand, is beschreven in Hoofdstuk 3. In oplossing is de polariteit gevarieerd door middel van het mengen van polaire en minder polaire oplosmiddelen. In de vaste toestand is een breed scala aan polymeerketens met een verschillende polariteit eindstandig gefunctionaliseerd met de BTA eenheid. In beide toestanden leidt een verhoging

van de polariteit tot een significante verlaging van de stabiliteit van BTA aggregaten. In de vaste toestand leidt dit zelfs tot een situatie waarin er niet langer fasescheiding optreedt en dus de eigenschappen van het polymeer niet verbeterd worden. Deze studie verschaft een gedetailleerd inzicht in het mogelijke gebruik van BTAs in verscheidene toepassingsgebieden.

In Hoofdstuk 4 is het gebruik van BTA gefunctionaliseerde polymeren als gelatoren voor water onderzocht. BTAs voorzien van twee alifatische zijketens zijn tweevoudig verbonden aan een lineair polyethyleen glycol, door middel van een kort apolair verbindingselement. Deze haltervormige polymeren vormen in water lange cilindrische aggregaten, die met elkaar verstrengeld zijn als gevolg van intermoleculaire waterstofbrugvorming, gestabiliseerd door hydrofobe interacties. Bij hogere concentraties werden sterke, elastische en transparante gels verkregen. De supramoleculaire structuur en de materiaaleigenschappen van deze gel zijn respectievelijk bepaald met CD spectroscopie en dynamische oscillerende afschuif rheologiemetingen.

Een supramoleculair polymeersysteem, bestaande uit een mengsel van BTA en ureidopyrimidinon enkelvoudig gefunctionaliseerde polymeren, zijn beschreven in Hoofdstuk 5. Beide supramoleculaire deeltjes zelf-assembleren op een orthogonale manier in twee aparte typen van cilindrische aggregaten. Na de toevoeging van een α, ω-telechelisch polymeer (compatibilizer) aan het polymeermengsel, werden de twee typen van aggregaten vernet. Deze netwerkvorming zorgt voor een transformatie van een viskeuze vloeistof naar een vast materiaal met elastische eigenschappen, en is gekwantificeerd met dynamische oscillerende afschuif rheologiemetingen. De beschreven resultaten laten zien dat orthogonale zelf-assemblage in de vaste fase gebaseerd op waterstofbruggen kan leiden tot een dramatische verbetering van de materiaaleigenschappen.

Het laatste Hoofdstuk 6 beschrijft de mogelijkheid om goed gedefinieerde nanodeeltjes met een helische structuur te verkrijgen uit BTA zij-gefunctionaliseerd polymethacrylaat. Deze polymeren vormen geordende enkele-keten polymeren nanodeeltjes op een gecontroleerde manier. Gecontroleerde vouwing is verkregen met behulp van fotochemische ontschermingschemie in combinatie met verwarmen en koelen. Het vouwproces en de structuur zijn beide gevisualiseerd met CD spectroscopie. De hoge stabiliteit en de chirale goed geordende structuur van de gevouwen deeltjes maken ze uitermate geschikt om gebruikt te worden in gecompartmenteliseerde katalytisch actieve systemen.

Curriculum Vitae

Tristan Mes werd geboren op 21 januari 1981 te Breda. Na zijn HAVO opleiding aan het Mgr Frencken College te Oosterhout, begon hij in 1999 aan de Bachelorstudie Chemie aan Avans Hogeschool. In 2004 is hij een Masterstudie Scheikundige Technologie begonnen aan de Technische Universiteit Eindhoven. Deze studie werd in 2007 afgerond met een afstudeerproject in de capaciteitsgroep Macromoleculaire en Organische Chemie, onder leiding van prof. dr. E.W. Meijer en dr. ir. A.R.A. Palmans. Aansluitend begon hij in september 2007 zijn promotieonderzoek binnen dezelfde capaciteitsgroep onder leiding van dr. ir. A.R.A. Palmans en prof. dr. E.W. Meijer. Het doel van dit onderzoek was het ontwikkelen en bestuderen van nieuwe supramoleculaire polymeren, die bestaan uit conventionele polymeren gekoppeld aan kleine supramoleculaire bouwstenen, met als doel om functionele supramoleculaire materialen te verkrijgen. De belangrijkste resultaten van dit onderzoek zijn beschreven in dit proefschrift.

Tristan Mes was born on Januray 21, 1981 in Breda, The Netherlands. After secondary education at the Mgr. Frencken College in Oosterhout, he started studying Chemistry at Avans Hogeschool where he obtained his Bachelor degree in Applied Sciences. In 2004, he started studying Chemical Engineering and Chemistry at the Eindhoven University of Technology. The Master of Science degree was obtained in 2007 after a graduation project in the Laboratory of Macromolecular and Organic Chemistry, under the supervision of prof. dr. E.W. Meijer en dr. ir. A.R.A. Palmans. From September 2007, he worked as a PhD student in the same laboratory, under the supervision of dr. ir. A.R.A. Palmans en prof. dr. E.W. Meijer. The aim of his research was to develop and study new supramolecular polymers, which consist of conventional polymers connected to small supramolecular motifs, to generate functional supramolecular materials. The most important results of this research are presented in this thesis.

List of Publications

Single-Chain Polymeric Nanoparticles by Stepwise Folding

T. Mes, R. van der Weegen, A.R.A. Palmans, E.W. Meijer, *Angew. Chem., Int. Ed.* **2011**, *50*, 5085-5089.

Single-Chain Folding of Polymers for Catalytic Systems in Water

T. Terashima, T. Mes, T.F.A. de Greef, M.A.J. Gillissen, P. Besenius, A.R.A. Palmans, E.W. Meijer, *J. Am. Chem. Soc.* **2011**, *133*, 4742-4745.

Hydrogen-Bond Engineering in Supramolecular Polymers: Polarity Influence on the Self-Assembly of Benzene-1,3,5-tricarboxamides

T. Mes, M.M.J. Smulders, A.R.A. Palmans, E.W. Meijer, *Macromolecules* **2010**, *43*, 1981-1991.

Self-assembly of Benzene-1,3,5-tricarboxamides in Polymeric Systems

T. Mes, A.R.A. Palmans, E.W. Meijer, *Polym. Prep.* **2010**, *51*, 150-151.

Probing the Limits of the Majority-rules Principle in a Dynamic Supramolecular Polymer

M.M.J. Smulders, P.J.M. Stals, T. Mes, T.F.E. Paffen, A.P.H.J. Schenning, A.R.A. Palmans, E.W. Meijer, *J. Am. Chem. Soc.* **2010**, *132*, 620-626.

Supramolecular Materials from Benzene-1,3,5-tricarboxamide Based Nanorods

J. Roosma, T. Mes, P.E.L.G. Leclère, A.R.A. Palmans, E.W. Meijer, *J. Am. Chem. Soc.* **2008**, *130*, 1120-1121.

Iterative Tandem Catalysis of Secondary Diols and Diesters to Chiral Polyesters

B.A.C. van As, J. van Buijtenen, T. Mes, A.R.A. Palmans, E.W. Meijer, *Chem Eur. J.* **2007**, *13*, 8325-8332.

(to be) submitted

Network Formation by Orthogonal Self-assembly

T. Mes, M.M.E. Koenigs, V.F. Scalfani, T.S. Bailey, A.R.A. Palmans, E.W. Meijer, submitted to *ACS Macro Letters*.

From Supramolecular Polymers to Supramolecular Hydrogels

T. Mes, C.M.A. Leenders, P. Besenius, M.M.E. Koenigs, A.R.A. Palmans, E.W. Meijer, to be submitted.

Dankwoord

Het best gelezen onderdeel van een proefschrift: het Dankwoord! Na bijna zeven jaar actief geweest te zijn als Spinoza-student, afstudeerder en AIO binnen de vakgroep SMO, kan ik gerust zeggen dat ik er deels ben opgevoed. Ik heb deze tijd als zeer plezierig en leerzaam ervaren en wil graag verschillende mensen hiervoor bedanken.

Ik wil als eerste mijn promotor Bert Meijer bedanken. Bert, jij hebt me de mogelijkheid gegeven om mijn promotieonderzoek uit te voeren in jouw groep. Jouw enthousiasme en creativiteit zijn zeer inspirerend voor mij geweest. Ondanks de grootte van de groep ben je goed op de hoogte waar iedereen mee bezig is en geef je toch altijd die ene suggestie voor dat vervolg experiment. Jij kijkt veel verder dan de experimenten en weet altijd een groter beeld te schetsen en dit heb ik erg verhelderend gevonden. Wat ik het meest waardeer, is dat je ondanks je hoge wetenschappelijke prestatie zo sociaal en goed met ons blijft omgaan.

Mijn copromotor Anja Palmans wil ik bedanken voor de begeleiding tijdens mijn promotieonderzoek. Anja, ik heb heel veel van je geleerd en wat ik erg fijn heb gevonden is de vrijheid die je mij hebt gegeven. Je kantoor stond voor mij altijd open, zowel op zakelijk als persoonlijk vlak. Ik ben erg onder de indruk van je doelgerichtheid en technische kennis maar vooral van je educatieve vaardigheden. Ik herinner me nog goed in welke bewoording en kleur ik mijn allereerste kwartaalverslag terug kreeg. Zeven jaar later is mijn proefschrift geschreven. Ook jouw directe manier van communiceren heb ik zeer gewaardeerd.

Prof. Dr. Rint Sijbesma en Prof. Dr. Jan van Esch wil ik graag bedanken voor het plaats willen nemen in de leescommissie. Furthermore, I am honored that Prof. Dr. Weder took part in the reading committee and has come to Eindhoven to be present at my defense. Ten slotte wil ik ook Prof. Dr. Roeland Nolte en Dr. Ilja Voets bedanken voor het deelnemen in de promotiecommissie.

Ik bedank Jorg Roosma voor de fijne initiële samenwerking. Jij hebt de basis gelegd voor de eerste BTA gefunctionaliseerde polymeren en dus ook voor dit proefschrift.

During my PhD project I have had the ability to work with Dr. Travis Bailey and Vincent Scalfani from Colorado State University. I would like to thank both of you for the synthesis of the heterofunctional polybutadiene and for performing rheology measurements. This work is described in Chapter 5 and is submitted in a mutual manuscript.

Ook wil ik Maarten Smulders bedanken voor zijn wetenschappelijke bijdrage aan Hoofdstuk 2 en 3. Verder zal ik nooit vergeten hoe wij onvoorbereid Bear Rock in de Rocky Mountains beklommen en ons daar elke dag opnieuw lieten verrassen door een te kort aan water.

Ik heb het voorrecht gehad om met een drietal afstudeerders te werken. Marcel Koenigs, heel erg bedankt dat je samen met mij hebt gewerkt aan de orthogonale zelf-assemblage van UPy/BTA moleculen. Je was mijn eerste afstudeerder en begon vrij kort na mijn eigen start en

171

daarom was het ook zeer leerzaam voor mij. Ik wens je veel succes met het afronden van je eigen promotieonderzoek. Rob van der Weegen, ook jou wil ik heel graag bedanken voor je inzet en bijdrage aan mijn promotieonderzoek. Jouw synthetisch doorzettingsvermogen heeft mede geleid tot het succes van de BTA nanodeeltjes. Ook jij, heel veel succes met je promotieonderzoek. Nabil Tahiri, heel erg bedankt voor je bijdrage aan mijn onderzoek. Soms zijn een paar kleine experimenten, die maanden werk gekost hebben, van groot belang. Ik ben erg blij dat je de keus hebt gemaakt om door te studeren, al is het dan niet hier.

Floris en Pol, heel erg bedankt dat jullie mijn paranimfen willen zijn. Ik ben erg blij met de vriendschap die we hebben opgebouwd. Floris, we zijn tegelijkertijd begonnen en hebben veel ervaringen gedeeld, heel veel succes met de afronding. Pol, heel veel succes met je academische carrière. Ik heb veel respect voor je gedrevenheid en ambitie.

Marko Nieuwenhuizen, jou wil ik bedanken omdat je altijd klaar stond mij te helpen of iets uit te leggen. Ook zijn de avonden Stratumseind van groot belang geweest.

Takaya, it has been a pleasure to me to work with you on the nanoparticle project. I'm still impressed by your polymerization skills. I wish you, Aya and your son all the best for the future.

Svetlana Borukhova, thank you very much for the synthesis of some BTA functionalized pEGs. These polymers are used in Chapter 4. I wish you all the best for the future.

Ik wil graag Tonny, Henk, Gaby en Michel F. Bedanken voor de overgebrachte kennis en gekregen materialen.

Natuurlijk wil ik ook de ondersteunde staf bedanken voor het creëren van een prima werksfeer binnen de vakgroep. Allereerst Ralf Bovee, Xianwen Lou en Joost van Dongen voor de hulp bij de analyses. Hans Damen, bedankt voor je behulpzaamheid. Je bent onmisbaar voor de vakgroep. Graag wil ik Henk, Nora, Angela, Patricia, Joke, Carine en Janna bedanken voor de geweldige ondersteuning waardoor het werken in de vakgroep veel gemakkelijker wordt. Ik wil de academische staf bedanken voor hun beschikbaarheid en bereidheid voor het beantwoorden van elk mogelijke vraag.

Ook de deelnemers aan de Compartmentelized systems lunchbijeenkomst wil ik graag bedanken voor hun bijdragen aan de bijeenkomsten en input betreffende mijn eigen werk. Ook veel dank aan mijn labgenoten en speciale dank aan Jolanda. Jolanda, ook al deelden we niet dezelfde manier van werken en muzieksmaak, toch heb ik met veel plezier gewerkt op het schoonste lab van Eindhoven. Verder, bedank ik mijn kamergenoten van STO 4.43, Seda, Wilco, Bram, Edith, Nicole en Kelly voor de goede sfeer op de kamer. Seda en Wilco, ik kijk met erg veel plezier terug aan onze Amerika reizen.

The social events after work have been of significant importance to me. I have met some great people that contributed to the great time I had. I want to thank Thorsten, Jean-Luc, Matt, Elisa, Davide, Erik, Dana G., Johan F., Melissa, Marcel, Peter, Patrick, Janus, Rob vd W., Bart, Martijn, Ewelina, Allesio, Michel v H., Thomas, Amparo, Stephanie P. Maarten S, Arjan,

Pim, Sagitta, Carel, Isja, Ilja, Mellany, Katja, Lech, Dana U., Marie-France, Renaud, Mindaugas, Yuko, Yoko, Takaya, Takashi, Nobu, Yumi, Bob, Pablo, Roxanne, Paco, Stefania, Lars vd M, Tom, Rob vd B., Bas, Bram, Patricia, Menno en Carlien.

Ik wil graag mijn Oosterhoutse / Bredase / Eindhovense vrienden bedanken voor een langdurige vriendschap maar ook voor de interesse in mijn onderzoek. De tijd die ik met jullie doorbreng is voor mij heel erg belangrijk en heeft de nodige ontspanning gebracht. Jeroen, Jorrit, Nicole, Wouter, Roel, Danielle, Roel, Linda, Hugo, Stijn, Roy, Bas, Britte, Steven, Soes, Cheryl en Marleen, bedankt! Ook wil ik graag Jacques, Ann, Casper en Kim bedanken voor jullie interesse in wat ik doe.

Ten slotte wil ik mijn familie bedanken. Jasper, Susan, Flore, Opa, Ica en Harry, bedankt voor alle steun en interesse in mijn onderzoek. Pap en mam, jullie hebben me ontzettend goed geholpen door altijd voor mij klaar te staan, te luisteren en te bieden wat ik nodig heb. De rust en de vrijheid die ik bij jullie thuis vind zijn voor mij zeer waardevol en deze hebben enorm bijgedragen aan de totstandkoming van mijn proefschrift. Bedankt dat jullie er altijd voor mij zijn.

Pascalle, deze laatste woorden zijn voor jou. Ik wil je ontzettend bedanken dat je mij altijd bent blijven steunen en klaar voor mij stond. Vanwege mijn regelmatige afwezigheid en mijn niet altijd gezellige stemming is het ook niet gemakkelijk voor jou geweest. Ik waardeer heel erg hoe je hiermee bent omgegaan.

Tristan